On the Evolution of
Accreting White Dwarfs
in Binary Systems

On the Evolution of Accreting White Dwarfs in Binary Systems

Over de Evolutie van Massa-Invagende Witte Dwergen in
Dubbelstersystemen

(met een samenvatting in het Nederlands)

Proefschrift

ter verkrijging van de graad van doctor aan
de Universiteit Utrecht op gezag van de
Rector Magnificus, Prof. Dr. W.H. Gispen, ingevolge het besluit van het
College voor Promoties in het openbaar te verdedigen op
woensdag 22 april 2004 des middags te 12.45 uur

door
Sung-Chul Yoon

geboren op 15 november 1970, te Seoul

Promoter: Prof. Dr. Norbert Langer

Sterrenkundig Instituut, Universiteit Utrecht

Contents

Chapter 1

Introduction

Observation of the heavens was of utmost importance in ancient far eastern countries like China, Japan and Korea (cf. Fig. 1.1). This is not only due to practical needs for agriculture, which was their major economic resource, but also due to their particular world-view that
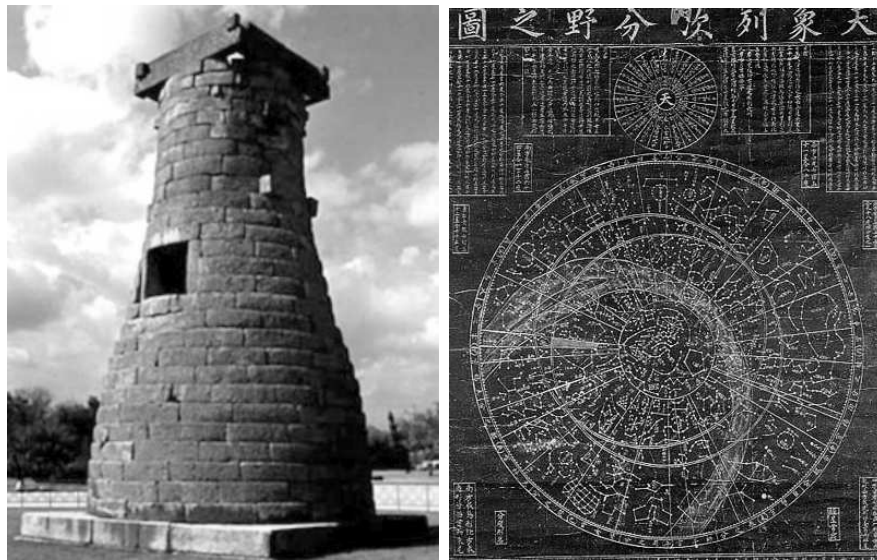
Figure 1.1: *Left)* Chum-Sung-Dae (Tower for star observations) at Kyung-Joo, Korea. The oldest existing astronomical observatory in Asia, constructed during the reign of queen Sun-Duk (AD 632 — AD 646) of the Shilla Dynasty. It was built from about 360 stones, which represent one year. *Right)* Chun-Sang-Yeol-Cha-Bun-Ya-Dji-Do — map of sky image according to zones and areas. This sky map was first constructed in 1396 by 12 royal astronomers during the reign of King Tae-Jo (AD 1392 — AD 1398), the founder of the Lee Dynasty which lasted from AD 1392 to AD 1910 in Korea. This photo is an updated version made in AD 1770, during the reign of King Young-Jo (AD 1724 — AD 1776).

heaven, earth and man are not separable entities, but one. Astronomical phenomena were always interpreted in terms of human activities on earth and affected significantly the political agenda. This is in sharp contrast to the situation of the ancient western world, which adhered to the belief of an unchanging universe which was considered rather independent of the human history.

It is not hence surprising that in far eastern countries great attention was drawn particularly to abnormal events like novae and supernovae (new stars), which were called *guest stars*. One example can be found in the detailed observations of a supernova in 1604, which were made over 6 months by Korean astronomers in the epoch of the King Seon-Jo. Their observational records were reported in the official chronicle of Lee Dynasty (*Lee-Jo Shillok*; Fig. 1.2). These observations, together with those by Kepler, enabled to reconstruct the daily variation of the brightness of this guest star. (see Fig. 11.1 in Clark & Stephenson 1977).

Interestingly, modern astrophysics has found that supernovae produce many important heavy elements such as oxygen, magnesium, calcium and iron, which are essential ingredients constituting human bodies as well as our planet. This discovery revives the old thought of the far eastern world – but in a somewhat different sense – that heaven is interwoven with earth and human being. This has provided, in part, a strong motivation for detailed studies on the nature of supernovae in astrophysics.

Figure 1.2: Lee-Jo Shillok – the official chronicle of the Lee Dynasty (AD 1392 - AD 1910 in Korea), where observations of a guest star in 1604 were reported.

Observational and theoretical studies indicate that at least two different kinds of supernovae exist in a broad sense. One is deaths of massive stars ($\gtrsim 8$ M$_\odot$), caused by the implosion of their inert central core when its nuclear fuel is exhausted. Such supernovae are classified as Type II or Type Ib/c according to their spectral features. Spectra of Type II supernovae show prominent hydrogen lines, while those of Type Ib/c supernovae do not. The other kind of supernovae originates from the thermonuclear explosion of white dwarfs in close binary systems (cf. Fig. 1.3; see explanations below), which is categorized as Type Ia (see Sect. 1.3). The guest star found in 1604 is also believed to be of this kind.

Recently, the use of the brightness and its time variation of Type Ia supernovae to measure extragalactic distances is radically changing our cosmological paradigm, intriguingly revealing the presence of so called dark energy in the universe (Sect. 1.3). However, evolutionary models of stars toward Type Ia supernovae have raised puzzling questions. Particularly, we still do not understand in which kinds of binary systems white dwarfs can evolve

into a thermonuclear explosion resembling a Type Ia supernova.

Thus motivated, this thesis aims at improving the knowledge of the physics and the evolution of accreting white dwarfs, especially by evoking one of the most classic, but often neglected topics in stellar astrophysics: rotation.

1.1 Accreting white dwarfs in binary systems

Stars spend most of their life for core hydrogen burning on the so called main sequence. Once hydrogen is exhausted at the center, helium burning follows in the core. In a star with its mass less than about 8 solar mass ($\lesssim 8 \ M_\odot$), a compact carbon and oxygen (CO) core is formed when core helium burning comes to an end. No further nuclear fusion occurs in the core, but thin layers of hydrogen and helium surrounding the CO core participate in thermonuclear reactions. Eventually, the outer hydrogen envelope is progressively thrown out of the star, leaving the CO core naked. Such stellar remnants are called *CO white dwarfs*.

A typical white dwarf has a mass of $0.6 \ M_\odot$ but only about the size of the earth. Due to this strong compactness, even in cold white dwarfs the electrons can not remain only in their lowest quantum energy states but are forced to fill high energy states according to Pauli's exclusion principle. Gases in such a state are referred as electron degenerate. It is the pressure due to the degenerate electron gas — as it dominates over the ideal gas pressure
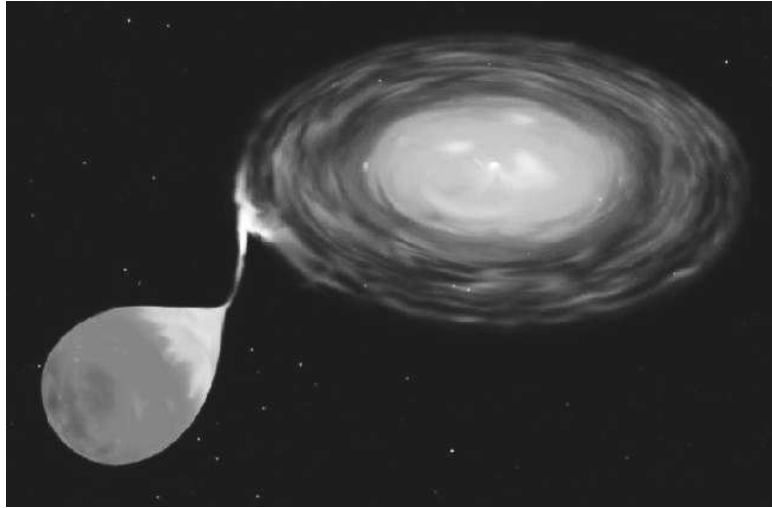
Figure 1.3: An artistic image of an accreting white dwarf with its non-degenerate companion star which transfers matter into the white dwarf via the Roche lobe overflow. A white dwarf is surrounded by the rapidly rotating accretion disk which is formed by the transfered matter.

— that supports white dwarfs against their own gravity. Interestingly, more massive white dwarfs are smaller in size and there exists a critical limit for the white dwarf mass above which the pressure inside a white dwarf can not balance its own gravity any more. This critical mass is called *Chandrasekhar mass*, which is about 1.4 $M_\odot$.

Since stellar populations are largely dominated by low and intermediate mass stars (i.e., more than 90 %), white dwarfs are the most commonly produced stellar remnants. For instance, about 10 percent of the stars in our galaxy are believed to be white dwarfs (cf. Oppenheimer et al. 2001). Isolated white dwarfs just radiate by spending their internal energy, doomed to quiescently fade out of our sight without showing any spectacle.

However, numerous white dwarfs are found in binary systems, like Sirius B, the first identified white dwarf. White dwarfs in close binaries may anticipate a very different fate than isolated ones. Once the companion star evolves and expands, or if the binary orbit shrinks due to gravitational wave radiation or other ways of angular momentum loss, the white dwarf companion may fill its critical volume in the binary, which is often called Roche lobe. The stellar matter which flows over the Roche lobe begins to be transferred to the white dwarf (see Fig. 1.3). Such binary systems where white dwarfs accrete matter from their companion stars are often called cataclysmic variables, of which more than 300 have been observed so far (Sion 1999; Downes et al. 2001). The accreted matter onto the white dwarf usually participates in unstable or even violent thermonuclear fusion as it is compressed to high density due to the white dwarf compactness. For example, so called nova outbursts represent such events that thermonuclear explosion of the accreted matter results in a drastic increase in the luminosity of the system by up to 18 magnitudes.

It is also suggested that steady nuclear burning of hydrogen or helium in a shell source close to the surface of accreting CO white dwarfs may explain the luminous objects observed in super-soft X-ray bands (super-soft X-ray sources; van den Heuvel et al. 1992; Iben & Tutukov 1994), which are characterized by luminosities of $10^{36} \ldots 10^{38}$ erg/s and surface temperatures of $10^5 \ldots 10^6$ K (Trümper et al. 1991; Greiner et al. 1991; Kahabka & van den Heuvel 1997).

Most importantly, one of the most spectacular events in the universe, namely Type Ia supernovae, are believed to originate from the thermonuclear disruptions of accreting white dwarfs (e.g. Hillebrandt & Niemeyer 2000; Livio 2001; see Sect. 1.3).

1.2   The evolution of accreting white dwarfs

The above mentioned nova and supernova phenomena are related to the way in which the accreted non-degenerate matter is incorporated into the strongly electron-degenerate white dwarf core. Theoretical studies in the last few decades indicate that the mass accretion rate is particularly important in determining the evolution and final fate of an accreting white white dwarf as follows.

Firstly, whether hydrogen or helium shell burning occurs steadily, in eruptions, or — at least for some time — not at all depends mostly on the mass accretion rate ($\dot{M}_{\rm acc}$) of the white dwarf (e.g. Paczyński & Żytkow 1978; Prialnik et al. 1978; Sion et al. 1979;
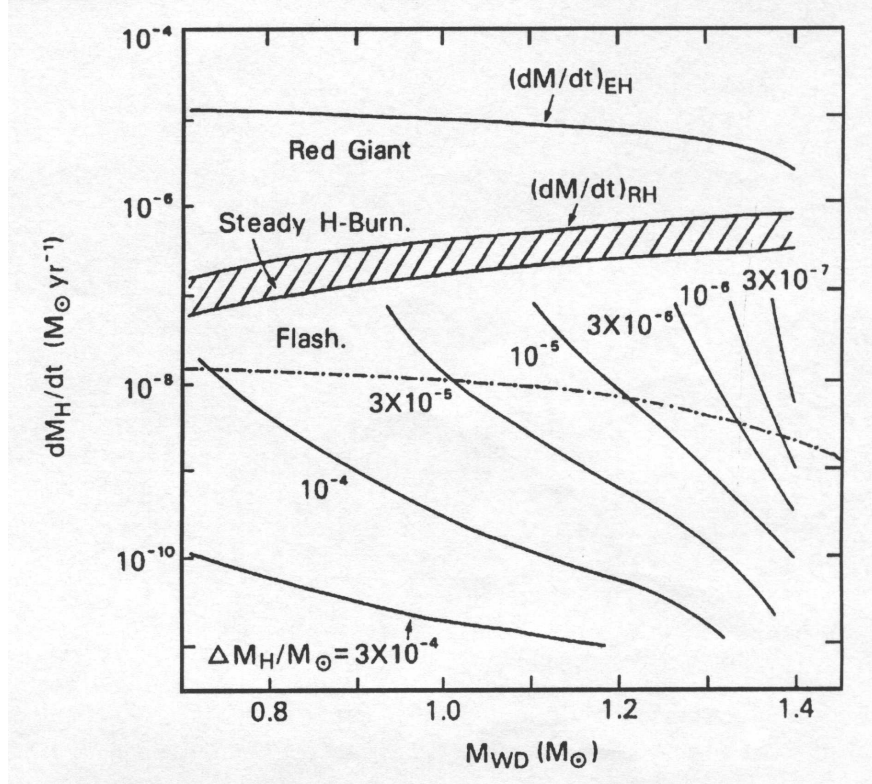
Figure 1.4: Schematic illustration of the outcome of the hydrogen shell burning, for different accretion rates and white dwarf masses. The solid lines marked by $(dM/dt)_{\rm EH}$ and $(dM/dt)_{\rm RH}$ denote the critical accretion rates above which the white dwarf reaches the Eddington limit (i.e., the limit above which the radiation pressure at stellar surface dominates over the gravity) and is driven to the red giant phase, respectively. The region which allows steady hydrogen shell burning is hatched. The numbers labeled at the solid lines below the steady hydrogen shell burning region give the mass of the accumulated hydrogen by the time when a hydrogen shell flash occurs. Below the dashed-dotted line, the hydrogen shell flash is expected strong enough to produce a nova explosion. From Kahabka and van den Heuvel (1997). See also Nomoto (1982a) and Fujimoto (1982b).

Iben 1982b; Nomoto 1982a; Fujimoto 1982a, 1982b; Cassisi et al. 1998; Piersanti et al. 2000). Fujimoto (1982b), Nomoto (1982a) and Kahabka & van den Heuvel (1997) summarize the accretion rate dependence of hydrogen shell burning as in Fig. 1.4. Too rapid accretion [$\dot{M}_{\rm acc} \gtrsim (dM/dt)_{\rm RH}$ in the figure] will lead the white dwarf to expand toward red giant dimensions such that the white dwarf envelope also fills the Roch lobe, which may result in significant mass outflow from the binary system. With too slow accretion ($\dot{M}_{\rm acc}$
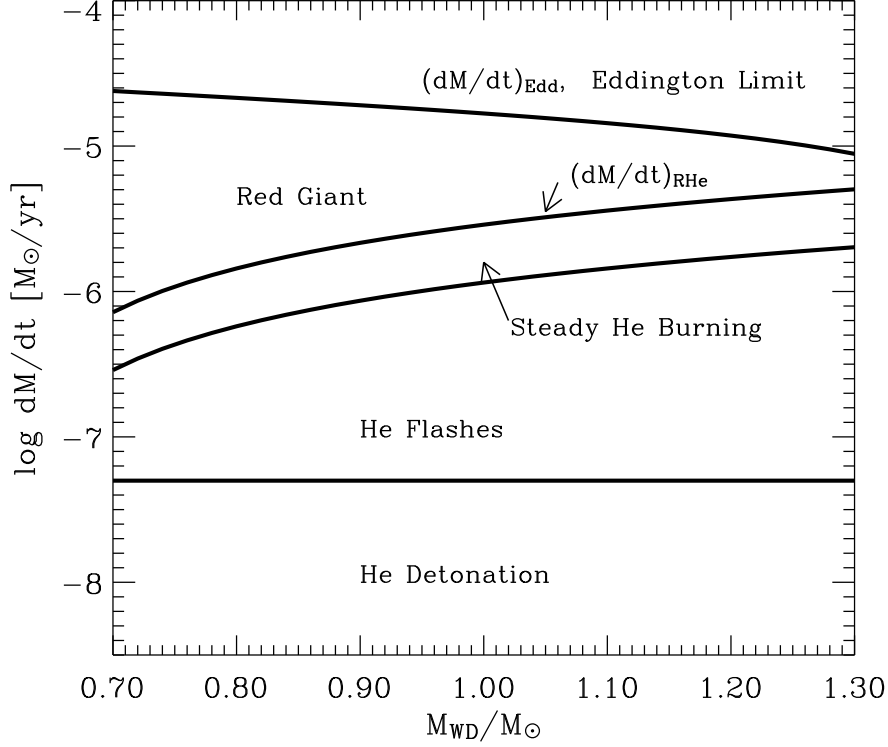
Figure 1.5: Same as in Fig. 1.4 but for helium accretion. The upper limit for the steady helium shell burning is taken from Nomoto (1982a): $(dM/dt)_{\rm RHe} = 7.2 \times 10^{-6}(M_{\rm WD}/M_{\odot} - 0.6)$ $M_{\odot}/$yr, while the lower limit is defined as $0.4(dM/dt)_{\rm RHe}$ (cf. Nomoto 1982a), below which helium shell burning is unstable in general.

$\lesssim 10^{-9} \ldots 10^{-8}$ $M_{\odot}/$yr; below the dashed-dotted line), the accreted hydrogen ignites under highly degenerate condition and the consequent hydrogen flashes produce strong nova explosions, which induce ejection of the accreted matter into space. Accretion with rates in-between these two limits allows steady burning of hydrogen or induces only mild recurrent shell flashes. Helium shell burning shows similar features but the accretion rates which allow steady helium shell burning are significantly higher, as shown in Fig. 1.5 (Nomoto 1982a; Iben & Tutukov 1989; cf. Cassisi et al. 1998). If $\dot{M}_{\rm acc}$ is lower than about 5×10^{-8} $M_{\odot}/$yr, helium ignition is expected to occur under such highly degenerate conditions that helium detonation is induced, which may lead to a supernova event if at least about 0.2 $M_{\odot}$ of helium have previously been accreted by the CO white dwarf (e.g. Nomoto 1982b; Iben & Tutukov 1991; Limongi & Tornamé 1991; Woosley & Weaver 1994; Livne

& Arnett 1995). If the accretion rate is between the detonation and steady burning regimes, weaker helium shell flashes will occur.

Secondly, the thermal evolution of the white dwarf core is a sensitive function of the accretion rate (e.g. Iben 1982b; Nomoto 1982a; Sion 1995; Townsley & Bildsten 2002). This has important implications for the final fate of accreting CO white dwarfs, as discussed by Nomoto & Kondo (1993). If accretion is fast ($\dot{M}_{\mathrm{acc}} \gtrsim 3 \times 10^{-6}$ M$_\odot$/yr) such that the accretion time scale is shorter than the thermal diffusion time in the white dwarf ($\tau_{\mathrm{acc}} \ll \tau_{\mathrm{diff}}$), the gravitational energy released due to the shrinkage of the white dwarf leads to off-center carbon ignition (Saio & Nomoto 1985, 1998; see also Fig. 1.6). Subsequently, carbon burning moves inward and transforms the CO white dwarf into an ONeMg white dwarf, which is likely to end as a neutron star due to electron capture induced collapse when it reaches the Chandrasekhar limit. On the other hand, if the accretion time scale is larger than the thermal diffusion time scale (i.e., $\dot{M}_{\mathrm{acc}} \lesssim 10^{-9}$ M$_\odot$/yr), the white dwarf temperature will continue to decrease such that the center will have crystallized ($\rho_{\mathrm{c}} \gtrsim 10^{10}$ g/cm^3) by the time its mass grows to the Chandrasekhar limit. The ensuing central carbon ignition fails to explode the white dwarf but results in a collapse and the formation of a neutron star (Nomoto & Kondo 1993). If the accretion rates are in-between these two limits, the whole white dwarf interior will be heated during mass accretion. As a result, when the white dwarf reaches the Chandrasekhar limit, carbon will ignite while the central core of the white dwarf is still in the liquid state (i.e., $\rho_{\mathrm{c}} \simeq 10^9$ g/cm^3 and $T_{\mathrm{c}} \simeq 10^8$ K). The following nuclear burning may be able to produce an SN Ia event, as confirmed by recent 3-dimensional numerical simulations (e.g. Reinecke et al. 2002; Gamezo et al. 2003).

1.3   Progenitors of Type Ia supernovae

1.3.1   Importance of SNe Ia in astrophysics

Type Ia supernovae (SNe Ia) are characterized mainly by two spectroscopic features: the lack of hydrogen and helium lines (see however, Hamuy et al. 2003) and the presence of strong Si II absorption near 6100 Å. Observations indicate that SNe Ia produce about 0.6 M$_\odot$ of ^{56}Ni on average (e.g. Leibundgut 2000; cf. Nomoto et al. 1984, 1997). The observed SNe Ia rate is as high as a few times 10^{-3} per year per galaxy. SNe Ia may critically affect the cosmic evolution as they produce most of iron in the universe (e.g. Renzini 1999; Kobayashi et al. 2000; Matteucci & Recchi 2001; Ferreras & Silk 2002). Since SNe Ia are likely to originate from low or intermediate mass stellar systems (see Sect. 1.3.2), they might begin to make contributions to the chemical evolution later than core collapse supernovae which are produced by massive stars.

Interestingly, before 1990 SNe Ia light curves were believed to be almost identical (e.g. Woosley & Weaver 1986), which enabled SNe Ia to acquire the honorable nickname *standard candles of the universe* (Branch & Tammann 1992). More recent systematic studies have revealed that, instead of being perfectly homogeneous, SNe Ia show an intrinsic and linear proportionality of their maximum brightness to the width of their light curve (Phillips

1993; Hamuy et al. 1996b). An important relevance of this property to astrophysics is that SNe Ia can be *standardized* as distance indicators of galaxies even beyond $z = 1$, which allows to derive cosmological parameters such as the Hubble constant with an unprecedented accuracy (e.g. Riess et al. 1996; Hamuy et al. 1996a; Branch 1998). Furthermore, two independent research programs for systematic observations of SNe Ia at large redshifts (Perlmutter et al. 1997; Riess et al. 1998) recently opened the new paradigm of the accelerating universe in modern cosmology, suggesting the presence of *dark energy* in the universe, of which the nature is still mysterious (cf. Perlmutter et al. 1999b; Livio 2000). Today, SNe Ia stand out as an indispensable tool in cosmology to probe the expansion history of the universe (e.g. Leibundgut 2001; Perlmutter & Schmidt 2003).

However, the use of SNe Ia for measuring extragalactic distances relies on extrapolating purely empirical results obtained from nearby galaxies. It is hence to question whether the nature of SNe Ia at high redshifts may remain analogous to those in nearby galaxies, given that stellar evolution might show consequential varieties to different metallicities and environments throughout the cosmic ages (e.g. Höflich et al. 1998; Langer et al. 2000). Together with the growing evidence for the diversity of SNe Ia (e.g. Branch 2001; Nomoto et al. 2003; Li et al. 2003; Wang 2003; Branch 2004), this requires to identify every possible evolutionary path of SNe Ia progenitors (cf. Weller & Albrecht 2002).

1.3.2   Possible SNe Ia progenitors

Even though progenitors of SNe Ia have not been identified yet, observations are most consistent with the scenario that SNe Ia result from the thermonuclear explosion of CO white dwarfs, of which the idea goes back to Hoyle & Fowler (1960). Given that isolated white dwarfs or CO cores in single stars can hardly experience such a thermonuclear explosion, SNe Ia are supposed to originate from binary systems in which CO white dwarfs accrete matter (e.g. Branch et al. 1995; Livio 2001).

SNe Ia are observed in nearly all types of galaxies including elliptical, spiral and irregular ones, unlike core collapse supernovae which favor spiral galaxies and do not appear in elliptical galaxies. In particular, SNe Ia in elliptical galaxies imply that their progenitors can be as old as $\sim 10^{10}$ yr. A high progenitor age of SNe Ia compared to core collapse supernovae is also confirmed by the indication that in spiral galaxies, Type II supernovae occur mostly in spiral arms, while SNe Ia tend to avoid active star forming regions (Maza & van den Bergh 1976; McMillan & Ciardullo 1996; Wang et al. 1997).

It is also found that over-luminous SNe Ia are observed only in spiral galaxies (e.g. Hamuy et al. 1995, 1996a), which might imply the existence of at least two different kinds of SNe Ia progenitors: one from old stellar populations ($\sim 10^{10}$ yr), the other from younger ones ($\sim 10^8$ yr) (Della Valle & Livio 1994; Howell 2001). The necessity of more than one SNe Ia progenitor scenario is also suggested by the observationally implied wide range of ^{56}Ni masses produced from SNe Ia, ranging from ~ 0.1 $M_\odot$ to ~ 1.0 $M_\odot$, even though more than 80 % of SNe Ia seem to be fairly homogeneous, giving about 0.6 $M_\odot$. (Hillebrandt & Niemeyer 2000).

Several types of binary systems have been suggested as SNe Ia progenitors, and we review the most studied systems as follows.

Double CO white dwarf systems: Whelan & Iben (1973) first suggested such binary systems consisting of two CO white dwarfs as SNe Ia progenitors, of which the period is short enough to merge the system due to angular momentum loss via gravitational wave radiation within a Hubble time (i.e., the age of the universe; see also Iben & Tutukov 1984; Webbink 1984). Systems with a total mass larger than the Chandrasekhar limit can be produced from intermediate mass main sequence binary stars, with frequencies of $\sim 10^{-4}$ yr^{-1} for old populations ($\sim 10^{10}$ yr) and $\sim 10^{-3}$ yr^{-1} for young populations ($\sim 10^{8}$ yr), which is consistent with the observed SNe Ia rate (Iben & Tutukov 1984; Iben & Livio 1993; Branch et al. 1995; Livio 2001). This scenario explains the absence of hydrogen or helium in observed SN Ia spectra, as well as a wide range of progenitor ages from 10^{7} yr to 10^{10} yr, which are mainly determined by the initial orbital periods of the double white dwarf systems. Several binary systems consisting of double white dwarfs which are expected to merge within a Hubble time have also been identified, including one near the Chandrasekhar limit (Napiwotzki et al. 2002, 2003; Karl et al. 2003). However, it is seriously questioned whether such systems can lead to SNe Ia at all. If the less massive CO white dwarf fills the Roche lobe, the consequent accretion onto the more massive one is expected to occur very rapidly (i.e., $\dot{M} \sim 10^{-5}$ M$_\odot$/yr; Cameron & Iben 1986; Benz et al. 1990; Mochkovitch & Livio 1990; Segretain et al. 1997; Han & Webbink 1999). With such high accretion rates, off-center carbon ignition is likely to occur in the accreting white dwarf well before it reaches the Chandrasekhar limit, as shown by Nomoto & Iben (1985) and Saio & Nomoto (1985, 1998), and as also demonstrated in Fig. 1.6 (see the figure caption for more details). The accreting CO white dwarf is transformed to an ONeMg white dwarf as the carbon burning flame propagates inward. As the center of an ONeMg white dwarf becomes susceptible to electron capture at densities higher than about 4×10^{9} g cm^{-3}, coalescence of double CO white dwarfs of which the total mass exceeds the Chandrasekhar limit are likely to end in a collapse induced by electron capture to form a neutron star, rather than in an SN Ia.

Helium main sequence star + CO white dwarf systems: Binary systems consisting of a CO white dwarf of $0.6 \dots 1.0$ M$_\odot$ plus a less massive helium star ("helium star cataclysmics") were investigated by Iben & Tutukov (1991) and Limongi & Tornambé (1991). Mass transfer in such systems is induced by angular momentum loss due to gravitational wave radiation, and the resultant accretion rates are found to be about $\sim 10^{-8}$ M$_\odot$/yr regardless of the exact masses of the two stellar components (Iben & Tutukov 1991). As implied in Fig. 1.5, such accretion rates will lead to a helium detonation when about 0.2 M$_\odot$ of helium is accumulated by the CO white dwarf, which may induce a detonation of carbon at the white dwarf center via an inward pressure wave, as shown by Livne (1990; see also Woosley & Weaver 1994; Livne & Arnett 1995). Although such a double detonation may appear as an SN Ia by definition, model calculations of such explosions fail to reproduce the light curves and spectra of observed SNe Ia (Höflich & Khoklov 1996; Nugent et al. 1997;
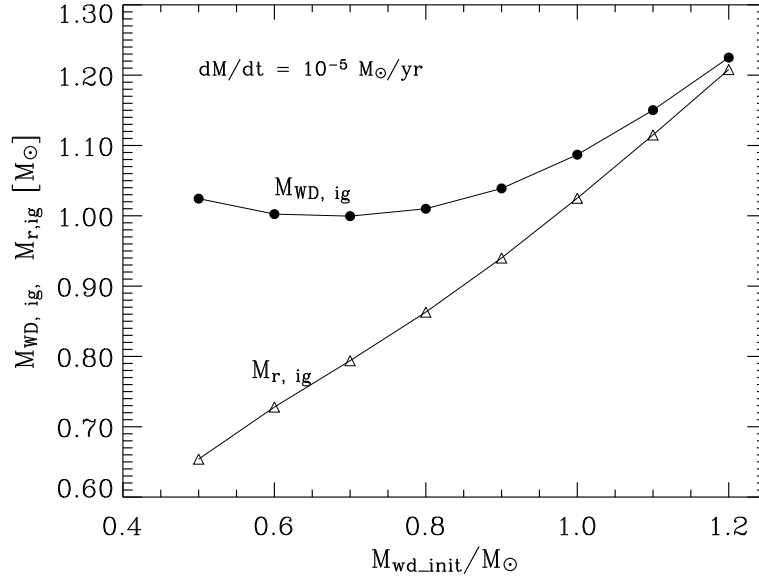
Figure 1.6: Mass at carbon ignition of CO white dwarfs which accrete CO-rich matter ($X_C = X_O = 0.487$) with a constant accretion rate of 10^{-5} $M_\odot$/yr, as function of their initial mass (line connecting the filled circles). The corresponding mass coordinate of carbon ignition inside the white dwarf is given by the line connecting the open triangles. The luminosity of the initial white dwarf models is about 0.01 $L_\odot$. From Yoon, Podsiadlowski & Langer (in preparation).

Pinto et al. 2001).

Main sequence star + CO white dwarf systems: These systems became a promising SN Ia progenitor candidate due to the discovery of luminous super-soft X-ray sources and their attribution to accreting white dwarfs with stationary hydrogen burning shells (van den Heuvel et al. 1992; Rappaport et al. 1994; Li & van den Heuvel 1997). Binaries where thermally unstable mass transfer from a MS star results in mass transfer rates of $\sim 10^{-7}$ $M_\odot$/yr allow a steady burning of the accreted hydrogen in the white dwarf with $L_{WD} \approx 10^{37}$ erg/s at $T_{\text{eff,WD}} \approx 10^5$ K (van den Heuvel et al. 1992). Recurrent novae from massive white dwarfs near the Chandrasekhar limit such as U Scorpii (Hachisu et al. 2000; Thoroughgood et al. 2001) may represent MS star + CO white dwarf binary systems in a late evolutionary stage, in which the mass transfer rate is significantly lowered (cf. Langer et al. 2000). If a white dwarf in such a binary system reaches the Chandrasekhar limit, the consequent thermonuclear explosion induced by carbon burning will be able to produce an SN Ia. The expected life time of $\sim 10^8$ yr of such systems indicates that this channel could be responsible for some of the observed SNe Ia in late type galaxies. On the other hand, it is debated
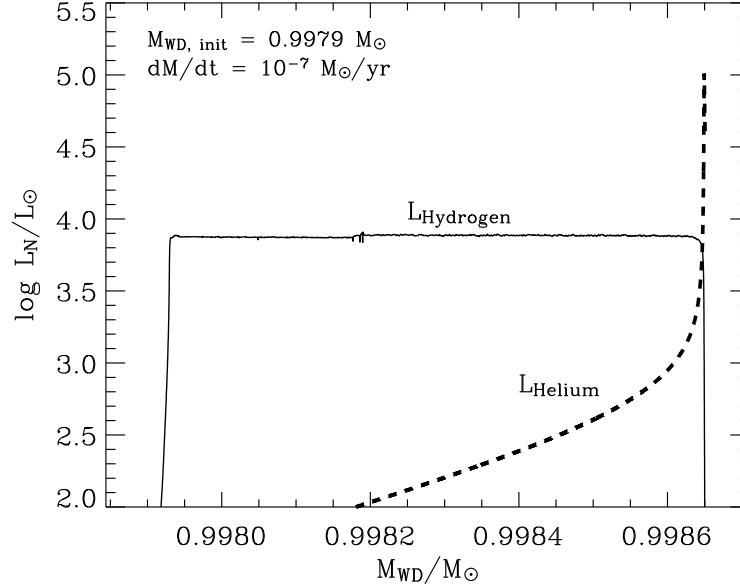
Figure 1.7: Evolution of the nuclear luminosity due to hydrogen (solid line) and helium (dashed line) shell burning in a white dwarf which accretes hydrogen rich matter at a constant rate of 10^{-7} $M_\odot$/yr. The initial mass and surface luminosity of the white is 0.9979 $M_\odot$ and 2383 $L_\odot$, respectively. From Yoon & Langer (in preparation).

whether this channel can be a major source of SNe Ia, or whether those systems can produce SNe Ia at all, since the growth of a white dwarf up to the Chandrasekhar limit by hydrogen accretion can not be easily achieved due to the following reasons. Firstly, the accretion rates for steady hydrogen shell burning are limited to a very narrow range, as shown in Fig. 1.4. Secondly, even if hydrogen is burned steadily, the following helium shell burning is generally unstable (Cassisi et al. 1998; Fig. 1.7), since the accretion rates for steady shell burning for hydrogen and helium do not correspond to each other, as indicated in Figs. 1.4 and 1.5. Figure 1.7 gives an example of the evolution of hydrogen and helium shell burning in an accreting white dwarf, which shows a helium shell flash preceded by steady hydrogen shell burning (see the figure caption for more details). Such unstable helium shell burning may drive the white dwarf envelope to reach the Eddington limit or to fill its Roche lobe radius (Cassisi et al 1998; Langer et al. 2002), which will lead to significant mass loss (cf. Kato & Hachisu 1999). Therefore, the mass accumulation efficiency in hydrogen accreting white dwarfs needs to be carefully investigated in order to evaluate the importance of MS star + CO white dwarf systems as SNe Ia progenitors.

Symbiotic systems: Symbiotic systems (red giant star + CO white dwarf binary systems) have the advantage that they can explain progenitors in elliptical galaxies, if the mass of the red giant star is sufficiently low. There exist two different possibilities for supernova explosion in these systems. One is the double detonation at sub-Chandrasekhar mass as a consequence of mass accretion from the red giant wind, after about 0.2 $M_\odot$ of helium is accumulated through hydrogen burning at a rate of $\sim 10^{-8}$ $M_\odot/yr$ (Kenyon et al. 1993; Yungelson et al. 1995; cf. Piersanti et al. 1999). The outcome of the explosion may be similar to that from a helium main sequence star + CO white dwarf system, and thus may have the same kind of problems in explaining the observed light curves and spectra of SNe Ia. The other is the explosion of the white dwarf at the Chandrasekhar mass, as in MS star + CO white dwarf systems, which can be achieved via mass accretion during Roche lobe overflow from a low mass RG star (Hachisu et al. 1996, 1999). This scenario invokes a strong wind from the white dwarf, to stabilize the mass accretion such that the conditions for steady hydrogen shell burning may be satisfied. However, the physics of such a strong wind from a white dwarf which leads the wind mass loss rates even up to $\sim 10^{-4}$ $M_\odot/yr$ (!) is not yet well understood, and further realistic radiation hydrodynamic studies are required for its justification. Furthermore, this scenario has the same problem of unstable helium shell burning as the MS star + CO white dwarf systems.

Helium giant + CO white dwarf systems: Iben & Tutukov (1994) investigated mass transfer from a evolved helium star with a CO core mass of ~ 0.6 $M_\odot$ (i.e., a helium giant) onto a CO white dwarf. The expected mass transfer rates are as high as $10^{-6}\ldots10^{-5}$ $M_\odot/yr$, and the resulting helium accretion may induce steady helium shell burning (see also Chapt. 3). The progenitor age of this channel is about 10^8 yr, which may be relevant to late type galaxies. These systems are free of complications involved in the double shell source models, as only helium is accreted. Nevertheless, the accretion rates for steady helium shell burning are limited to a narrow range as shown in Fig. 1.5, and the production rate of SNe Ia through this channel is not well known.

In the literature, the above mentioned binary systems are often categorized into three different scenarios:

- **The double degenerate scenario**: double CO white dwarfs

- **The sub-Chandrasekhar mass single degenerate scenario**: helium main sequence star + CO white dwarf, symbiotic systems with wind accretion

- **The Chandrasekhar mass single degenerate scenario**: MS star + CO white dwarf, symbiotic systems with Roche lobe overflow, helium giant+CO white dwarf

Currently, the third category represents the favored SNe Ia progenitor scenario, since explosion models of a Chandrasekhar mass CO white dwarf give good fits to observed SN Ia light curves and spectra, compared to double detonation models, while the Chandrasekhar mass

white dwarf produced via the coalescence of two CO white dwarfs may fail to produce an SN Ia due to the off-center carbon ignition, as discussed above.

1.4 This Thesis

1.4.1 Motivation and Outline

It is remarkable that the above discussion of possible SNe Ia progenitors is based on theoretical studies in which mostly constant accretion rates and spherical symmetry for the accreting white dwarf model have been assumed. In reality, close binary systems experience orbit changes due to mass transfer, stellar wind mass loss, gravitational wave radiations, etc, which in turn leads to a time evolution of the mass accretion rate (e.g. Langer et al. 2000). More importantly, the effects of rotation have been neglected in most previous studies. It is now well established that rotation strongly affects the evolution of massive stars (e.g. Langer 1998; Heger et al. 2000; Maeder & Meynet 2000). Langer et al. (2003) pointed out that the effects of rotation become even more important in the stellar components of close binary systems, where mass exchange can involve a large angular momentum gain or loss. We suggest that this can be also the case in accreting white dwarfs, since the transfered matter in a close binary system generally forms a centrifugally supported disk around the accreting white dwarf, and the accreted matter may carry a large amount angular momentum, spinning up the white dwarf (e.g. Durisen 1977; Ritter 1985; Langer et al. 2000, 2002, 2003).

Although a few studies addressed the effects of rotation on accreting white dwarfs, the transport of angular momentum was not properly treated in those studies, assuming either solid body rotation — i.e., extremely efficient angular momentum transport —, or angular momentum redistribution by the degenerate electron viscosity — which is very inefficient This work explores systematically the effects of rotation on the SNe Ia progenitor evolution, using a realistic description of the transport of angular momentum and of chemical species due to rotationally induced hydrodynamic instabilities (see Sects. 4.2 and 4.3 for more details).

This thesis is organized is as follows.

Chapter 2   We investigate the stability conditions of thermonuclear shell sources analytically, which is crucial for the understanding the evolution of hydrogen or helium accreting white dwarfs. Several studies on the stability of shell sources have already been presented (see Sect. 2.1), but here we unify the existing results in terms of the shell source geometry, temperature, and density, and provide a quantitative tool for investigating the shell burning stability in stellar evolution models.

Chapter3 Although the Chandrasekhar mass single degenerate scenario for SNe Ia pro-
genitors is currently the most favored one, its realization in nature has not yet been unam-
biguously confirmed, neither observationally nor theoretically. From the theoretical point
of view, this is mainly due to the occurrence of unstable helium shell burning in correspond-
ing progenitor evolution models, as discussed in Sect. 1.3.2, which causes severe numerical
difficulties for realistic simulations. In this chapter, we present theoretical evidence for the
functioning of this scenario, by constructing the first self-consistent binary star evolution
model which produces a Chandrasekhar mass white dwarf. Motivated by the work of Iben
& Tutukov (1994), helium giant + CO white dwarf binary systems are considered here.

Chapter 4 The physics of angular momentum transport in white dwarfs due to various
hydrodynamic instabilities is investigated in detail. After briefly reviewing the existing
literature on rotating white dwarfs, numerical methods to describe the effects of rotation and
angular momentum redistribution are explained in detail. It is shown that strong differential
rotation, with the shear strength near the threshold value for the onset of the dynamical shear
instability, is expected to be retained in white dwarfs which accrete matter with rates of
$10^{-7} \ldots 10^{-6}$ $M_\odot$/yr, affecting their thermal and mechanical conditions significantly. We
discuss implications for SNe Ia progenitors, for the diversity of SNe Ia, and for explosion
models, in the context of the Chandrasekhar mass single degenerate scenario. It is also
suggested that progenitors of SNe Ia may be detectable sources of gravitational waves.

Chapter 5 We investigate the evolution of helium accreting CO white dwarfs with accre-
tion rates of $10^{-7} \ldots 10^{-6}$ $M_\odot$/yr, including the effects of rotation. An important role of
rotationally induced chemical mixing is identified, as it is shown to affect the stability of
the helium shell source as well as the resulting nucleosynthesis. We analyse the physical
conditions of the helium shell sources in rotating models, which are found more stable com-
pared to the corresponding non-rotating case, utilizing the stability criterion developed in
Chapt. 2.

Chapter 6 The role of rotation in the context of the sub-Chandrasekhar mass scenario
is explored. I.e., the evolution of helium white dwarfs with accretion rates of a few times
10^{-8} $M_\odot$/yr is investigated for both, rotating and non-rotating cases. Here we suggest that,
with rotation, helium detonation might be avoided altogether, and that binary systems con-
sisting of a CO white dwarf and a less massive helium star may be progenitors of recurrent
helium novae, rather than supernovae as believed before.

1.4.2   Results

Technical aspects

The numerical routines for the transport of angular momentum in the stellar evolution code
used in this study were originally developed in the context of massive stars (Heger et al.

2000). For the present study of accreting white dwarfs, several modifications such as the inclusion of the degenerate electron viscosity were necessary for properly describing transport processes in degenerate matter (Sect. 4.3.2). Frictional energy dissipation in differentially rotating layers, which is usually negligible in stars, was found to play a significant role in accreting white dwarfs (Chapt.4 and Chapt.6) and is also newly included (Sect. 4.3.2). Furthermore, we showed that, unlike in non-degenerate stars, the dynamical shear instability can be important in highly degenerate stars (Sect. 4.2). The linear way of solving the diffusion equation (Heger et al. 2000) cannot properly describe such a fast process, since the time steps in the stellar evolution code are determined on the basis of secular time scales. We improved this by treating the diffusive angular momentum transport as a non-linear process, as described in Appendix A. This new treatment enabled to identify the important role of the dynamical shear instability in highly degenerate white dwarf cores as discussed in Chapt. 4.

The nuclear network is updated to consider the $^{14}\mathrm{N}(e^-, \nu)^{14}\mathrm{C}(\alpha, \gamma)^{18}\mathrm{O}$ reaction, which becomes active when $\rho \gtrsim 10^6$ g cm^{-3} (Hashimoto et al. 1984), for which a data table by Gabriel Martinez (2002, private communication) is used for the $^{14}\mathrm{N}(e^-, \nu)^{14}\mathrm{C}$ reaction rate (see Sect. 6.2). The effect of orbital angular momentum loss via gravitational waves is also included to properly describe the evolution of the orbital separation of binary systems with short periods (Sect. 3.2).

Spin-up of accreting white dwarfs and angular momentum redistribution

In mass exchanging binary systems consisting of a CO white dwarf and a Roche lobe filling non-degenerate star, a centrifugally supported accretion disk (i.e., a Keplerian disk) is supposed to form around the white dwarf. The white dwarf is spun up as it accretes matter, and angular momentum is transported inside the white dwarf by rotationally induced hydrodynamic instabilities such as Eddington Sweet circulations, the dynamical and secular shear instability and the Goldreich–Schubert–Fricke (GSF) instability. It is shown that, if the accretion is fast enough (i.e., $\gtrsim 10^{-7}$ M$_\odot$/yr), turbulent diffusion of angular momentum can not lead the white dwarf to rotate rigidly during the accretion phase, even though the degenerate white dwarf core is susceptible to the dynamical shear instability (Sect. 4.2). This is due to the fact that, once the shear strength decreases below the threshold value for the onset of the dynamical shear instability, the subsequent redistribution of angular momentum by Eddington sweet circulations and degenerate electron viscosity — given that the secular shear and GSF instabilities are likely suppressed at high degeneracy (Sect. 4.2) — usually requires a larger time scale than the accretion time scale (Sect. 4.2 and 4.4).

SNe Ia progenitors in the context of the single degenerate Chandrasekhar mass scenario, where white dwarfs are assumed to grow to the Chandrasekhar limit by steady nuclear shell burning with $\dot{M} \simeq 10^{-7} \ldots 10^{-6}$ M$_\odot$/yr, are thus expected to rotate differentially during the accretion phase. In accord with previous results, our differentially rotating white dwarf models do not ignite carbon at the center even when they reach the canonical Chandrasekhar limit of 1.4 M$_\odot$. Efficient angular momentum loss is therefore required for such centrifugally supported super-Chandrasekhar mass white dwarfs to end in supernova explosions if

mass accretion ceases before reaching carbon ignition. The secular instability to the reaction of gravitational wave radiation of the bar mode or the r-mode is suggested to play an important role to determine the final fate of such rapidly rotating white dwarfs, since its growth timescale in our white dwarf models is found to be rather short ($\lesssim 10^7$ yr; Sect. 4.5).

An important consequence of our results is an expected diversity of exploding white dwarfs, as their mass may range from the canonical Chandrasekhar mass of 1.4 $M_\odot$ to the maximum achievable mass during the mass accretion phase, which is as high as $\sim 2.0\ M_\odot$ (Sect. 4.5 and 4.6). Since the spin rate at the moment of the white dwarf explosion may vary, the polarization strength in SNe Ia is expected to show a significant diversity (Sect. 4.6). Furthermore, we speculate how rotation can change the physics of the explosion itself (Sect. 4.7), and show that rapidly rotating SNe Ia progenitors may be detectable sources of gravitational waves (Sect. 4.8).

Stability and nucleosynthesis of thermonuclear shell sources

The conditions for stable thermonuclear fusion in helium shell sources of accreting white dwarfs are important for the so called single degenerate Chandrasekhar mass scenario (see Sect. 1.2.2), which assumes an efficient mass increase of white dwarfs by hydrogen or helium accretion. We developed a quantitative stability criterion to unravel the most important physical factors which determine the behavior of nuclear shell burning (Chapt. 2). The main result is that a shell source is more stable when it is thicker, hotter and less degenerate (Sect.2.4). This result allows a detailed understanding of the influence of rotation on helium shell burning in accreting white dwarfs (Chapt. 5). Interestingly, helium shell sources in accreting white dwarfs are found to be significantly stabilized if the spin-up by angular momentum accretion is considered, compared to the case where rotation is neglected (Sect. 5.4). This is because accreted helium is mixed deeply into the CO core due to rotationally induced hydrodynamic instabilities (Sect. 5.5), and because the centrifugal force lifts the degeneracy of the shell source (Sect. 5.6). I.e., rotation renders a wider, less degenerate and thus more stable shell source in an accreting white dwarf, compared to the corresponding non-rotating case. This result leads to the straightforward implication that rotation may increase the parameter range for white dwarfs to grow to the Chandrasekhar limit by mass accretion. Rotationally induced chemical mixing also affects the nucleosynthesis in the helium shell source in a significant way. Due to the active participation of alpha particles to the $^{12}\mathrm{C}(\alpha,\gamma)^{16}\mathrm{O}$ reaction in layers where accreted helium is significantly mixed with core material, the carbon–to–oxygen ratio is reduced in the accreted envelope compared to the non-rotating case (Sect. 5.5), which affects the energetics and spectra of SNe Ia,

Support for the single degenerate Chandrasekhar mass scenario

Although it is still a matter of debate whether an SN Ia explosion is induced by an off-center detonation in the degenerate helium envelope of a sub-Chandrasekhar mass CO white dwarf (sub-Chandrasekhar mass scenario), explosion models of Chandrasekhar mass white

dwarfs correspond much better to observed SNe Ia. Since the coalescence of double CO white dwarfs is likely to result in a neutron star rather than an SN Ia (see Sect. 1.2.2), the production of Chandrasekhar mass white dwarfs in close binary systems consisting of a CO white dwarf and a non-degenerate star is the currently favored scenario (i.e., single degenerate Chandrasekhar mass scenario). Our results add strong support to the single degenerate scenario for the following reasons.

Firstly, our self-consistent binary star evolution model in Chapt. 3 demonstrates for the first time that a Chandrasekhar mass white dwarf *can* be produced in a single degenerate binary system. Starting from a zero-age main sequence helium star of 1.6 $M_\odot$ and a CO white dwarf of 1.0 $M_\odot$ in a 0.124 day orbit, the evolution of this binary has been simulated until the center of the white dwarf ignites carbon when its mass reaches about 1.37 $M_\odot$. Therefore, this progenitor channel for SNe Ia has been convincingly identified as a reliable route for the production of Chandrasekhar mass white dwarfs. Furthermore, as discussed above, helium shell sources in accreting white dwarfs with accretion rates of $10^{-7} \ldots 10^{-6}$ $M_\odot$/yr are found more stable with rotation (Chapt. 5), which may significantly increase the probability for the production of Chandrasekhar mass white dwarfs in systems of the considered kind.

Secondly, helium detonation is found to be avoided in our white dwarf models which accrete helium with rates of a few times 10^{-8} $M_\odot$/yr when the effects of rotation are included. As the accretion induced spin-up in the white dwarf creates strong shear motions, energy is dissipated due to friction in the spun-up layers, and the helium envelope is heated up efficiently. Helium ignition is accordingly induced earlier than in the corresponding non-rotating case. For instance, with an initial CO white dwarf mass of 0.8 $M_\odot$, helium ignition starts after only about 0.02 $M_\odot$ of helium is accreted when the effects of rotation are considered, while about 10 times more helium (~ 0.2 $M_\odot$) needs to be accreted in the corresponding non-rotating case. Degeneracy at the helium ignition point in the rotating models is therefore too weak to produce a detonation, ruling out the sub-Chandrasekhar mass scenario for SNe Ia. This finding offers a plausible solution to the long-standing question why the peculiar type of supernovae predicted from the off-center detonation models have never been observed, despite their theoretically expected high birth rate of $\sim 10^{-3}$ yr^{-1} per galaxy.

Summary: The main conclusion of the present study is that the evolution of accreting white dwarfs is seriously affected by rotation if the spin-up effects by mass and angular momentum accretion is properly considered, which requires substantial adjustments to the current picture on SNe Ia progenitors.

1.4.3 Future plans

Our binary star evolution model producing a Chandrasekhar mass white dwarf in Chapt. 3 indicates that binary systems consisting of a helium giant with a CO core of $\gtrsim 0.5$ $M_\odot$ and a massive CO white dwarf ($\gtrsim 0.8$ $M_\odot$) are promising SNe Ia progenitors. The formation

of such systems requires initial main sequence star masses of $7 - 10 \ M_{\odot}$, which leads to evolutionary timescales of $\sim 10^8$ yr. The relevance of the considered channel is thus limited to SNe Ia from late type galaxies. An important question is which fraction of the observed SNe Ia in late type galaxies is produced by this channel. Different evolutionary paths from intermediate mass stars to helium giant + CO white dwarf binaries may be possible, as discussed by Iben & Tutukov (1994). Since they usually involve complicated processes such as mass exchange and common envelope evolution, an appropriate evaluation of the frequency of SNe Ia through helium giant + CO white dwarf channel demands a careful investigation through detailed binary star evolution models.

Our numerical simulations in Chapt. 4, 5 and 6 suggest that rotation might be a primary factor to critically affect the evolution and the final fate of accreting white dwarfs. One of the most intriguing predictions from our models is the formation of rapidly rotating super-Chandrasekhar mass ($\gtrsim 1.4 \ M_{\odot}$) white dwarfs. If the mass transfer from the companion ceases before carbon ignites, the explosion of the white dwarfs is expected to be delayed until they lose enough angular momentum through the secular instability. Therefore, the pre-explosion conditions in a super-Chandrasekhar mass white dwarf may be determined by the secular evolution induced by gravitational wave radiation, and its detailed investigation is important for identifying possible causes for the observed diversity in SNe Ia. For instance, for a larger time scale of angular momentum loss, the central temperature in a white dwarf will decrease more and carbon is expected to ignite at a higher density, which may have observable consequences. Another important question is whether a long delay of carbon ignition by 10^{10} yr will prevent an SN Ia or not. If such a slow angular momentum loss from a super-Chandrasekhar mass would still lead to a supernova explosion rather than to electron-capture induced collapse, it might be a plausible explanation for SNe Ia observed in elliptical galaxies, which require progenitor ages as high as a Hubble time. On the other hand, although the possibility of the detection of gravitational waves from SNe Ia progenitors is briefly discussed in Sect. 4.8, a quantitative understanding of the nature of gravitational waves due to the bar mode or the r-mode instability from differentially rotating white dwarfs should be better approached by means of multi-dimensional white dwarf models, given that the one dimensional approximation of the rotation physics adopted in our simulations might underestimate the effect of the centrifugal force in describing the white dwarf structure, especially in the outer layers which rotate at near the critical value.

Finally, as emphasized in the following chapters, the effects of magnetic fields are neglected in our simulations. Magnetic torques are known as an effective mechanism to transport angular momentum. I.e., even with initially weak seed fields, differential rotation can induce magnetic instabilities which may enhance the transport of angular momentum (Spruit 2002; Heger et al. 2003; Maeder & Meynet 2003). Thus, the effects of magnetic fields might have significance for the evolution of accreting white dwarfs and deserve a careful examination.

Chapter 2

On the stability of thermonuclear shell sources in stars

S.-C. Yoon, N. Langer and M. van der Sluys

Abstract   We present a quantitative criterion for the thermal stability of thermonuclear shell sources. We find the thermal stability of shell sources to depend on exactly three factors: they are more stable when they are geometrically thicker, less degenerate and hotter. This confirms and unifies previously obtained results in terms of the geometry, temperature and density of the shell source, by a simplified but quantitative approach to the physics of shell nuclear burning. We present instability diagrams in the temperature-density plane for hydrogen and helium shell burning, which allow a simple evaluation of the stability conditions of such shell sources in stellar models. The performance of our stability criterion is demonstrated in various numerical models: in a 3 $M_\odot$ AGB star, in helium accreting CO white dwarfs and in a helium white dwarf which is covered by a thin hydrogen envelope.

2.1   Introduction

Thermonuclear fusion is the main source of energy in stars. To use fusion as main energy supply over long time scales requires extreme stability, since the thermonuclear reaction rates are sensitive functions of the temperature. I.e., a slight temperature increase may enhance the nuclear burning rate drastically; if this results in an even higher temperature, a thermal runaway occurs. In most stars, such a runaway does not occur, since an increased energy output due to an enhancement of the nuclear burning rate leads to an overpressure and thus to an expansion of the burning region (Kippenhahn & Weigert 1990). However, two different circumstances have been shown to be able to prevent such a pressure increase.

The first one is electron degeneracy. If nuclear burning starts in a degenerate gas, the increased energy production will lead to a higher temperature. But as — for complete degeneracy — the pressure does not depend on the temperature, it remains constant. This situation is realized during the core helium flash in low mass stars, at carbon ignition in Chandrasekhar-mass CO white dwarf, i.e. in a Type Ia supernova explosion, and in strong nova shell flashes.

The second circumstance is a strong geometrical confinement of the burning region. As discovered by Schwarzshild & Härm (1965) and Weigert (1966), geometrically thin helium shell sources in red giants can become unstable. Since the local gravity in a thin shell source remains constant even when it expands in response to an increased energy production, hydrostatic equilibrium will enforce a constant pressure in the shell. The thin shell instability is prone to occur in nuclear shell sources around compact cores, as the small scale heights induced by the compactness of the core ensures the geometrical confinement of the shells. Examples are thermal pulses in asymptotic giant branch stars (e.g. Iben & Renzini 1983; Busso et al. 2001; Lugaro et al. 2003), hydrogen or helium shells on white dwarfs (e.g. Fujimoto 1982a, 1982b; Cassisi et al. 1998; Langer et al. 2002; Yoon et al. 2004), and X-ray bursts on neutron stars (e.g. Fujimoto et al. 1981; Taam & Woosley 1996).

In principle, both destabilizing circumstances may occur together. In central burning regions, however, the degeneracy aspect dominates, as gravity and thus pressure will not be constant in an expanding core. In nuclear shell sources, degeneracy and geometrical confinement may simultaneously contribute to the instability of shell sources. Among various authors investigating the stability of nuclear shell sources (e.g. Giannone & Weigert 1967; Unno 1970; Dennis 1971; Härm & Schwarzshild 1972; Stothers & Chin 1972; Sackmann 1977), Kippenhahn & Weigert (1990) developed a semi-quantitative understanding of the relevance of both destabilizing factors.

The purpose of this paper is to develop the insight into the shell stability mechanism further such that a quantitative tool is obtained, which allows to assess the thermal stability of shell sources in numerical stellar models. This will allow for a physical interpretation of fluctuating nuclear shell sources found in non-linear time-dependent stellar evolution calculations. As described in Section 2, we essentially follow the method by Giannone & Weigert (1967), but assume homology in the region of the shell source as in Kippenhahn & Weigert (1990). In Section 3, we derive thermodynamic parameters for partial degenerate

conditions, which we use in Section 4 to formulate and investigate the stability criterion in idealized situations. In Section 5, we apply the criterion to various numerical stellar models, and give a summary and discussion of our results in Section 6.

2.2 Secular behavior of shell burning

2.2.1 Gravothermal specific heat

Let us consider a shell source with a geometrical thickness D. The mass of the shell source is given as $\Delta M_{\mathrm{s}} = \int_{r_0}^{r_{\mathrm{s}}} 4\pi r^2 \rho dr$, where r_0 is the radius of the bottom of the shell source and $r_{\mathrm{s}} = r_0 + D$, its upper boundary. Assuming r_0 is constant, the relation between density and radius perturbation is given from $d\Delta M_{\mathrm{s}} = 0$ as

$$\frac{\delta \rho}{\rho} = -\frac{3}{3D/r_{\mathrm{s}} - 3(D/r_{\mathrm{s}})^2 + (D/r_{\mathrm{s}})^3} \frac{\delta r_{\mathrm{s}}}{r_{\mathrm{s}}}$$

(Huang & Yu 1998). If we assume that the matter in the shell source expands or contracts homologously, we have $\delta P/P = -4\delta r/r$ from the hydrostatic equation and we obtain:

$$\frac{\delta P}{P} = \alpha_{\mathrm{s}} \frac{\delta \rho}{\rho} \tag{2.1}$$

where

$$\alpha_{\mathrm{s}} = \frac{4}{3} \left(3D/r_{\mathrm{s}} - 3(D/r_{\mathrm{s}})^2 + (D/r_{\mathrm{s}})^3 \right). \tag{2.2}$$

Kippenhahn & Weigert's value α_{s}=4D/r_{s} is restored when $D/r_{\mathrm{s}} \ll 1$, while it becomes 4/3 with D/r_{s}=1, which is the case when the whole star contracts or expands homologously.

Using the thermodynamic relation $\delta \rho/\rho = \alpha_P \delta P/P + \alpha_T \delta T/T$, it follows from Eq. 2.2 that

$$\frac{\delta P}{P} = \frac{\alpha_{\mathrm{s}} \alpha_T}{\alpha_{\mathrm{s}} \alpha_P - 1} \frac{\delta T}{T}, \quad \frac{\delta \rho}{\rho} = \frac{\alpha_T}{\alpha_{\mathrm{s}} \alpha_P - 1} \frac{\delta T}{T} \tag{2.3}$$

where $\alpha_P = (\partial \ln \rho/\partial \ln P)_T$ and $\alpha_T = -(\partial \ln \rho/\partial \ln T)_P$ (Kippenhahn & Weigert 1990). As we will see in the next section, α_T and α_P are functions of the degree of degeneracy and are not constant over a shell source. However, since we are interested in the mean properties of a shell source in this study, we will assume that like the density and the pressure perturbation, the temperature change is also homologous in the shell, and mean values over the shell source will be used for α_P and α_T.

The heat perturbation in the shell source can be obtained from the first law of the thermodynamics as shown by Kippenhahn & Weigert (1990):

$$\delta q = c^* \delta T \tag{2.4}$$

with

$$c^* := c_{\mathrm{P}} \left(1 - \nabla_{\mathrm{ad}} \frac{\alpha_{\mathrm{s}} \alpha_T}{\alpha_{\mathrm{s}} \alpha_P - 1} \right), \tag{2.5}$$

where c_P denotes the specific heat at constant pressure and $\nabla_{\text{ad}} = (d\ln P/d\ln T)_{\text{ad}}$.

The quantity c^* is called the gravothermal specific heat (Kippenhahn & Weigert 1990). When the heat δq is added to the shell source, more energy than δq is consumed by the expansion work if $c^* < 0$, thereby decreasing the internal energy. However, if $c^* > 0$, the additional energy heats up the matter and thus favors instability.

2.2.2 The stability criterion

The gravothermal specific heat alone does not describe the thermal reaction of a shell source, as it is also influenced by its thermal interaction with its surroundings. The energy conservation in a star is expressed by the following equation:

$$\frac{\partial L_r}{\partial M_r} = \epsilon_{\text{N}} - \frac{dq}{dt}. \tag{2.6}$$

For a shell source with the thickness $D = r_{\text{s}} - r_0$ and the mass ΔM_{s}, integration over the burning shell gives

$$L_{r_{\text{s}}} - L_{r_0} = L_{\text{N}} - L_{\text{g}}. \tag{2.7}$$

$L_{r_{\text{s}}}$ and L_{r_0} are the luminosities at $r = r_{\text{s}}$ and $r = r_0$, respectively. L_{N} is the luminosity due to the nuclear burning in the shell: $L_{\text{N}} = \int_{\Delta M_{\text{s}}} \epsilon_{\text{N}} dM_r$ where ϵ_{N} is the nuclear energy generation rate in the shell source. L_{g} is defined as $\int_{\Delta M_{\text{s}}} \frac{dq}{dt} dM_r$. In AGB stars or accreting white dwarfs the main contribution to L_{g} is due to the gravitational energy release by contraction. This term is not significant compared to L_{N} in general, and we will assume that the shell source is initially in a stationary state (i.e., $dq/dt = 0$).

Perturbing Eq. 2.7 yields

$$\delta L_{r_s} = \Delta M_{\text{s}} \delta \epsilon_{\text{N}} - \Delta M_{\text{s}} \frac{d\delta q}{dt} \tag{2.8}$$

where $L_{r_0} \ll L_{r_s}$ has been assumed. With the use of equations 2.1-2.5 and with assuming radiative heat transfer, i.e.,

$$\frac{\partial T}{\partial M_r} = -\frac{3}{64\pi^2 ac} \frac{\kappa L_r}{r^4 T^3},$$

gives the following equation for the temperature perturbation $\theta = \delta T/T$:

$$\tau_{\text{th}} \dot{\theta} = \sigma \theta, \tag{2.9}$$

with

$$\tau_{\text{th}} = \frac{\Delta M_{\text{s}} T c_P}{L_{r_s}}, \tag{2.10}$$

and

$$\sigma = \frac{\nu - 4 + \kappa_{\text{T}} + \dfrac{\alpha_T}{\alpha_{\text{s}} \alpha_P - 1}(\lambda + \alpha_{\text{s}} + \kappa_\rho)}{c^*/c_p}. \tag{2.11}$$

Here, $\kappa_{\mathrm{T}} = (\partial \ln \kappa / \partial \ln T)_\rho$, $\kappa_{\mathrm{P}} = (\partial \ln \kappa / \partial \ln \rho)_T$, $\nu = (\partial \ln \epsilon / \partial \ln T)_\rho$, and $\lambda = (\partial \ln \epsilon / \partial \ln \rho)_T$. The quantity τ_{th} defined in Eq. 2.10 corresponds to the thermal time scale of the shell source. Note that Eq. 2.9 is essentially the same as the equation (16) in Giannone & Weigert (1967), for the case that the assumption of homology in the shell source is adopted in their analysis.

When $\sigma > 0$ the shell source becomes thermally unstable and the perturbation growth time scale becomes

$$\tau_{\mathrm{growth}} = \tau_{\mathrm{th}}/\sigma. \tag{2.12}$$

The larger the value of σ, the more rapidly the thermal instability grows. If $\sigma < 0$, nuclear burning in a shell source is thermally stable, and, upon a temperature increase, the temperature drops faster for larger σ. Therefore, σ can serve as a measure of the susceptibility of a shell source to thermal instability.

For the following discussions, let us define the numerator in Eq. 2.11 as σ_{E} such that $\sigma = \sigma_{\mathrm{E}}/(c^*/c_P)$ and

$$\sigma_{\mathrm{E}} = \nu - 4 + \kappa_{\mathrm{T}} + \frac{\alpha_T}{\alpha_{\mathrm{s}}\alpha_P - 1}(\lambda + \alpha_{\mathrm{s}} + \kappa_\rho). \tag{2.13}$$

The first 3 terms in Eq. 2.13 are related to the temperature perturbation and the remaining terms to the density perturbation.

For a given c^*, i.e. a given equation of state, the stability of a shell source is determined by the sign of σ_{E}. Physically, $\sigma_{\mathrm{E}} > 0$ means that that the additional energy production in response to a positive temperature perturbation exceeds the additional energy loss by radiation. In other words, for $\delta T > 0$, we have $\delta q > 0$ if $\sigma_{\mathrm{E}} > 0$, in which case a shell source is stable if $c^* < 0$, since the additional heat is consumed mostly for the expansion work of the shell source as discussed in section 2.2.1. If $\sigma_{\mathrm{E}} < 0$, the additional energy loss by radiation is larger than the additional energy production (i.e., $\delta q < 0$) in response to $\delta T > 0$. If $c^* < 0$ and $\sigma_{\mathrm{E}} < 0$, this results in further increase in the temperature perturbation since the net energy loss is compensated by the contraction of the system, increasing the internal energy of the shell source. However, this instability mode has little relevance as in stars σ_{E} hardly becomes negative if $c^* < 0$, as we will see in Sect. 2.3.1. If $c^* > 0$ and $\sigma_{\mathrm{E}} < 0$, the net energy loss results in the decrease in temperature and stable burning is established.

In the following sections, we will investigate the possible modes of stability/instability of a shell source in a more quantitative way.

2.3 Physical conditions for stability/instability

In order to discuss the stability of shell source in realistic stars, it is necessary to understand the behaviour of the thermodynamic quantities such as α_P, α_T and c^* in various equation-of-state regimes.

For non-relativistic partially degenerate conditions, electron density and pressure are given by

$$n_{\mathrm{e}} = \frac{\rho}{\mu_{\mathrm{e}} m_{\mathrm{H}}} = \frac{4\pi}{h^3}(2m_{\mathrm{e}}kT)^{3/2}F_{1/2}(\eta) \tag{2.14}$$

and

$$P_{\mathrm{e}} = \frac{\rho kT}{\mu_{\mathrm{e}} m_{\mathrm{H}}}\frac{2F_{3/2}(\eta)}{3F_{1/2}(\eta)} \tag{2.15}$$

where $F_{3/2}$ and $F_{1/2}$ are the Fermi-Dirac functions and $\eta := \psi/kT$ is the degeneracy parameter (e.g. Clayton 1968). The equation of state is thus given as:

$$P = P_{\mathrm{g}} + P_{\mathrm{r}} = \frac{\rho kT}{\mu_{\mathrm{I}} m_{\mathrm{H}}} + \frac{\rho kT}{\mu_{\mathrm{e}} m_{\mathrm{H}}}\frac{2F_{3/2}(\eta)}{3F_{1/2}(\eta)} + \frac{1}{3}aT^4. \tag{2.16}$$

With the definition of $\beta := P_{\mathrm{g}}/P$, the above equation can be rewritten as

$$F(\eta) + \frac{\mu_{\mathrm{e}}}{\mu_{\mathrm{I}}} = \frac{\mu_{\mathrm{e}} m_{\mathrm{H}} \beta P}{\rho kT}, \tag{2.17}$$

where $F := 2F_{3/2}/3F_{1/2}$. Differentiating this equation, we get

$$\frac{F}{F + \mu_{\mathrm{e}}/\mu_{\mathrm{I}}}d\ln F = \frac{1}{\beta}d\ln P - \frac{4 - 3\beta}{\beta}d\ln T - d\ln\rho \tag{2.18}$$

where $(\partial\ln\beta/\partial\ln P)_T = (1-\beta)/\beta$ and $(\partial\ln\beta/\partial\ln T)_P = 4(\beta-1)/\beta$ were used. From Eq. 2.18 and by differentiating Eq. 2.14, we can obtain α_P and α_T as function of η:

$$\alpha_P = \frac{\dfrac{1}{\beta}\dfrac{d\ln F_{1/2}}{d\eta}}{\dfrac{d\ln F_{1/2}}{d\eta} + \dfrac{F}{F + \mu_{\mathrm{e}}/\mu_{\mathrm{I}}}\dfrac{d\ln F}{d\eta}} \tag{2.19}$$

and

$$\alpha_T = \frac{\dfrac{4 - 3\beta}{\beta}\dfrac{d\ln F_{1/2}}{d\eta} - \dfrac{3}{2}\dfrac{F}{F + \mu_{\mathrm{e}}/\mu_{\mathrm{I}}}\dfrac{d\ln F}{d\eta}}{\dfrac{d\ln F_{1/2}}{d\eta} + \dfrac{F}{F + \mu_{\mathrm{e}}/\mu_{\mathrm{I}}}\dfrac{d\ln F}{d\eta}}. \tag{2.20}$$

When $\beta = 1$, we get $\alpha_P = \alpha_T = 1$ for an ideal gas ($\eta \to -\infty$, Fig. 2.1), and $\alpha_P = 0.6$ and $\alpha_T = 0$ for complete degeneracy ($\eta \to \infty$).

The specific heat at constant pressure is given by $c_{\mathrm{P}} = \left(\frac{\partial u}{\partial T}\right)_P - \frac{P}{\rho^2}\left(\frac{\partial\rho}{\partial T}\right)_P$ (Kippenhahn & Weigert 1990). From $u = \left(\frac{3}{2}P_{\mathrm{g}} + 3P_{\mathrm{r}}\right)/\rho = (3 - \frac{3}{2}\beta)P/\rho$, we have

$$c_{\mathrm{P}} = \frac{P}{\rho T}\left[\left(\frac{5}{2} + \frac{3}{2}(1 - \beta)\right)\alpha_T + 6(1 - \beta)\right] \tag{2.21}$$
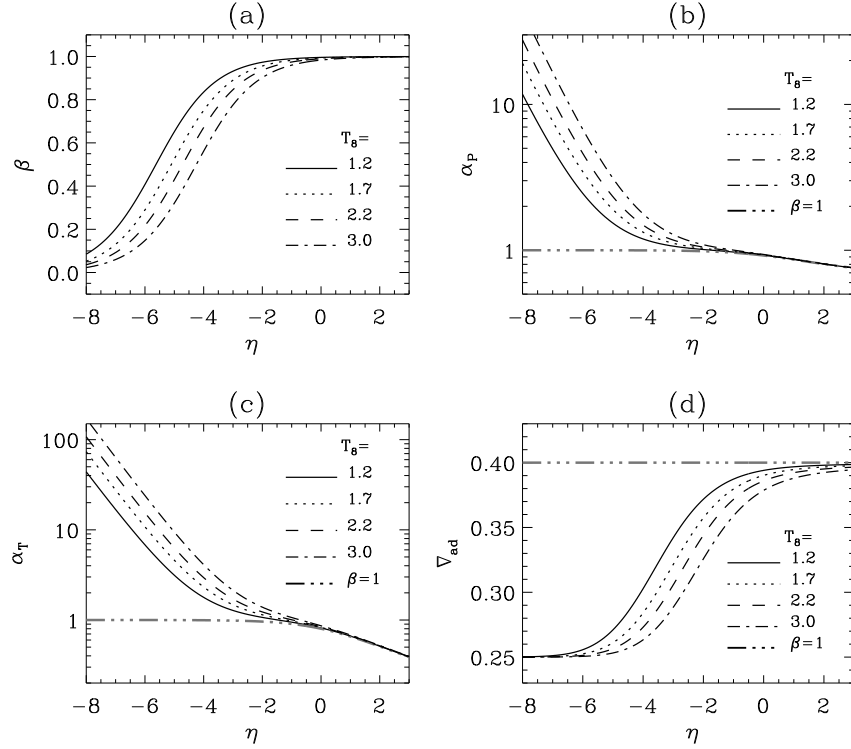
Figure 2.1: Thermodynamic quantities as function of the degeneracy parameter η for 4 different temperatures as indicated. Here, T_8 denotes temperature in unit of 10^8K. As a reference, the case of $\beta = 1$ is also shown for α_P, α_T and $\nabla_{\rm ad}$. (a) - Ratio of gas pressure to total pressure, β, as function of the degeneracy parameter. (b), (c) - $\alpha_P (:= (\partial \ln \rho / \partial \ln P)_T)$ and $\alpha_T [:= (\partial \ln \rho / \partial \ln T)_P]$ calculated from Eq. 2.18 and 2.19 using β given in (a). (d) - $\nabla_{\rm ad} [:= (\partial \ln P / \partial \ln T)_{\rm ad}]$ calculated from Eq. 2.20 using β and α_T given in (a) and (c) respectively.

and

$$\nabla_{\rm ad} = \frac{P \alpha_T}{\rho T c_{\rm P}} = \frac{\alpha_T}{\left(\frac{5}{2} + \frac{3}{2}(1 - \beta)\right) \alpha_T + 6(1 - \beta)}. \tag{2.22}$$

Since $P/\rho T$ in Eq. 2.21 can also be given as function of η from Eq. 2.17, the gravothermal specific heat c^* can be obtained as function of η for a specified β.

The value of β can be obtained as function of η at a given temperature from the equation of state. In Fig. 2.1a, we show β as function of η for 4 different temperatures which may be relevant to the helium shell burning. Here, $\mu_{\rm e} = 2$ and $\mu_{\rm e}/\mu_{\rm I} = 0.38$ have been assumed. In this temperature range, β reaches 1 when $\eta \gtrsim 0$ since the gas pressure becomes dominant.

Figure 2.2: Lines of vanishing gravothermal specific heat c^* in the plane spanned by the degeneracy parameter η and the relative thickness of the shell source D/r_s, for four different temperatures. These lines are computed by using the thermodynamic quantities given in Fig. 2.1. The line labeled $\beta = 1$ shows the case where radiation pressure is neglected.

As discussed in Sections 2.3.1—2.4, the values of α_T and α_P and the sign of c^* affect the stability of a shell source critically. Fig. 2.1b and 2.1c show α_P and α_T as function of η, obtained using the values of β given in Fig. 2.1a. The case when the radiation pressure is neglected (i.e., $\beta = 1$) is also shown in these figures. Since changes in the total pressure become more sensitive to changes in temperature than in density as radiation pressure becomes significant, we find larger values of α_P and α_T when radiation pressure is considered than in the case of $\beta = 1$. Since ∇_{ad} varies little compared to α_P and α_T, the sign of c^* is mainly determined by the sign of $\alpha_s \alpha_P - 1$ (see Eq. 2.5).

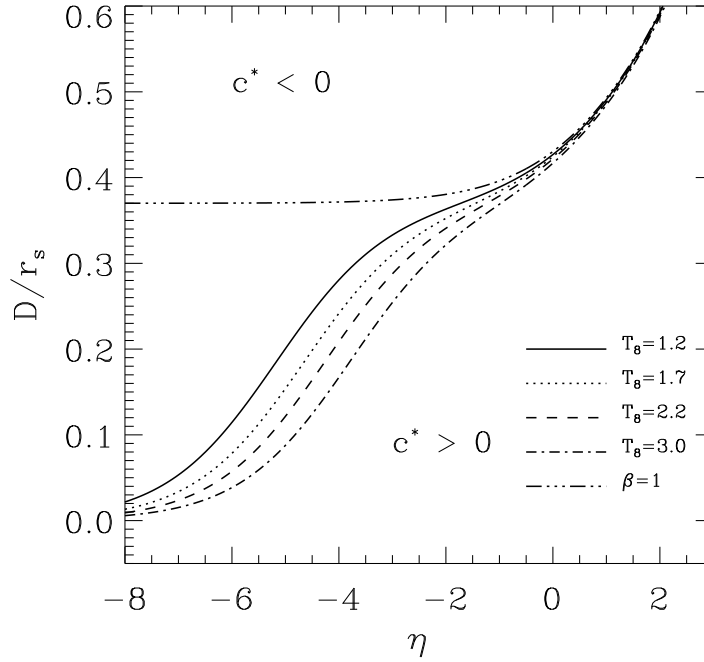Figure 2.2 shows the lines of zero gravothermal specific heat c^*, in the plane spanned by the degeneracy parameter η and the relative thickness of the shell source D/r_s, for 4 different temperatures. These lines have been determined using the values of β, α_T, α_P and ∇_{ad} given in Fig. 2.1. For $\beta = 1$, the thickness of the shell source should be larger
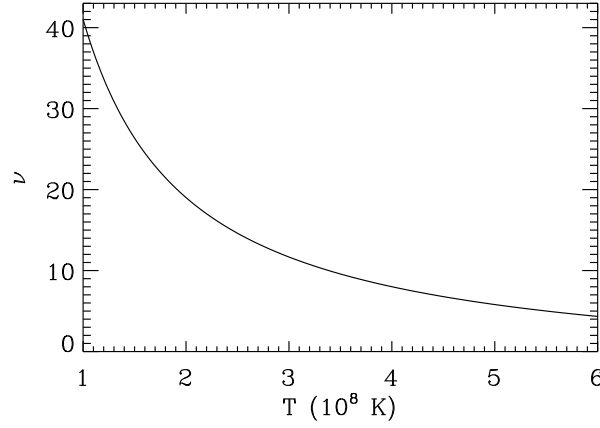
Figure 2.3: The logarithmic derivative of the 3α reaction with respect to temperature: $\nu = (\partial \ln \epsilon_{3\alpha} / \partial \ln T)_\rho$. The reaction rate given by Harris et al. (1983) has been used in the calculation.

than $0.37 r_{\rm s}$ for the gravothermal specific heat to be negative in the non-degenerate region ($\eta \lesssim -2$). As the electron degeneracy becomes more significant, the minimum thickness which gives $c^* < 0$ becomes larger.

In the non-degenerate region, c^* remains negative for much smaller shell thicknesses when the effect of the radiation pressure is considered. This is due to the fact that α_P and α_T become large when radiation pressure is significant. Since shell sources are generally stable when $c^* < 0$ as discussed in Sect. 2.3.1, this indicates that radiation pressure serves as a stabilizing factor for a shell source. The stabilizing effect of radiation pressure, which has already been discussed by many authors (e.g. Dennis 1971; Stothers & Chin 1972; Sackmann 1977), is due to the fact that a small increase in temperature induces considerable expansion of the shell source when radiation pressure is significant (cf. Eq. 2.3).

2.3.1 The case of $c^* < 0$

When $c^* < 0$, the following two conditions are fulfilled from Eq. 2.5:

$$\alpha_{\rm s} \alpha_P - 1 > 0 \quad \text{and} \quad \alpha_{\rm s} \alpha_P - 1 < \nabla_{\rm ad} \alpha_{\rm s} \alpha_T$$

With these conditions, the term $\alpha_T / (\alpha_{\rm s} \alpha_P - 1)$ in Eq. 2.13 is always positive, and it is generally $\sigma_{\rm E} > 0$ since ν dominates over κ_T and κ_ρ in most cases.

For example, let us consider a helium shell source powered by the 3α-reaction. Figure 2.3 shows ν as function of temperature, calculated from the 3α reaction rate given by Harris et al. (1983). The density dependence λ is equal to 2 regardless of temperature. In
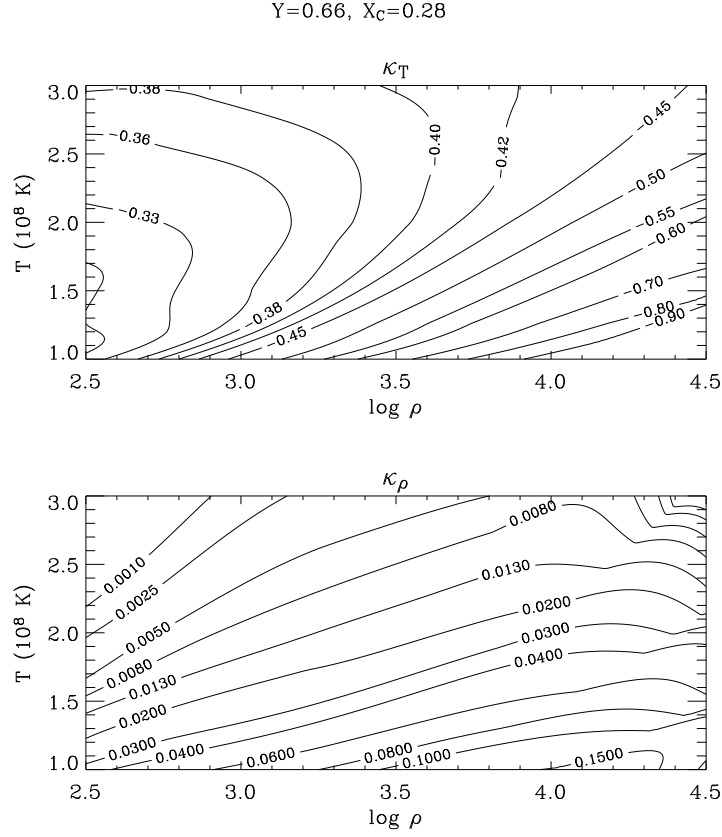
Figure 2.4: The logarithmic derivatives of the opacity with respect to to temperature and density: $\kappa_T = (\partial \ln \kappa / \partial \ln T)_\rho$ and $\kappa_\rho = (\partial \ln \kappa / \partial \ln \rho)_T$. The OPAL opacity table by Igelsias & Rogers (1996) has been used in the calculation. $Y = 0.66$, $X_C = 0.28$ and $Z = 0.02$ have been assumed.

AGB stars or in accreting white dwarfs, the temperature of the helium shell source varies according to the core mass or the accretion rate within the range $1 < T/10^8 \ K < 3$, giving $\nu = 40 \cdots 12$. Figure 2.4 shows the contour levels of κ_T and κ_ρ in the $T - \rho$ plane, calculated from the OPAL opacity table by Iglesias & Rogers (1996). The helium abundance has been assumed to be 0.66 in this calculation since the energy generation reaches its maximum around this value in a helium shell source. This figure shows that $\kappa_T > -1$ and $\kappa_\rho \ll 1$ in the given temperature and density range. Therefore, $\sigma_E > 0$ is guaranteed as long as $\alpha_T/(\alpha_s \alpha_P - 1) > 0$. The situation is very similar even in hydrogen shell sources if

they are powered by the CNO cycle. In conclusion, the shell source is generally stable (i.e., $\sigma < 0$) under the condition $c^* < 0$, i.e. for negative gravothermal specific heat.

2.3.2 The case of $c^* > 0$

For $c^* > 0$, we have

$$\alpha_s \alpha_P - 1 < 0 \quad \text{or} \quad \alpha_s \alpha_P - 1 > \nabla_{\mathrm{ad}} \alpha_s \alpha_{\mathrm{T}}.$$

With the second condition, we have usually $\sigma_{\mathrm{E}} > 0$, for the same reason discussed in Sect 2.3.1 Then, the shell source is unstable when $a_s a_P - 1 > \nabla_{\mathrm{ad}} a_s a_T$.

When the first condition is fulfilled, we have $\alpha_T/(\alpha_s \alpha_P - 1) < 0$. In general, a shell source is prone to thermal instability when $\alpha_T/(\alpha_s \alpha_P - 1) < 0$ since any density decrease due to expansion will lead to a further temperature increase (Eq. 2.3). However, if the absolute value of $\alpha_T/(\alpha_s \alpha_P - 1)$ is large enough, a small increase in temperature induces such a large decrease in density that the nuclear energy generation may be considerably reduced. In this case, we have $\sigma_{\mathrm{E}} < 0$ and the shell is thermally stable.

This can be realized when α_T becomes very large or/and when $|\alpha_s \alpha_P - 1| \ll 1$. A large α_T can be obtained if radiation pressure becomes substantial (Fig. 2.1c), showing again its stabilizing effect. When $|\alpha_s \alpha_P - 1| \ll 1$ is satisfied, we have $\delta\rho/\rho = \frac{1}{\alpha_s}\delta P/P \simeq \alpha_P \delta P/P$. This means that the shell source behaves as if it were isothermal when $\alpha_s \alpha_P \simeq 1$. As a consequence, the influence of the temperature perturbation becomes negligible compared to that of the density perturbation, resulting in $\sigma_{\mathrm{E}} < 0$. For an ideal gas with $\beta = 1$, this condition means $\alpha_s \simeq 1$: the shell source is stable if its thickness D is not much less than $0.37 r_s$, even when $c^* > 0$ (see Fig. 2.5). This mode of stability has been already noted by Fujimoto (1982b): he found that a very large c^* can render a shell source stable, which is the case when $|a_s a_P - 1| \ll 1$ (Eq. 2.5). As shown in Sect. 2.5, this situation may occur in the helium shell sources of AGB stars and accreting white dwarfs.

2.3.3 Infinitely thin shell sources

If a shell source is infinitely thin, we have $\alpha_s \to 0$, $c^* \to c_P$ and

$$\sigma = \nu - 4 + \kappa_{\mathrm{T}} - \alpha_T(\lambda + \kappa_\rho). \tag{2.23}$$

The shell burning can be stable if the dependence of the nuclear reaction on temperature is weak or/and when radiation pressure is significant, in which case α_T becomes large (cf. Fig. 2.5). An astrophysical application for such a case is shell burning in accreting neutron stars, for which the compactness of the gravitating body enforces a constant pressure in the shell source, such that $\alpha_s \to 0$. In fact, the criterion for thermal instability in this case is very similar to that given by Fujimoto et al. (1981), who studied shell flashes on accreting neutron stars. Numerical calculations by Taam et al. (1996) show that the helium shell burning in a neutron star can be stable when the temperature of the helium shell source is as high as 5.6×10^8K, for which the temperature sensitivity of the 3α reaction is considerably
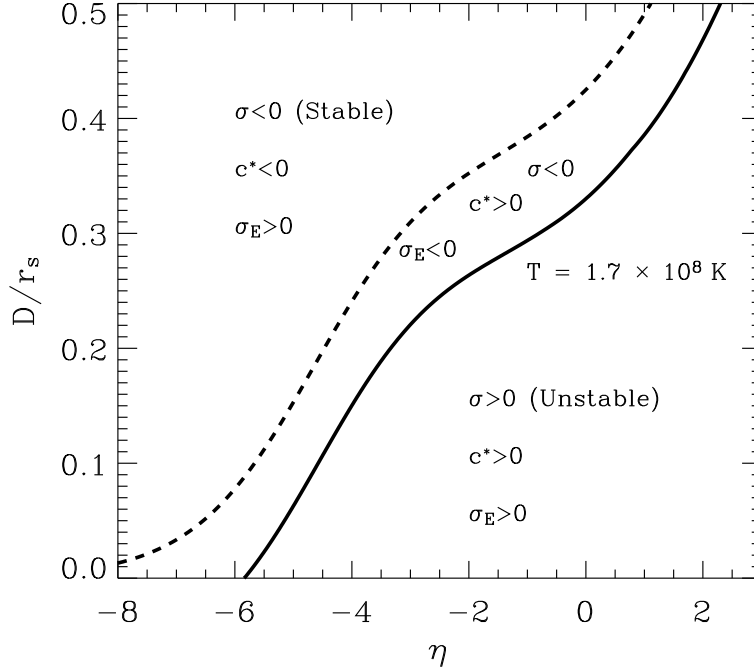
Figure 2.5: Loci of σ and c^* for their sign in $\eta - D/r_s$ plane when $T = 1.7 \times 10^8$K. The solid line separates the thermally unstable ($\sigma > 0$) from the stable ($\sigma < 0$) region, while the dashed line separates the region with negative c^* from that with positive c^*. The same chemical composition as in Fig. 2.4 is assumed.

weakened ($\nu \simeq 5$, Fig. 2.3). This can be easily understood by our stability criterion with Eq. 2.23 (see also Fig. 2.7 and discussions given in Sect. 2.4).

2.3.4   Complete degeneracy

In completely degenerate gas ($\eta \to \infty$), we have $\alpha_T = 0$ and σ becomes

$$\sigma = \nu - 4 + \kappa_T. \tag{2.24}$$

Since heat in a strongly degenerate gas is transfered mainly by electron conduction, with $\kappa_T \simeq 2$ (e.g. Kippenhahn & Weigert 1990), any nuclear reaction with $\nu > 2$ will give $\sigma > 0$, resulting in unstable nuclear burning. An example for the shell burning in strongly degenerate conditions is provided by the sub-Chandrasekhar mass progenitor model for Type Ia supernovae. In this model, helium ignites at the bottom of a helium layer of some tenth of solar mass accumulated on a CO white dwarf with low accretion rates (e.g. Woosley
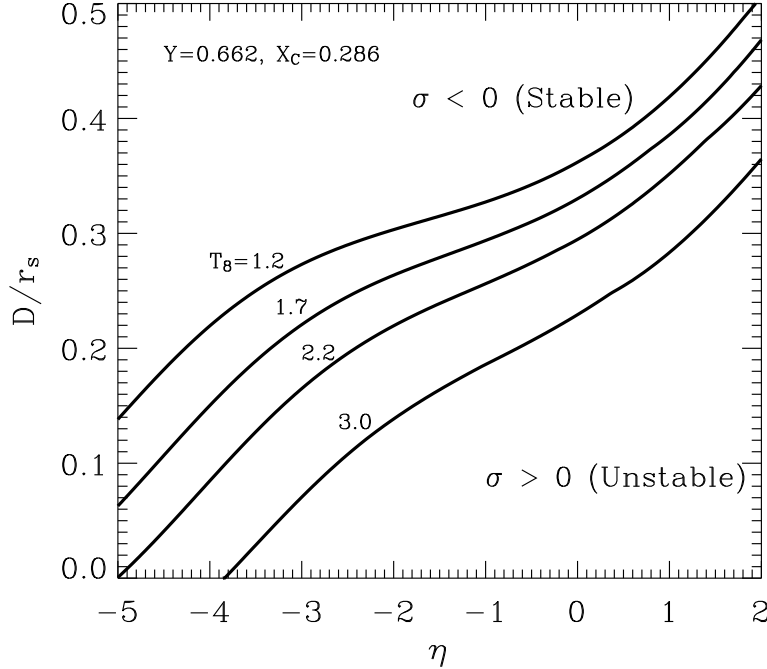
Figure 2.6: Loci for the sign of σ at 4 different temperatures: $T = 1.2, 1.7, 2.2$ and 3.0×10^8K in $\eta - D/r_s$ plane.

& Weaver 1994). At the ignition point, the helium envelope is highly degenerate ($\eta > 10$, e.g. Yoon & Langer 2004b), rendering complete degeneracy as a good approximation.

2.4   Instability diagrams

Figure 2.5 gives an example of the stability criterion for a He shell source in $\eta - D/r_s$ parameter space, using a specific chemical composition as indicated in the figure caption, which are typical for helium shell sources in AGB stars or in accreting white dwarfs.

   This figure shows the two modes of stability as discussed in sections 2.3.1 and 2.3.2: one with $c^* < 0$ & $\sigma_E > 0$ and the other with $c^* > 0$ & $\sigma_E < 0$. As expected, a shell source becomes more susceptible to thermal instability when it is thinner and more degenerate. For $\eta \gtrsim 2$, where the electron degeneracy is significant ($F(\eta) \gtrsim 1.5$), the shell source can not be stable even with $D/r_s > 0.5$, which is because a pressure change becomes less sensitive to a temperature change as the electrons become more degenerate. On the other hand, the shell source can be stable even with $D/r_s = 0$ when $\eta \lesssim -5.8$ (see also Fig. 2.7), where the radiation pressure is dominant over the gas pressure.
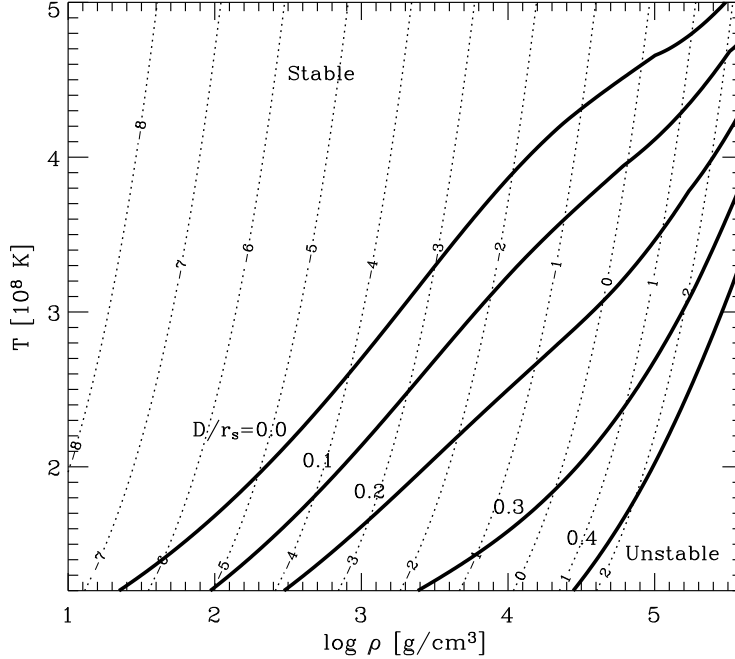
Figure 2.7: Stability conditions for a helium shell source in the density-temperature plane. The solid
line separates the thermally unstable ($\sigma > 0$, lower right part) from the stable ($\sigma < 0$) region, for 5
different relative shell source thicknesses (i.e., $D/r_s = 0.0$, 0.1, 0.2, 0.3 and 0.4). The dotted contour
lines denote the degeneracy parameter η. $X_{He} = 0.662, X_C = 0.286$ and $Z = 0.02$ have been
assumed.

As shown in Fig. 2.4, κ_T and κ_ρ remain to be small compared to ν in the given tem-
perature and density range. The quantities α_P and α_T do not depend strongly on μ_e/μ_I.
The main factor which determines the stability at given η and D/r_s is thus the temperature
of the shell source. Figure 2.6 shows that the stability criterion is more relaxed for higher
temperature. This is because the temperature dependence of the energy generation is weak-
ened (Fig. 2.3), and because radiation pressure becomes more significant at a given degree
of degeneracy as the temperature increases. This temperature dependence of the stability
of shell burning explains, why the accretion rates which allow steady burning solutions de-
pend on the mass of accreting white dwarf (e.g. Fujimoto 1982b; Nomoto & Kondo 1993;
Cassisi et al. 1998). I.e., higher accretion rates are required to have stable shell burning
for more massive white dwarfs, in which shell sources are thinner. This is mainly because
shell sources becomes hotter with higher accretion rates if the accreted matter is burned in
a steady way.

In Fig. 2.7, we show the stability conditions in the density-temperature plane for 5 dif-
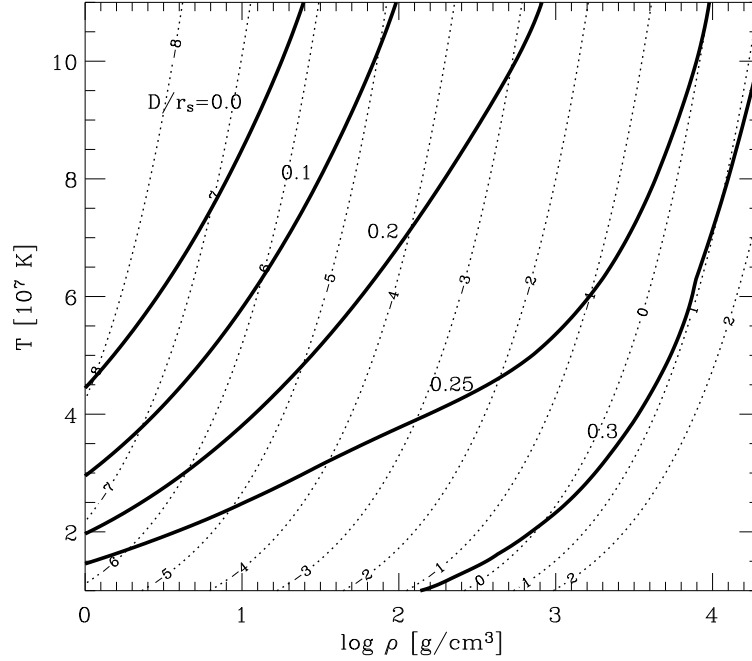
Figure 2.8: Stability conditions for hydrogen shell source powered by the CNO cycle, in density and temperature plane. The solid line separates the thermally unstable ($\sigma > 0$) from stable ($\sigma < 0$) region at 5 different relative thicknesses of shell source (i.e., $D/r_{\rm s} = 0.0$, 0.1, 0.2, 0.25 and 0.3). A shell source with each $D/r_{\rm s}$ is expected to be stable in the upper region of the each locus. The dotted contour lines denote the degeneracy parameter η. $X_{\rm H} = 0.502$, $X_{\rm He} = 0.478$ and $Z = 0.02$ have been assumed. Note that the hot CNO cycle is not considered in the calculation.

ferent relative shell source thicknesses. As discussed in Sect. 2.3.3, this figure shows that a shell source can be stable even when it is infinitely thin ($D/r_{\rm s} = 0$), if the temperature is high enough, since with high temperature the dependence of the energy generation on temperature becomes weakened and the role of radiation pressure becomes important, giving a large α_T. The stability conditions are relaxed as $D/r_{\rm s}$ increases. The conditions for stability in hydrogen shell source show a similar behaviour (Fig. 2.8), where the shell source is assumed to be powered by the CNO cycle. I.e., thinner, cooler and more degenerate shell sources are more prone to thermal instability. Note, however, that in the calculation, we did not consider the so called *hot CNO cycle*, which may be active at high temperatures ($T > 8 \times 10^7$ K).

2.5   Applications

In this section, we apply the stability criterion to various numerical stellar models: a 3 $M_\odot$ AGB star, helium accreting CO white dwarfs, and a cooling helium white dwarf with a thin hydrogen envelope. All models have been computed with a stellar evolution code (Langer 1998 and references therein) which solves the hydrodynamic form of the stellar structure equations (Kippenhahn & Weigert 1990). Opacities are taken from Iglesias & Rogers (1996). We define the thickness of a shell source D such that the energy generation rate at each boundary is 2×10^{-3} times its peak value. The mean values weighted by the energy generation rate over the shell source are used for density, temperature and chemical abundances to estimate physical quantities which appear in Eq. 2.11.

2.5.1   Helium shell burning on the AGB

It is well known that asymptotic giant branch (AGB) stars suffer thermally unstable helium shell burning in their advanced evolution (e.g. Iben & Renzini 1983). We investigate this phase by computing a 3 $M_\odot$ evolutionary model with $Z = 0.02$, starting at the zero age main sequence (Langer et al. 1999). After passing through hydrogen and helium core burning, the star enters the helium shell burning stage. Fig. 2.9a shows the nuclear luminosity due to helium burning as function of time at the onset of the thermal pulses ($T \simeq 4.306 \times 10^8$yrs). We analyzed those models indicated by a filled circle in Fig. 2.9a, in which the helium shell burning is still stable, and computed c^* and σ for each model. (Fig. 2.9b and Fig. 2.9c). During the stable shell burning stage, the mean temperature in the shell source is nearly constant at $T \simeq 1.4 \times 10^8$K (Fig. 2.9d). The shell source becomes thinner and more degenerate as the CO core mass increases as shown in Fig. 2.9e.

   The gravothermal specific heat of the shell source is positive in the chosen models, indicating that the shell burning is kept to be stable, until the onset of the thermal pulses by the second mode of the stability discussed in Sect. 2.3.2. However, it becomes smaller as the CO core mass increases, mainly because $\alpha_s \alpha_P - 1$ deviates from 1 more significantly as D/r_s decreases (see Eq. 2.5), and partly because degeneracy in the shell source becomes stronger (Fig. 2.9e). The thermal pulses start when the relative thickness of the shell source becomes as low as 0.316.

2.5.2   Helium shell burning in accreting white dwarfs

Here, we consider the helium shell source in hot helium accreting CO white dwarfs. Two different initial white dwarf models are considered: $M_{init} = 0.8\,M_\odot$ with $\log L_s = 2.948\,L_\odot$ and M_{init} $0.998\,M_\odot$ and $\log L_s = 3.379\,L_\odot$, where M_{init} and $\log L_s$ are the initial mass and surface luminosity, respectively. The accreted matter is assumed to be helium enriched such that $Y = 0.98$. We have performed simulations with 6 different combinations of initial mass and accretion rate (see Table 1). The helium shell burning is initially stable in each model sequence, and eventually turns unstable as the white dwarf mass increases (see Fig. 2.10 for an example). The value of σ for the shell source of the last analysed model in
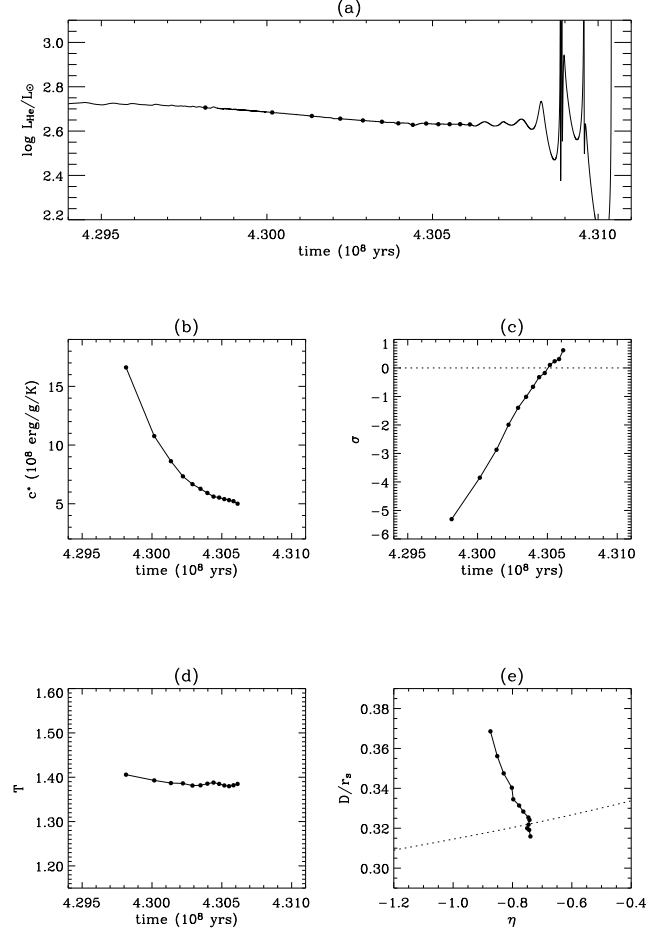
Figure 2.9: Evolution of the helium shell source in a $3M_\odot$ AGB star. (a) Nuclear luminosity due to helium burning as function of time, for shortly before and during the onset of thermal pulses. The mean values of c^*, σ, and temperature in the shell sources of the models marked by a filled circle are shown in (b), (c) and (d) respectively. (e) Evolution of the shell source in the $\eta - D/r_s$ plane. The dotted line corresponds to $\sigma = 0$ computed for the physical conditions in the shell source of the last analysed model.

each sequence is given in the last column of the table. In all sequences, the last analysed models, from which the thermal pulses grow significantly, have $|\sigma| \lesssim 0.6$, indicating that our stability criterion predicts the onset of the instability with good accuracy.

Table 2.1: Properties of the computed helium accreting white dwarf models. The first column denotes the model sequence number. The second column shows the initial mass and the third gives the accretion rate. The forth column gives the amount of accreted material until the onset of the helium shell instability. The value of σ estimated in the shell source of the last analysed model is given in the last column.

No.	M_{init} (M$_\odot$)	$\dot{M}$ (M$_\odot$/yr)	ΔM (M$_\odot$)	σ
No.1	0.800	$4.0 \cdot 10^{-7}$	0.0212	-0.429
No.2	0.800	$5.0 \cdot 10^{-7}$	0.0238	-0.291
No.3	0.800	$7.0 \cdot 10^{-7}$	0.1141	-0.598
No.4	0.800	$8.0 \cdot 10^{-7}$	0.1455	-0.471
No.5	0.998	$8.0 \cdot 10^{-7}$	0.0028	-0.114
No.6	0.998	$1.0 \cdot 10^{-6}$	0.0048	-0.035

As an example, results for sequence No.6 are shown in Fig. 2.10. In Fig. 2.10a, the nuclear luminosity due to helium burning is given as function of the total white dwarf mass, which serves as a linear measure of time. Thermal pulses are induced when the white dwarf mass reaches ~ 1.028 M$_\odot$. The evolution of c^* and σ shown in Fig. 2.10b and 2.10c is very similar to that in the AGB model discussed above. The mean temperature in the shell source is about 2×10^8 K (Fig. 2.10d). The shell source becomes thinner and more dense as the white dwarf mass increases (Fig. 2.10). The last analysed model is at the edge of stability as shown in Fig. 2.10c and the thermal pulses grow significantly from this point.

2.5.3   hydrogen shell burning in cooling helium white dwarfs

Here, we discuss a hydrogen shell flash in a cooling helium white dwarf model (cf., Driebe et al. 1999), which has been obtained by evolving a 2.4 M$_\odot$ zero age main sequence star with $Z = 0.02$ in a binary system with the initial orbital period of 1.76 days. Its companion was a 2 M$_\odot$ zero age main sequence star. It loses most of it hydrogen-rich envelope during the hydrogen shell burning stage through so-called case B mass transfer, ending in a helium white dwarf of $M = 0.324$ M$_\odot$ with a hydrogen envelope of $M \simeq 0.005$ M$_\odot$ when the mass transfer stops. The luminosity and surface temperature at this moment are $10^{2.2}$ L$_\odot$ and 1.4×10^4 K, respectively.

The hydrogen shell burning is weakened progressively as the white dwarf cools (Fig. 2.11a). At $t \simeq 5.905 \times 10^8$ yr, further weakening of the shell burning stops due to the increase in density. The hydrogen burning increases slowly as the helium core contracts further and ends in a strong flash at $t \simeq 5.98 \times 10^8$ yr. The thickness and degree of degeneracy of the shell source have been computed for the model marked by a filled circle in Fig. 2.11a, and positioned in $D/r_s - \eta$ plane in Fig. 2.11b. The shell source at this point is in the unstable regime as expected from the fact that the nuclear luminosity reaches its peak very soon thereafter. The contour levels for the perturbation growth timescale from Eq. 2.12 are
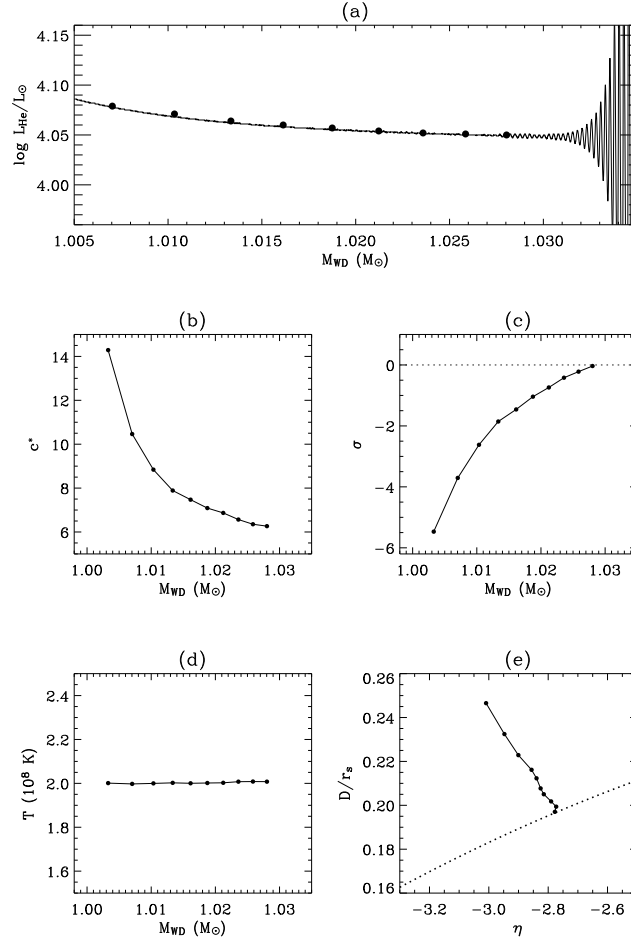
Figure 2.10: Evolution of the helium shell source in an accreting white dwarf with an initial mass of 0.998 $M_\odot$ and a constant accretion rate of 10^{-6} $M_\odot/yr$. (a) Nuclear luminosity due to helium burning as function of the total white dwarf mass. The mean values of c^*, σ, and temperature in the shell sources of the models marked by a filled circle are shown in (b), (c) and (d) respectively. (e) Evolution of the shell source in the $\eta - D/r_s$ plane. The dotted line corresponds to $\sigma = 0$ computed for the physical conditions in the shell source of the last analysed model.

also given in the same figure. The perturbation growth time estimated at the point is about 2.4×10^4yrs, which is in good agreement with the time interval from the marked model to the peak in L_H ($\simeq 3 \times 10^4$yrs).
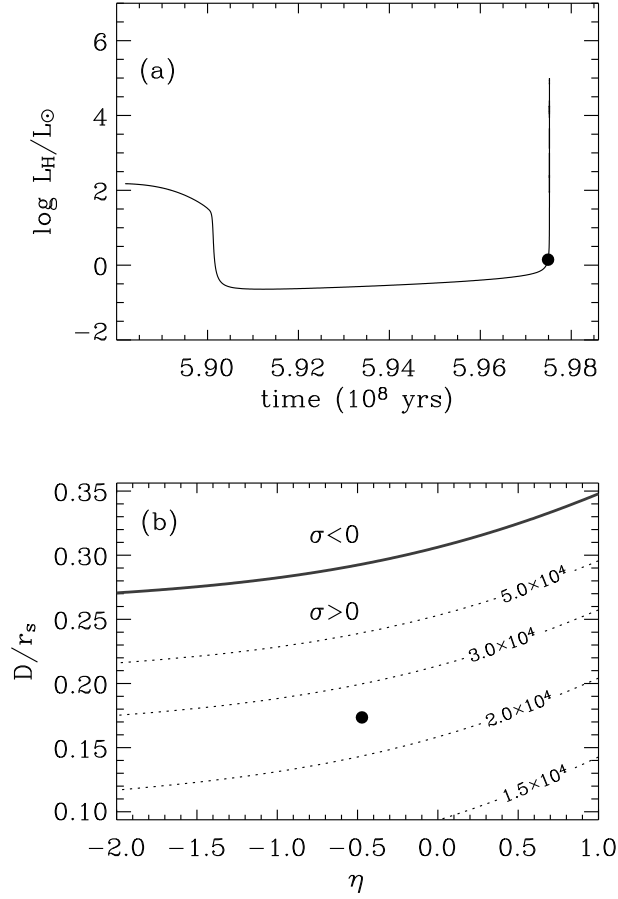
Figure 2.11: (a) Nuclear luminosity due to hydrogen burning at the onset of the hydrogen shell flash in the hydrogen envelope in a cooling helium white dwarf of $0.324 M_\odot$. (b) Contour levels of the perturbation growth time scale in the $\eta - D/r_s$ plane, obtained from Eq. 2.12. Here, σ and τ_{th} have been estimated for the physical conditions in the shell source of the marked model. The solid line corresponds to $\sigma = 0$.

2.6   Conclusion

We have developed a stability criterion for thermonuclear shell sources which can be easily applied to numerical stellar models in a quantitative way. The stabilizing/destabilizing factors have been identified unambiguously: a shell source is less prone to the thermal in-

stability when it is thicker, less degenerate and hotter (Sect. 2.3, Figs. 2.6, 2.7 and 2.8). If a shell source is sufficiently thick at a given degree of degeneracy, the gravothermal specific heat becomes negative and any excessive energy gain is consumed mostly for the expansion work, preventing thermal runaway. It is shown that the shell source can remain stable even with a positive gravothermal specific heat as long as temperature at a given degree of degeneracy is high enough such that the sensitivity of nuclear reactions to temperature is significantly weakened or/and that radiation pressure becomes substantial. In such a case, the energy loss rate by radiation begins to dominate over the additional nuclear energy production rate. Interestingly, this effect allows even an infinitely thin shell source to be thermally stable (Sect. 2.3.3, Fig. 2.7 and 2.8), which may have interesting consequences in accreting neutron stars (Sect. 2.3.3; cf. in 't Zand et al. 2003).

We have applied the stability criterion developed in this study to a 3 $M_\odot$ AGB star, to helium accreting CO white dwarfs and to a helium white dwarf with a thin hydrogen shell (Sect. 2.5). In spite of the simple approach of using homology assumption in the shell source and not relying on the full linear stability analysis, it is demonstrated that this criterion can predict the onset of thermal pulses or flashes with a reasonably good accuracy.

In conclusion, being simple and robust, our stability criterion may serve as a useful tool for analysing shell burning in various types of stars. One example can be found in Yoon et al. (2004), who discuss the effects of rotationally induced chemical mixing on the behaviour of helium shell burning in accreting white dwarfs.

Chapter 3

The first binary star evolution model producing a Chandrasekhar mass white dwarf

S.-C. Yoon and N. Langer

Abstract   Today, Type Ia supernovae are essential tools for cosmology, and recognized as major contributors to the chemical evolution of galaxies. The construction of detailed supernova progenitor models, however, was so far prevented by various physical and numerical difficulties in simulating binary systems with an accreting white dwarf component, e.g., unstable helium shell burning which may cause significant expansion and mass loss. Here, we present the first binary evolution calculation which models both stellar components and the binary interaction simultaneously, and where the white dwarf mass grows up to the Chandrasekhar limit by mass accretion. Our model starts with a 1.6 $M_\odot$ helium star and a 1.0 $M_\odot$ CO white dwarf in a 0.124 day orbit. Thermally unstable mass transfer starts when the CO core of the helium star reaches $0.53 M_\odot$, with mass transfer rates of $1 \ldots 8 \times 10^{-6}$ $M_\odot/\mathrm{yr}$. The white dwarf burns the accreted helium steadily until the white dwarf mass has reached ~ 1.3 $M_\odot$ and weak thermal pulses follow until carbon ignites in the center when the white dwarf reaches 1.37 $M_\odot$. Although the supernova production rate through this channel is not well known, and this channel can not be the only one as its progenitor life time is rather short ($\sim 10^7 - 10^8$ yr), our results indicate that helium star plus white dwarf systems form a reliable route for producing Type Ia supernovae.

3.1   Introduction

Type Ia supernovae (SNe Ia) are of particular importance in astrophysics: They are the major source for iron group elements in the universe and are thus an essential contributor to the chemical evolution of galaxies (e.g. Renzini 1999). And their light curve properties allow it to measure their distances with an excellent accuracy even out to redshifts beyond $z = 1$, which makes them a powerful tool to determine the cosmological parameters (e.g. Hamuy et al. 1996a; Branch 1998; Leibundgut 2000). In particular, the recent suggestion of a non-zero cosmological constant is in part based on SNe Ia data (Perlmutter et al. 1999a; Riess et al. 2000). An understanding of the progenitors of these supernovae is clearly required as a basis for these fundamental astrophysical phenomena.

However, even though there seems no doubt that SNe Ia are produced by the thermonu-clear explosion of a white dwarf, it is currently unclear in which kinds of binary systems such an event can occur (Livio 2001). Among the scenarios which have been put forward as possibilities, the so called single degenerate scenario is currently favored, where a CO white dwarf accretes mass from a non-degenerate companion and thereby grows up to the Chandrasekhar mass (e.g. Hillebrandt & Niemeyer 2000; Livio 2001). However, hydrogen as well as helium accretion rates which allow an increase of the CO white dwarf mass due to shell burning are limited to narrow ranges (e.g. Nomoto 1982a; Fujimoto 1982b; Iben & Tutukov 1989). While hydrogen and helium shell sources are prone to degeneracy effects and related thermonuclear instabilities (e.g., nova explosions) at low accretion rates, the helium shell source in accreting white dwarf models has been found to be thermally unstable even for cases where the electron degeneracy is negligible (e.g. Cassisi et al. 1998; Langer et al. 2002). This affects in particular the potentially most frequent SN Ia progenitor systems, where a hydrogen rich star (main sequence star or red giant) is considered as white dwarf companion (e.g. Li & van den Heuvel 1997; Hachisu et al. 1999; Langer et al. 2000). The hydrogen accretion rates in those systems which may allow steady hydrogen shell burning are about a few 10^{-7} M$_\odot$/yr. With these rates, the subsequent helium shell burning is usually found to be unstable (Iben & Tutukov 1989; Cassisi et al. 1998; Kato & Hachisu 1999), and no model sequences which cover the major part of the white dwarf accretion phase could be constructed so far.

In an effort towards overcoming this shortcoming, we consider here the evolution of close helium star plus CO white dwarf systems. In those, the white dwarf develops only a helium shell source, thus avoiding complications involved in double shell source models (e.g. Iben & Tutukov 1989). Such systems form a predicted binary evolution channel (Iben & Tutukov 1994), which is confirmed — even though for lower masses than considered here — by Maxted et al. (2000). Further evidence for the existence of close helium star plus CO white dwarf systems comes from the recent discovery of a helium nova (Ashok & Banerjee 2003; Kato & Hachisu 2003).

Simplified binary evolution considerations provided us with an estimate for the optimal initial parameters of our model system. As a result, we embarked on calculating the detailed evolution of a 1.6 M$_\odot$ helium star and a 1 M$_\odot$ CO white dwarf in a 0.124 d orbit. We

introduce our computational method and physical assumptions in Sect. 3.2. In Sect. 3.3, the evolution of the considered binary system is presented. We discuss our results in Sect. 3.4.

3.2 Numerical method and physical assumptions

The numerical model has been computed with a binary stellar evolution code which computes the evolution of two binary components, and the evolution of the mass transfer rate and of the orbital separation simultaneously through an implicit coupling scheme (Braun 1997). We use Eggleton's (1983) approximation for the Roche lobe radius. Mass loss from the Roche lobe filling star through the first Lagrangian point is computed according to Ritter (1988). The orbital change due to stellar wind and mass transfer is followed according to Podsiadlowski et al. (1992). The specific angular momentum carried away by the stellar wind is computed following Brookshaw & Tavani (1993). Orbital angular momentum loss due to the gravitational wave radiation is also taken into account. Opacities are taken from Iglesias & Rogers (1996). Mass loss due to a stellar wind is considered as $\dot{M} = 10^{-2}RL/[GM(1-\Gamma)]$, with Γ being the ratio of photospheric to Eddington luminosity. This mass loss rate is based on dimensional arguments and normalized for Wolf-Rayet stars (Langer 1989). However, the particular choice of the stellar wind mass loss formula does not affect our final results significantly, given that the value of the mass loss rate is largely determined by Γ, as the luminosity of the white dwarf during the mass accretion phase is close to the Eddington limit. Effects of rotation are not considered here (cf. Langer et al. 2002, Yoon et al. 2004). For more details about the code, see Wellstein & Langer (1999) and Wellstein et al (2001).

We start with a zero age main sequence helium star of 1.6 $M_\odot$ and a 1.0 $M_\odot$ white dwarf, in 0.124 day orbit. The metallicity of the helium star is set to 0.02. In order to avoid the numerical difficulty in following the initial strong helium shell flash in the white dwarf which might be induced soon after the onset of mass accretion, the white dwarf is approximated by a point mass until the mass transfer rate from the helium star reaches about 10^{-6} $M_\odot$/yr (see Fig. 3.3 in Sect. 3.3). To mimic the heating by the initial shell flash, we exchange the point mass by a hot and bright ($\log L_{\rm s}/L_\odot = 4.175$) white dwarf model at this time. The initial central temperature and density of the white dwarf are $T_{\rm c} = 1.8 \times 10^8$ K and 2×10^7 g cm^{-3} respectively. Although the central temperature may be much lower in reality when the mass accretion starts, the initial temperature structure is unimportant for the advanced evolution due to the self-heating of the white dwarfs (cf. Sect. 3.3).

The calculations presented here required high space and time resolution: About 500 000 binary models were computed, where both stars were resolved into ~ 1000 mass shells.

3.3 Results

The evolution of our 1.6 $M_\odot$ helium star + 1 $M_\odot$ CO white dwarf binary system proceeds as follows (see Figs. 3.1 and 3.2, and Table 1). The helium star undergoes the core helium

Table 3.1: Component masses, orbital period, and central density of both stars, for five different times during the mass transfer, including the beginning of mass transfer (defines t=0), the time of minimum orbital separation (t=73 000 yr), and the time of central carbon ignition (t=148 000 yr).

| t | $M_{\rm He}$ | $M_{\rm WD}$ | P | $\rho_{\rm c,He}$ | $\rho_{\rm c,WD}$ |
10^3 yr	$M_\odot$	$M_\odot$	h	10^5 g cm^{-3}	10^8 g cm^{-3}
0	1.60	1.00	2.97	1.31	0.20
35	1.39	1.10	2.70	1.53	0.51
73	1.25	1.21	2.65	1.86	1.45
110	1.15	1.30	2.69	2.30	4.70
148	1.08	1.37	2.78	2.92	23.5
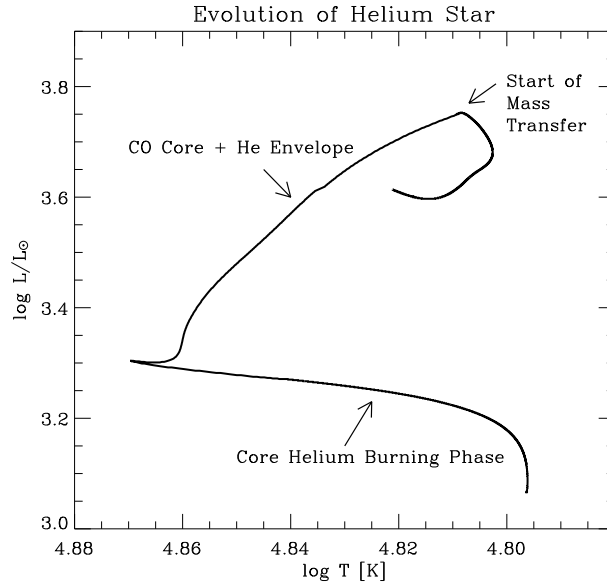
Figure 3.1: Evolution of the 1.6 $M_\odot$ helium star in the HR diagram.

burning for 4.28 million years. After core helium exhaustion, the envelope of the helium star expands and starts to fill its Roche lobe (Fig. 3.1) when the radius of the helium star reaches 0.61 $R_\odot$. At this point, the CO core mass of the helium star reaches 0.53 $M_\odot$ and mass transfer from the helium star commences. Even though at this time the helium star expands on the nuclear timescale of helium shell burning, the mass transfer shrinks the orbit and thus proceeds on the thermal timescale of the helium star. The resulting mass transfer rates are in the range $1 \ldots 8 \times 10^6$ $M_\odot$/yr, as shown by the dotted line in Fig. 3.3.
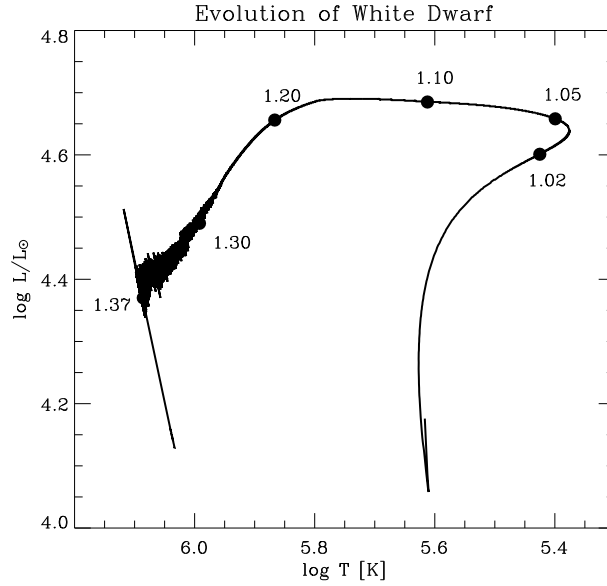
Figure 3.2: Evolution of the CO white dwarf during the mass accretion phase in the HR diagram. The numbers at the filled circles denote the white dwarf mass in the unit of solar mass at the given points.

A part of the transferred matter is blown off by the stellar wind at the white dwarf surface without being burned into carbon and oxygen, and thus without affecting the thermal evolution of the CO core. The rest is transformed into CO in the helium burning shell source and accreted into the CO core. As the mass transfer rate from the helium star increases, the surface luminosity of the white dwarf reaches about 40% of its Eddington luminosity (see Fig. 3.2). A radiation driven wind from the white dwarf surface is induced, with a peak of 4.8×10^{-6} M$_\odot$/yr at $M_{\mathrm{WD}} \simeq 1.04$ M$_\odot$. As the mass transfer rate decreases, the stellar wind from the white dwarf becomes weaker. The upper dashed lines in Fig. 3.3 denotes the critical mass accretion rate above which the helium envelope is expected to expand to giant dimensions, $\dot{M}_{\mathrm{Rhe}} = 7.2 \times 10^{-6}(M_{\mathrm{CO}}/M_\odot - 0.60)$ M$_\odot$/yr, based on white dwarf models computed with constant mass accretion rates (Nomoto 1982a). The helium shell source is expected to be stable when $0.4\dot{M}_{\mathrm{Rhe}} < \dot{M} < \dot{M}_{\mathrm{Rhe}}$. The accretion rate in the white dwarf remains in the steady helium shell burning regime until $M \simeq 1.3$ M$_\odot$ and the white dwarf mass grows efficiently (Fig. 3.2). Thereafter, the white dwarf undergoes weak thermal pulses.

During the mass accretion, the surface temperature of the white dwarf varies from 2.5×10^5 K to 12×10^5 K and the luminosity reaches $2.5 \ldots 5 \times 10^4$ L$_\odot$ (Fig. 3.2), with which the white dwarf will appear as a super-soft X-ray source (e.g. Kahabka & van den
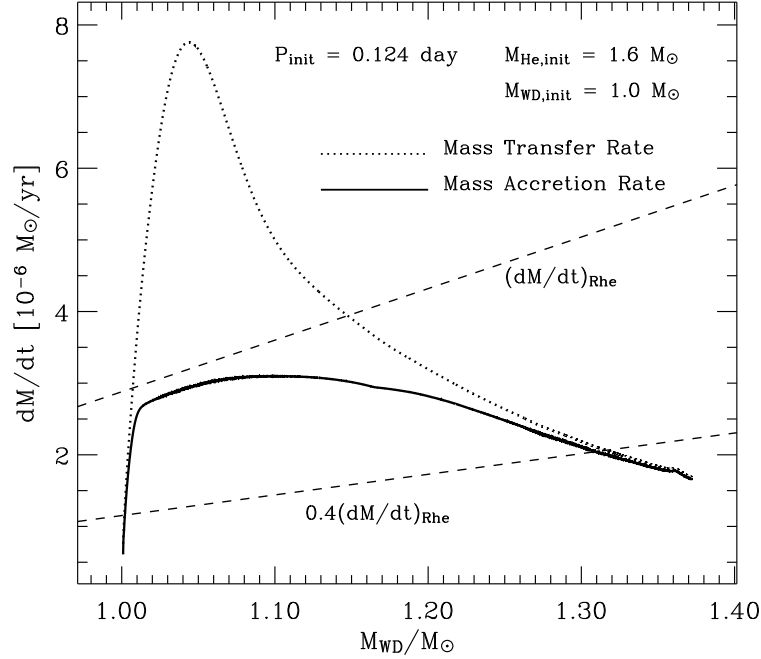
Figure 3.3: Mass transfer rate (dotted line) and white dwarf mass accretion rate (solid line) as a function of the white dwarf mass, for the considered binary model. The upper dashed line denotes the critical mass accretion rate above which the helium envelope is expected to expands to giant dimensions (Nomoto 1982a). For accretion rates below the lower dashed line helium shell burning is usually unstable.

Heuvel 1997; Greiner 2000). The central temperature of the white dwarf decreases initially, mainly due to neutrino emission. When $M_{\rm WD} \gtrsim 1.1$ $M_\odot$, the compressional heating begins to dominate, and the central temperature of the white dwarf increases. The dashed line in Fig. 3.4 indicates where the energy generation rate due to the carbon burning equals to the neutrino energy loss rate. The white dwarf reaches this line at $\rho_{\rm c} = 1.92 \times 10^9$ g/cm^3 and $T_{\rm c} = 2.71 \times 10^8$ K, from where the central temperature increases rapidly. About 1700 years thereafter, when $T_{\rm c} \simeq 2.9 \times 10^8$ K, the central region becomes convectively unstable. About 1800 years later, in our last model, the convection zone extends to $\simeq 0.5$ $M_\odot$ when $T_{\rm c} = 4.6 \times 10^8$ K (Fig. 3.5).

The convective URCA process, which is not considered in our study, may affect the evolution during this stage (Paczynski 1972; Iben 1982a). It is currently still debated whether it leads to heating or to cooling of the convective core (e.g. Mochkovitch 1996; Stein et al. 1999). Thus we have to consider the spatial extent and duration of the convective phase, as obtained from our models, as uncertain. When the temperature exceeds $5 \ldots 8 \times 10^8$
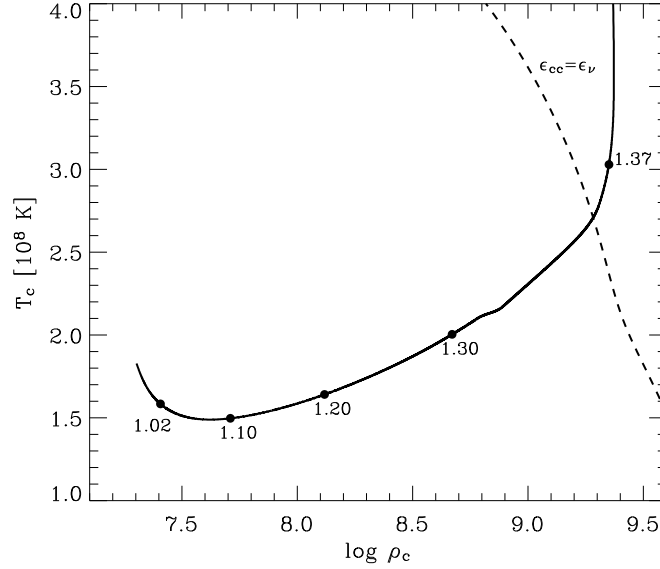
Figure 3.4: Evolution of central density and temperature in the white dwarf during the mass accretion phase. The dashed line gives the locus where the energy generate rate due to the carbon burning equals to the neutrino cooling rate. The numbers at the filled circles denote the white dwarf mass in the unit of solar mass at the given points.

K, the nuclear time scale becomes comparable to the convective time scale. In this case, convection is not able to efficiently carry away the released nuclear energy, and the mixing length theory becomes inadequate to describe the convective energy transport. Therefore, we stop the calculation at this point; see, however, Höflich & Stein (2002) for the further evolution.

In our last model, the helium star has a mass of 1.08 $M_\odot$ and a CO core mass of 0.64 $M_\odot$. If the white dwarf explodes, the helium star may survive but suffer stripping off small amounts of mass by the supernova ejecta (Marrietta et al. 2000). Its space velocity will be close to its final orbital velocity of 330 km/s. It will evolve into a massive CO white dwarf of ~ 1.0 $M_\odot$ eventually.

3.4 Discussion

The model described above is (to our knowledge) the first self-consistent binary evolution calculation which leads to a Chandrasekhar-mass white dwarf. Its relevance is in part the realistic construction of a supernova progenitor white dwarf model, but even more the fact that it provides for the first time hard evidence of the functioning of an SN Ia progenitor
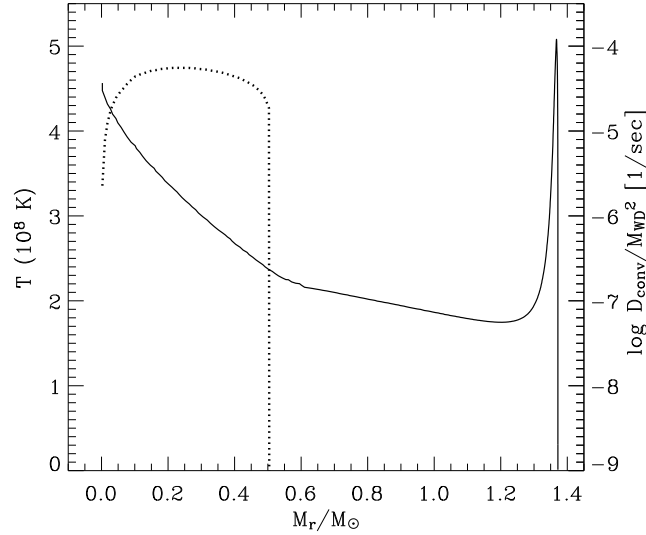
Figure 3.5: Temperature as a function of the mass coordinate in the last white dwarf model. The dotted lines show the convective diffusion coefficient (in the unit of g^2/s) divided by the square of the total mass of the white dwarf.

channel: Our results leave little doubts that some helium star plus white dwarf systems will in fact produce a Type Ia supernova.

The considered system may have evolved from a wide 8.0 $M_\odot$ giant star + 1.0 $M_\odot$ white dwarf system though a common envelope phase, which in turn may be the result of two intermediate mass stars in a close orbit. This indicates a system life time of the order of $\sim 10^7 - 10^8$ yr, which is too short to explain SNe Ia in elliptical galaxies. Therefore, our results support the idea that at least two SN Ia progenitor scenarios are realized in nature (e.g., della Valle & Livio 1994). Iben & Tutukov (1994) estimated the potential SN Ia production rate through white dwarf + helium giant binary systems to 1.7×10^{-3} yr^{-1}, which may constitute a significant fraction of SNe Ia observed in late type galaxies.

As previously mentioned, SNe Ia progenitors of the kind considered here will appear as a super-soft X-ray source (SSS). We note that, since a wide range of orbital separations is possible for helium star plus white dwarf systems (Iben & Tutukov 1994), this may explain SSSs with various orbital periods. For instance, short period systems such as RX J0537.7-7034 (3.5h, Greiner et al. 2000) and 1E0035.4-7230 (4.1h, Schmidtke et al. 1996) can not be easily explained within the canonical model which invokes hydrogen rich donor stars (e.g., Rappaport et al. 1994; Kahabka and van den Heuvel 1997), except at low metallicity (Langer et al. 2000). Orbital periods of the binary system in the present study in the range

$2.65 - 2.97$ h indicate that helium star plus white dwarf systems might be another natural possibility to explain short period SSSs.

Chapter 4

Presupernova evolution of accreting white dwarfs with rotation

S.-C. Yoon and N. Langer

Abstract   We discuss the effects of rotation on the evolution of accreting carbon-oxygen white dwarfs, with the emphasis on possible consequences in Type Ia supernova (SN Ia) progenitors. Starting with a slowly rotating CO white dwarf, we consider the accretion of matter and angular momentum from a quasi-Keplerian accretion disk. Numerical simulations with initial white dwarf masses of 0.8, 0.9 and 1.0 $M_\odot$ and accretion of carbon-oxygen rich matter at rates of $3 \ldots 10 \times 10^{-7}$ $M_\odot/\mathrm{yr}$ are performed. The models are evolved either up to a ratio of rotational to potential energy of $T/W = 0.18$ — as angular momentum loss through gravitational wave radiation will become important for $T/W < 0.18$ — or to central carbon ignition. The role of the various rotationally induced hydrodynamic instabilities for the transport of angular momentum inside the white dwarf is investigated. We find that the dynamical shear instability is the most important one in the highly degenerate core, while Eddington Sweet circulations, the Goldreich-Schubert-Fricke instability and the secular shear instability are most relevant in the non-degenerate envelope. Our results imply that accreting white dwarfs rotate differentially throughout, with a shear rate close to the threshold value for the onset of the dynamical shear instability. As the latter depends on the temperature of the white dwarf, the thermal evolution of the white dwarf core is found to be relevant for the angular momentum redistribution. As found previously, significant rotation is shown to lead to carbon ignition masses well above 1.4 $M_\odot$. Our models suggest a wide range of white dwarf explosion masses, which could be responsible for some aspects of the diversity observed in SNe Ia. We analyze the potential role of the bar-mode and the r-mode instability in rapidly rotating white dwarfs, which may impose angular momentum loss by gravitational wave radiation. We discuss the consequences of the resulting spin-down for the fate of the white dwarf, and the possibility to detect the emitted gravitational waves at frequencies of $0.1 \ldots 1.0$ Hz in nearby galaxies with LISA. Possible implications of fast and differentially rotating white dwarf cores for the flame propagation in exploding white dwarfs are also briefly discussed.

4.1 Introduction

Type Ia Supernovae (SNe Ia) have a particular importance in astrophysics. Observations of SNe Ia at low redshift showed a clear correlation between the peak brightness and the width of the light curve (Phillips 1993; Phillips' relation), which allowed to use SNe Ia as distance indicators for galaxies even beyond $z = 1$. This made SNe Ia an indispensable tool for cosmology, in particular to determine the cosmological parameters (e.g. Hamuy et al. 1996a; Branch 1998; Leibundgut 2000, 2001). The new cosmology with a non-zero cosmological constant has been initiated by the observational evidence deduced from observations of SNe Ia at high redshift (Perlmutter et al. 1999a; Riess et al. 2000).

Recent analyses of SNe Ia have revealed, however, that SNe Ia are not perfectly homogeneous but show some diversity in their light curves and spectra (e.g. Branch 2001; Nomoto et al. 2003; Li et al. 2003). This leaves concerns about applying the Phillips' relation to very distant SNe Ia. An understanding of the origin of the diversity observed in SNe Ia is thus a crucial task for stellar evolution theory, which requires to identify the detailed evolutionary paths of SNe Ia progenitors.

Unlike core collapse supernovae, Type Ia supernovae (SNe Ia) are believed to occur exclusively in binary systems (e.g. Livio 2001). Although it is still unclear which kinds of binary systems lead to SNe Ia, non-degenerate stars such as main sequence stars, red giants or helium stars are often assumed as white dwarf companion (e.g. Li & van den Heuvel 1997; Hachisu et al. 1999; Langer et al. 2000; Yoon & Langer 2003). The white dwarf is then assumed to grow to the Chandrasekhar limit by mass accretion from its companion, with accretion rates which allow steady shell hydrogen and helium burning ($\dot{M} \gtrsim 10^{-7}$ $M_{\odot}/\mathrm{yr}$). An understanding of the physics of mass accretion is therefore indispensable to investigate the evolution of accreting white dwarfs.

Although the mass accretion process in white dwarfs has been discussed by many authors (e.g. Iben 1982b; Nomoto 1982a; Fujimoto & Sugimoto 1982; Saio & Nomoto 1985, 1998; Kawai et al. 1988; Cassisi et al. 1998; Piersanti et al. 2000; Langer et al. 2002), little attention has so far been devoted to the effects of angular momentum accretion and the ensuing white dwarf rotation (see Sect. 4.3.1). As the evolution of stars can generally be affected by rotation (e.g. Heger & Langer 2000; Maeder & Meynet 2000), this might be particularly so in accreting white dwarfs: Since the transferred matter may form a Keplerian disk which carries a large amount of angular momentum, the resultant accretion of angular momentum will lead to the spin-up of the white dwarf (e.g. Durisen 1977; Ritter 1985; Narayan & Popham 1989; Langer et al. 2000, 2002, 2003). The observation that white dwarfs in cataclysmic variables rotate much faster than isolated ones (Sion 1999) provides evidence for accreting white dwarfs indeed being spun up. Rapidly rotating progenitors may also lead to aspherical explosions, which may give rise to the observed polarization of SNe Ia (Howell et al. 2001; Wang et al. 2003).

Here, we make an effort to investigate in detail the possibility of angular momentum accretion, and the role of the various rotationally induced hydrodynamic instabilities in transporting angular momentum into the white dwarf core, and in establishing the the pre-

explosion angular momentum profile. The remainder of this paper is organized as follows. We evaluate the possible mechanisms for angular momentum transport in accreting white dwarfs in Sect. 4.2. Our approach to the problem, including the numerical methods and physical assumptions, is discussed in Sect. 4.3, where previous papers on rotating white dwarf models are also reviewed (Sect. 4.3.1). Numerical results are presented in Sect. 4.4, with the emphasis on the process of angular momentum transport in the white dwarf interior. Pre-explosion conditions of accreting white dwarfs and their implications for the diversity of SNe Ia are discussed in Sect. 4.5, 4.6 and 4.7. The possibility of detecting gravitational waves from SNe Ia progenitors is examined in Sect. 4.8. Our conclusions are summarized in Sect. 4.9.

4.2 Angular momentum transport in white dwarfs

Inside a white dwarf, angular momentum can be transported by Eddington Sweet circulations and by turbulent diffusion induced by hydrodynamic instabilities. Our discussion below is limited to angular momentum transport in the vertical direction.

4.2.1 Eddington Sweet circulation

Eddington Sweet circulations are induced by the thermal imbalance between the equator and the poles of a rotating star. Its time scale is roughly given by $\tau_{\rm ES} \simeq \tau_{\rm KH}/\chi^2$ (Maeder & Meynet 2000), where $\tau_{\rm KH}$ is the Kelvin-Helmholtz time scale and χ is the angular velocity normalized to the Keplerian value, i.e., $\chi = \omega/\omega_{\rm Kep}$. In a white dwarf which accretes at rates of $\dot{M} > 10^{-7}$ $M_\odot$/yr, the surface luminosity reaches 10^4 $L_\odot$ due to compressional heating and nuclear burning. The quantity χ is close to 1 in the outer envelope as we shall see in Sect. 4.4.3. As a result, we expect an Eddington Sweet circulation time scale in the non-degenerate envelope which is shorter than or comparable to the accretion time scale:

$$\tau_{\rm ES} \approx \frac{G \Delta M_{\rm env}^2}{R L \chi^2}$$
$$\approx 1.3 \cdot 10^3 {\rm yr} \frac{(\Delta M_{\rm env}/0.05 {\rm M}_\odot)^2}{(R/0.01 {\rm R}_\odot)(L/10^4 {\rm L}_\odot)(\chi/0.8)^2}. \tag{4.1}$$

In the degenerate core, on the other hand, we have $\tau_{\rm ES} \gg \tau_{\rm acc}$ since the Kelvin-Helmholtz time scale is typically much larger than 10^7 yr. Furthermore, χ is usually significantly smaller than 1 in the inner core:

$$\tau_{\rm ES} \approx \frac{G M_{\rm core}^2}{R_{\rm core} L_{\rm core} \chi^2}$$
$$\approx 7 \cdot 10^9 {\rm yr} \frac{(M_{\rm core}/{\rm M}_\odot)^2}{(R_{\rm core}/0.005 {\rm R}_\odot)(L_{\rm core}/10 {\rm L}_\odot)(\chi/0.3)^2} \tag{4.2}$$

Consequently, Eddington Sweet circulations are only important in the white dwarf envelope.

4.2.2   Shear instability

The dynamical shear instability (DSI) occurs when the energy of the shear motion dominates over the buoyancy potential. In a rotating flow, the linear condition for instability is given by

$$\frac{N^2}{\sigma^2} < R_{\mathrm{i,c}} \approx 1/4, \tag{4.3}$$

where $R_{\mathrm{i,c}}$ denotes the critical Richardson number which is about 0.25, N^2 the Brunt-Väisälä frequency, and σ the shear factor (Zahn 1974):

$$N^2 = N_{\mathrm{T}}^2 + N_\mu^2, \tag{4.4}$$

$$N_{\mathrm{T}}^2 = \frac{g\delta}{H_P}(\nabla_{\mathrm{ad}} - \nabla), \quad N_\mu^2 = \frac{g\varphi\nabla_\mu}{H_{\mathrm{P}}} \tag{4.5}$$

and

$$\sigma = \frac{\partial\omega}{\partial\ln r} . \tag{4.6}$$

Here, ω is the angular velocity and other symbols have their usual meaning. The equation of state of electron degenerate matter is given by $P = P(\rho, T, \mu_{\mathrm{e}}, \mu_{\mathrm{I}})$ and the factor $\varphi\nabla_\mu$ in Eq. 4.5 needs to be replaced by $\varphi_{\mathrm{e}}\nabla_{\mu_{\mathrm{e}}} + \varphi_{\mathrm{I}}\nabla_{\mu_{\mathrm{I}}}$, where $\varphi_{\mathrm{e}} = (\partial\ln\rho/\partial\ln\mu_{\mathrm{e}})_{P,T,\mu_{\mathrm{I}}}$ and $\varphi_{\mathrm{I}} = (\partial\ln\rho/\partial\ln\mu_{\mathrm{I}})_{P,T,\mu_{\mathrm{e}}}$. In a typical CO white dwarf, N_μ^2 is generally smaller than N_{T}^2 and has minor effects on the angular momentum transport as discussed in Sect. 4.4.3.

With constant temperature and homogeneous chemical composition, which is a good approximation for the central region of a CO white dwarf, the critical value of σ for the DSI can be given as

$$\sigma_{\mathrm{DSI,crit}}^2 = N^2/R_{\mathrm{i,c}}$$

$$\simeq 0.2 \left(\frac{g}{10^9\,\mathrm{cm/s^2}}\right) \left(\frac{\delta}{0.01}\right) \left(\frac{H_{\mathrm{P}}}{8\cdot10^7\mathrm{cm}}\right)^{-1} \left(\frac{\nabla_{\mathrm{ad}}}{0.4}\right) \tag{4.7}$$

where $R_{\mathrm{i,c}} = 0.25$ is assumed. Fig. 4.1 shows $|\sigma_{\mathrm{DSI,crit}}|$ as a function of density, with other physical assumptions as indicated in the figure caption. This figure shows that the condition for the DSI becomes more relaxed with increasing density, which is due to the buoyancy force becoming weaker with stronger degeneracy. This implies that the highly degenerate core in a white dwarf is more susceptible to the dynamical shear instability than the outer envelope.

The stability criterion for the shear instability can be relaxed if thermal diffusion reduces the buoyancy force such that

$$R_{\mathrm{is,1}} := \frac{\nu R_{\mathrm{e,c}} N_{\mathrm{T}}^2}{K\sigma^2} < R_{\mathrm{i,c}}, \tag{4.8}$$

where $R_{\mathrm{e,c}}$ is the critical Reynolds number, ν the kinetic viscosity and $K = (4acT^3)/(3C_{\mathrm{p}}\kappa\rho^2)$ the thermal diffusivity (e.g. Maeder & Meynet 2000). Since the μ gradient is not affected by
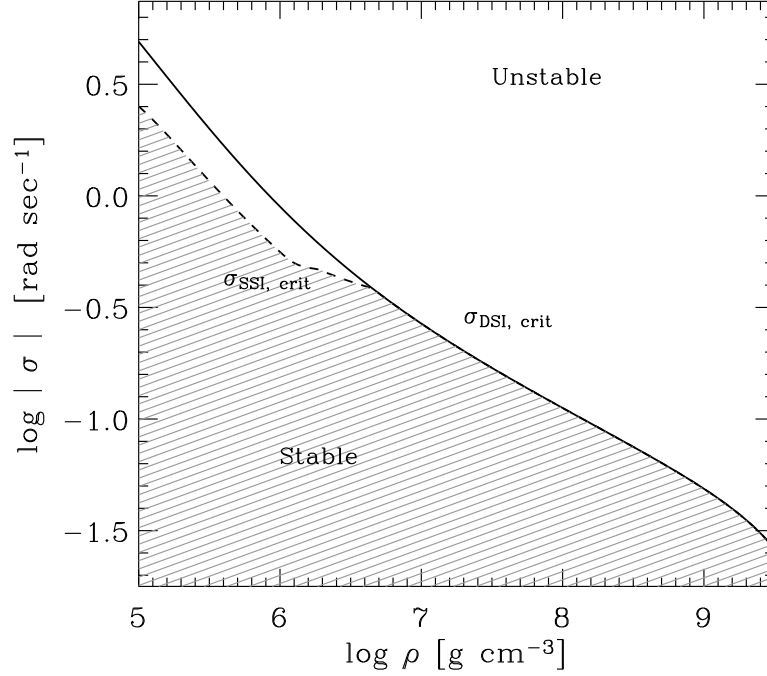
Figure 4.1: Threshold values of the shear factor $\sigma = (\partial\omega/\partial\ln r)$ for the dynamical (solid line) and the secular (dashed line) shear instability. Constant gravity and temperature, i.e., $g = 10^9$ cm/s^2, $T = 5 \times 10^7$ K, are assumed. The chemical composition is also assumed to be constant, with $X_C = 0.43$ and $X_O = 0.54$. For the critical Richardson number, $R_{i,c} = 1/4$ is employed. $R_{e,c} = 2500$ is used for the critical Reynolds number.

the thermal diffusion, this condition needs to be supplemented by the following additional condition (Endal & Sofia 1976):

$$R_{is,2} := \frac{N_\mu^2}{\sigma^2} < R_{i,c} \qquad (4.9)$$

The thermally induced shear instability is often called 'secular shear instability' (SSI).

This instability can occur only when the thermal diffusion time scale is shorter than the turbulent viscous time scale (i.e., $\nu R_{e,c} < K$), which is often the case in non-degenerate stars. However, this condition is not always fulfilled in white dwarfs. In Fig. 4.2, the critical density $\rho_{SSI,crit}$ above which the secular shear instability is not allowed is plotted as a function of temperature. In this calculation, the ion and electron viscosity as well as the radiative and conductive opacities are estimated as described in Sect. 4.3.2. This figure indicates that the SSI may play a role only for relatively weakly degenerate regions. The threshold value
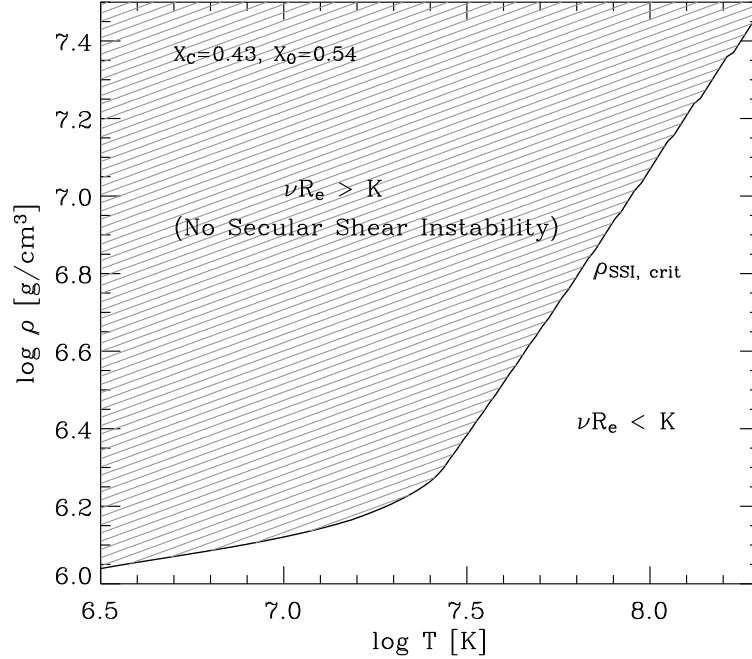
Figure 4.2: The critical density $\rho_{\mathrm{SSI,crit}}$, above which the secular shear instability can not occur, as function of temperature (solid line). The region where the thermal diffusion time scale exceeds the turbulent viscous time scale is hatched. Abundances of $X_{\mathrm{C}} = 0.43$ and $X_{\mathrm{O}} = 0.54$ are assumed. $R_{\mathrm{e,c}} = 2500$ is used for the critical Reynolds number.

of the shear factor for this instability is given by $\sigma_{\mathrm{SSI,crit}}^2 = \nu R_{\mathrm{e,c}} N_{\mathrm{T}}^2/(K R_{\mathrm{i,c}})$ if $N_{\mu}^2 = 0$, and plotted in Fig 4.1, with the assumptions as indicated in the figure caption. As shown in the figure and as discussed above, thermal diffusion can not weaken the restoring buoyancy force for $\rho \gtrsim 5 \times 10^6$ g/cm^3 under the chosen conditions, and only the dynamical shear instability can occur for higher densities.

Zahn (1992) derives the diffusion coefficient for the SSI as

$$D_{\mathrm{SSI}} = \frac{1}{3} \frac{K \sigma^2 R_{\mathrm{i,c}}}{N^2}. \tag{4.10}$$

The time scale of the SSI when $\sigma = \sigma_{\mathrm{DSI,crit}}$ thus becomes simply the thermal diffusion time scale: τ_{SSI} (at $\sigma = \sigma_{\mathrm{DSI,crit}}$) $\approx 3R^2/K$. In the degenerate core of a CO white dwarf with $\rho \lesssim \rho_{\mathrm{SSI,crit}}$, we have $\tau_{\mathrm{SSI}} \approx 7.6 \times 10^6 \left(\frac{R_{\mathrm{core}}}{2 \cdot 10^8 \text{ cm}}\right)^2/\left(\frac{K}{500 \text{ cm}^2\text{s}^{-1}}\right)$ yr.

As a consequence of these considerations, any shear motion with $\sigma > \sigma_{\mathrm{DSI,crit}}$ will decay such that σ approaches $\sigma_{\mathrm{DSI,crit}}$ on the dynamical time scale. Further angular mo-

mentum transport will operate on the thermal diffusion time scale until σ reaches $\sigma_{\mathrm{SSI,crit}}$ for $\rho \lesssim \rho_{\mathrm{SSI,crit}}$. For $\sigma < \sigma_{\mathrm{SSI,crit}}$ and $\sigma < \sigma_{\mathrm{DSI,crit}}$ (hatched region in Fig. 4.1), angular momentum will be transported only via the electron viscosity or via Eddington Sweet circulations on much longer time scales (unless other kinds of instabilities are invoked). Therefore, if we consider accretion at rates required by the single degenerate SN Ia progenitor scenario ($\dot{M} > 10^{-7}$ M$_\odot$/yr), the degree of shear may not be far from the threshold value for the dynamical shear instability throughout the degenerate white dwarf interior. This conjecture is confirmed by the numerical results presented in Sect. 4.4.2.

4.2.3 GSF and magnetic instabilities

The Goldreich, Schubert and Fricke instability (GSF instability) can be induced if a star is in a baroclinic condition (Goldreich & Schubert 1967; Fricke 1968). In an accreting white dwarf, this instability may be important in the non-degenerate envelope, but is likely suppressed in the degenerate core where the barotropic condition will be retained through a dynamical meridional circulation (Kippenhahn & Möllenhoff 1974; see also Durisen 1977). Magnetic instabilities such as the Tayler instability (Spruit 2002) may be potentially important, and their role will be investigated in the near future. In the present study, we restrict our discussions to non-magnetized white dwarfs.

4.3   Simulations of accreting white dwarfs

For the detailed investigation of the angular momentum transport and its role in the evolution of accreting white dwarfs, we have simulated accreting CO white dwarfs with various initial masses and accretion rates.

4.3.1 Previous work on rotating white dwarfs

In order to compare our results with previously obtained ones, here we briefly discuss the models of rotating white dwarfs in the literature. Most rotating white dwarf equilibrium models have been constructed assuming a barotropic equation of state and axial symmetry for both, rigidly and differentially rotating cases (e.g. James 1964; Roxburgh 1965; Monaghan 1966; Ostriker 1966; Anand 1968; Ostriker & Mark 1968; Hachisu 1986). These models have mainly been used to investigate the stability of rapidly rotating zero temperature white dwarfs (e.g. James 1964; Lynden-Bell & Ostriker 1967; Ostriker & Bodenheimer 1968; Durisen 1975b; Durisen & Imammura 1981). One of the main results of these studies is that the Chandrasekhar limit increases slightly in rigidly rotating white dwarfs ($\sim$ 1.48 M$_\odot$), while differentially rotating white dwarfs can be dynamically stable even with masses up to ~ 4.0 M$_\odot$. It was also found that differentially rotating white dwarfs become secularly unstable to gravitational wave radiation if the ratio of the rotational energy to the gravitational energy exceeds a certain limit (see Sect. 4.5 for more detailed discussions).

The evolution of rotating white dwarfs was investigated by Durisen (1973a, 1973b, 1975a) for the first time. Evolution and spin-up of mass accreting white dwarfs were probed by Durisen (1977). In his studies based on two-dimensional barotropic differentially rotating white dwarf models, Durisen assumed that angular momentum in the white dwarf interior is only transported by electron viscosity, and angular momentum transport time scales of the order of 10^{10} yr have been obtained. In all these models, the thermal history and the energy transport in the white dwarf matter were neglected, assuming zero temperature.

Recently, Piersanti et al. (2003) investigated the effect of rotation on the thermal evolution of CO-accreting white dwarfs, using a one dimensional stellar evolution code. They also discussed angular momentum loss by gravitational wave radiation (cf. Sect. 4.5). However, the detailed history of the angular momentum transport inside the white dwarf was neglected, but rigid body rotation was assumed. I.e., while Durisen assumed much slower angular momentum redistribution by restricting his considerations to electron diffusion, Piersanti et al. assume instant angular momentum redistribution with a maximum efficiency.

Uenishi et al. (2003) did consider a finite spin-up time of accreting white dwarfs by dividing their two-dimensional white dwarf models into a non-rotating central core and a fast rotating outer envelope. However, rigid body rotation is again assumed for the spun-up region, introducing a discontinuity in the angular velocity profile.

In the present study on the evolution of accreting white dwarfs, we consider the effects of the accretion induced heating and energy transport, the angular momentum transport by various instabilities, and the effect of rotation on the white dwarf structure. However, our numerical models are calculated in a one dimensional approximation as described in the next section, and thus the structure of rapidly rotating white dwarfs is described less accurately than in multi-dimensional models mentioned above. Furthermore, by assuming CO-accretion we do not consider effects of nuclear shell burning. These, and the feedback between rotation and nuclear shell burning, as well as rotationally induced chemical mixing, are discussed in a separate paper (Yoon et al. 2004). The effects of rotation with respect to the off-center helium detonation models — i.e., helium accreting CO white dwarf models with $\dot{M} = \sim 10^{-8}$ M$_\odot$/yr — are investigated in Yoon & Langer (2004b).

4.3.2   Numerical method

We use a hydrodynamic stellar evolution code (Langer et al. 1988) for the accreting white dwarf model calculations. Radiative opacities are taken from Iglesias & Rogers (1996). For the electron conductive opacity, we follow Hubbard & Lampe (1969) in the non-relativistic case, and Canuto (1970) in the relativistic case. The accreted matter is assumed to have the same entropy as that of the surface of the accreting white dwarf, and the accretion induced compressional heating is treated as in Neo et al (1977).

The effect of rotation on the stellar structure is approximated in one dimension by introducing the factors f_P and f_T in the momentum and energy conservation equations (cf. Heger et al. 2000), following the method of Kippenhahn & Thomas (1970) and Endal &

Sofia (1976). This method is well suited for the case where the effective gravity can be derived from an effective potential. This is indeed a good assumption for a CO white dwarf, since it should be in a barotropic condition except for the non-degenerate outer envelope. Note that this method is also applicable in the case of shellular rotation as discussed by Meynet & Maeder (1997).

However, our method of computing the effective gravitational potential in a rotating star limits the accuracy of our results for very rapid rotation. The potential is expanded in terms of spherical harmonics, of which we only consider terms up to the second order (cf., Kippenhahn & Thomas 1970). Fliegner (1993) showed this method to accurately reproduce the shapes of rigidly rotating polytropes up to a rotation rate of about 60% critical, corresponding to correction factors of $f_{\mathrm{P}} \simeq 0.75$ and $f_{\mathrm{T}} \simeq 0.95$ in the stellar structure equations (cf. Heger et al. 2000). We therefore limit these factors to the quoted values, with the consequence that we underestimate the effect of the centrifugal force in layers which rotate faster than about 60% critical. As in our models the layers near the surface are always close to critical rotation, the stellar radius of our models may be underestimated. Furthermore, our models are per definition rotationally symmetric. Therefore, we are in principle unable to investigate the onset of triaxial instabilities, which may affect the final fate of a rapidly rotating white dwarf (Sect. 4.5).

The angular momentum transport induced by the instabilities mentioned in Sect. 4.2 is described as a diffusion process (Heger et al. 2000), while this approximation neglects the possibility of advective angular momentum redistribution by Eddington Sweet circulations (Maeder & Meynet 2000). Note also that this approach is based on the assumption of shellular rotation (see Heger et al. 2000 for a detailed discussion), which might not be appropriate for white dwarfs. Nevertheless, our models can represent the case of cylindrical rotation to some degree, since most of the total angular momentum is confined to layers near the equatorial plane in both cases. Since the dynamical shear instability is important in the present study, the diffusion solver has been improved as a non-linear process, as explained in Appendix A, in order to deal properly with such a fast angular momentum redistribution as on a dynamical time scale during the secular evolution of accreting white dwarfs. Diffusion coefficients for each of the instabilities are taken from Heger et al. (2000) and Heger & Langer (2000), with some modifications as follows.

As mentioned in Sect. 4.2.3, the GSF instability may be suppressed in the degenerate barotropic core, and we describe this effect as

$$D_{\mathrm{GSF}} = D^*_{\mathrm{GSF}} \left(1 - \min \left[1, \frac{P_{\mathrm{e}}}{P_{\mathrm{ideal}}} \right] \right) . \tag{4.11}$$

Here, D^*_{GSF} is the diffusion coefficient for the GSF instability as estimated in Heger et al. (2000). P_{e} is the electron pressure for complete non-relativistic degeneracy, and P_{ideal} is the ideal gas pressure:

$$P_{\mathrm{e}} = 9.91 \cdot 10^{12} \left(\frac{\rho}{\mu_{\mathrm{e}}} \right)^{5/3} , \quad P_{\mathrm{ideal}} = \frac{\rho k T}{\mu m_{\mathrm{H}}} . \tag{4.12}$$

For the secular instability, Zahn's (1992) prescription is employed (Eq. 4.10), with a correction factor as in Heger et al. (2000) to ensure a smooth turn-on of the instability and to relate its strength to the deviation from the Richardson criterion:

$$D_{\mathrm{SSI}} = \frac{1}{3} \frac{K \sigma^2 R_{\mathrm{i,c}}}{N^2} \left(1 - \frac{\max\{R_{\mathrm{is},1}, \ R_{\mathrm{is},2}\}}{R_{\mathrm{i,c}}} \right)^2 , \qquad (4.13)$$

where $R_{\mathrm{is},1}$ and $R_{\mathrm{is},2}$ are defined in Eq. 4.8 and 4.9. As already discussed in Sect. 4.2.2, the viscosity is an important factor for the stability of the secular shear instability. The former way of computing the ion viscosity in Heger et al. (2000) and Heger & Langer (2000), following Spitzer (1962), is not well adapted for matter in the ion liquid state: here we follow the work of Wallenborn & Bauss (1978), as described in Itoh et al. (1987):

$$\eta_{\mathrm{i}} = 5.53 \cdot 10^3 Z A^{-1/3} (\rho/10^6)^{5/6} \eta^* \ \ (\mathrm{g \, cm^{-1} \, s^{-1}}) . \qquad (4.14)$$

We constructed a fitting formula for the dimensionless parameter η^* from the table in Itoh et al. as

$$\eta^* = -0.016321227 + 1.0198850 \, \Gamma^{-1.9217970}$$
$$+ 0.024113535 \, \Gamma^{0.49999098} , \qquad (4.15)$$

where $\Gamma = (Ze)^2/[(3/4\pi n_{\mathrm{i}})^{1/3} kT]$. The electron viscosity, which is dominant over the ion viscosity in degenerate matter, is estimated according to Nandkumar & Pethick (1984).

When differential rotation is present in a star, rotational energy is dissipated through frictional heating. We estimate the rotational energy dissipation rate as (Kippenhahn & Thomas 1978; Mochkovitch & Livio 1989)

$$\epsilon_{\mathrm{diss}} = \frac{1}{2} \nu_{\mathrm{turb}} \sigma^2 \ \ (\mathrm{erg \, g^{-1} \, sec^{-1}}) , \qquad (4.16)$$

where ν_{turb} is the turbulent viscosity, which is the sum of all the diffusion coefficients related to the rotationally induced instabilities considered in the present study (Heger et al. 2000).

As discussed in Sect. 4.2.2, the calculation of $\varphi_{\mu_{\mathrm{e}}}$ and $\varphi_{\mu_{\mathrm{I}}}$ is required for considering chemical composition effects in degenerate matter on the rotationally induced instabilities. We can make use of the thermodynamic relation:

$$\varphi_{\mathrm{e}} \nabla_{\mu_{\mathrm{e}}} + \varphi_{\mathrm{I}} \nabla_{\mu_{\mathrm{I}}} = \frac{d \ln \rho}{d \ln P} - \alpha + \delta \nabla , \qquad (4.17)$$

where all the thermodynamic quantities on the right hand side are obtained from the equation of state used in our stellar evolution code (Blinnikov et al. 1996).

4.3.3 Physical assumptions

Our CO white dwarf models start mass accretion at three different initial masses: 0.8, 0.9 and 1.0 $M_{\odot}$. Isolated white dwarfs are observationally found to rotate slowly ($v_{\mathrm{WD}} \lesssim 40$

Table 4.1: Physical quantities of the initial white dwarf models: mass, surface luminosity, central temperature, central density, radius and rotation velocity

$M_{\mathrm{WD,init}}$	$L_{\mathrm{s,init}}$	$T_{\mathrm{c,init}}$	$\rho_{\mathrm{c,init}}$	$R_{\mathrm{WD,init}}$	$v_{\mathrm{rot,init}}$
$M_\odot$	$L_\odot$	10^8 K	10^7 g/cm^3	$R_\odot$	km/s
0.8	0.80	0.79	0.97	0.0115	10
0.9	0.88	0.85	1.68	0.0100	10
1.0	0.81	0.94	3.14	0.0086	10
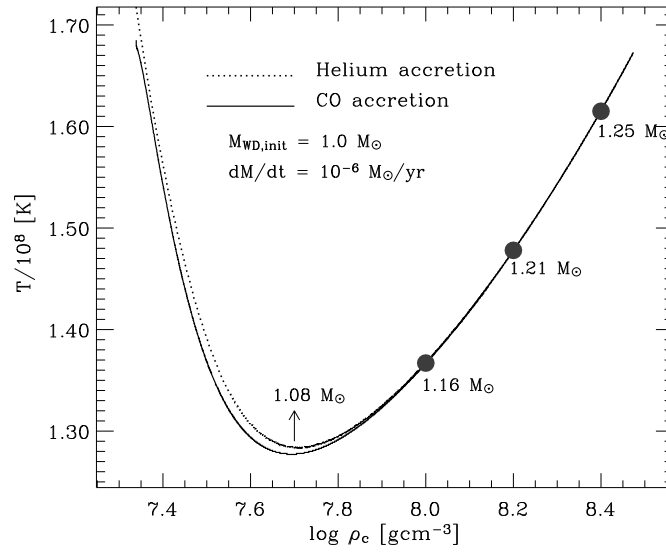
Figure 4.3: Evolution of central density and temperature in non-rotating accreting CO white dwarfs. The initial mass is 1.0 $M_\odot$ and the accretion rate is 10^{-6} $M_\odot$/yr. The dotted line denotes the case of helium accretion, while the dashed line the case of carbon-oxygen accretion. The initial central temperature was $T_{\mathrm{c,init}} = 2.29 \cdot 10^8$ K for the helium accreting white dwarf and and $T_{\mathrm{c,init}} = 1.69 \cdot 10^8$ K for the CO accreting one. The numbers next to the filled circles denote the white dwarf mass in solar masses.

km/s ; Heber et al. 1997; Koester et al. 1998; Kawaler 2003), as also predicted by stellar evolution models (Langer et al. 1999). We thus consider slow rigid rotation in our initial models, and the surface velocity at the white dwarf equator is set to 10 km/s. Other physical quantities of the initial models are summarized in Table 4.1.

For the accretion rate four different values are considered: $3 \cdot 10^{-7}$, $5 \cdot 10^{-7}$, $7 \cdot 10^{-7}$ and 10^{-6} $M_\odot$/yr. These accretion rates are chosen in the context of the single degenerate

Chandrasekhar mass scenario for SNe Ia progenitors, in which steady nuclear shell burning of hydrogen or helium is assumed (Nomoto 1982a; Li & van den Heuvel 1997; Langer et al. 2000; Yoon & Langer 2003). The accreted matter is carbon-oxygen enriched such that $X_C = X_O = 0.487$. In this way, we assume that the accreted hydrogen or helium is immediately converted to carbon and oxygen by shell burning. This assumption, however, does not affect the advanced thermal evolution of the degenerate core of a white dwarf as demonstrated in Fig. 4.3. In this figure, the evolution of the central density and temperature of a non-rotating white dwarf that accretes matter at a rate of with $\dot{M} = 10^{-6}$ M$_\odot$/yr is shown for two cases. One case assumes CO accretion, the other case assumes helium accretion. In the latter case, we have followed the helium shell burning and thereby induced thermal pulses up to $M_{WD} = 1.2$ M$_\odot$. Although a slight difference appears when $M_{WD} \lesssim 1.1$ M$_\odot$, which is due to the different initial temperatures as indicated in the figure caption, the two sequences converge when $M_{WD} \gtrsim 1.1$ M$_\odot$ due to the dominance of the compressional heating for the thermal structure. Therefore, we can assume safely that the thermal evolution of the white dwarf interior does not change significantly even if we neglect the shell burning, as long as rapid accretion is ensured.

Since non-magnetic white dwarfs in close binary systems are thought to accrete matter through a Keplerian disk, the accreted matter may carry angular momentum of about the local Keplerian value at the white dwarf equator (cf. Durisen 1977; Ritter 1985). Langer et al. (2000) pointed out that a white dwarf will reach overcritical rotation well before growing to the Chandrasekhar limit if the white dwarf gains angular momentum with the Keplerian value, when the assumption of rigid body rotation is made (see also Livio & Pringle 1998; Uenishi et al. 2003). Our preliminary calculations show that overcritical rotation may be reached even earlier at the white dwarf surface, as the angular momentum transport time scale is finite (Yoon & Langer 2002). Interestingly, Paczyński (1991) and Popham & Narayan (1991) found a possibility for the angular momentum to be transported from the white dwarf onto the disk by viscous effects when the white dwarf rotates at near break-up velocity, without preventing the continued efficient mass accretion. Based on this picture, we limit the angular momentum gain such that no angular momentum is allowed to be transfered into an accreting white dwarf when its surface rotates at the Keplerian value at its equator:

$$j_{acc} = \begin{cases} f \cdot j_K & \text{if } v_s < v_K \\ 0 & \text{if } v_s = v_K \end{cases} \tag{4.18}$$

where j_{acc} denotes the specific angular momentum carried by the accreted matter, v_s the surface velocity of the accreting white dwarf at its equator, v_K and j_K the Keplerian value of the rotation velocity and the specific angular momentum at the white dwarf equator, respectively: $v_K = (GM_{WD}/R_{WD})^{1/2}$ and $j_K = v_K R_{WD}$. The dimensionless parameter f determines which fraction of the Keplerian value is actually accreted in a white dwarf when $v_s < v_K$.

As mentioned earlier, we do not consider nuclear shell burning in our simulations. Although this may not change the thermal history in the white dwarf core, the surface conditions can be affected by this simplification: the white dwarf envelope may be hotter and

more extended with shell burning, which may lead to a stronger Eddington Sweet circulation and different values for j_K. In order to investigate how the results are affected by this uncertainty, we consider three different values for f: 0.3, 0.5 and 1.0.

In calibrating the chemical mixing efficiencies in massive stars, Heger et al. (2000) introduced the factor f_μ such that ∇_μ is replaced by $f_\mu \nabla_\mu$, with $f_\mu = 0.05$ giving the best reproduction of the observed enhancement of nitrogen at the stellar surface in the mass range 10 $M_\odot$ to 20 $M_\odot$. Although this result is deduced from massive stars and might not apply to white dwarfs, we keep the value of $f_\mu = 0.05$ for most of our models. However, in order to check the sensitivity of our results to this parameter, models with $f_\mu = 1.0$ are also calculated (Sect. 4.4.3).

Table 4.2 gives an overview of the computed model sequences. The first column gives the model sequence designation, where the letters A, B and C denote the cases with $f = 1.0$, 0.5 and 0.3 respectively, all for a fixed f_μ of 0.05. Model sequences with index D have $f = 1.0$ and $f_\mu = 1.0$. The index T indicates test sequences where the effects of rotational energy dissipation (Eq. 4.16) are neglected.

4.4 Results

In this section, we present the results of our simulations, which are summarized in Tables 4.2 and 4.3. In these tables, key properties of the white dwarf models are given for three different epochs, i.e., when the ratio of the rotational energy to the gravitational potential energy $E_{\rm rot}/|W|$ reaches 0.10, 0.14 and 0.18. The implications of these numbers are discussed in Sect. 4.5. In the following subsections, after discussing the thermal evolution of our models, we focus on the processes of the angular momentum transport in the interior of accreting white dwarfs and its consequences for the white dwarf structure.

4.4.1 Thermal evolution

The thermal evolution of non-rotating accreting white dwarfs has been studied by many authors (e.g. Iben 1982b; Nomoto 1982a; Sion 1995; Townsley & Bildsten 2002). Piersanti et al. (2003) compared rigidly rotating white dwarf models with non-rotating ones for CO-accretion at various accretion rates. They found that a rotating white dwarf is generally cooler than its non-rotating counterpart, which is a natural consequence of the lifting effect of the centrifugal force. This conclusion holds also in our differentially rotating white dwarf models (Fig. 4.4). However, as we shall see in Sect. 4.4.2, the thermal structure in an accreting white dwarf is found to have an interesting consequence for the redistribution of angular momentum, as it affects the stability criterion for the dynamical shear instability. Therefore, before discussing the angular momentum transport, we examine the evolution of the thermal structure in our white dwarf models.

Fig. 4.4 displays the temperature profiles of selected white dwarf models of different sequences. The non-rotating models (Fig. 4.4a) show a rapid increase of the central temperature, from 10^8 K when $M_{\rm WD} = 0.96$ $M_\odot$ to $2.7 \cdot 10^8$ K when $M_{\rm WD} = 1.37$ $M_\odot$. In the

Table 4.2: Properties of the computed model sequences. The first column gives the system number. The other columns have the following meanings. M_{init}: initial mass, $\dot{M}$: accretion rate, f: fraction of j_{K} of the accreted matter (see Eq. 4.18), f_μ : efficiency parameter of the μ gradient, $\dot{E}_{\mathrm{rot}}$: rotational energy dissipation by friction, $M_{0.10}$: white dwarf mass when the ratio of the rotational energy to the gravitational potential energy (T/W) reaches 0.10. The remaining physical quantities are also estimated at this point, i.e., when $T/W = 0.10$. $\rho_{\mathrm{c},0.10}$ and $T_{\mathrm{c},0.10}$: central density and temperature. $R_{0.10}$: radius of white dwarf defined on the sphere of the volume of the equipotential surface. $J_{0.10}$: total angular momentum, $\Omega_{0.10}$: moment - of - inertia - weighted mean of angular velocity.

No.	M_{init}	$\dot{M}$	f	f_μ	$\dot{E}_{\mathrm{rot}}$	$M_{0.10}$	$\rho_{\mathrm{c},0.10}$	$T_{\mathrm{c},0.10}$	$R_{0.10}$	$J_{0.10}$	$\Omega_{0.10}$
		10^{-7}					10^8	10^8	0.01	10^{50}	
	$M_\odot$	$M_\odot/\mathrm{yr}$				$M_\odot$	g/cm^3	K	$R_\odot$	erg s	rad/s
A1	0.8	3.0	1.0	0.05	Yes	1.16	0.29	0.92	1.22	1.10	0.68
A2	0.8	5.0	1.0	0.05	Yes	1.18	0.32	0.97	1.26	1.13	0.70
A3	0.8	7.0	1.0	0.05	Yes	1.19	0.33	1.01	1.34	1.14	0.69
A4	0.8	10.0	1.0	0.05	Yes	1.21	0.35	1.07	1.39	1.17	0.71
A5	0.9	3.0	1.0	0.05	Yes	1.28	0.58	1.02	1.02	1.18	0.95
A6	0.9	5.0	1.0	0.05	Yes	1.30	0.64	1.11	1.03	1.21	0.99
A7	0.9	7.0	1.0	0.05	Yes	1.32	0.69	1.17	1.03	1.23	1.02
A8	0.9	10.0	1.0	0.05	Yes	1.34	0.75	1.23	1.05	1.25	1.06
A9	1.0	3.0	1.0	0.05	Yes	1.41	1.30	1.14	0.82	1.26	1.40
A10	1.0	5.0	1.0	0.05	Yes	1.42	1.39	1.22	0.83	1.25	1.43
A11	1.0	7.0	1.0	0.05	Yes	1.43	1.52	1.28	0.82	1.27	1.49
A12	1.0	10.0	1.0	0.05	Yes	1.45	1.67	1.36	0.83	1.28	1.56
B1	0.8	3.0	0.5	0.05	Yes	1.21	0.36	0.96	1.17	1.17	0.76
B2	0.8	5.0	0.5	0.05	Yes	1.25	0.42	1.04	1.20	1.22	0.81
B3	0.8	7.0	0.5	0.05	Yes	1.26	0.44	1.09	1.24	1.23	0.82
B4	0.8	10.0	0.5	0.05	Yes	1.30	0.52	1.16	1.23	1.27	0.89
B5	0.9	3.0	0.5	0.05	Yes	1.32	0.69	1.03	0.97	1.24	1.04
B6	0.9	5.0	0.5	0.05	Yes	1.35	0.79	1.12	0.97	1.27	1.11
B7	0.9	7.0	0.5	0.05	Yes	1.38	0.90	1.12	0.96	1.29	1.18
B8	0.9	10.0	0.5	0.05	Yes	1.41	1.04	1.27	0.97	1.32	1.26
B9	1.0	3.0	0.5	0.05	Yes	1.45	1.61	1.18	0.78	1.30	1.56
B10	1.0	5.0	0.5	0.05	Yes	1.46	1.76	1.27	0.78	1.30	1.62
B11	1.0	7.0	0.5	0.05	Yes	1.48	2.00	1.34	0.78	1.31	1.72
B12	1.0	10.0	0.5	0.05	Yes	1.51	2.33	1.44	0.77	1.32	1.84
C1	0.8	3.0	0.3	0.05	Yes	1.53	1.55	1.17	0.77	1.48	1.57
C2	0.8	5.0	0.3	0.05	Yes	1.50	1.25	1.19	0.84	1.46	1.41
C3	0.8	7.0	0.3	0.05	Yes	1.46	1.05	1.20	0.90	1.44	1.29
C4	0.8	10.0	0.3	0.05	Yes	1.42	0.85	1.21	1.01	1.40	1.15
C9	1.0	3.0	0.3	0.05	Yes	1.73	19.0	2.16	0.42	1.25	5.03
C10	1.0	5.0	0.3	0.05	Yes	1.72	16.2	2.04	0.44	1.27	4.65
C11	1.0	7.0	0.3	0.05	Yes	1.72	14.3	2.06	0.46	1.29	4.38
C12	1.0	7.0	0.3	0.05	Yes	1.71	12.1	2.01	0.49	1.31	4.04
D2	0.8	5.0	1.0	1.00	Yes	1.18	0.32	0.97	1.27	1.13	0.69
D6	0.9	5.0	1.0	1.00	Yes	1.30	0.64	1.11	1.03	1.21	0.99
T2	0.8	5.0	1.0	0.05	No	1.12	0.27	0.95	1.24	1.02	0.63
T6	0.9	5.0	1.0	0.05	No	1.26	0.56	1.03	0.97	1.15	0.93
T10	1.0	5.0	1.0	0.05	No	1.40	1.24	1.14	0.81	1.24	1.37

Table 4.3: Continued from Table 4.2. The symbols in the columns have the same meaning with those in Table 4.2, but when $T/W = 0.14$ and $T/W = 0.18$ for the indices 0.14 and 0.18, respectively.

| No.	$M_{0.14}$	$\rho_{c,0.14}$	$T_{c,0.14}$	$R_{0.14}$	$J_{0.14}$	$\Omega_{0.14}$	$M_{0.18}$	$\rho_{c,0.18}$	$T_{c,0.18}$	$R_{0.18}$	$J_{0.18}$	$\Omega_{0.18}$
	10^8	10^8	0.01	10^{50}			10^8	10^8	0.01	10^{50}	
	$M_\odot$	g/cm^3	K	$R_\odot$	erg s	rad/s	$M_\odot$	g/cm^3	K	$R_\odot$	erg s	rad/s
A1	1.31	0.42	0.94	1.10	1.54	0.97	1.45	0.56	0.96	1.01	1.97	1.26
A2	1.34	0.47	1.01	1.11	1.58	1.02	1.47	0.63	1.04	1.01	1.99	1.32
A3	1.35	0.49	1.06	1.13	1.59	1.03	1.48	0.66	1.09	1.03	2.00	1.34
A4	1.37	0.54	1.12	1.15	1.63	1.07	1.50	0.73	1.15	1.04	2.03	1.40
A5	1.42	0.78	1.03	0.93	1.62	1.30	1.55	1.04	1.74	0.87	2.02	1.68
A6	1.44	0.87	1.11	0.93	1.63	1.36	1.56	1.15	1.15	0.87	2.01	1.74
A7	1.46	0.97	1.17	0.93	1.65	1.42	1.58	1.28	1.21	0.85	2.03	1.83
A8	1.48	1.07	1.23	0.93	1.67	1.48	1.60	1.42	1.28	0.85	2.04	1.92
A9	1.55	1.78	1.18	0.76	1.66	1.90	1.69	2.56	1.28	0.69	2.03	2.54
A10	1.55	1.88	1.26	0.77	1.65	1.94	1.67	2.55	1.33	0.71	2.01	2.52
A11	1.57	2.08	1.33	0.76	1.66	2.03	1.69	2.82	1.40	0.70	2.00	2.63
A12	1.58	2.31	1.40	0.75	1.66	2.12	1.70	3.13	1.49	0.70	2.00	2.75
B1	1.36	0.51	0.96	1.06	1.61	1.07	1.50	0.71	1.00	0.97	2.03	1.41
B2	1.40	0.62	1.05	1.05	1.66	1.16	1.54	0.85	1.09	0.96	2.07	1.53
B3	1.41	0.65	1.10	1.05	1.67	1.19	1.55	0.89	1.14	0.96	2.07	1.55
B4	1.45	0.78	1.17	1.06	1.71	1.28	1.58	1.07	1.22	0.95	2.09	1.69
B5	1.46	0.95	1.06	0.90	1.66	1.43	1.60	1.32	1.12	0.82	2.06	1.88
B6	1.49	1.12	1.15	0.89	1.68	1.54	1.63	1.56	1.22	0.81	2.07	2.02
B7	1.52	1.28	1.22	0.86	1.70	1.63	1.65	1.79	1.29	0.81	2.07	2.15
B8	1.55	1.52	1.31	0.87	1.72	1.76	1.67	2.12	1.39	0.77	2.07	2.32
B9	1.60	2.38	1.36	0.71	1.70	2.19	1.75	3.94	1.40	0.62	2.05	3.13
B10	1.60	2.52	1.34	0.72	1.68	2.23	1.74	3.81	1.46	0.64	2.02	3.05
B11	1.62	2.90	1.42	0.70	1.68	2.38	1.75	4.32	1.54	0.64	2.01	3.22
B12	1.64	3.43	1.53	0.68	1.68	2.56	1.75	4.91	1.65	0.61	1.98	3.42
C1	1.74	3.36	1.36	0.64	1.87	2.62	1.87	6.30	1.57	0.54	2.13	3.99
C2	1.71	2.66	1.38	0.69	1.89	2.35	1.86	5.02	1.58	0.59	2.17	3.58
C3	1.68	2.18	1.37	0.74	1.89	2.13	1.84	4.13	1.57	0.63	2.20	3.27
C4	1.64	1.69	1.35	0.81	1.88	1.88	1.81	3.20	1.54	0.69	2.23	2.89
D2	1.34	0.47	1.01	1.11	1.58	1.02	1.47	0.63	1.04	1.01	1.99	1.32
D6	1.44	0.87	1.11	0.94	1.63	1.36	1.56	1.15	1.15	0.87	2.01	1.74
T2	1.26	0.37	0.95	1.12	1.45	0.90	1.38	0.47	0.95	1.05	1.85	1.14
T6	1.39	0.72	1.02	0.94	1.57	1.25	1.51	0.72	1.02	0.94	1.57	1.25
T10	1.52	1.57	1.15	0.76	1.63	1.79	1.64	2.06	1.21	0.71	2.00	2.29
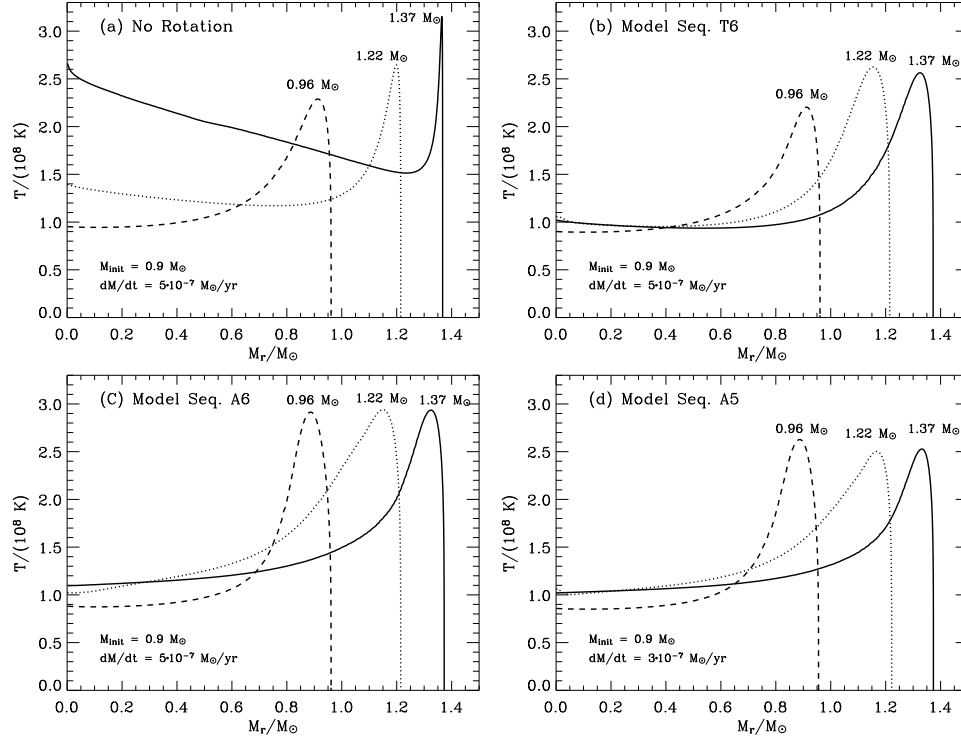
Figure 4.4: Temperature as a function of the mass coordinate in white dwarf models when M_{WD} = 0.96, 1.22 and 1.37 M$_\odot$. (a) non-rotating case with M_{init} = 0.9 M$_\odot$ and $\dot{M}$ = 5 · 10^{-7}, (b) model sequence T6, (c) model sequence A6, (d) model sequence A6.

corresponding rotating models (Fig. 4.4b & c), the change in the central temperature is not significant in the considered period.

A comparison of Fig. 4.4b and Fig. 4.4c shows the effects of rotational energy dissipation ($\dot{E}_{\mathrm{rot}}$) described by Eq. 4.16. In model sequence T6 (Fig. 4.4b), where $\dot{E}_{\mathrm{rot}}$ is neglected, the white dwarf models are cooler than in the corresponding models with $\dot{E}_{\mathrm{rot}}$ considered (sequence A6, Fig. 4.4c). As shown in Fig. 4.5, the rotational energy dissipation rate can be as high as $10^3 \ldots 10^4$ erg/g/s in the degenerate core, and even higher close to the surface. The integrated energy dissipation rate $\dot{E}_{\mathrm{rot}} = \int \epsilon_{\mathrm{diss}} dM_{\mathrm{r}}$ reaches several times 10^2 L$_\odot$ in these models. This results in a heating of the region with a strong shear motion (cf. Fig. 4.6 below), with the consequence that the temperature maxima when M_{WD} = 0.96, 1.22 and 1.37 M$_\odot$ in models of sequence A6 are higher than in the models of sequence T6. The accretion induced heating is a sensitive function of the accretion rate: comparison of Fig. 4.4c with Fig. 4.4d indicates that the white dwarf becomes significantly hotter with a higher accretion rate. The effects of the accretion rate and of $\dot{E}_{\mathrm{rot}}$ for the angular
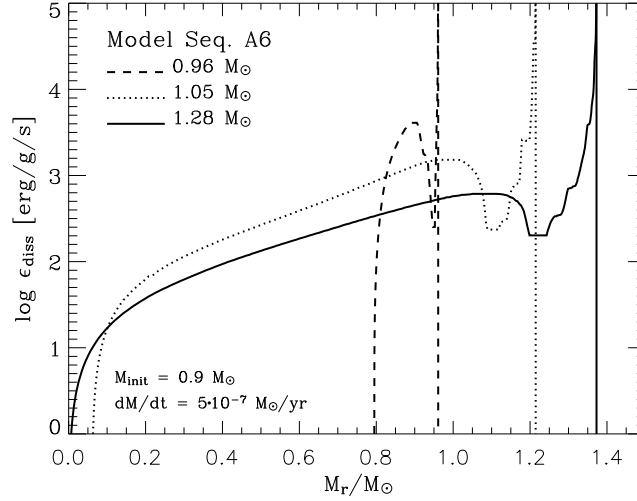
Figure 4.5: Rotational energy dissipation rate (see Eq. 4.16) as function of the mass coordinate, when $M_{WD} = 0.98$, 1.22 and 1.37 $M_\odot$ in model sequence A6.

momentum transport are discussed in Sect. 4.4.3.

Note that in all white dwarf models, there exists an absolute temperature maximum in the outer layers of the degenerate core. Below this temperature peak, the temperature gradient ∇ becomes negative and large. This produces a strong buoyancy force in this region, since the Brunt-Väisälä frequency is proportional to $\nabla_{ad} - \nabla$. The temperature peak moves outward as the white dwarf accretes more mass. This leads to changes in the local thermodynamic condition which plays a key role for the angular momentum transport from the outer envelope into the inner core, as shown in the next section.

4.4.2 White dwarf spin and angular momentum transport

Our white dwarf models are spun up as they gain angular momentum from the accreted matter, as described in Sect. 4.3.3. Fig. 4.6 shows the evolution of the angular velocity profiles in model sequences A2, A6, A10 and D6. Most strikingly, all white dwarf models rotate differentially, as predicted from the discussions in Sect. 4.2. Note also that in every white dwarf model in Fig. 4.6, a maximum angular velocity occurs, such that $\sigma > 0$ in the inner core and $\sigma < 0$ in the outer layers. This maximum comes into existence soon after the onset of mass accretion because the slowly rotating inner part contracts faster than the rapidly rotating surface layers as the total mass increases.

Since angular momentum is transported in the direction of decreasing angular velocity, this peak in ω serves as a bottleneck for the angular momentum transport from the outer
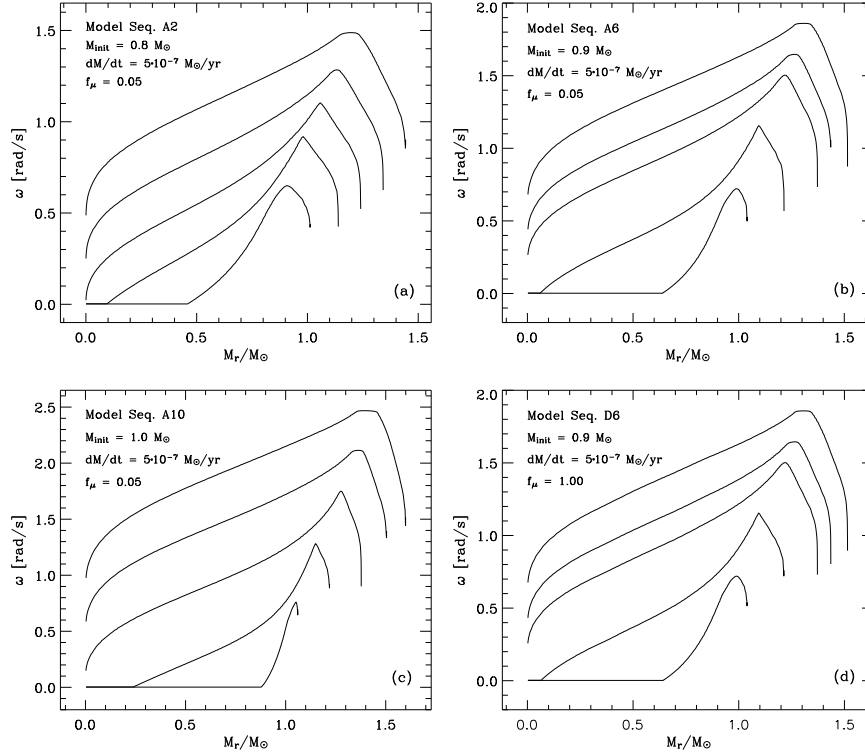
Figure 4.6: Angular velocity as a function of the mass coordinate at different white dwarf masses. Panels (a), (b), (c) & (d) give results for model sequences A2, A6, A10 and D6, respectively (see Table 4.2).

envelope into the core. It prevents the outer envelope from slowing down efficiently by inward angular momentum transport. As a result, the surface remains to rotate close to the critical value throughout the evolution, severely limiting the angular momentum gain from the accreted matter. I.e., about 60 % of the angular momentum of the accreted matter is rejected by the condition posed in Eq. 4.18, and only about 40 % is actually retained by the time the white dwarf mass reaches $1.4 \, M_{\odot}$, in all model sequences (see Fig. 4.11 below).

Fig. 4.7 shows the shear factor σ as a function of the mass coordinate at two different evolutionary epochs ($M_{\mathrm{WD}} = 1.26$ & $1.37 \, M_{\odot}$) in model sequence A6. The dashed line gives the threshold value of the shear factor ($\sigma_{\mathrm{DSI,crit}}$). Note that the two, i.e., σ and $\sigma_{\mathrm{DSI,crit}}$ converge remarkably well in the white dwarf interior, i.e., in $M_{\mathrm{r}} \lesssim 1.1 \, M_{\odot}$ when $M_{\mathrm{WD}} = 1.26 \, M_{\odot}$ and $M_{\mathrm{r}} \lesssim 1.2 \, M_{\odot}$ when $M_{\mathrm{WD}} = 1.37 \, M_{\odot}$. This confirms the conclusion given in Sect. 4.2 that the degenerate core of an accreting white dwarf will rotate differ-
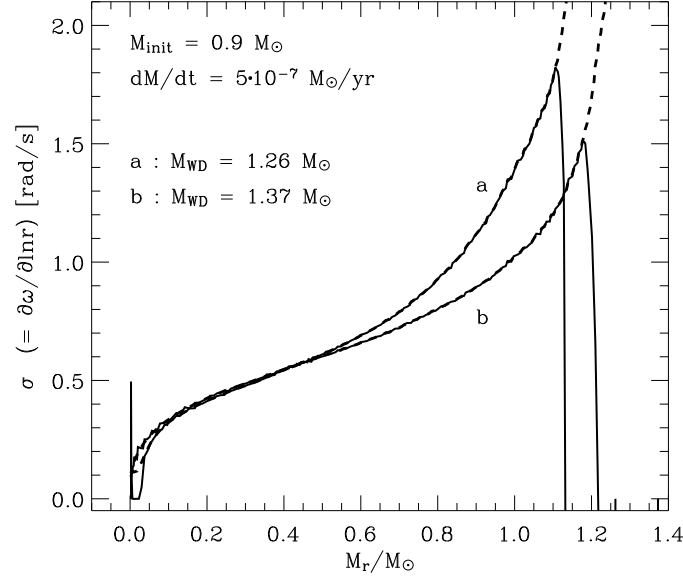
Figure 4.7: Shear factor σ $(= \partial\omega/\partial \ln r)$ as a function of the mass coordinate in two different white dwarf models at $M_{WD} = 1.26$ $M_\odot$ and 1.37 $M_\odot$ from model sequence A6. The dashed lines denote the threshold value of σ for the dynamical shear instability (i.e., $\sigma_{DSI,crit} = (N^2/R_{i,c})^{1/2}$, see Eq. 4.7).

entially with the shear strength near the threshold value for the dynamical instability. As already discussed in Sect. 4.2.2, this is because any strong shear motion with $\sigma > \sigma_{DSI,crit}$ can not be retained for a long time and should decay to $\sigma_{DSI,crit}$ quickly via the dynamical shear instability, and because further angular momentum transport by other mechanisms requires a longer time scale compared to the accretion time scale.

Fig. 4.8 depicts the situation in more detail. The right hand panel of this figure shows the various diffusion coefficients as a function of the mass coordinate in the white dwarf models of sequence A6 when $M_{WD} = 1.26$ and 1.37 $M_\odot$. This figure shows that the white dwarf consists of an inner dynamical shear unstable region and an outer region dominated by the secular shear instability and Eddington Sweet circulations. Let us define $M_{r,DSI}$ as the mass coordinate at the point which divides the white dwarf into these two regions. $M_{r,DSI}$ changes with time not only due to the change of the shear strength, but also due to the evolution of the thermodynamic properties as explained below.

As shown in Sect. 4.4.1, the accretion induced heating results in a temperature maximum in the outer region of an accreting white dwarf. A steep negative temperature gradient (i.e., $\nabla < 0$) thus appears just below this temperature peak. The buoyancy force is enhanced in
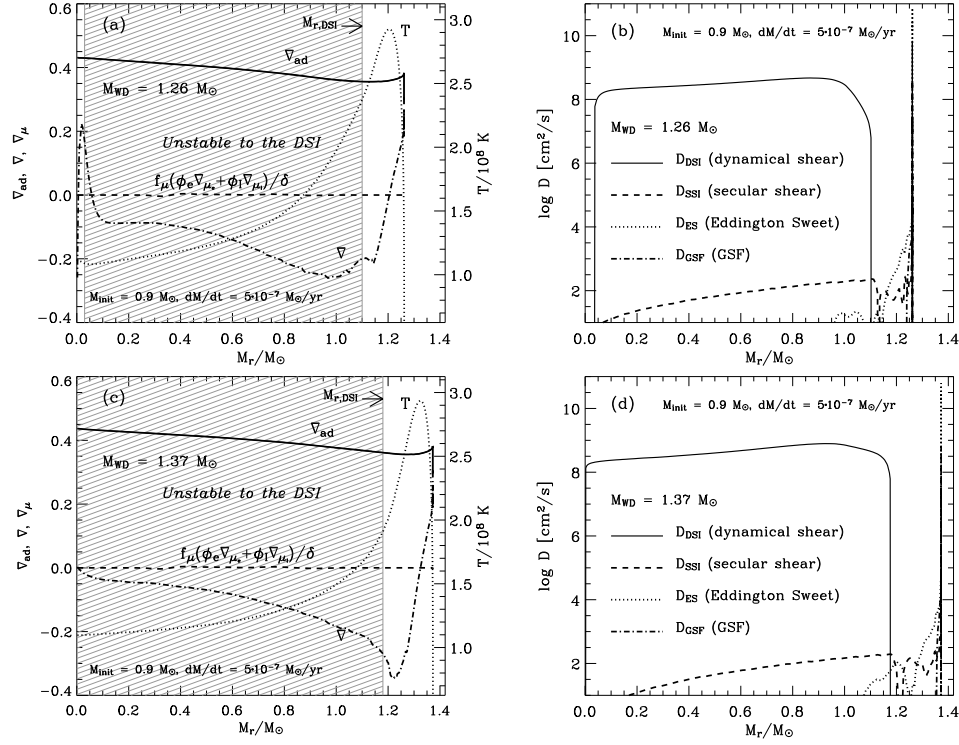
Figure 4.8: (a) Thermodynamic quantities as a function of the mass coordinate, in the white dwarf model of sequence A6 when $M_{WD} = 1.26\ M_\odot$: ∇_{ad} (solid line), ∇ (dot-dashed line), $f_\mu(\varphi_e \nabla_{\mu_e} + \varphi_I \nabla_{\mu_I})/\delta$ where $f_\mu = 0.05$ (dashed line) and temperature (dotted line). The region where the white dwarf is unstable to the dynamical shear instability is hatched. (b) Diffusion coefficients for rotationally induced hydrodynamic instabilities, as a function of the mass coordinate, in the white dwarf model of sequence A6 at $M_{WD} = 1.26\ M_\odot$. The solid line denotes the diffusion coefficient for the dynamical shear instability, the dashed line, the dotted line and the dashed-dotted lines are for the secular shear instability, the Eddington Sweet circulation, and the GSF instability respectively. (c) Same as in (a) but for $M_{WD} = 1.27\ M_\odot$ (d) Same as in (b) but for $M_{WD} = 1.37\ M_\odot$

this region, which leads to stability against the dynamical shear instability (See Eqs. 4.3–4.6). Therefore, the location of $M_{r,DSI}$ is below the region containing the strong temperature gradient, as demonstrated in Fig. 4.8.

According to Fig. 4.8, $M_{r,DSI}$ moves outward as the white dwarf mass increases (See also Fig. 4.7 and Fig. 4.9). This outward shift of $M_{r,DSI}$ can be understood as follows. As shown in Fig. 4.7, the threshold value $\sigma_{DSI,crit}$ becomes smaller near $M_{r,DSI}$ as the white dwarf mass increases. Two processes contribute to this effect. First, the degeneracy at a given M_r becomes stronger as the white dwarf mass increases, reducing the buoyancy
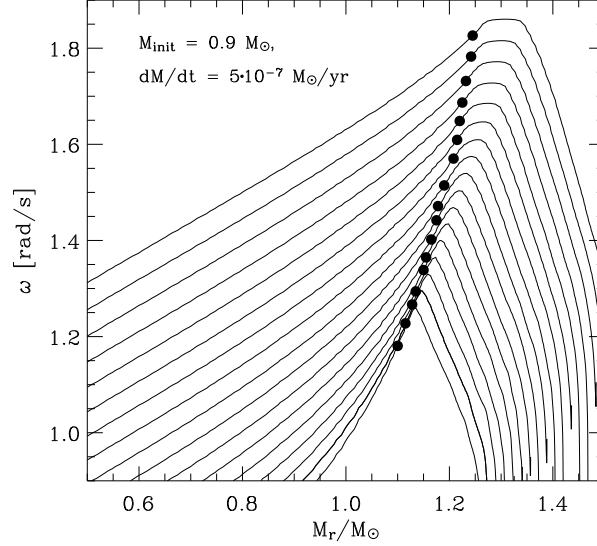
Figure 4.9: Angular velocity profiles given as a function of the mass coordinate at 17 different evolutionary epochs of sequence A6: 1.26, 1.28, 1.30, 1.31, 1.33, 1.34, 1.36, 1.37, 1.38, 1.40, 1.42, 1.44, 1.45, 1.47, 1.48, 1.50, 1.52 $M_\odot$, from the bottom to the top. The filled circles designate the mass coordinate $M_{\rm rm,DSI}$, below which the white dwarf interior is dynamical shear unstable.

force. Second, the region with strong temperature stratification with $\nabla < 0$ moves outward as indicated in Fig. 4.8a and Fig. 4.8c. Consequently the dynamical shear unstable region gets extended outward with time as shown in Figs. 4.8 and 4.9. The outward shift of $M_{\rm r,DSI}$ allows the angular momentum from the outer layers to be transported inward, and thus leads to the outward shift of the position of the maximum angular velocity as shown in Fig. 4.9.

Fig. 4.10 shows how much angular momentum is actually transported into the white dwarf interior in model sequence A6. Here $J(M_{\rm r}) = \int_0^{M_{\rm r}} j(m)dm$ is the integrated angular momentum. In a rigidly rotating homogeneous body, we have $J(M_{\rm r})/M_r^{5/3} = {\rm const.}$, and therefore any deviation from the zero gradient in $J(M_{\rm r})/M_r^{5/3}$ may serve as a measure of the degree of differential rotation. A comparison of different evolutionary epochs demonstrates the flow of angular momentum through the mass shells, as $J(M_{\rm r})$ and $J(M_{\rm r})/M_r^{5/3}$ would remain constant in a given mass shell throughout the evolution if no angular momentum were transported through this shell. Note that all the white dwarf models in this figure have a similar amount of angular momentum ($J \simeq 10^{50}$ erg s) at around $M_{\rm r} \sim 1.2$ $M_\odot$, which is close to the angular velocity peaks shown in Fig. 4.9. The angular momentum transport from this point into the further interior is shown to be efficient, due to the dynam-
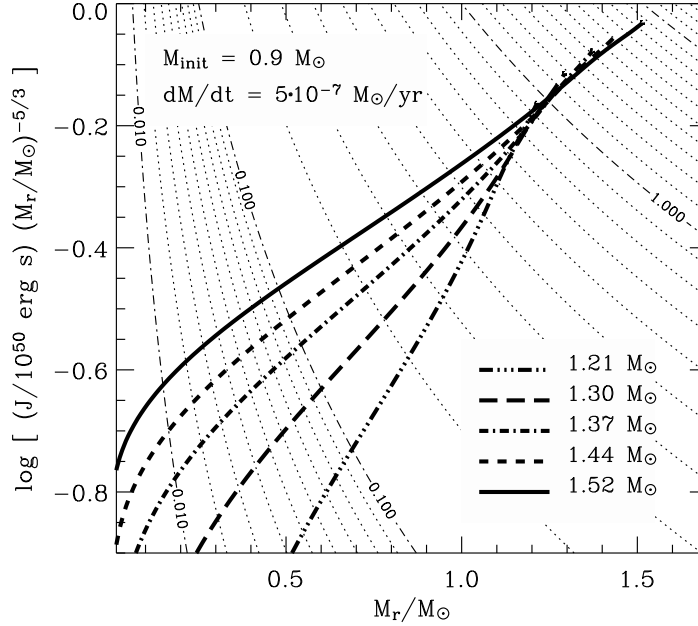
Figure 4.10: Integrated angular momentum $J(M_r) = \int_0^{M_r} j(m)dm$ divided by $M_r^{5/3}$, as a function of the mass coordinate at five different evolutionary epochs of sequence A6: M_{WD} = 1.21, 1.30, 1.37, 1.44 and 1.52 $M_\odot$. The thin contour lines denote levels of constant J in logarithmic scale, labeled with $\log(J/10^{50}\text{ergs})$.

ical shear instability as described above.

We summarize the main conclusions from this section as follows. a) We find accreting white dwarf models to rotate differentially throughout their evolution. b) The dynamical shear instability is the most important mechanism for angular momentum transport in the highly degenerate core of our white dwarf models. c) The angular momentum gain from the accreted matter and the spin-up of our accreting white dwarfs is closely related to their restructuring and thermal evolution as their mass increases.

4.4.3 Influence of physical assumptions

Having understood the detailed processes of the angular momentum transport in an accreting white dwarf, let us consider the influence of the different initial conditions and physical assumptions on the evolution of accreting white dwarfs.

Influence of the initial white dwarf mass

Tables 4.2 and 4.3 give the white dwarf mass when the ratio of the rotational energy to the gravitational potential energy ($E_{\mathrm{rot}}/|W|$) in each model sequence reaches 0.1, 0.14 and 0.18 ($M_{0.1}$, $M_{0.14}$ and $M_{0.18}$). It is believed that a rapidly rotating white dwarf becomes secularly unstable when $E_{\mathrm{rot}}/|W| \simeq 0.14$ (e.g. Durisen & Imamura 1981). Imamura et al (1995) found that this critical value can be lowered to about 0.1 for strong differential rotation (see detailed discussion in Sect. 4.5).

The tables show that the lower the initial mass, the higher the values of $M_{0.10}$ and $M_{0.14}$ become. For example, $M_{0.14}$ increases from 1.34 $M_\odot$ to 1.55 $M_\odot$ with a change of the initial mass from 0.8 $M_\odot$ to 1.0 $M_\odot$ in the case of $f = 1$ (sequences A2 and A10). The total angular momentum also increases at a given $E_{\mathrm{rot}}/|W|$ with higher initial mass. This tendency is simply due to the fact that more angular momentum gain is necessary to reach a certain amount of $E_{\mathrm{rot}}/|W|$ if a white dwarf is more massive.

Influence of the angular momentum gain parameter f

As indicated in Tables 4.2 and 4.3, model sequences with $f = 1.0$ and those with $f = 0.5$ show some differences in the results. The adoption of $f = 0.5$ yields a larger white dwarf mass at a given $E_{\mathrm{rot}}/|W|$, by about $0.05 - 0.06$ $M_\odot$, which is a natural consequence of less angular momentum being accreted per unit time (Eq. 4.18). This effect becomes more prominent with $f = 0.3$, and $M_{0.1}$ increases by about 24 % and 17 % for $M_{\mathrm{init}} = 0.8$ $M_\odot$ and $M_{\mathrm{init}} = 1.0$ $M_\odot$ respectively, compared to the case of $f = 1$. Furthermore, the models with $M_{\mathrm{init}} = 1.0$ $M_\odot$ and $f = 0.3$ reach central carbon ignition when $E_{\mathrm{rot}}/|W|$ reaches about 0.11.

Interestingly, the helium accreting white dwarf models by Yoon et al. (2004), where $f = 1$ is adopted, show similar $E_{\mathrm{rot}}/|W|$ values at a given mass as the present CO accreting white dwarf models with $f = 0.3$. As mentioned in Sect. 4.3.2, this difference is mainly due to the fact that the angular momentum transport efficiency in the outermost layers is affected by the energy generation in the helium burning shell. In particular, the Eddington Sweet circulation becomes more efficient due to shell burning, resulting in a more efficient outward angular momentum transport in the non-degenerate envelope (cf. Fig. 4.6). This causes a more severe restriction of the angular momentum gain from the accreted matter, due to the condition posed by Eq. 4.18. This implies that the history of the angular momentum gain may also be different for hydrogen accreting cases.

However, these ambiguities concern only the actual amount of the angular momentum gain from the accreted matter, but do not affect the history of the angular momentum redistribution in the degenerate core, where differential rotation persists during the mass accretion phase (Sect. 4.2.2 and 4.4.2). In fact, despite big differences in f, all model sequences show the same remarkable feature that carbon ignition is not reached even when $M_{\mathrm{WD}} \gtrsim 1.4$ $M_\odot$, due to differential rotation.

Influence of accretion rate and dissipation

Tables 4.2 and 4.3 show that with a given initial mass, the white dwarf mass at given $E_{\rm rot}/|W|$ increases for higher accretion rate. Fig. 4.11 gives the accumulated angular momentum ($\Delta J_{\rm accreted}$) in the white dwarf, as well as the accumulated rejected angular momentum ($\Delta J_{\rm rejected}$) according to Eq. 4.18, as a function of the white dwarf mass, for sequences with $M_{\rm init} = 0.9~{\rm M}_\odot$, and for three different accretion rates as indicated in the figure. It is shown that the higher the accretion rate, the more angular momentum is rejected and the less angular momentum is accreted, which is the reason for the higher white dwarf mass at a given $E_{\rm rot}/|W|$ for a higher accretion rate.

This accretion rate dependence can be explained by two factors. First, with a lower accretion rate, a white dwarf gains a smaller amount of angular momentum per time and thus has more time to transport angular momentum into the white dwarf interior. Second, as already pointed out in Sect. 4.4.1, a higher accretion rate results in a stronger accretion induced heating, which leads to higher temperatures inside the white dwarf (Fig. 4.4). This reduces the degeneracy in the white dwarf interior, and the buoyancy force becomes accordingly stronger. This thermal effect changes the stability condition for the dynamical shear instability in the white dwarf interior: the higher the accretion rate, the less susceptible to the dynamical shear instability it is, which in turn limits the angular momentum transfer from the outer envelope into the interior more severely.

We can also understand why the white dwarf mass at a given $E_{\rm rot}/|W|$ is smaller when $\dot{E}_{\rm rot}$ is neglected (Tables 4.2 and 4.3) in terms of different thermal structures: the white dwarf temperature becomes significantly lower without $\dot{E}_{\rm rot}$ as shown in Fig. 4.4, resulting in a lower buoyancy force in the white dwarf interior and thus a more efficient angular momentum transport.

Influence of chemical gradients

In the model sequences discussed in the previous sections, the effect of μ-gradients is significantly reduced by using $f_\mu = 0.05$, as described in Sect. 4.3.3. In order to understand the importance of chemical gradients for the angular momentum evolution, two model sequences (D2 and D6) are computed with $f_\mu = 1.0$. The results are presented in Table 4.2 and 4.3. Interestingly, it is found that the adoption of different f_μ has hardly any effect. For instance, we have exactly the same values for $M_{0.1}$, $M_{0.14}$ and $M_{0.18}$ in the two corresponding model sequences A2 and D2, as well as in A6 and D6.

Fig. 4.12a shows the chemical structure in two white dwarf models of sequence D6, in the initial model (0.9 ${\rm M}_\odot$) and when $M_{\rm WD} = 1.37~{\rm M}_\odot$. The model at 1.37 ${\rm M}_\odot$ shows that although the rotationally induced chemical mixing smoothes out the chemical structure significantly, a strong stratification in the chemical composition persists in the range $M_{\rm r} = 0.4 - 0.8~{\rm M}_\odot$. Nevertheless, its contribution to the total buoyancy force turns out to be too small to suppress the dynamical shear instability, as implied in Fig. 4.12b. The term $(\varphi_{\rm e}\nabla_{\mu_{\rm e}} + \varphi_{\rm I}\nabla_{\mu_{\rm I}})/\delta$ has a maximum value of about 0.1, which is only 25 % of $\nabla_{\rm ad}$.

In conclusion, the effect of chemical gradients on the angular momentum transport is
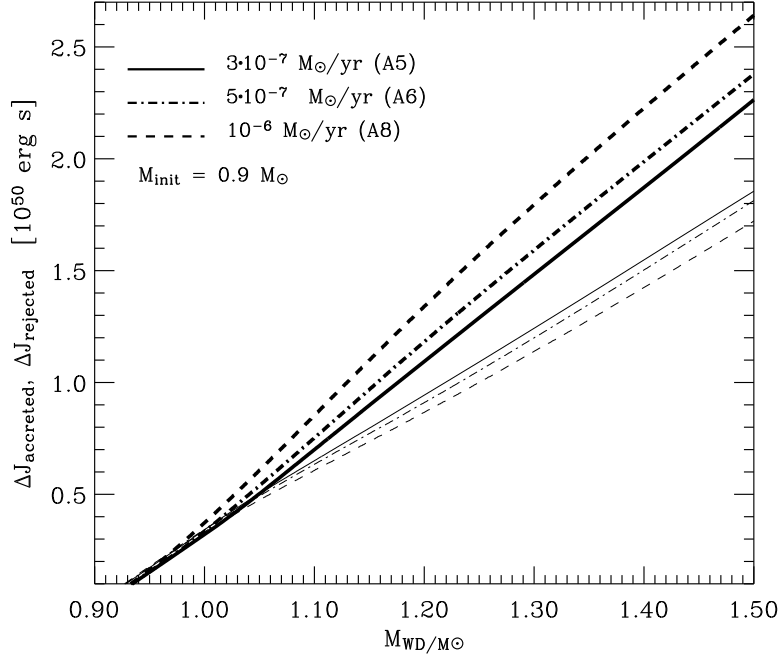
Figure 4.11: The evolution of the accumulated angular momentum in model sequences A5, A6 and A10, given as a function of the white dwarf mass. The thin lines denote the accumulated total angular momentum in the white dwarf models. The thick lines give the accumulated rejected angular momentum by Eq. 4.18.

negligible in the white dwarf interior, unlike in non-degenerate stars.

Limitations of our 1D approximation

As pointed out in Sect. 4.3.3, our one-dimensional description of rotation works accurately up to about 60% of Keplerian rotation. In our white dwarf models, however, the fast rotating outer layers exceed this limit (cf. Fig. 4.13). For instance, in model sequence A6, the outer 19 % in mass rotate faster than 60 % of the Keplerian value when $E_{\rm rot}/|W| = 0.1$. This fast rotating region increases to 27 % in mass when $E_{\rm rot}/|W|$ reaches 0.14. This means that our numerical models underestimate the effect of the centrifugal force on the white dwarf structure.

The accreting white dwarf models by Durisen (1977) may be the most appropriate to evaluate the uncertainty due to the underestimation of the centrifugal force in the outer envelope. In his two dimensional models, the inner dense core with $\rho > 0.1\rho_{\rm c}$ remains close
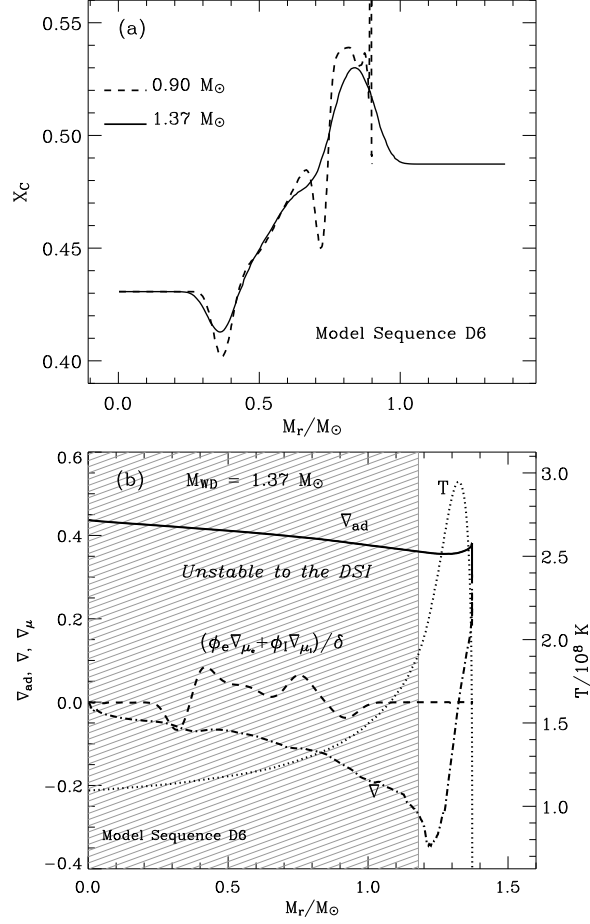
Figure 4.12: (a) Mass fraction of carbon as a function of the mass coordinate in two white dwarf models of sequence D6, at $M_{WD} = 0.9$ M$_\odot$ (initial model, dashed line) and 1.37 M$_\odot$ (solid line). (b) Thermodynamic quantities as a function of the mass coordinate for the same models: ∇_{ad} (solid line), ∇ (dot-dashed line), $(\varphi_e \nabla_{\mu_e} + \varphi_I \nabla_{\mu_I})/\delta$ (dashed line) and temperature (dotted line). The region where the white dwarf is unstable to the dynamical shear instability is hatched.

to spherical, and the outer layers with $\rho < 0.1\rho_c$ start deviating from spherical symmetry, becoming toroidal. Consequently, the outer envelope is considerably extended, and the ratio of the polar to the equatorial radius (R_p/R_e) becomes as small as 0.4 when $E_{rot}/|W|$ reaches 0.1.

Figure 4.13: Angular velocity normalized to the local Keplerian value, as a function of the mass coordinate in white dwarf models of sequence A6, when $E_{\rm rot}/|W| = 0.04$, 0.07, 0.10 and 0.14
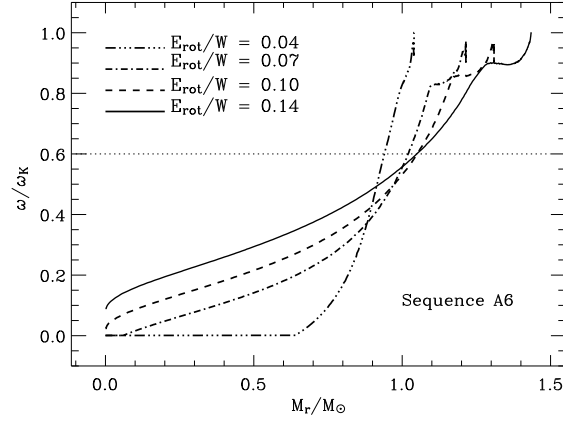
In our models, the inner slowly rotating core ($\omega < 0.6\omega_{\rm Kepler}$) has density $\rho \gtrsim 0.1\rho_{\rm c}$ in general, and therefore we may conclude that the inner core is accurately described in our calculations, although it could be implicitly affected by the underestimation of the centrifugal force in the outer envelope. However, the major qualitative conclusions of our study are not affected by this uncertainty: accreting white dwarfs will rotate differentially and can grow beyond the canonical Chandrasekhar mass without suffering central carbon ignition, unless they lose angular momentum through secular instabilities (Sect. 4.5).

4.5 On the final fate of rapidly rotating massive white dwarfs

A remarkable feature of our models is that the white dwarfs can not reach central carbon ignition even when their mass becomes significantly larger than the canonical Chandrasekhar mass of $1.4\,\rm M_\odot$ (Tables 4.2 and 4.3). For example, in model sequence A12, the central density at $M_{\rm WD} = 1.70\,\rm M_\odot$ is only $3.13 \times 10^8\,\rm g/cm^3$ (see Table 4.3), which is still far from the carbon ignition density (a few $10^9\,\rm g/cm^3$ at $T \gtrsim 10^8$ K). This is in good agreement with the conclusion of previous studies of rotating white dwarfs (cf. Sect. 4.3.1) that a white dwarf can be dynamically stable for masses up to $\sim 4.0\,\rm M_\odot$ if it rotates differentially.

If a rapidly rotating massive white dwarf would not lose angular momentum, it could not produce a Type Ia supernova. However, it is well known that rapidly rotating compact stars become secularly unstable to non-axisymmetric perturbations due to the gravitational wave radiation reaction (Chandrasekhar 1970; Friedman & Schutz 1978), which is often named CFS (Chandrasekhar, Friedman and Schutz) instability. Two representative modes are believed to be the most important ones for this instability. One is the bar-mode, i.e., the

f-mode with $l = m = 2$, of which the restoring force is the buoyancy force. Here, l and m denote the nodal numbers of the spherical harmonics. Although Friedman & Schutz (1978) found that f-modes with a higher m are more susceptible to the CFS instability compared to the case $m = 2$, their growth time is usually too long to be of astrophysical interest (e.g. Shapiro & Teukolsky 1983). Hereafter, we will refer to the CFS instability with $m = 2$ as the bar-mode instability. Recently it has been found that the CFS instability can also excite the r-mode, of which the restoring force is the Coriolis force (hereafter, r-mode instability, see Andersson & Kokkotas 2001 for a review). Here again, the mode with $m = l = 2$ is most relevant because it gives the smallest time scale for the growth of the instability.

In the following, we discuss the importance of these instabilities for our white dwarf models, and derive implications for the final fate of rapidly rotating massive white dwarfs.

4.5.1 Bar-mode instability

The bar-mode instability can operate when $E_{\rm rot}/|W|$ exceeds a certain critical value in a rotating star, as studied by many authors (Ostriker & Tassoul 1969; Ostriker & Bodenheimer 1973; Durisen 1975b, 1977; Bardeen et al. 1977; Durisen & Imamura 1981). Although the critical value $(E_{\rm rot}/|W|)_{\rm b,c}$ is found to be about 0.14 for a wide range of rotation laws and equations of state (e.g. Durisen 1975b; Karino & Eriguchi 2002), Imamura et al. (1995) showed that it tends to decrease for strong differential rotation. In particular, we note that the rotation law in our models bears a similarity to one of their rotating polytrope models with $n' = \infty$ (see Imamura et al. for the definition of n'), in which the spin rate shows a maximum where the gradient in ω changes its sign, as in our models (Fig. 4.6). In these models, $(E_{\rm rot}/|W|)_{\rm b,c}$ turns out to be as small as 0.09, which is significantly smaller than the canonical value of 0.14.

According to Chandrasekhar (1970) and Friedman & Schutz (1975), the growth time of the bar-mode instability in Maclaurin spheroids is given by

$$
\tau_{\rm bar} \sim 10^{-8} \frac{R}{c} \left(\frac{R\Omega}{c} \right)^{-6} \left[\frac{E_{\rm rot}}{|W|} - \left(\frac{E_{\rm rot}}{|W|} \right)_{\rm b,c} \right]^{-5} \text{ sec,} \tag{4.19}
$$

for $0 < E_{\rm rot}/|W| - (E_{\rm rot}/|W|)_{\rm b,c} \ll 1$, where Ω is the mean angular velocity and R is the radius.

Since we have $E_{\rm rot} \simeq k^2 M R^2 \Omega^2$ and $|W| \simeq G M^2/R$ (where k is the dimensionless radius of gyration), the growth time of the instability can be rewritten as (cf. Friedman and Schutz 1975; Hayashi et al. 1998)

$$
\tau_{\rm bar} \sim 1.6 \left(\frac{R}{0.01 {\rm R}_\odot} \right)^4 \left(\frac{M}{{\rm M}_\odot} \right)^{-3} \left(\frac{E_{\rm rot}}{|W|} \right)^{-3}
$$
$$
\times \left[\frac{E_{\rm rot}}{|W|} - \left(\frac{E_{\rm rot}}{|W|} \right)_{\rm c} \right]^{-5} \text{ sec,} \tag{4.20}
$$

where $k^2 = 0.4$ has been used. Although our white dwarf models deviate significantly from the Maclaurin spheroids, this approximation may give an order of magnitude estimate for the growth time scale of the bar-mode instability.

Fig. 4.14 shows τ_{bar} as a function of $E_{\mathrm{rot}}/|W|$ for four different masses as indicated in the figure caption. Here, $R = 0.01\,\mathrm{R}_\odot$ is assumed since the mean radii of our white dwarf models do not differ much from $0.01\,\mathrm{R}_\odot$ for all $E_{\mathrm{rot}}/|W|$ values. Two different values for $(E_{\mathrm{rot}}/|W|)_{\mathrm{b,c}}$, i.e., 0.1 and 0.14 are considered in the figure. The growth time scale of the bar-mode instability is a sensitive function of $E_{\mathrm{rot}}/|W|$, while it does not change much for different white dwarf masses: For $(E_{\mathrm{rot}}/|W|)_{\mathrm{b,c}} = 0.10$, τ_{bar} is as large as 10^{10} yr at $E_{\mathrm{rot}}/|W| \simeq (E_{\mathrm{rot}}/|W|)_{\mathrm{b,c}}$, but it drops to 10^4 yr when $E_{\mathrm{rot}}/|W| \simeq 0.12$. Furthermore, τ_{bar} becomes only about 10 yrs when $E_{\mathrm{rot}}/|W|$ approaches 0.15.

Durisen (1977) found that the angular momentum loss time scale is comparable to the growth time scale of the instability ($\tau_{J,\mathrm{bar}} \simeq \tau_{\mathrm{bar}}$), and therefore we may conclude that the bar-mode instability can be an efficient mechanism to remove angular momentum for white dwarfs with $E_{\mathrm{rot}}/|W| > (E_{\mathrm{rot}}/|W|)_{\mathrm{b,c}}$, as long as it is not suppressed by turbulent motions (see Sect. 4.5.3).

4.5.2 r-mode instability

Recently, Andersson (1998) and Friedman & Morsink (1998) have found that r-modes in all rotating inviscid stars are unstable to the CFS instability. The possibility of gravitational wave radiation from fast rotating white dwarfs due to the r-mode instability was also discussed by Hiscock (1998), Andersson et al. (1999) and Lindblom (1999). Lindblom (1999) gives the growth time scale for this instability with $m = l = 2$ as

$$\frac{1}{\tau_{\mathrm{r}}} = \frac{2\pi}{25}\left(\frac{4}{3}\right)^8 \frac{G}{c} \int_0^R \rho \left(\frac{r\Omega}{c}\right)^6 dr. \tag{4.21}$$

This time scale is plotted in Fig. 4.14 for two model sequences (A6 and A12). Interestingly, we find that the r-mode instability becomes important when $E_{\mathrm{rot}}/|W| \lesssim (E_{\mathrm{rot}}/|W|)_{\mathrm{b,c}}$, compared to the bar-mode instability. The sensitivity of the time scale τ_{r} to $E_{\mathrm{rot}}/|W|$ is much weaker than that of τ_{bar}, and τ_{r} remains in the range $10^5 \ldots 10^8$ yr for $E_{\mathrm{rot}}/|W| < (E_{\mathrm{rot}}/|W|)_{\mathrm{b,c}}$. Note that τ_{r} in our models has much smaller values than in Lindblom (1999), who found τ_{r} to be larger than 6×10^9 yr in the observed DQ Her objects. This difference is mainly due to the fact that our white dwarf models are rotating differentially, with the outer layer rotating faster than the inner core. More precise estimates of τ_{r} require, of course, a multidimensional study, which is beyond the scope of this paper. Nevertheless, the present estimates indicate that the r-mode instability might be a promising mechanism for the removal of angular momentum in a differentially rotating massive white dwarf within an interestingly short time scale ($\lesssim 10^8$ yr), when $E_{\mathrm{rot}}/|W| < (E_{\mathrm{rot}}/|W|)_{\mathrm{b,c}}$
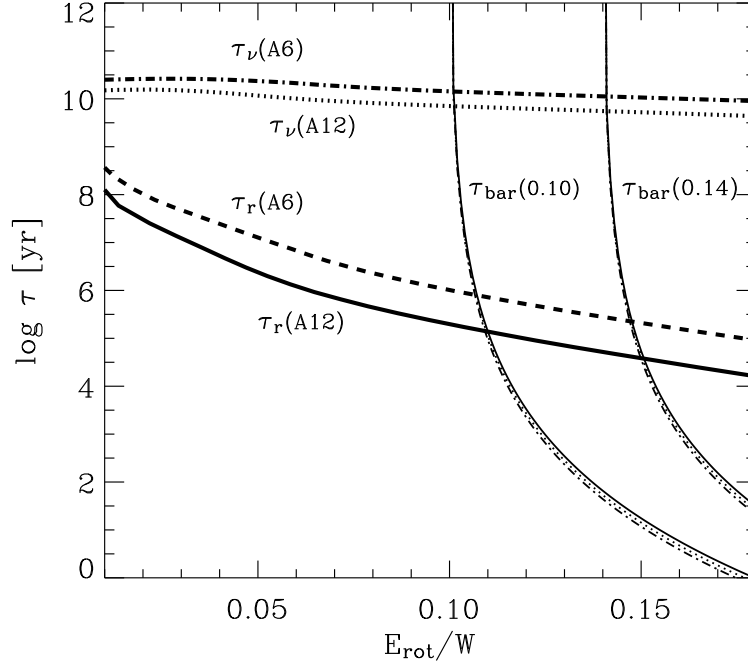
Figure 4.14: Growth time scales for the bar - mode instability (τ_{bar}, Eq. 4.20) as well as for the r-mode instability (τ_{r}, Eq. 4.21). τ_{bar} is plotted as a function of $E_{\mathrm{rot}}/|W|$, with thin lines for 3 different masses: 1.4 $M_\odot$ (solid line), 1.5 $M_\odot$ (dotted line) and 1.6 $M_\odot$ (dashed-dotted line). Two different values of $(E_{\mathrm{rot}}/|W|)_{\mathrm{b,c}}$ (0.1 and 0.14) for the bar-mode instability are considered as indicated in the figure. The thick dashed line denotes τ_{r} in the models of sequence A6, while the thick solid line is for sequence A12. The thick dashed-dotted and dotted lines give the viscous time scale for sequences A6 and A12 respectively.

4.5.3   Implications for the final fate of accreting white dwarfs

The previous sections imply that our differentially rotating massive white dwarfs can lose angular momentum via the bar-mode instability if $E_{\mathrm{rot}}/|W| \gtrsim (E_{\mathrm{rot}}/|W|)_{\mathrm{b,c}}$, and via the r-mode instability if $E_{\mathrm{rot}}/|W| \lesssim (E_{\mathrm{rot}}/|W|)_{\mathrm{b,c}}$. These instabilities would remove angular momentum from the outer layers of the white dwarfs — as shown in the numerical simulations of rotating neutron stars (Lindblom et al. 2002) — where most of the white dwarf angular momentum is located in our models.

Although the CFS instability is likely suppressed in the presence of strong viscosity for both, the r-mode and the bar-mode (e.g. Andersson & Kokkotas 2001), Imamura et al. (1995) suggest that secularly unstable modes may not necessarily be damped in the

presence of a large effective viscosity due to turbulence. Given this uncertainty, we consider both cases, i.e., we assume strong damping of secular instabilities due to turbulence induced by the shear instability as Case I, and a persistence of secular modes even when the shear instability is present, where the CFS instability is only affected by the microscopic viscosity (Case II).

Case I

If the unstable CFS modes are damped by turbulence, an accreting white dwarf will not experience any angular momentum loss due to the CFS instability during the mass accretion phase in which the dynamical and secular shear instability persist throughout the white dwarf interior (see Sect. 4.4.2), no matter how large $E_{\mathrm{rot}}/|W|$ becomes. Once the mass accretion ceases, the angular momentum redistribution in the white dwarf will continue until the degree of the differential rotation becomes weak enough for the shear instability to disappear. Once the fluid motion in the white dwarf becomes laminar, only the electron and ion viscosities will contribute to the viscous friction.

The time scale of viscous dissipation (τ_ν) through the electron and ion viscosity is plotted in Fig. 4.14 for model sequences A6 and A10. Here τ_ν is calculated following Eq. (4.2) in Lindblom (1999). It is found that τ_ν is far larger than τ_{r} and τ_{bar} (except for τ_{bar} at $E_{\mathrm{rot}}/|W| \simeq (E_{\mathrm{rot}}/|W|)_{\mathrm{b,c}}$). This implies that the unstable modes of the CFS instability will not be damped by the microscopic viscosity before they grow to a dynamically meaningful level, once the shear instability has decayed.

If the white dwarf mass has grown to $M_{\mathrm{WD}} \gtrsim 1.4\,\mathrm{M}_\odot$ by the end of the mass accretion phase, carbon ignition at the white dwarf center will be delayed as follows. After the mass accretion stops, the white dwarf will evolve without losing angular momentum until the shear instability decays. When the white dwarf interior becomes laminar, the white dwarf will begin to lose the angular momentum either by the bar-mode instability if $E_{\mathrm{rot}}/|W| > (E_{\mathrm{rot}}/|W|)_{\mathrm{b,c}}$, or by the r-mode instability if $E_{\mathrm{rot}}/|W| \lesssim (E_{\mathrm{rot}}/|W|)_{\mathrm{b,c}}$. The core density will increase as it loses angular momentum and eventually carbon will ignite at the center.

Can such a white dwarf end in a Type Ia supernova? It depends on how much time is spent from the halt of mass accretion to carbon ignition, the time scale to which we will refer as τ_{delay}. Nomoto & Kondo (1993) found that if the core of a white dwarf has solidified, core carbon ignition is likely to end in a collapse rather than an explosion. I.e., to obtain an SN Ia, carbon ignition should occur before the white dwarf core is crystallized.

In an attempt to estimate τ_{delay}, we have selected a white dwarf model which has grown in mass to $1.50\,\mathrm{M}_\odot$ in model sequence A12, and let it evolve without further mass accretion. The evolution of the angular velocity in the white dwarf model is shown in Fig. 4.15. The initial model of this calculation is characterized by $T_{\mathrm{c}} = 1.37 \times 10^8$ K, $\rho_{\mathrm{c}} = 1.87 \times 10^8$ g/cm^3 and $E_{\mathrm{rot}}/|W| = 1.11$. As the white dwarf cools, the buoyancy force in the white dwarf interior becomes weaker and thus the dynamical shear instability continues to operate in the central core even though the degree of differential rotation becomes continuously smaller. Only when $t \simeq 1.1 \times 10^8$ yr, the shear strength becomes so weak that the shear instability finally decays. The central temperature and density at this moment are 4×10^7
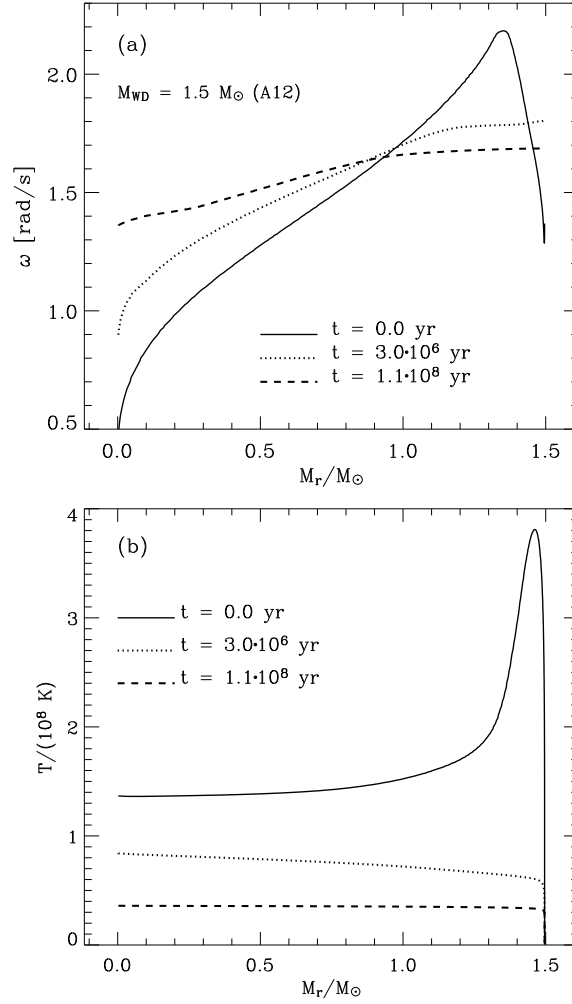
Figure 4.15: Evolution of the angular velocity in (a), and temperature in (b), of a rapidly rotating 1.50 $M_\odot$ white dwarf after the mass accretion stops. The initial model at $t = 0$ has been taken from model sequence A12.

K and 1.57×10^8 g/cm^3 respectively. This example indicates that the CFS instability can begin to operate about 10^8 yr after the end of the mass accretion. Which instability mode is responsible for the following angular momentum loss depends on the value of $(E_{\rm rot}/|W|)_{\rm b,c}$ of the white dwarf configuration at this point.

If the angular momentum loss time scale is short enough, (i.e., $\tau_J \lesssim 10^7$), the white dwarf may end in a Type Ia supernova, since the central temperature is still relatively high, and it will increase by the contraction of the core as the white dwarf loses angular momentum. Piersanti et al. (2003) showed that an initially cool Chandrasekhar mass white dwarf with $T_c \simeq 5.6 \times 10^7$ K is heated to $T_c \sim 10^8$ K if the white dwarf loses angular momentum on a time scale of $10^4 \ldots 10^7$ yr.

In the example given above, $E_{\rm rot}/|W|$ decreases from 0.11 to 0.10 during the evolution. If $(E_{\rm rot}/|W|)_{\rm b,c}$ at this point is less than 0.1, the bar-mode instability will remove angular momentum in $\tau_{J,\rm bar}$, which may be short enough (i.e., $\lesssim 10^7$ yr) to produce an SN Ia. On the other hand, if $(E_{\rm rot}/|W|)_{\rm b,c}$ is larger than 0.1 at the given moment, the r-mode instability will become dominant. The value of $\tau_{\rm r}$ at this point is about 2×10^5 yr. If the time scale for the following angular momentum loss is of the order of $\tau_{\rm r}$, the white dwarf will safely end in an SN Ia.

Although this discussion is somewhat speculative, it may suggest an interesting implication for the masses of white dwarfs in SNe Ia explosions. If the CFS instability is suppressed by the shear instability, white dwarfs can grow in principle until they become dynamically unstable ($E_{\rm rot}/|W| \gtrsim 0.27$) without becoming secularly unstable. In most close binary systems, the mass accretion will stop before reaching this point, given that the mass at $E_{\rm rot}/|W| = 0.18$ ($M_{0.18}$) in our models can be already as high as 1.45 $M_\odot$ – 1.75 $M_\odot$ (Table 4.3). Therefore, the upper limit for the white dwarf mass at the moment of the supernova explosion ($M_{\rm SN}$) is determined by the maximum possible mass a white dwarf can achieve by mass accretion, ($M_{\rm max}$). The lower limit for $M_{\rm SN}$ is simply 1.4 $M_\odot$. I.e., the white dwarf mass at the moment of supernova explosion will be inbetween 1.4 $M_\odot$ and $M_{\rm max}$ (1.4 $M_\odot \lesssim M_{\rm SN} \lesssim M_{\rm max}$).

The lower limit for $M_{\rm SN}$ (1.4 $M_\odot$) can not be different for different initial masses. However, the upper limit ($M_{\rm max}$) may be systematically larger for higher initial masses. I.e., Langer et al. (2000), found that $M_{\rm max}$ is larger for a higher $M_{\rm init}$ in main sequence star + white dwarf binary systems. Furthermore, $M_{\rm max}$ is expected to show a dependence on the metallicity of the mass donor. Langer et al. (2000) showed that $M_{\rm max}$ for main sequence star + white dwarf binary systems decreases for lower metallicity. This implies a higher probability to obtain massive exploding white dwarfs for higher metallicity. If more massive white dwarfs gave brighter SNe Ia as Fisher et al. (1999) speculate, the brightest SNe Ia observed at low metallicity may be dimmer than those at higher metallicity, while the luminosity of the dimmest may not be much different (unless affected by the CO ratio; Umeda et al. 1999, Höflich et al. 2000).

Case II

If the CFS instability is not affected by the shear instability, an accreting white dwarf will start losing angular momentum when $\tau_{\rm r}$ or $\tau_{\rm bar}$ becomes smaller than the accretion time scale ($\tau_{\rm acc} \simeq \Delta M/\dot{M}$).

If we consider sequence A6 as an example, $\tau_{\rm r}$ becomes comparable to $\tau_{\rm acc}$ only when $E_{\rm rot}/|W| \simeq 0.14$. Therefore, if we assume $(E_{\rm rot}/|W|)_{\rm b,c} = 0.1$, the bar-mode instability

will dominate before the r-mode instability becomes important. Once $E_{\rm rot}/|W|$ becomes larger than 0.1, the white dwarf will lose angular momentum via the bar-mode instability while gaining angular momentum continuously from the accreted matter. It is likely that $E_{\rm rot}/|W|$ will not change much after $\tau_{\rm bar} \approx \tau_{\rm acc}$ is obtained. This means that $E_{\rm rot}/|W|$ can not increase much from the critical value of 0.1, since $\tau_{\rm bar}$ drops rapidly as it deviates from $(E_{\rm rot}/|W|)_{\rm b,c}$ (Fig. 4.14). If mass accretion continues, the white dwarf will finally reach carbon ignition at $M_{\rm WD} \simeq 1.76$ M$_\odot$, according to the results of sequences C9 ... C12, where carbon ignites at the center when $M_{\rm WD} \simeq 1.76$ M$_\odot$, with $E_{\rm rot}/|W| \simeq 0.11$ (see also Sect. 4.7). If mass accretion stops before carbon ignition is reached but after the white dwarf mass has grown beyond 1.4 M$_\odot$, carbon ignition will be delayed until the white dwarf loses enough angular momentum.

In summary, we can expect that even in Case II the mass of exploding white dwarfs will show a significant diversity, as in Case I. The lower limit for $M_{\rm SN}$ should be $\sim$1.4 M$_\odot$ in both cases, but the upper limit may be either the critical mass for carbon ignition at that $E_{\rm rot}/|W|$ which gives $\tau_{\rm J} \approx \tau_{\rm acc}$, or the maximum possible achievable mass by mass accretion.

Other uncertainties

In reality, the mass transfer rate in a close binary system does not remain constant. For instance, in a binary system consisting of a main sequence star + a white dwarf, where thermally unstable mass transfer occurs, the mass transfer rate increases rapidly from the onset of the mass transfer, followed by slow decrease to the point that the nuclear shell burning can not be stable any more (Langer et al. 2000). Although shell sources may be more stable with rotation (Yoon et al. 2004), the white dwarf will experience strong shell flashes if the mass accretion rate decreases below 10^{-7} M$_\odot$/yr. This may cause a significant loss of mass, which may even decrease the white dwarf mass. This may also lead to a removal of angular momentum from the white dwarf (Livio & Pringle 1998). Effects of magnetic fields, if they are strongly amplified due to the differential rotation (Spruit 2002), may also serve to brake the white dwarf by magnetic torques and/or by magnetic dipole radiation. These possibilities will be the subject of further studies.

4.6   Implications for the SNe Ia diversity

We note that for all considered circumstances, the effects of rotation in accreting white dwarfs offer the possibility of SN Ia explosions from white dwarfs more massive than $\sim$1.4 M$_\odot$ (hereafter designated as super-Chandrasekhar mass). The observational signatures of super-Chandrasekhar mass explosions are currently difficult to predict. The peak brightness values and light curves of SNe Ia might be a sensitive function of the ignition conditions such as the CO ratio, the density at the moment of carbon ignition, the speed of the deflagration front, the core rotation rate, and possibly the transition density at which the deflagration turns into a detonation (e.g. Khokholov 1991a, 1991b; Höflich & Khokhlov

1996; Niemeyer & Woosley 1997; Höflich et al. 1998; Iwamoto et al. 1999; Umeda et al. 1999; Hillebrandt & Niemeyer 2000; Woosley et al. 2003).

If the ignition conditions are not strongly affected by the mass of the exploding white dwarf, it is likely that more massive one gives a brighter SN Ia, since a more massive white dwarf can provide more fuel to produce ^{56}Ni. For instance, progenitors with a super-Chandrasekhar mass are often invoked to explain such an anomalous SN Ia as SN 1991T. Fisher et al. (1999) note that the mass of ^{56}Ni produced from the explosion models of a Chandrasekhar mass white dwarf remains smaller than about 0.9 $M_\odot$ even in the case where a pure detonation is considered (e.g. Höflich & Khokhlov 1996). Although the nickel masses derived from the luminosities of normal SNe Ia are constrained to 0.4 ... 0.8 $M_\odot$ (Leibundgut 2000), the existing models fail to explain such a peculiar SN Ia as 1991T, whose brightness implies the production of about 1.0 $M_\odot$ of ^{56}Ni. The fact that explosion models with the canonical Chandrasekhar mass could not explain the peculiarity of SN 1991T suggests that it is worthwhile to investigate the possible outcome of super-Chandrasekhar mass explosions, even if we can not exclude the possibility that the luminosity of 1991T is biased by the uncertainty in determining the distance of its host galaxy (Hanato et al. 2002).

On the other hand, Fisher et al. (1999) suggested the explosion of a super-Chandrasekhar mass white dwarf from the merger of double CO white dwarfs as explanation of the over-luminosity found in SN 1991T. We note that differentially rotating single degenerate progenitors may be a more natural explanation for the super-Chandrasekhar mass scenario than double degenerate mergers, which fail to produce SNe Ia in numerical models due to the off-center carbon ignition induced by the fast mass accretion with $\dot{M} \gtrsim 10^{-5}$ $M_\odot/\mathrm{yr}$ (Saio & Nomoto 1985, 1998).

Rotation also has implications for the polarization of SNe Ia. According to our results, the rotation velocity of exploding white dwarfs may strongly depend on the history of angular momentum loss via gravitational wave radiation. The more angular momentum is lost, the slower the white dwarf rotation will be, which means that the polarization strength in SNe Ia may show significant diversity. Some white dwarfs may have a chance to end in an SN Ia while they are rotating very rapidly, as in sequences C9, C10, C11 and C12, where carbon ignition occurs at the white dwarf center when $M_{\mathrm{WD}} \simeq 1.76$ $M_\odot$ and $E_{\mathrm{rot}}/|W| \simeq 0.11$. Such exploding white dwarfs will show strong features of asphericity in the explosion, which might give a plausible explanation for the polarization observations in SN 1999by (Howell et al. 2001) and SN 2001 el (Wang et al. 2003; Kasen et al. 2003).

4.7   Pre-explosion conditions of a fast rotating white dwarf

Rotation may have interesting consequences for the supernova explosion itself. Fig. 4.16 shows the physical properties of the white dwarf model of sequence C9 when $M_{\mathrm{WD}} = 1.76 \, M_\odot$, where the central temperature and density reach 5.5×10^8 K and 2.2×10^9 g cm^{-3}, respectively. The central region ($0.0 \lesssim M_{\mathrm{r}} \lesssim 0.6 M_\odot$) is found to be convectively unstable due to carbon burning, rotating rigidly due to the convective angular momentum redistribution. A thermonuclear runaway is expected to develop when the central temperature reaches a
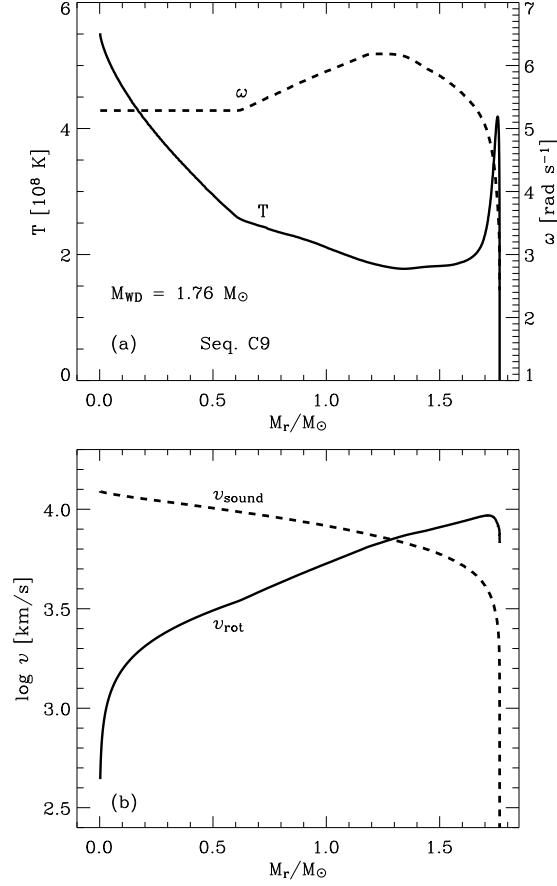
Figure 4.16: (a) Temperature (solid line) and angular velocity (dashed line) as a function of the mass coordinate in the last computed model of sequence C9. (b) Equatorial rotational velocity (solid line) for the same model as in (a) as a function of the mass coordinate. The dashed line denotes the sound speed as a function of the mass coordinate.

few times 10^9 K. The convective core will be more extended by then, spinning up the central region further. In the model shown in Fig. 4.16, the central region rotates with $v_{\rm rot} \simeq 1000$ km/s, which is well above the convective velocity (~ 100 km/s; e.g. Höflich & Stein 2002) and somewhat larger than the expected initial velocity of the deflagration front ($v_{\rm def,init} \simeq 0.03 v_{\rm sound}$, e.g. Nomoto et al. 1984). The equatorial rotation velocity increases sharply from the center to the edge of the convective layer ($M_{\rm r} = 0.6$ M$_\odot$), by a factor of 10.

This fast rotation in the central carbon burning core may affect the explosion as follows. Numerous studies indicate that the combustion front develops large scale turbulent motions, especially due to the Rayleigh-Taylor instability (e.g. Reinecke et al. 2002; Gamezo et al. 2003 and references therein). It is a crucial question whether this turbulence can induce a detonation (Khokhlov 1991a, 1991b; Niemeyer & Woosley 1997; Khokhlov et al. 1997). Although pure deflagration models show a good agreement with observations (Nomoto et al. 1984; Höflich & Khokhlov 1996), recent three dimensional calculations show that large amounts of unburned and partially burnt materials are left even at the center (Reinecke et al. 2002; Gamezo et al. 2003), which is not supported by observations (however, see Baron et al. 2003). This problem would disappear if a detonation were triggered by the turbulent deflagration ('delayed detonation', Khokhlov 1991a). Furthermore, delayed detonation models are shown to reproduce the light curves and spectra of well observed SNe Ia (Höflich & Khokhlov 1996; Höflich et al. 1996). A study of the nucleosynthesis output of SNe Ia by Iwamoto et al. (1999) also favors the delayed detonation scenario.

Several authors conclude that the probability of triggering a detonation can be enhanced if the turbulence is strong enough to form a thick mixed region of unburned and burning materials with a constant temperature gradient (Khokhlov 1991b; Niemeyer & Woosley 1997; Khokhlov et al. 1997; Lisewski et al. 2000). However, no robust mechanism for the formation of such a strong turbulence has yet been suggested. (Niemeyer 1999).

A rapidly rotating white dwarf like the one shown in Fig. 4.16 will be spun down due to expansion once the thermal runaway occurs, as the deflagration wave propagates. However, the outer layers will still rotate rapidly at $v_{\mathrm{rot}} \sim 10^3$ km/s. Lisewski et al. (2000) show that strong turbulence, i.e. $v_{\mathrm{turb}} \approx 10^3$ km/s, is necessary for a detonation to form successfully. Since the rotation velocity in the outer region will be of this order, the shear motion may provide enough kinetic energy for the turbulence intensity to satisfy the condition for a transition of the deflagration into a detonation, which might not be possible in the non-rotating case since the maximum value for v_{turb} is $\sim 10^2$ km/s in the Rayleigh-Taylor-driven turbulence. Alternatively, the fast rotation in the outer region can tear the turbulent deflagration front and enhance the nuclear burning surface, which may be another way to trigger a detonation (Höflich 2003, private communication). Future multi-dimensional calculations are required to test the validity of these scenarios.

4.8 Gravitational wave radiation in pre-explosion white dwarfs?

Rotation may have another important and exciting observational consequence. Our results indicate that the white dwarfs in SN Ia progenitor systems may emit gravitational wave radiation (GWR). Therefore, if we could observe GWR preceding an SN Ia event, this would provide strong evidence for the scenarios outlined in Sect. 4.5.

The GWR due to the CFS bar-mode instability may be much stronger than the r-mode signal, since perturbations due to the bar-mode involve larger density changes than those due

Table 4.4: Expected properties of the gravitational waves from the selected accreting white dwarfs.

No.	M $M_\odot$	$E_{\rm rot}/|W|$	$h_{\rm bar}$ at 10 Mpc 10^{-24}	$f_{\rm GW}$ Hz
A2	1.18	0.10	1.7	0.22
A6	1.30	0.10	2.9	0.32
A10	1.42	0.10	4.3	0.46
A2	1.34	0.14	3.7	0.32
A6	1.44	0.14	5.0	0.43
A10	1.55	0.14	7.5	0.62

to the r-mode (e.g. Andersson & Kokkotas 2001). Fryer et al. (2002) derive the gravitational wave amplitude observed at Earth from a source which undergoes the bar-mode instability at a distance d as

$$h_{\rm bar} = \left(\frac{32}{45}\right)^{1/2} \frac{G}{c^4} \frac{MR^2\Omega^2}{d}, \qquad (4.22)$$

where R denotes the equatorial radius of the source, M the mass and Ω the angular velocity. The frequency of the gravitational waves ($f_{\rm GW}$) due to the bar-mode instability is twice the rotation frequency of the source. We estimate $h_{\rm bar}$ and $f_{\rm GW}$ for selected white dwarf models in Tables 4.4. For these calculations, we used mean values for Ω and R given in Table 4.2 and 4.3.

Table 4.4 indicates that $f_{\rm GW}$ is within the range of $0.1 \ldots 1.0$ Hz. Observation of GWs with such frequencies may be performed by low frequency gravitational wave detectors such as LISA, which will cover the range $10^{-4} - 1.0$ Hz (e.g. Cutler & Thorne 2002). The expected strength of the gravitational wave signal is about 10^{-24} at $d = 10$ Mpc. Hiscock (1998) estimated the strength of GWs due to the r-mode instability from white dwarfs in the observed DQ Her systems as $h \sim 10^{-23}$. His calculations show that this strength is well above the detection limit of the LISA interferometer. Therefore, the results shown in Table 4.4 imply that SNe Ia progenitors in nearby galaxies could be within the observable range. Given that GWs from SN Ia progenitors will be emitted over a secular time, and that SNe Ia are observed with a relatively high rate of $\sim 3 \times 10^{-3}$ yr^{-1} per galaxy, the probability to detect the GW signal may be considerable.

Even if a white dwarf would not reach the bar-mode instability at $(E_{\rm rot}/|W|)_{\rm b,c}$, it might still emit gravitational waves via the r-mode instability. Although their strength is rather unclear and may be much weaker than that of the bar-mode, they may still be detectable if the source is close enough.

4.9   Conclusion

We summarize the results of this paper as follows.

1. The role of Eddington Sweet circulations, the GSF instability and the shear instability for the transport of angular momentum in non-magnetized white dwarfs has been investigated (Sect. 4.2). Although Eddington Sweet circulations and the GSF instability are important for the redistribution of angular momentum in the non-degenerate envelope, their importance is small in the degenerate core compared to the shear instability. The secular shear instability can not operate in the strongly degenerate core, since the thermal diffusion time becomes longer than the turbulent viscous time for densities higher than a critical value (i.e., $\rho \gtrsim 10^6 \ldots 10^7$ g/cm^3, Fig. 4.2). On the other hand, the criterion for the dynamical shear instability is significantly relaxed for higher density because the buoyancy force becomes weaker with stronger degeneracy (Fig. 4.1). As a result, the degenerate inner core is dominated by the dynamical shear instability in accreting white dwarfs as shown in Sect. 4.4.2.

2. We have followed the redistribution of the angular momentum in accreting white dwarfs by the above mentioned processes (Sect. 4.4.2). We find that accreting white dwarfs do not rotate rigidly, but differentially throughout their evolution, for the considered accretion rates ($\dot{M} = 3 \ldots 10 \times 10^{-7}$ M$_\odot$/yr). In the degenerate core, once the shear factor decreases to the threshold value for the onset of the dynamical shear instability, the time scale for further angular momentum transport becomes larger than the accretion time scale. Accordingly, strong differential rotation is retained in the inner core with a shear strength near the threshold value for the dynamical shear instability (Fig. 4.7).

3. Accreting white dwarfs, as they rotate differentially, may not reach central carbon ignition even when they grow beyond the canonical Chandrasekhar limit of ~ 1.4 M$_\odot$. This is in accordance with previously obtained results based on other methods (Ostriker & Bodenheimer 1968, 1973; Durisen 1975b; Durisen & Imamura 1981). A secular instability to gravitational wave radiation through the r-mode or the bar-mode may be important for determining the final fate of accreting white dwarfs. The masses of exploding white dwarfs are expected to vary in the range from the canonical Chandrasekhar mass (~ 1.4 M$_\odot$) to the maximum possible mass that the white dwarf can achieve by mass accretion in a binary system (~ 2.0 M$_\odot$, Langer et al. 2000). This may have consequences for the diversity in the brightness and polarization of SNe Ia.

4. Fast rotation in the white dwarf core may change the supernova explosion since it can affect the evolution of the turbulent nuclear burning flames by providing a large amount of turbulent kinetic energy and/or by enhancing the burning surface significantly. It needs to be clarified whether this may be a plausible mechanism to induce the transition from deflagration to detonation.

5. White dwarfs that have accreted enough angular momentum may be detectable sources of gravitational waves in the near future. Our models show that these will emit gravitational waves with frequencies of $0.1 - 1.0$ Hz. Space-based interferometric gravitational wave detectors such as LISA could observe such signals from rapidly rotating SNe Ia progenitors in nearby galaxies.

Chapter 5

Effects of rotation on the helium burning shell source in accreting white dwarfs

S.-C. Yoon, N. Langer and S. Scheithauer

Astronomy & Astrophysics, 2004, submitted

Abstract   We investigate the effects of rotation on the behavior of the helium burning shell source in accreting carbon-oxygen white dwarfs, in the context of the single degenerate Chandrasekhar mass progenitor scenario for Type Ia supernovae (SNe Ia). We model the evolution of helium accreting white dwarfs of initially 1 $M_\odot$, assuming four different constant accretion rates (2, 3, 5 and 10×10^{-7} $M_\odot/yr$). In a one-dimensional approximation, we compute the mass accretion and subsequent nuclear fusion of helium into carbon and oxygen, as well as angular momentum accretion, angular momentum transport inside the white dwarf, and rotationally induced chemical mixing. Our models show two major effects of rotation: **a)** The helium burning nuclear shell source in the rotating models is much more stable as in corresponding non-rotating models — which increases the likelihood of accreting white dwarfs to reach the stage of central carbon ignition. This effect is mainly due to rotationally induced mixing at the CO/He interface which widens the shell source, and due to the centrifugal force lowering the density and degeneracy at the shell source location. **b)** The C/O-ratio in the layers which experience helium shell burning — which may affect the energy of an SN Ia explosion — is strongly decreased by the rotationally induced mixing of α-particles into the carbon-rich layers. We discuss implications of our results for the evolution of SNe Ia progenitors.

5.1 Introduction

Accreting white dwarfs in close binary systems are considered to be responsible for such important astrophysical phenomena as nova explosions, cataclysmic variables and super-soft X-ray sources. Especially, there is general agreement that accreting CO white dwarfs are progenitors of Type Ia supernovae (SNe Ia) (e.g., Woosley & Weaver 1986; Branch et al. 1995; Wheeler 1996; Nomoto et al. 1997, Hillebrandt & Niemeyer 2000; Livio 2001).

The fairly homogeneous properties of light curves and spectra of SNe Ia have made them a valuable distance indicator to determine cosmological parameters (e.g, Hamuy et al. 1996a; Branch 1998; Leibundgut 2001). One of the most intriguing results obtained from SNe Ia data may be the recent suggestion of a finite cosmological constant, which implies that the universe is currently accelerating its expansion (Perlmutter et al. 1999a; Riess et al. 2000).

The observational properties of SNe Ia demand a thermonuclear explosion of a CO white dwarf as their origin. However, despite the far-reaching observational achievements, self-consistent progenitor evolution model calculations which explain the existence of SNe Ia are still lacking (but see Yoon & Langer 2003). Models for the evolution of SN Ia progenitors studied until now can be divided into two groups, one where the white dwarf explosion is triggered close to the center, and the other where the white dwarf explosion is triggered in the helium shell (see Livio 2001 for a review).

Two scenarios exist for close-to-center ignition. One is the double degenerate scenario, in which two CO white dwarfs in a binary system merge due to the angular momentum loss by gravitational radiation. If the system mass exceeds the Chandrasekhar mass, carbon must ignite, with the possible outcome of a thermonuclear explosion. Although there is observational evidence for double white dwarf systems (e.g., Koester et al. 2001) including one with the total mass near the Chandrasekhar limit (Napiwotzki et al. 2002), this scenario is criticized mainly by the fact that the merging of two white dwarfs is likely to end in an accretion-induced collapse rather than an SN explosion (Saio & Nomoto 1985, 1998).

The currently favored scenario for close-to-center ignition is the single degenerate scenario, in which a CO white dwarf in a close binary system accretes hydrogen or helium rich matter from a non-degenerate companion at a relatively high accretion rate ($\sim 10^{-7} M_\odot/yr$). The super-soft X-ray sources, which are believed to consist of a non-degenerate star and a white dwarf, are promising observed counterparts of this scenario. The idea of steady nuclear burning due to a high accretion rate fits well to these sources (e.g., Li & van den Heuvel 1997; Kahabka & van den Heuvel 1997; Langer et al. 2000; Yoon & Langer 2003). Symbiotic systems (e.g., Hachisu et al. 1999) and recurrent novae (e.g., Hachisu & Kato 2001; Thoroughgood et al. 2001) may also belong to this scenario. However, it is still not clear whether this scenario can explain the observed SN Ia frequency since the accretion rates which allow steady burning are limited to a very narrow range. Furthermore, helium shell burning is generally found to be unstable, leading to strong shell flashes with the consequence of a strong expansion of the white dwarf, i.e., a possible merging of the binary, and/or strong mass loss (e.g. Nomoto 1982a; Hachisu, Kato & Nomoto 1996; Cassisi et

al. 1998; Kato & Hachisu 1999; Langer et al. 2002).

In the so called 'Edge Lit Detonation' (ELD) models, corresponding to sub-Chandrasekhar mass models, helium ignites at the bottom of a helium layer of a few tenth of a solar mass, accumulated on a CO white dwarf at a relatively low accretion rate ($\sim 10^{-8} M_\odot/\mathrm{yr}$) (e.g. Nomoto 1982b; Limongi & Tornambé 1991; Woosley & Weaver 1994; Livne & Arnett 1995). These models are favoured in terms of statistics (e.g. Iben & Tutukov 1991; Tout et al. 2001) but disfavoured by the fact that the spectra and light curves produced by these models are not in agreement with observations (Höflich et al. 1996; Nugent et al. 1997; Pinto et al. 2001). Yoon & Langer (2004b) showed that a helium detonation in such models may be avoided altogether due to a strong shear layer inside an accreting white dwarf.

Most previous studies of accreting white dwarfs as SN Ia progenitors have assumed spherical symmetry. However, in a close binary system which contains a white dwarf, an accretion disk is formed around the white dwarf. The matter coming from the accretion disk which is incorporated into the white dwarf carries high specific angular momentum, i.e. up to the value corresponding to Keplerian rotation at the white dwarf equator. Consequently, not only the accreted layer may be spinning very fast, but also the rest of the white dwarf, as angular momentum may be transported into the stellar interior (e.g. Ritter 1985; Langer et al. 2000).

Recent polarization observations provide evidence for the aspherical nature in SNe Ia (Howell et al. 2001; Wang et al 2003). The observation that white dwarfs in Cataclysmic Variables rotate much faster than isolated ones (Sion 1999; Starrfield 2003) supports the idea that accreting white dwarfs are indeed spun up. A possible explanation for this asphericity may be a rapidly rotating progenitor. In this picture, differential rotation inside the accreting white dwarf is inevitable, unless the angular momentum transport in the white dwarf is extremely efficient (Yoon & Langer 2004a). Rotationally induced instabilities such as the shear instability may lead to chemical mixing between the CO white dwarf material and the accreted matter. This effect has been discussed by several authors mainly with respect to the chemical enrichment of CNO and other heavier elements observed in nova ejecta (e.g., Kippenhahn & Thomas 1978; MacDonald 1983; Livio & Truran 1987; Fujimoto 1988, Fujimoto & Iben 1997).

In this paper, we investigate the effects of rotation on the evolution of accreting white dwarfs in relation to the single degenerate Chandrasekhar mass scenario for SNe Ia progenitors. For this purpose, we carry out numerical simulations of helium accreting white dwarfs considering high accretion rates ($> 10^{-7} M_\odot/\mathrm{yr}$) which allow steady shell burning for hydrogen and/or helium. Our discussions in this study is focused on the rotationally induced chemical mixing and their consequences for the behavior of the helium shell source. Comprehensive discussions on the rotational induced hydrodynamic instabilities and their role in the redistribution of angular momentum in accreting white dwarfs are given in a separate paper (Yoon & Langer 2004a). Effects of rotation on sub-Chandrasekhar mass models, i.e., on accreting white dwarfs with relatively low accretion rates ($\sim 10^{-8} M_\odot/\mathrm{yr}$), are discussed in Yoon & Langer (2004b). Our computational method is introduced in Sect. 2, and the initial model and physical assumptions are discussed in Sect. 3. In Sect. 4, we present

the evolution of various physical quantities of our white dwarf models. We discuss rotationally induced chemical mixing and the stability of shell burning in Sect. 5 and 6 respectively. Finally, we discuss our results in Sect. 7.

5.2   Computational method

The numerical models have been computed with a hydrodynamic stellar evolution code (cf, Langer 1998; Heger, Langer & Woosley 2000). Opacities are taken from Iglesias & Rogers(1996). Changes in the chemical composition are computed using a nuclear network with more than 60 nuclear reactions, of which 31 reactions are relevant to helium burning such as 3α, $^{12}C(\alpha,\gamma)^{16}O(\alpha,\gamma)^{20}Ne$ and $^{20}Ne(\alpha,\gamma)^{24}Mg(\alpha,\gamma)^{28}Si$ reactions. For the $^{12}C(\alpha,\gamma)^{16}O$ reaction rate, which has an important role in our study, we use the rate of Caughlan et al. (1985) reduced by a factor of 0.63, as suggested by Weaver & Woosley (1993).

The effect of the centrifugal force on the stellar structure, and rotationally induced transport of angular momentum and chemical species are treated in a one-dimensional approximation (Heger et al. 2000). We consider rotationally induced transport processes as Eddington Sweet circulations, the Goldreich-Schubert-Fricke instability, and the dynamical and secular shear instability, by solving a non-linear diffusion equation, with diffusion coefficients for each of the instabilities computed as in Heger et al. (2000) and Yoon & Langer (2004a). The viscous dissipation of the rotational energy is also considered as described by Yoon & Langer (2004a). More details about the numerical methods are given in Yoon & Langer (2004a)

A comparison of our method with previously used ones for rotating white dwarf models is already given in Yoon & Langer (2004a) in detail. Here we give some additional comments on the rotation physics in relation to helium accreting white dwarfs.

Our approach to include rotation is based on the method given by Kippenhahn & Thomas (1970), with the mass shells of a star defined by isobars instead of spherical shells. In describing effects of rotationally induced chemical mixing, the chemical abundances are assumed to be constant on isobars. This is justified by theoretical achievements of Zahn (1975), Chaboyer & Zahn (1992) and Zahn (1992), who showed that anisotropic turbulence acts much more efficiently in the horizontal than in the vertical direction. Shellular rotation and chemical homogeneity on isobars can be thus achieved (Meynet & Maeder 1997), enabling us to use a one dimensional approximation (see also Maeder 2003).

However, our assumption of shellular rotation may be questionable for helium accreting white dwarfs, on two accounts. Kippenhahn & Thomas (1978) argued that the accreted matter cannot spread over the whole surface of white dwarf but rather forms an accretion belt, since the angular momentum transport time scale based on the electron viscosity is longer than the accretion time scale. However, calculations by Sparks & Kutter (1987) failed in obtaining nova-like outbursts when the prescription of accretion belts was employed. Livio & Truran (1987) argued that if a turbulent viscosity is used, the angular momentum transport becomes much more efficient than discussed by Kippenhanh & Thomas. They

concluded that the accreted matter can spread over the entire star with the consequence that mass accretion onto white dwarfs may result in nova outbursts, which was not possible in the accretion belt prescription due to the too strong centrifugal force at the equator. A local stability analysis by MacDonald (1983) and a theoretical study by Fujimoto (1988) also concluded that the accreted matter will not remain confined to the equatorial belt due to efficient angular momentum transport toward the poles. We therefore conclude that the assumption of shellular rotation employed in our study may still be well-grounded, at least in the non-degenerate helium envelope, although multi-dimensional simulations are ultimately required for its justification (cf. Hujeirat 1995).

Secondly, as degenerate matter is barotropic, perturbations which create $\partial j/\partial z \neq 0$, with j as specific angular momentum and z being the distance to the equatorial plane, are eliminated on a short time scale. Thus, cylindrical rotation may be enforced in the inner CO core (e.g. Kippenhahn & Möllenhoff 1974; Durisen 1977). This means that accreting white dwarfs may consist of two different rotation laws: shellular in the non-degenerate envelope and cylindrical rotation in the degenerate core. However, our numerical models can still represent the cylindrically rotating degenerate inner core to some degree, since most of the total angular momentum is confined at the equatorial plane in both the shellular and the cylindrical cases. It is harder to estimate the angular momentum transport efficiency in the semidegenerate transition layer, as non-barotropic perturbations in the degenerate core may induce dynamical meridional flows (Kippenhahn & Möllenhoff 1974; Müller 2003, private communication). Since it is poorly known how these meridional flows may affect the angular momentum redistribution, we have to leave the detailed investigation of this effect to future work.

Finally, the accuracy of our results for very rapid rotation is limited due to the one dimensional approximation. In computing the effective gravitational potential in a rotating star, the potential is expanded in terms of spherical harmonics, of which we only consider terms up to the second order (Kippenhahn & Thomas 1970; Endal & Sofia 1976). This method can reproduce the shapes of rigidly rotating polytropes accurately up to a rotation rate of about 60% of the critical value, corresponding to correction factors of $f_P \simeq 0.75$ and $f_T \simeq 0.95$ in the stellar structure equations (Fliegner 1993; Heger et al. 2000). We therefore limit these factors to the quoted values, with the consequence that we underestimate the effect of the centrifugal force in layers which rotate faster than about 60% critical. We shall see below that this affects only a very small fraction of our stellar models in most cases. However, as the surface layers are always very close to critical rotation, the stellar radius of our models may be somewhat underestimated. In addition, since our models are rotationally symmetric, three dimensional effects such as a triaxial deformation can not be described with our numerical code.

5.3 Physical assumptions

We begin with a hot carbon-oxygen white dwarf of $\log L_s/L_\odot = 3.379$ in order to avoid the numerical difficulty of a strong initial helium shell flash. The initial mass of our model is

Table 5.1: Properties of the computed models. The first column denotes the sequence number, where 'NR', 'R' and 'RT' denote the non-rotating models and rotating models with $f_c = 1/30$ and 1/3 respectively. The second column gives the accretion rate in the unit of 10^{-7} $M_\odot/\mathrm{yr}$. The third column denotes the factor f_c for the chemical mixing efficiency in rotating models. Columns 4, 5, 6 and 7 give mass, central density, central temperature and $E_{\mathrm{rot}}/|W|$ of the last computed model of each evolutionary sequence. The eighth column gives the amount of accreted material until the onset of the helium shell instability. The column with L_{Edd} indicates whether the last computed model reached the Eddington limit or not. The last column gives the total number of the computed models for each sequence.

No.	$\dot{M}$ 10^{-7} $M_\odot/\mathrm{yr}$	f_c	M_{last} $M_\odot$	$\rho_{c,\mathrm{last}}$ 10^8 g cm^{-3}	$T_{c,\mathrm{last}}$ 10^8 K	$\left(\frac{E_{\mathrm{rot}}}{|W|}\right)_{\mathrm{last}}$	ΔM $M_\odot$	L_{Edd}	No. of models
NR1	2.0	–	1.0026	0.25	1.45	–	0.00	Yes	4342
NR2	3.0	–	1.0042	0.25	1.45	–	0.00	Yes	5164
NR3	5.0	–	1.0130	0.28	1.37	–	0.00	Yes	10324
NR4	10.0	–	1.1984	1.39	1.44	–	0.03	No	383637
R1	2.0	1/30	1.0074	0.28	1.25	0.0018	0.00	Yes	18021
R2	3.0	1/30	1.0224	0.32	1.17	0.0025	0.00	Yes	28449
R3	5.0	1/30	1.2241	1.05	1.21	0.0197	0.14	No	180004
R4	10	1/30	1.4773	5.14	1.72	0.0578	0.48	No	490026
RT1	2.0	1/3	1.0665	0.42	0.99	0.0081	0.01	No	174270
RT2	3.0	1/3	1.1537	0.77	1.22	0.0080	0.01	No	212730

0.998 $M_\odot$. The central temperature and density are initially such that $T_c = 2.288 \times 10^8$ K and $\rho_c = 1.64 \times 10^6$ g cm^{-3}, respectively. Although in reality white dwarfs may be much colder when mass accretion starts, the thermal evolution of the white dwarf core is not influenced by the different initial conditions due to the self heating of white dwarfs (cf. Yoon & Langer 2003). Since observations (Heber et al. 1997; Koester et al. 1998; Kawaler 2003) and stellar evolution models (Langer et al. 1999) find small spin rates of isolated white dwarfs, we adopt a slow and rigid rotation in our initial model: the initial rotation velocity at the white dwarf equator is set to $1.0\ \mathrm{km s}^{-1}$.

We consider 4 different accretion rates: $2 \times 10^{-7}, 3 \times 10^{-7}, 5 \times 10^{-7}$ and 10^{-6} $M_\odot/\mathrm{yr}$. The accreted matter is assumed to be helium-rich with $Y = 0.98$ and $Z = 0.02$. The abundances for heavier elements are chosen to be the same as in a helium core which results from core hydrogen burning in a main sequence star through the CNO cycle.

The specific angular momentum of the accreted matter is assumed to have the local Keplerian value, as most white dwarfs with a non-degenerate companion are believed to accrete matter through an accretion disk. However, analytic considerations can show this to cause an angular momentum problem: Assuming rigid rotation and a usual white dwarf mass-radius relation, the white dwarf reaches overcritical rotation much before reaching the Chandrasekhar limit (Livio & Pringle 1998; Langer et al. 2000). For finite angular momentum redistribution times, as realized by our preliminary calculations (Yoon & Langer 2002),

overcritical rotation is even reached earlier.

Livio & Pringle (1998) suggested nova explosions as a possible mechanism for angular momentum loss to explain the white dwarf rotation velocity in typical CV systems. However, within the single degenerate SNe Ia progenitor scenario in which the white dwarf must grow to the Chandrasekhar limit by mass accretion, we need another mechanism to solve the angular momentum problem. To prevent the white dwarf from rotating over-critically, in our calculations, we limited the angular momentum gain in a simple way as follow. If the surface velocity at the white dwarf equator is below the Keplerian value, the specific angular momentum of the accreted matter is assumed to have the Keplerian value. Otherwise, no angular momentum is allowed to be accreted onto the white dwarf while mass is still accreted:

$$j(\text{accreted matter}) = \left\{ \begin{array}{ll} v_{\text{Kepler}} R_{\text{WD}} & \text{if } v_{\text{s}} < v_{\text{Kepler}} \\ 0 & \text{if } v_{\text{s}} = v_{\text{Kepler}} \end{array} \right., \tag{5.1}$$

where $v_{\text{Kepler}} = \sqrt{GM_{\text{WD}}/R_{\text{WD}}}$, and v_{s} is the surface rotation velocity of the accreting white dwarf at its equator. This assumption may be justified by considerations of Paczyński (1991) and Popham & Narayan (1991) to allow angular momentum transport from the white surface through the boundary layer into the accretion disk by turbulent viscosity.

As discussed in Heger et al. (2000), the contribution of the rotationally induced instabilities to the chemical diffusion is considered by introducing a factor $f_{\text{c}} \in [0, 1]$, which describes the ratio of the chemical diffusion coefficient to turbulent viscosity. Heger et al. (2000) and Heger and Langer (2000) chose a value of $f_{\text{c}} = 1/30$ following Chaboyer & Zahn (1992) (See also Pinsonneault et al. 1989). In the present study, we consider two different values for f_{c}, i.e., 1/30 and 1/3 (see Table 5.1), in order to investigate how the strength of chemical mixing affects the nuclear shell burning.

For a comparative study, rotating and non-rotating models with the same initial conditions have been investigated. The properties of all computed models are summarized in Table 5.1.

5.4 Evolution

The results of our calculations are summarized in Table 5.1. For sequences NR1, NR2, NR3, R1 and R2, we followed the evolution until the helium shell flashes become strong enough to drive the surface luminosity to the Eddington limit. For the rest, calculations are stopped after a large number of models has been calculated (cf. Tab. 5.1).

5.4.1 Helium shell burning and luminosity

In Fig. 5.1, the nuclear luminosity due to the helium burning in the sequences with $\dot{M} = 2 \times 10^{-7}$ $M_{\odot}/\text{yr}$ (NR1, R1 & RT1) is shown as a function of the total mass of white dwarf. In sequence NR1, helium shell burning is not stable but undergoes thermal pulses, which are driven by the thin shell instability (e.g. Schwarzshild & Härm 1965; Weigert 1966). It is

well known that this phenomenon occurs also in intermediate mass stars in their thermally pulsating asymptotic giant branch (TP-AGB) phase (e.g. Iben & Renzini 1983). The thermal pulses in sequence NR1 become stronger as the white dwarf accretes more matter (cf. Fujimoto & Sugimoto 1979). Finally, the shell flash at the sixth pulse drives the surface luminosity to the Eddington limit when $M_{\mathrm{WD}} \simeq 1.002\ \mathrm{M_{\odot}}$ (cf. Fig. 5.2), at which point we stop the calculation. Perhaps, the white dwarf would experience a radiation driven optically thick outflow at this stage, which would reduce the mass accumulation efficiency (Kato & Hachisu 1999). It is beyond the purpose of this paper to consider the ensuing evolution in detail.

In the rotating sequence R1 with the same accretion rate, the thermal pulses become significantly weaker compared to the non-rotating case. For instance, the helium shell source reaches $\log L_{\mathrm{N}}/L_{\odot} \simeq 6.5$ in the non-rotating case when the white dwarf has accreted about $0.004\ \mathrm{M_{\odot}}$, while the rotating sequence reaches only $\log L_{\mathrm{N}}/L_{\odot} \simeq 4.0$ at the same epoch (see Fig. 5.1). As a consequence, the white dwarf can accrete more mass ($\Delta M_{\mathrm{acc}} \simeq 0.0096$ $\mathrm{M_{\odot}}$) than in sequence NR1 ($\Delta M_{\mathrm{acc}} \simeq 0.0039\ \mathrm{M_{\odot}}$) before the surface luminosity reaches the Eddington limit. In the HR diagram (Fig. 5.2), the rotating sequence is located in lower effective temperatures than the non-rotating sequence, since the white dwarf envelope is expanded by the centrifugal force.

The helium shell source becomes more stable with stronger chemical mixing. Results of sequence RT1 in Fig. 5.1c, where the chemical mixing is 10 times stronger than in sequence R1, show that the helium is burned more or less steadily until $M_{\mathrm{WD}} \simeq 1.01\ \mathrm{M_{\odot}}$. More than 100 pulses were followed thereafter, but the surface luminosity still did not reach the Eddington limit.

The evolution of sequence NR2 ($\dot{M} = 3 \times 10^{-7}\ \mathrm{M_{\odot}/yr}$) shown in Fig. 5.3 is similar to that of NR1, only the white dwarf reaches the Eddington limit somewhat later, i.e., when $M_{\mathrm{WD}} \simeq 1.004\ \mathrm{M_{\odot}}$. The thermal pulses are weakened in the corresponding rotating sequence with $f_{\mathrm{c}} = 1/30$ (R2, Fig. 5.3b), and about 4 times more mass could be accreted in the white dwarf of sequence R2 before reaching the Eddington limit. With a stronger chemical mixing ($f_{\mathrm{c}} = 1/3$, RT2, Fig. 5.3c), steady helium shell burning continues until $M_{\mathrm{WD}} \simeq 1.01\ \mathrm{M_{\odot}}$, and weak thermal pulses with $\log L_{\mathrm{N}}/L_{\odot} \lesssim 5.0$ follow. The evolution of this sequence was stopped when $M_{\mathrm{WD}} \simeq 1.15\ \mathrm{M_{\odot}}$, as the number of thermal pulses before reaching the Chandrasekhar mass would exceed 10^4.

The stabilizing effect of rotation appears more prominently at $\dot{M} = 5 \times 10^{-7}\ \mathrm{M_{\odot}/yr}$. In the non-rotating case (NR3), the helium shell burning is still unstable even with such a high accretion rate, as shown in Fig. 5.4a, and the white dwarf reaches the Eddington limit when $M_{\mathrm{WD}} \simeq 1.013\ \mathrm{M_{\odot}}$. In the corresponding rotating sequence (R3), very weak thermal pulses appear when $M_{\mathrm{WD}} \simeq 1.005\ \mathrm{M_{\odot}}$, but are suppressed when $M_{\mathrm{WD}} \gtrsim 1.02\ \mathrm{M_{\odot}}$. Steady helium shell burning continues until $M_{\mathrm{WD}} \simeq 1.14\ \mathrm{M_{\odot}}$, from which the shell source becomes again unstable. Note that the thermal pulses shown in Fig.5.4b look like noise but are actually many successive thermal pulses, each of which is resolved by about 10^3 models.

With an accretion rate of $\dot{M} = 10^{-6}\ \mathrm{M_{\odot}/yr}$, the non-rotating white dwarf undergoes unstable helium shell burning after $M_{\mathrm{WD}} \simeq 1.03\ \mathrm{M_{\odot}}$ (NR4, Fig. 5.4c). We have followed
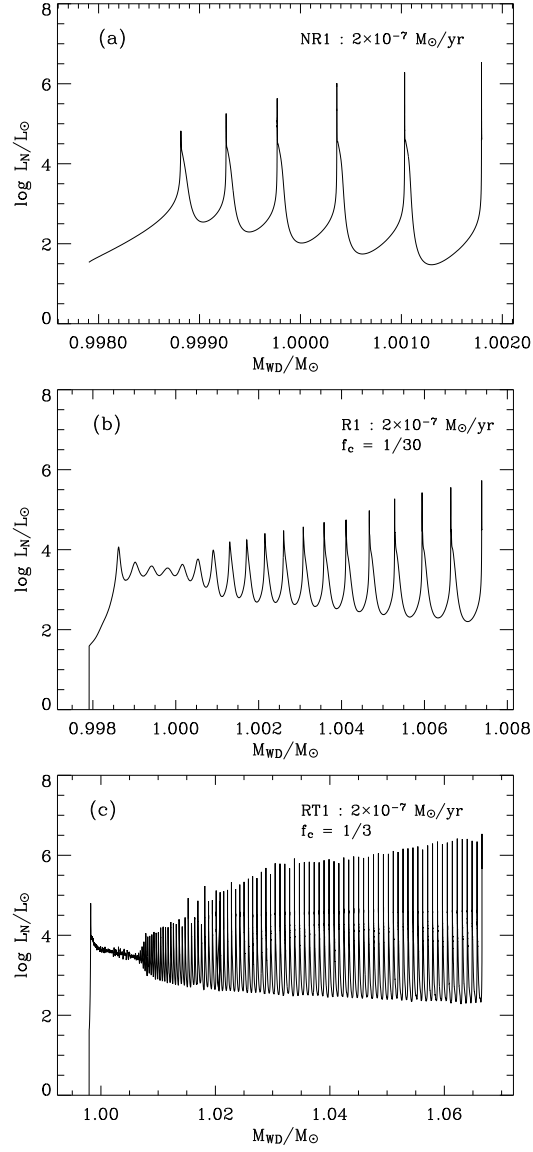
Figure 5.1: Evolution of nuclear luminosity due to helium burning in the helium accreting white dwarf models with $\dot{M} = 2 \times 10^{-7}$. The box in the top panel gives the result from the non-rotating case (NR1) while the results from the rotating models with $f_c = 1/30$ (R1) and $f_c = 1/3$ (RT1) are shown in the next panels. The abscissa denotes the total mass of white dwarf, which serves as a measure of time.
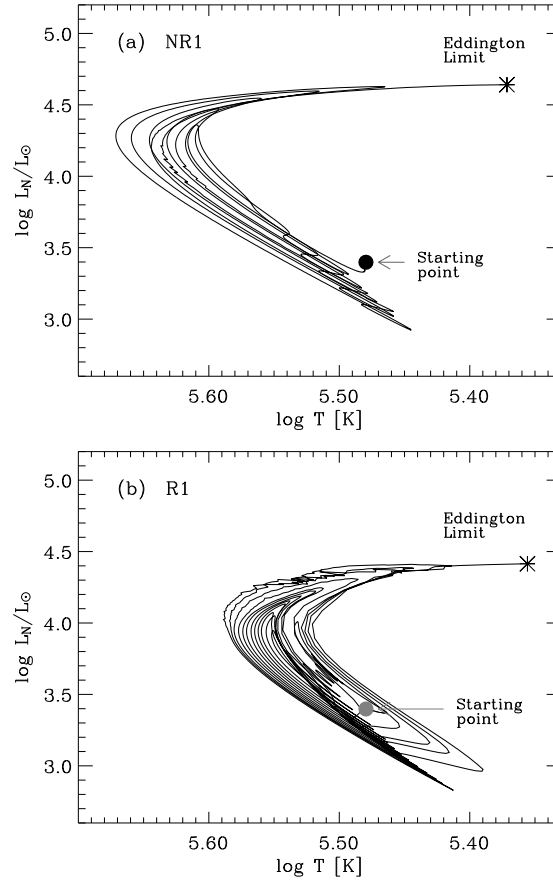
Figure 5.2: Evolution of white dwarf in the sequences NR1 (upper panel) and R1 (lower panel) in the Hertzsprung-Russell diagram. The starting point is marked by a filled circle. The ending point, where the surface luminosity reaches the Eddington limit, is marked by an asterisk for each case.
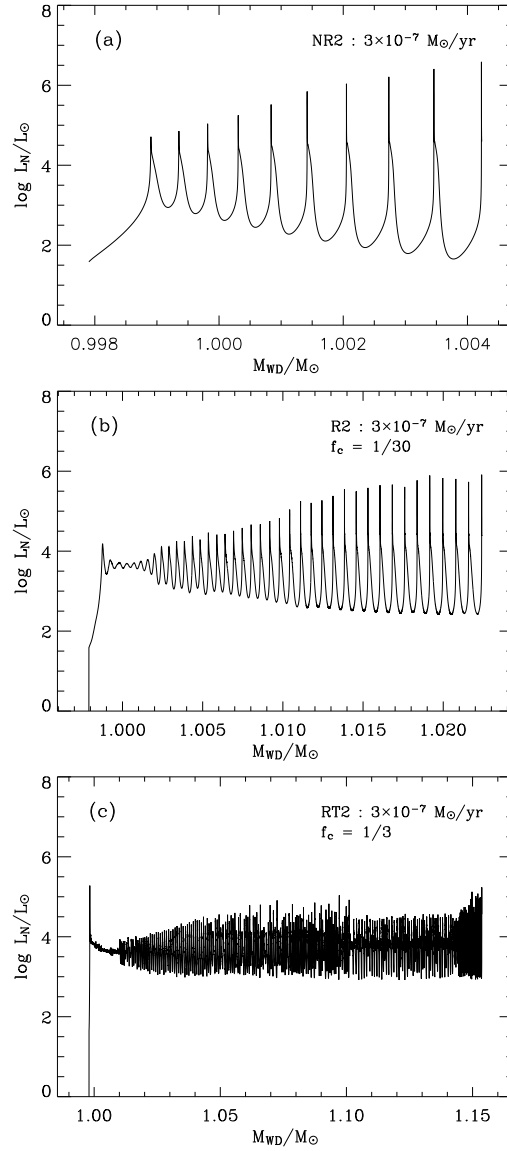
Figure 5.3: Same as in Fig. 5.1 but with $\dot{M} = 3 \times 10^{-7}$ (NR2, R2, RT2).
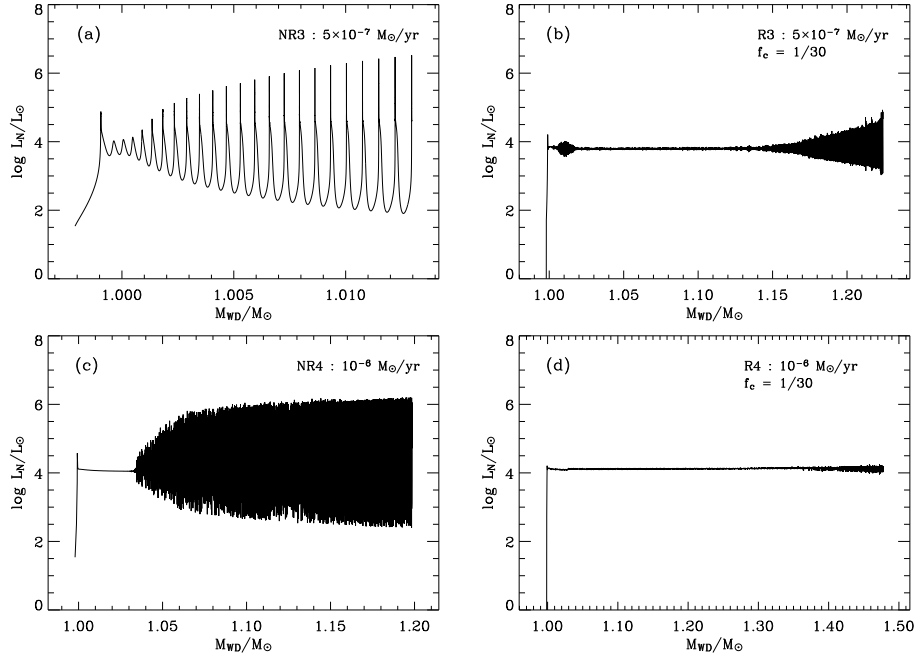
Figure 5.4: Evolution of nuclear luminosity due to helium burning in the helium accreting white dwarf models for $\dot{M} = 5 \times 10^{-7}$ (NR3 and R3) and $\dot{M} = 10^{-6}$ (NR4 and R4). The abscissa denotes the total mass of white dwarf, which serves as a measure of time. We note that what appears to look like noise in the plots for R3 and NR4 corresponds to many successive thermal pulses each of which being as well resolved in time (i.e., by roughly 10^3 time steps) as those in the plots in Fig 5.1 and 5.3.

the evolution until $M_{\mathrm{WD}} = 1.2$ M$_\odot$ and find that the thermal pulses do not become strong enough to lead the white dwarf to the Eddington limit. On the other hand, in the rotating sequence R4 (Fig. 5.4d), the white dwarf can grow up to $M_{\mathrm{WD}} \simeq 1.48M_\odot$ without encountering significant thermal pulses.

The evolution of the white dwarf of sequence R4 in HR diagram is shown in Fig. 5.5. The surface luminosity remains nearly constant at $\log L_{\mathrm{s}}/L_\odot \simeq 4.2$, while the surface temperature increases from $\log T = 5.3$ to $\log T = 5.88$, with which the white dwarf will appear as a super-soft X-ray source (e.g. Kahabka & van den Heuvel 1997; Greiner 2000).

Results presented in this section show that the helium shell source becomes more stable with rotation, and that the stronger the chemical mixing the more stable the shell burning becomes. We discuss the physical reasons for this behavior in Sect. 5.6.
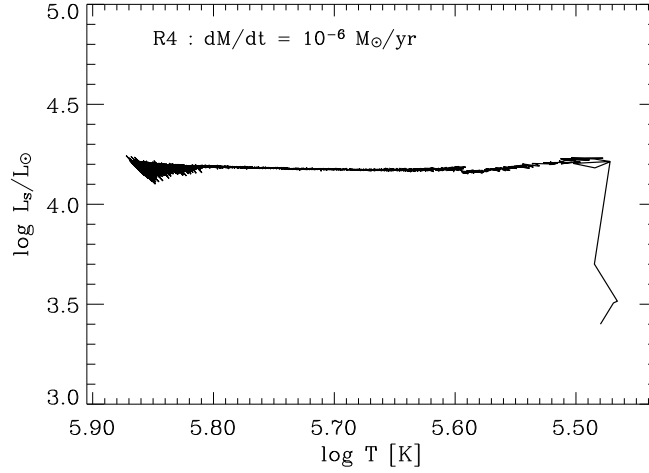
Figure 5.5: Evolution of white dwarf in sequence R4 in the Hertzsprung-Russell diagram.

5.4.2 White dwarf spin and angular momentum transport

According to Yoon & Langer (2004a), who considered accretion of carbon-oxygen rich matter, non-magnetic accreting white dwarfs with $\dot{M} \gtrsim 10^7$ M$_\odot$/yr show the following features in relation to the angular momentum redistribution. a) Eddington-Sweet circulations, the secular shear instability, and the GSF instability are dominating the angular momentum redistribution in the non-degenerate outer envelope, while the dynamical shear instability is the most important in the degenerate core. b) The degree of differential rotation in the degenerate core remains strong throughout the evolution, with a shear strength near the threshold value for the onset of the dynamical shear instability. c) The resulting differential rotation changes the white dwarf structure such that the center does not reach carbon ignition even when the white dwarf reaches the Chandrasekhar limit (~ 1.4 M$_\odot$). d) More than 60 % of the angular momentum of the accreted matter is rejected by the condition that the white dwarf should not gain angular momentum when its surface rotates critically (Eq. 5.1).

It is found that all these features remain the same in the present study, where helium accretion is considered. Fig. 5.6 shows angular velocity profiles throughout white dwarf models of sequence RT1, R3 and R4, at various times, where the angular velocity is given in units of the local Keplerian value (i.e., $\omega_{\mathrm{Kep}} = \sqrt{GM_r/r^3}$). Note that the spin rate remains well below the local Keplerian value throughout the whole star in all cases.

The white dwarf model with $M_{\mathrm{WD}} \simeq 1.4$ M$_\odot$ in sequence R4 has a central density of 3.54×10^8 g/cm^3, which is still far from the carbon ignition density. (cf. Ostriker & Bodenheimer 1968; Durisen 1975b; Durisen & Imamura 1981). As shown in the mentioned papers, a differentially rotating white dwarf can be dynamically stable up to ~ 4.0 M$_\odot$.
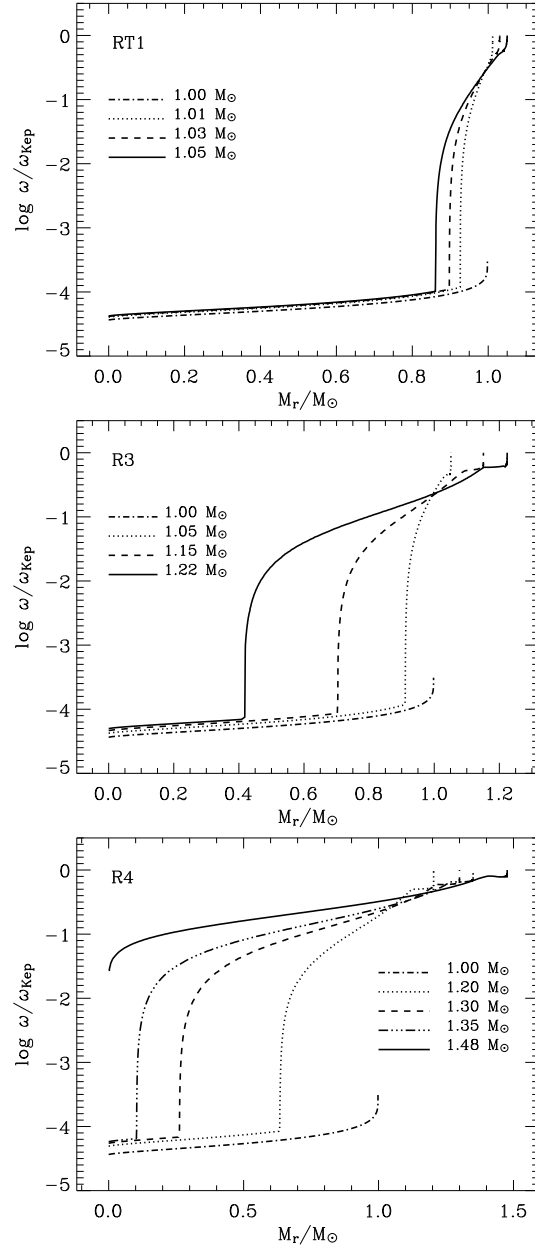
Figure 5.6: Spin velocity at different white dwarf masses, normalized to the local Keplerian value, as function of the mass coordinate for RT1, R3 & R4.

As discussed in Yoon & Langer (2004a), this suggests that the secular instability to the gravitational wave radiation reaction, which is often called as the 'CFS instability' (Chandrasekhar 1970; Friedman & Schutz 1978), might be important for the final fate of accreting white dwarfs at near or above the Chandrasekhar limit. The ratio of the rotational energy to the gravitational energy ($E_{\rm rot}/|W|$), which determines the growth time scale of the CFS instability via the bar-mode or the r-mode (see Yoon & Langer 2004a), remains smaller than 0.1 in the white dwarf models of sequence R4, and the last model ($M_{\rm WD} = 1.48\ {\rm M}_\odot$) has $E_{\rm rot}/|W| = 0.06$. Since $E_{\rm rot}/|W| \gtrsim 0.1$ is required in white dwarfs with strong differential rotation for the onset of the bar-mode instability (Imamura et al. 1995), only the r-mode may be relevant at this point. The expected growth time of the r-mode instability in this model is about 1.1×10^5 yr (see Yoon & Langer 2004a; Lindblom 1999). We refer to Yoon & Langer (2004a) for a detailed discussion of the final fate of fast rotating massive white dwarfs.

5.5 Chemical mixing and nucleosynthesis

The mixing of α-particles into the CO-core and of carbon into the helium envelope has consequences for the helium burning shell source. Here, we discuss the resulting changes in chemical structure of the white dwarf, while in the next section we analyze how rotation and rotationally induced chemical mixing affects the stability properties of the shell source.

Fig. 5.7 shows the chemical structure and the nuclear energy generation rate in the helium burning shell in the white dwarf models of sequences R4 and NR4 when $M_{\rm WD} = 1.0305\ {\rm M}_\odot$. The helium layer in the rotating model extends farther into the CO core, compared to the non-rotating case, due to the rotationally induced chemical mixing. This renders the $^{12}{\rm C}(\alpha, \gamma)^{16}{\rm O}$ reaction more active in the rotating model, with two main consequences.

Firstly, the contribution of the $^{12}{\rm C}(\alpha, \gamma)^{16}{\rm O}$ reaction to the total energy production is considerably increased. In the given models in Fig. 5.7, the rotating model gives $\log L_{3\alpha}/L_\odot = 3.938$ and $\log L_{^{12}C(\alpha,\gamma)}/L_\odot = 3.562$, while the non-rotating model gives $\log L_{3\alpha}/L_\odot = 3.963$ and $\log L_{^{12}C(\alpha,\gamma)}/L_\odot = 3.338$, where $L_{3\alpha}$ and $L_{^{12}C(\alpha,\gamma)}$ are the integrated nuclear energy generation rate over the shell source in the unit of erg/s, due to the triple alpha reaction and the $^{12}{\rm C}(\alpha, \gamma)^{16}{\rm O}$ reaction, respectively. The 3α reaction is weaker in the rotating model than in the non-rotating one due to a lower density in the helium envelope (cf. Fig. 5.9 in Sect. 5.6) and due to a smaller mass fraction of helium at the peak of the nuclear energy generation rate caused by rotationally induced mixing (Fig. 5.7). However, the increase of the energy generation by the $^{12}{\rm C}(\alpha, \gamma)^{16}{\rm O}$ reaction is more important on the whole, leading to a higher nuclear luminosity in the rotating model ($\log L_{\rm N}/{\rm L}_\odot = 4.094$) compared to the non-rotating model ($\log L_{\rm N}/{\rm L}_\odot = 4.060$), for the models given in Fig. 5.7. Furthermore, the shell source is hotter in the rotating model, $T_{\rm shell}/(10^8\ {\rm K}) = 2.16$ than in the comparable non-rotating model [$T_{\rm shell}/(10^8\ {\rm K}) = 2.03$], which affects the stability of the shell source as discussed in Sect. 5.6.

Secondly, the enhanced $^{12}C(\alpha, \gamma)$-efficiency results in an increased oxygen abundance in the ashes of the helium burning shell, at the expense of carbon. Fig. 5.8 shows the carbon
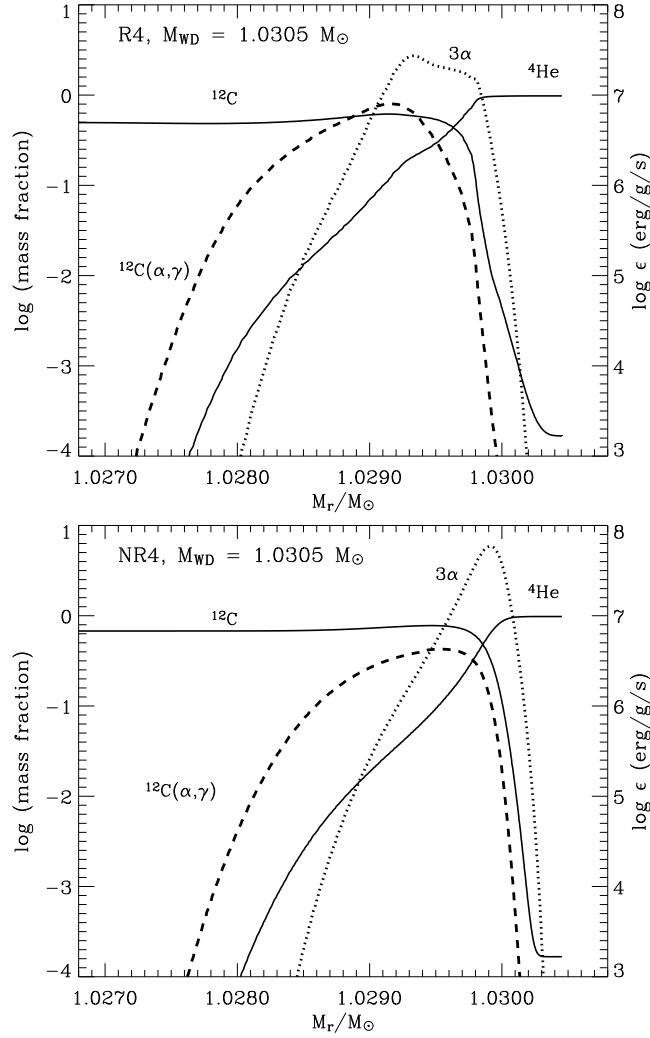
Figure 5.7: Logarithm of the mass fractions of helium and carbon as function of the mass coordinate (solid line), in the white dwarf models of sequences NR4 (upper panel) and R4 (lower panel) at a time when $M_{\mathrm{WD}} = 1.02178$ M$_\odot$. The dotted and dashed lines denote the corresponding energy generation rate (left scale) for the 3α and $^{12}C(\alpha, \gamma)$ reactions respectively.

mass fraction throughout the white dwarf for the last computed models of sequences NR3 and R3. In the non-rotating model, the carbon mass fraction produced by the shell source reaches almost $X_{\mathrm{C}} \simeq 0.68$ at a white dwarf mass of 1.03 M$_\odot$. At this time, the helium shell
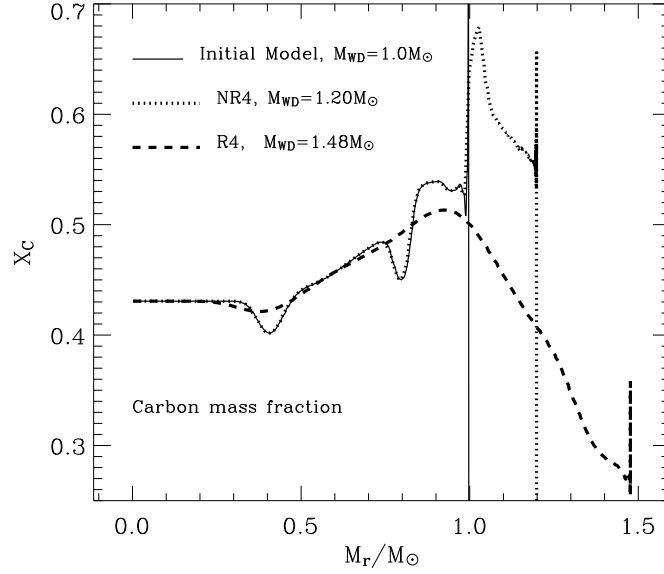
Figure 5.8: Carbon mass fraction as a function of the mass coordinate for the last computed models of sequences R4 (dashed line) and NR4 (dotted line). The thin solid line corresponds to the initial model. Note that the mass of the helium envelope is only of the order of 10^{-4} M$_\odot$, which is not resolved in this figure.

source becomes unstable and develops thermal pulses. As the layers at and above the shell source become convectively unstable during each pulse, the resulting carbon abundance is reduced. The convective mixing becomes more and more significant as the thermal pulse becomes stronger (cf. Fig. 5.4c), which is reflected in the drop of X_C from about 0.68 to 0.55 in the range 1.03 M$_\odot \lesssim M_\mathrm{r} \lesssim$ 1.20 M$_\odot$ in Fig. 5.8. A comparison with the rotating model shows that the carbon mass fraction is mostly below 0.5, even though the rotating model does not suffer from thermal pulses for most of the time. While the average carbon mass fraction in the accreted layer is 0.58 in the non-rotating model, it is 0.45 in the layer with $1.0 < M_r/\mathrm{M}_\odot < 1.2$ of the rotating model. The average carbon mass fraction in the accreted layer is 0.38 in the last calculated model ($M_\mathrm{WD} \simeq 1.48$ M$_\odot$).

The carbon and oxygen mass fractions in the accreted envelope of an SN Ia progenitor are important from the point of view of nucleosynthesis and supernova spectroscopy, and may even affect the peak brightness of the supernova explosion (Umeda et al. 1999; Höflich et al. 2000; Domínguez et al. 2001).

5.6   Stability of helium shell burning

Our results show that helium shell burning is more stable with rotation, compared to the non-rotating case (Figs. 5.1, 5.3, 5.4). The stability of a helium shell source is mainly determined by three factors: geometrical thickness, degree of degeneracy and temperature of the shell source. In other words, a helium shell source is more stable if it is thicker, less degenerate and hotter. While a general and quantitative stability criterion for shell sources is worked out in a separate paper (Yoon, Langer & van der Sluys 2004), we discuss the qualitative effects of rotation on the shell source stability of the models presented in Sect. 3 in the following.

Fig. 5.9 shows the evolution of the helium shell sources of sequences NR4 and R4 in the plane of the degeneracy parameter η ($:= \psi/kT$, e.g. Clayton 1968) and the relative thickness of the shell source D/r_s, where D and r_s are the thickness and the radius of the shell source, respectively. Here, the energy generation rate weighted mean over the shell source is used for the degeneracy parameter. The thickness of the shell source is defined such that the energy generation rate at each boundary is 2×10^{-3} times its peak value. Figure 5.9 illustrates the evolution toward instability for the example of sequences NR4 and R4. In sequence NR4, the mean temperature in the shell source remains nearly constant, around $T \simeq 2.02 \times 10^8$ K during the stable shell burning phase. Fig. 5.9 shows the border between stability and instability for $T = 2 \times 10^8$ K, as obtained by Yoon, Langer & van der Sluys (2004), as dotted line. Shell source becomes more degenerate and thinner as the white dwarf mass grows, and finally enters the unstable regime when $M_{WD} \simeq 1.03$ M$_\odot$, resulting in the onset of thermal pulses as shown in Fig. 5.4c.

As already discussed in Sect. 5.5, the shell source in the rotating models extends over a wider mass range due to rotationally induced chemical mixing. I.e., significant amounts of α-particles are mixed into the CO core and participate in the ^{12}C$(\alpha, \gamma)^{16}$O reaction. The presence of the centrifugal force lowers the density, and were it not for the effect of mixing, the shell source temperature would decrease with rotation. However, due to the enhanced ^{12}C$(\alpha, \gamma)^{16}$O reaction, temperature and nuclear energy production are increased, despite the lower density. In summary, rotation changes all three physical properties which affect the stability — thickness, degeneracy and temperature — such that stability becomes more likely. Fig. 5.9 shows that this effect is quite significant. While the evolutionary tracks of sequences NR4 and R4 are close to each other in the shell thickness-degeneracy plane, *at a given mass* the shell thickness is much larger and the degeneracy much lower in the rotating models. For example, at $M_{WD} = 1.01$ M$_\odot$, the non-rotating model gives $\eta \simeq -2.9$ and $D/r_s \simeq 0.225$ and the corresponding rotating model gives $\eta \simeq -3.0$ and $D/r_s \simeq 0.281$. Furthermore, we have $\eta \simeq -2.8$ and $D/r_s \simeq 0.19$ at $M_{WD} = 1.03$ M$_\odot$, which is the last analysed model in sequence NR4, while $\eta \simeq -2.9$ and $D/r_s \simeq 0.25$ even when M_{WD} is as large as 1.14 M$_\odot$ (Fig. 5.9).

Additionally, the instability border which is given by the thin lines in Fig. 5.9 is located lower at a given mass in the rotating case, due to the higher shell source temperature in the rotating models, which leads to a later onset of the instability. For instance, the shell source
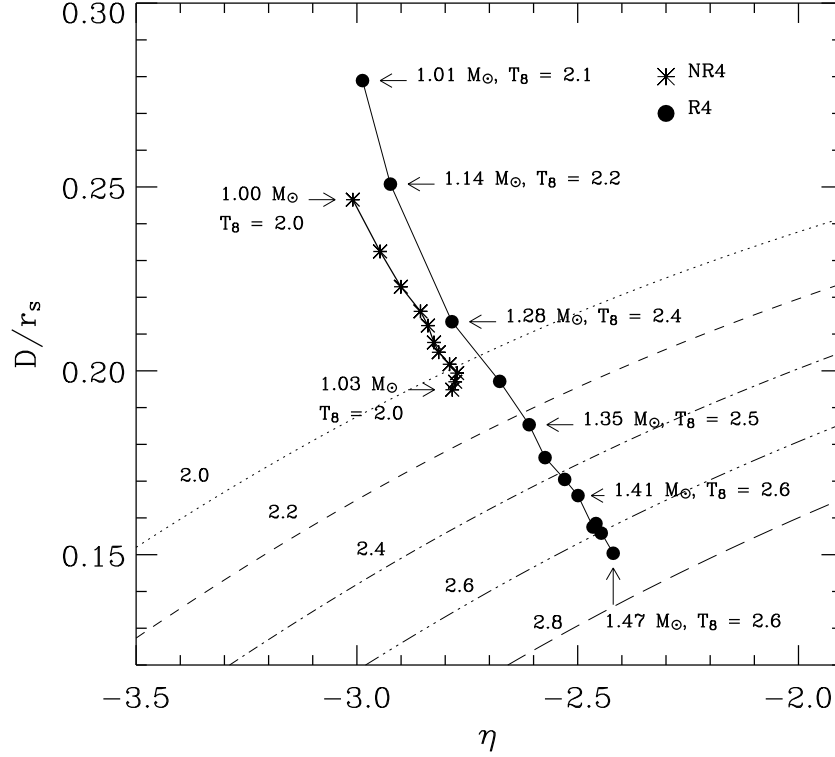
Figure 5.9: Evolution of the helium shell source in the sequences NR4 and R4 during stable shell burning phase, in the plane spanned by the degeneracy parameter η and the relative thickness of shell source D/r_s. Here D denotes the thickness of shell source and r_s its radius. Each asterisk and black dot represents one selected stellar model in sequence NR4 and R4, respectively. The white dwarf mass in solar masses and the temperature of the shell source in the unit of 10^8 K are indicated for various models. The thin lines separate the stable and unstable regime, for $T/(10^8 \; \mathrm{K}) = 2.0$ (dotted line), 2.2 (short dashed line), 2.4 (dotted-dashed line), 2.6 (three dotted - dashed line) and 2.8 (long dashed line) according to the analytic stability criterion of Yoon, Langer & van der Sluys (2004). I.e., helium shell burning is predicted to be stable (unstable) above (below) the lines, while thermal pulses become significant from $M_\mathrm{WD} \simeq 1.03 \; \mathrm{M}_\odot$ in sequence NR4, and weak thermal pulses appear from $M_\mathrm{WD} \simeq 1.41 \; \mathrm{M}_\odot$ in sequence R4.

temperature in the rotating model when $M_\mathrm{WD} = 1.01 \; \mathrm{M}_\odot$ is about 2.1×10^8 K, which is higher than in the non-rotating models, where T_shell remains at $\sim 2.0 \times 10^8$ K during the steady shell burning phase. The stability limit for the relative thickness of the shell source at this temperature is given by the dotted line as a function of the degeneracy parameter. The last analysed model in NR4 is already in the unstable regime ($D/r_\mathrm{s} \simeq 0.19$) and thermal

pulses grow significantly right after as expected from the stability criterion. On the other hand, the shell source temperature increases up to 2.6×10^8 K when $M_{WD} = 1.41$ M$_\odot$, which explains why the shell source is stable until $M_{WD} \simeq 1.41$ M$_\odot$ even though D/r_s at this moment is smaller than in the last analyzed model of NR4. As shown in Fig. 5.4d (see also Fig. 5.5), the ensuing thermal pulses which appear when $M_{WD} \gtrsim 1.41$ M$_\odot$ in sequence R4 remain very weak until the last model ($M_{WD} = 1.48$ M$_\odot$ with $T_{shell} = \simeq 2.6 \times 10^8$ K), which is still near the stability border line for $T = 2.6 \times 10^8$ K in Fig. 5.9.

In summary, rotation stabilizes the instability of the burning shell in our models significantly. Shell sources in realistic white dwarfs, however, may be even more stable than our models predict, due to two reasons. Firstly, as outlined in Sect. 5.2, our method forces us to limit the structural effects of rotation to that obtained at about 60% of critical rotation. This means that we underestimate the centrifugal force in the layers which contain the shell source. Secondly, our models are one-dimensional, which restricts the pressure response due to any perturbation to the radial direction — which is generally not true in the realistic situation. In a fast rotating star, the pressure can also respond to a perturbation horizontally, unless the shell source is located at the poles. We believe that this multidimensional effects can stabilize the shell source further. It is also possible that the physical conditions in the shell source vary with latitude, which may lead to interesting consequences such as non-spherical stellar winds (cf. Owocki & Gayely 1997; Maeder 1999) . We leave the systematic investigation of these effects to future work.

5.7   Final discussion

We have performed numerical simulations of helium accreting CO white dwarfs with an initial mass of 0.998 M$_\odot$ and 4 different mass accretion rates (2, 3, 5 and 10×10^{-7} M$_\odot$/yr), considering spin-up by mass accretion. The main feature of the spin-up is the angular momentum transport from the accreted matter into the white dwarf, which creates differential rotation in the white dwarf interior. This induces transport of chemical species from the accreted matter into the CO core, through the shear instability, Eddington Sweet circulations, and the GSF instability.

It is shown that the helium burning layer becomes spatially more extended compared to the non-rotating case, since the accreted α-particles are mixed into the carbon-rich layer, participating actively in the $^{12}C(\alpha, \gamma)^{16}O$ reaction (Sect. 5.5). The carbon-to-oxygen ratio is significantly reduced in the accreted layer. The centrifugal force lowers density in the shell source and degeneracy is significantly lifted. The total energy generation in the helium shell source increases with rotation, due to the increased contribution from the $^{12}C(\alpha, \gamma)^{16}O$ reaction, rendering the helium shell source as hot as in the non-rotating cases, despite the lowered density. All these effects contribute to stabilizing the helium shell burning significantly (Sect. 5.6). Thermal pulses, if they occur, are considerably weakened with rotation.

As mentioned previously, and as discussed by Cassisi et al. (1998), Kato & Hachisu (1999) and Langer et al. (2002), a high mass accumulation efficiency on a white dwarf by hydrogen accretion has been seriously questioned due to the unstable helium shell burning

which is found when helium is accreted at a rate which gives steady hydrogen shell burning. Note that the accretion rate of 5×10^{-7} corresponds roughly to the maximum rate for the steady hydrogen burning in a $1.0\,M_\odot$ white dwarf (Nomoto 1982a). Our results indicate that even if hydrogen is accreted and burned steadily, the subsequent helium shell burning may be unstable, with strong helium shell flashes driving the stellar envelope to the Eddington limit, unless effects of rotation are considered. Cassisi et al. (1998) pointed out that the white dwarf will fill its Roche lobe once helium flashes occur during hydrogen accretion, leaving doubts about the mass increase of a white dwarf by hydrogen accretion. Kato & Hachisu (1999) suggested that if the new OPAL opacities are adopted, an optically thick wind can remove mass from the system without the white dwarf's filling its Roche lobe. They also suggested that the effective mass accumulation rate can remain high enough for the white dwarf to grow to the Chandrasekhar mass.

Although our results imply that rotation can help a white dwarf to grow in mass by stabilizing helium shell burning, we still cannot answer the question whether rotation may be a potential solution in explaining the observed SNe Ia rate from the canonical single degenerate scenario, where a main sequence star or a red giant is considered as the white dwarf companion (Li & van den Heuvel 1997; Hachisu et al. 1999; Langer et al. 2000), without investigating the effects of rotation in the case of hydrogen accretion. However, given that the stability conditions for hydrogen shell burning are not qualitatively different from that for helium shell burning (Yoon, Langer & van der Sluys 2004), the effects of rotation on the hydrogen shell source are likely to give a similar conclusion as for the helium shell burning.

On the other hand, hydrogen accretion with a rate of $10^{-6}\,M_\odot/yr$, with which our rotating sequence reaches the Chandrasekhar limit without undergoing ustable helium shell flashes, is supposed to lead a $1.0\,M_\odot$ white dwarf into a red giant phase (Nomoto 1982a; Nomoto & Kondo 1993; Cassisi et al. 1998). In a close binary system, the hydrogen envelope expanded to the red giant phase will fill the Roche lobe, causing significant mass loss or the merging of both stars, unless the mass accretion rate is not reduced by an optically thick stellar wind, as suggested by Hachisu et al (1996, 1999). However, steady helium accretion with such a high accretion rate can be realized, for example, in a binary system which consists of a white dwarf and a helium giant star ("helium Algols", Iben & Tutukov 1994), in which the mass transfer rate can amount to $10^{-6} - 10^{-5}\,M_\odot/yr$, as shown by Yoon & Langer (2003). Our results indicate clearly that the mass accumulation efficiency can be significantly enhanced by rotation for helium giant star + white dwarf binary systems. Although the production rate of SNe Ia via this route is currently rather uncertain (Iben & Tutukov 1994; Branch et al. 1998), rotation may increase it strongly.

Finally, we note that an increase in the uncertain efficiency of rotationally induced chemical mixing results in more stable shell burning (Fig. 5.1 and 5.3), than the case where the calibration by Heger et al. (2000) and Heger & Langer (2000) is adopted. Their calibration gives a similar chemical mixing efficiency as in Pinsonneault et al. (1989) who made a calibration to reproduce the solar surface ^{7}Li abundance, as well as to the theoretical estimate by Chaboyer & Zahn (1992). The physical conditions in the helium shell source in white

dwarfs do not qualitatively differ from those in main sequence stars. However, for accreting white dwarfs, another mixing mechanism which was not considered in the present study may be important: magnetic instability induced by differential rotation in radiative layers (Spruit 2002). Heger et al. (2003) and Maeder & Meynet (2003) show that the turbulent diffusion can become stronger by several orders of magnitude due to the magnetic instability, compared to the case where only rotational effects are considered. The differential rotation induced magnetic instability can be even more important in accreting white dwarfs, in which a strong shear motion is retained due to the continuous angular momentum transport from the accreted matter, as shown in Sect. 5.4.2. The efficiency of the chemical mixing may increase accordingly, which may stabilize the shell source even further than in the present study. This possibility is currently under investigation.

Chapter 6

Helium accreting CO white dwarfs with rotation: helium novae instead of double detonation

S.-C. Yoon and N. Langer

Abstract   We present evolutionary models of helium accreting carbon-oxygen white dwarfs in which we include the effects of the spin-up of the accreting star induced by angular momentum accretion, rotationally induced chemical mixing and rotational energy dissipation. Initial masses of 0.6 $M_\odot$ and 0.8 $M_\odot$ and constant accretion rates of a few times $10^{-8} M_\odot/\mathrm{yr}$ of helium rich matter have been considered, which is typical for the sub-Chandrasekhar mass progenitor scenario for Type Ia supernovae. It is found that the helium envelope in an accreting white dwarf is heated efficiently by friction in the differentially rotating spun-up layers. As a result, helium ignites much earlier and under much less degenerate conditions compared to the corresponding non-rotating case. Consequently, a helium detonation may be avoided, which questions the sub-Chandrasekhar mass progenitor scenario for Type Ia supernovae. We discuss implications of our results for the evolution of helium star plus white dwarf binary systems as possible progenitors of recurrent helium novae.

6.1   Introduction

Type Ia supernovae are of key importance for the chemical evolution of galaxies, as they are a major producer of iron group elements (e.g. Nomoto et al. 1984; Renzini 1999). They were also found to be excellent distance indicator and have become an indispensable tool in cosmology (Phillips 1993; Hamuy et al. 1996a; Branch 1998). The recent suggestion of a non-zero cosmological constant is partly based on observations of SNe Ia at high redshift (Leibundgut 2001). Given that distance determinations at high redshift through SNe Ia depend on the assumption of the homogeneity of SNe Ia light curves throughout the ages, an understanding of the possible diversity of their progenitors is crucial to evaluate this approach. Nevertheless, the progenitors of Type Ia supernovae have not been identified yet, and the debate on their exact nature continues (e.g., Livio 2001).

One possibility to obtain an SN Ia is the detonation of the degenerate helium layer accumulated on top of a CO white dwarf due to mass transfer from its low mass helium star companion in a close binary system, which triggers a carbon detonation in the white dwarf core. This is the so called double detonation or sub-Chandrasekhar mass scenario for SNe Ia, as it may allow to explode white dwarfs with masses well below the Chandrasekhar mass (e.g. Nomoto 1982b; Fujimoto & Sugimoto 1982; Limongi & Tornambé 1991; Livne 1990; Woosley & Weaver 1994; Livne & Arnett 1995). While the capability of the helium detonation to ignite the CO core is still debated (e.g., Livio 2001), the helium detonation by itself would produce an explosion of supernova scale.

Currently, the sub-Chandrasekhar mass scenario is not favored as a major source of SNe Ia mainly because the light curves and spectra obtained from this model are not in good agreement with observations (e.g. Höflich & Khokhlov 1996; Nugent et al. 1997). Especially, the predicted presence of high velocity Ni and He is most stringently criticized (e.g. Hillebrandt & Niemeyer 2000; Livio 2001).

On the other hand, stellar and binary evolution theory predicts a realization frequency of binary systems such as helium star cataclysmics — which might produce double detonating sub-Chandrasekhar mass white dwarfs — which amounts to a few times 10^{-3} yr^{-1} per galaxy (e.g. Iben & Tutukov 1991; Regös et al. 2002) which is comparable to the expected total SN Ia rate in the Milky Way. This raises the question why such explosions are practically never observed.

We note that the sub-Chandrasekhar mass SN progenitor models which have been constructed so far neglected the effects of rotation, which can be one of the primary factors determining the evolution of stars, in particular of massive stars (Langer 1998; Maeder & Meynet 2000). Iben & Tutukov (1991) pointed out that rotation may indeed be important in helium star cataclysmic systems. Yoon & Langer (2002, 2004a) and Yoon et al. (2004) showed that effects of rotation might be essential for the evolution of accreting white dwarfs when the accreted matter contains a high specific angular momentum. The induced spin-up was found to change the white dwarf structure significantly and to produce rotationally induced chemical mixing.

In this paper, we suggest that rotation could play a key role in helium accreting white

dwarfs such that in model which would produce a helium detonation this phenomenon is completely avoided when the white dwarf spin-up is considered. After explaining the numerical method and physical assumptions of the present study in Sect. 6.2, we investigate the evolution of helium accreting carbon-oxygen white dwarfs with accretion rates of $\sim 10^{-8}$ M$_\odot$/yr, with the effects of rotation considered, in Sect. 6.3. Implications of our results for helium novae and neutron capture nucleosynthesis are discussed in Sect. 6.4. Our main conclusions are summarized in Sect. 6.5

6.2 Numerical method and physical assumptions

We have computed the numerical models with a hydrodynamic stellar evolution code (Langer et al. 1988), which incorporates the effect of the centrifugal force on the stellar structure and rotationally induced transport of angular momentum and chemical species due to the dynamical and secular shear instability, the Goldreich-Schubert-Fricke instability and the Eddington-Sweet circulations (Heger et al. 2000; Yoon & Langer 2004a). Conservation of angular momentum and energy of viscous fluids requires dissipation of rotational energy as angular momentum is transported by viscous friction in differentially rotating layers (e.g. Landau & Lifshitz 1984). This effect is considered in our calculations following Mochkovitch & Livio (1989) as:

$$\epsilon_{\mathrm{diss,r}} = \frac{1}{2}\nu_{\mathrm{turb}} \left(\frac{\partial \omega}{\partial \ln r}\right)^2 \; \left(\mathrm{erg\ g}^{-1}\mathrm{sec}^{-1}\right), \qquad (6.1)$$

where ω is the angular velocity, r the radius and ν_{turb} the turbulent viscosity due to the above mentioned rotationally induced instabilities (Heger et al. 2000; Yoon & Langer 2004a).

Nuclear networks for the changes in chemical composition and the nuclear energy generation include more than 60 reactions (see Heger et al. 2000 for more details). In particular, the $^{14}\mathrm{N}(e^-,\nu)^{14}\mathrm{C}(\alpha,\gamma)^{18}\mathrm{O}$ reaction (hereafter NCO reaction), which becomes active when $\rho \gtrsim 10^6$ g cm^{-3} (Hashimoto et al. 1984), has been newly included for this study. We have used the $^{14}\mathrm{N}(e^-,\nu)^{14}\mathrm{C}$ reaction rate given by Martinez (2002, Private communication) and followed Caughlan and Fowler (1988) for the $^{14}\mathrm{C}(\alpha,\gamma)^{18}\mathrm{O}$ reaction rate. The accretion induced heating is described following Neo et al. (1977), and the accreted matter is assumed to have the same entropy as that of the surface of the accreting star.

Two initial masses, 0.6 and 0.8 M$_\odot$, are considered for the CO white dwarf models. Since isolated white dwarfs are generally found to rotate with a surface velocity of $v_{\mathrm{s}} \lesssim 40$ km/s (Heber et al. 1997; Koester et al. 1998; Kawaler 2003), the initial rotation velocity of our models is assumed to be as slow as 10 km/s at the white dwarf equator (see also Langer et al. 1999). Other physical properties of the white dwarf initial models are summarized in Table 6.1. While most of our simulations start with a cold white dwarf with $\log L_{\mathrm{s}}/\mathrm{L}_\odot \simeq -2.0$, an initially hot white dwarf with $\log L_{\mathrm{s}}/\mathrm{L}_\odot \simeq 2.508$ is also considered for one model sequence (TC, Table 6.2; cf. Sect. 6.4.1). The accreted matter, received with

Table 6.1: Physical quantities of the initial white dwarf models: mass, surface luminosity, central temperature, central density, radius and rotation velocity. The hot white dwarf model in the third row is only used for sequence TC (see Table 6.2).

$M_{\mathrm{WD,init}}$ $\mathrm{M}_\odot$	$\log L_{\mathrm{s,init}}/\mathrm{L}_\odot$	$T_{\mathrm{c,init}}$ 10^7 K	$\rho_{\mathrm{c,init}}$ 10^6 g/cm^3	$R_{\mathrm{WD,init}}$ $\mathrm{R}_\odot$	$v_{\mathrm{rot,init}}$ km/s
0.6	-2.049	1.69	3.64	0.0126	10
0.8	-2.024	1.59	10.7	0.0101	10
0.8	2.508	14.4	6.44	0.0186	10

two different constant accretion rates of $\dot{M} = 2 \times 10^{-8}$ and 3×10^{-8} M$_\odot$/yr, is assumed to have $Y = 0.982$ and $X_{\mathrm{N}} = 0.012$, where Y and X_{N} are the mass fraction of helium and nitrogen, respectively.

In a close binary system, the white dwarf is believed to receive matter through a Keplerian accretion disk if its magnetic field is not considerable. The accreted matter may thus carry an amount of specific angular momentum which corresponds to critical rotation at the white dwarf equator. However, continuous angular momentum gain under these conditions leads to over-critical rotation soon after the onset of mass transfer in the outer part of the accreting star (Yoon & Langer 2002). Therefore, we limit the angular momentum gain such that the accreting star may not rotate over-critically, as follows:

$$j_{\mathrm{acc}} = \left\{ \begin{array}{ll} f \cdot j_{\mathrm{Kepler}} & \text{if } v_{\mathrm{s}} < f \cdot v_{\mathrm{Kepler}} \\ 0 & \text{if } v_{\mathrm{s}} = f \cdot v_{\mathrm{Kepler}} \end{array} \right. \tag{6.2}$$

where v_{s} denotes the surface velocity at the white dwarf equator, j_{acc} the specific angular momentum of the accreted matter, and v_{Kepler} and j_{Kep} the Keplerian value of the surface velocity and the specific angular momentum at the white dwarf equator, respectively. The dimensionless parameter f represents the fraction of the Keplerian value of the specific angular momentum which is contained in the accreted matter, and also the maximum fraction of the critical rotational velocity with which the white dwarf equator may rotate.

The use of $f = 1$ might be the most natural choice to describe the realistic situation, as Paczyǹski (1991) and Popham & Narayan (1991) argue that a critically rotating star may continue to accrete matter from a Keplerian disk by transporting angular momentum from the star back into the disk due to turbulent viscosity. However, as the correct treatment of close-to-critical rotation is beyond the capabilities of our numerical code, we also consider the case $f < 1$. As discussed in Yoon & Langer (2004a), the correction factors of f_{P} and f_{T} which are included in the stellar structure equations for describing the effects of rotation (cf. Heger et al. 2000) are limited to 0.75 and 0.95, respectively. This limit corresponds to a rotation rate of about 60% of critical rotation, up to which our one dimensional approximation in computing the effective gravitation potential can accurately describe the structure of the rotating star. In our models with $f = 1$, where the outer envelope rotates close to critically, the centrifugal force is accordingly underestimated. Although the region which

Table 6.2: Properties of the computed model sequences. M_{init} : initial mass, $\dot{M}$: accretion rate, f : fraction of the Keplerian value of the accreted specific angular momentum (see Eq. 6.2). $\dot{E}_{\mathrm{diss}}$: Rotational energy dissipation due to frictional heating. Yes (or No) means that this effect is considered (or not). ΔM_{He} : accumulated helium mass until the helium ignition point. T_{c} and ρ_{c} : central temperature and density in the last computed model. T_{He} : maximum temperature in the helium envelope in the last computed model. ρ_{He} and η_{He} : density and degeneracy parameter at the position of the maximum temperature in the helium envelope in the last computed model. The last column indicates whether the model sequence will finally result in helium detonation or not.

No.	M_{init}	$\dot{M}$	f	$\dot{E}_{\mathrm{diss}}$	ΔM_{He}	T_{c}	ρ_{c}	T_{He}	ρ_{He}	η_{He}	Detonation?
		10^{-8}				10^8	10^6	10^8	10^6		
	$\mathrm{M}_\odot$	$\mathrm{M}_\odot/\mathrm{yr}$			$\mathrm{M}_\odot$	K	$\mathrm{g\,cm}^{-3}$	K	$\mathrm{g\,cm}^{-3}$		
N1	0.6	2.0	–	–	0.229	0.60	10.9	2.0	1.48	11	Yes
N2	0.6	3.0	–	–	0.185	0.54	8.8	1.4	0.55	9	No
N3	0.8	2.0	–	–	0.168	0.55	26.1	2.0	1.58	13	Yes
N4	0.8	3.0	–	–	0.150	0.46	23.6	1.2	1.50	19	Yes
R1	0.6	2.0	1.0	Yes	0.080	0.39	4.4	1.2	0.22	6	No
R2	0.6	3.0	1.0	Yes	0.061	0.23	4.2	1.4	0.15	4	No
R3	0.8	2.0	1.0	Yes	0.022	0.14	11.0	1.5	0.15	4	No
R4	0.8	3.0	1.0	Yes	0.017	0.14	10.6	3.8	0.03	0.3	No
TA1	0.6	2.0	0.6	Yes	0.149	0.50	5.97	1.2	0.42	9	No
TA2	0.6	3.0	0.6	Yes	0.106	0.45	4.70	3.5	0.16	2	No
TA3	0.8	2.0	0.6	Yes	0.073	0.21	14.2	1.3	0.38	8	No
TA4	0.8	3.0	0.6	Yes	0.045	0.18	12.7	1.4	0.28	6	No
TB1	0.6	2.0	1.0	No	0.402	0.59	9.6	1.1	1.14	22	Yes
TB3	0.8	2.0	1.0	No	0.233	0.65	21.3	1.2	1.36	21	Yes
TC	0.8	1.0	1.0	Yes	0.002	0.95	8.5	2.8	0.001	0.06	No

rotates faster than 60% critical contains only little mass (see Sect. 6.3), we also consider the case $f = 0.6$, apart from the case $f = 1.0$. With $f = 0.6$, the white dwarf never rotates faster than 60 % of the Keplerian value, and thus the stellar structure is accurately described throughout the white dwarf interior.

For comparison, we also compute rotating models where the rotational energy dissipation is neglected, as well as non-rotating models, with otherwise identical initial conditions. In Table 6.2 we list all computed model sequences. The index N in the model number indicates a non-rotating model sequence, while R denotes a rotating one with $f = 1.0$. The index TA is for rotating test models with $f = 0.6$, while TB is used for rotating test models with $f = 1.0$ without rotational energy dissipation (i.e., $\epsilon_{\mathrm{diss,r}} = 0.0$). The sequence TC designates the only model starting with a hot white dwarf. All sequences are computed up to the point where the accumulated helium shell ignites.

6.3   Results

We summarize the results of our simulations in Table 6.2. Here, T_{He}, ρ_{He} and η_{He} denote, for the last computed model, the maximum temperature in the helium envelope and the corresponding density and the degeneracy parameter (ψ/kT, e.g. Kippenhahn & Weigert 1990). ΔM_{He} gives the accumulated helium mass until helium ignition.

At helium ignition we stop our calculations, and our models are per se not able to predict whether the helium burning develops into a helium detonation or not. However, from the literature (e.g., Woosley & Weaver 1994) we conclude that a helium detonation can not develop if the ignition density is smaller than $\sim 10^6$ g cm^{-3}, due to the quenching of the thermonuclear runaway by expansion. For $\rho_{\mathrm{He}} < 10^6$ g cm^{-3}, therefore, the helium ignition may result only in a nova-like shell flash, which will not be able to trigger core carbon ignition.

Our results for the non-rotating model sequences are found in good agreement with similar models computed by Woosley & Weaver (1994) and Piersanti et al. (2001). For instance, for a sequence with the same initial mass and accretion rate as for our sequence N1, Piersanti et al. obtained $\Delta M_{\mathrm{He}} = 0.244$ M$_\odot$, which does not differ much from our result of $\Delta M_{\mathrm{He}} = 0.229$ M$_\odot$. The slightly smaller value of the present study may be attributed to a small difference in the initial nitrogen mass fraction, which triggers the NCO reaction when $\rho_c \gtrsim 10^6$ g cm^{-3} and initiates helium burning.

Fig. 6.1 illustrates the evolution of our white dwarf models with $M_{\mathrm{init}} = 0.8$ M$_\odot$ and $\dot{M} = 2\times10^{-8}$ M$_\odot$/yr (sequences N3, R3 and TB3). In the non-rotating case, the temperature of the helium envelope continues to increase due to accretion induced heating. When the white dwarf mass reaches about 0.9 M$_\odot$, the density at the bottom of the helium envelope starts exceeding 10^6 g cm^{-3} and the NCO reaction becomes active, accelerating the temperature increase. Finally, helium burning starts when M_{WD} reaches 0.968 M$_\odot$. The density at the helium ignition point is about 1.6×10^6 g cm^{-3} and a detonation is likely to follow.

The evolution of the corresponding rotating model (R3) in Fig. 6.1 looks similar, but helium ignites much earlier than in the non-rotating case. The maximum temperature in the helium envelope reaches 10^8 K when $M_{\mathrm{WD}} \simeq 0.818$ M$_\odot$. Helium burning develops quickly thereafter, and the nuclear energy generation amounts to $\log L_{\mathrm{He}}/L_\odot \simeq 5.0$ when $M_{\mathrm{WD}} \simeq 0.822$ M$_\odot$. Only 0.022 M$_\odot$ of helium has been accumulated by then, which is about 10 times less than in the non-rotating case. Importantly, the ignition density ρ_{He} is also found about 10 times lower (1.5×10^5 g cm^{-3}) than in the non-rotating case, implying that a helium detonation may be avoided.

The reason for the early helium ignition in the rotating sequence is as follows. As explained above, the white dwarf obtains angular momentum carried by the accreted matter. The angular momentum is thus transported from the surface into the interior by various rotationally induced hydrodynamic instabilities. In our white dwarf models, Eddington Sweet circulation, the secular shear and the GSF instability dominate in the non-degenerate envelope, while the dynamical shear instability is most important in the degenerate interior, as discussed in detail by Yoon & Langer (2004a). The white dwarf interior is spun up
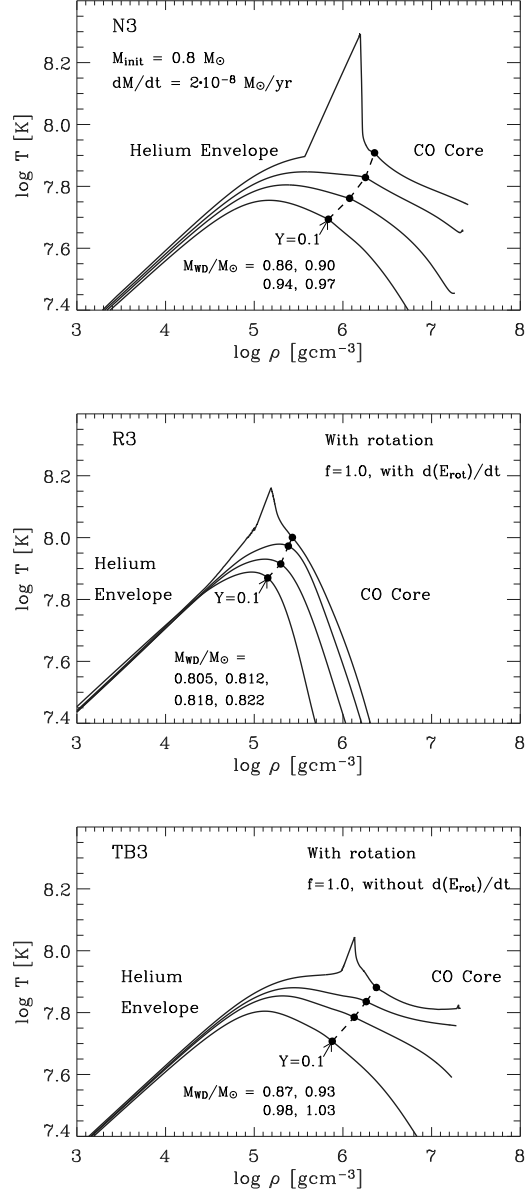
Figure 6.1: Evolution of accreting white dwarf models of sequence N3, R3 & TB3, for which $M_{\text{init}}=$ 0.8 $M_\odot$ and $\dot{M} = 2 \times 10^{-8}$ $M_\odot$/yr, in the $\log \rho - \log T$ plane. The boundary between the CO core and the helium envelope, defined though $Y = 0.1$, is indicated by a filled circle for each model.
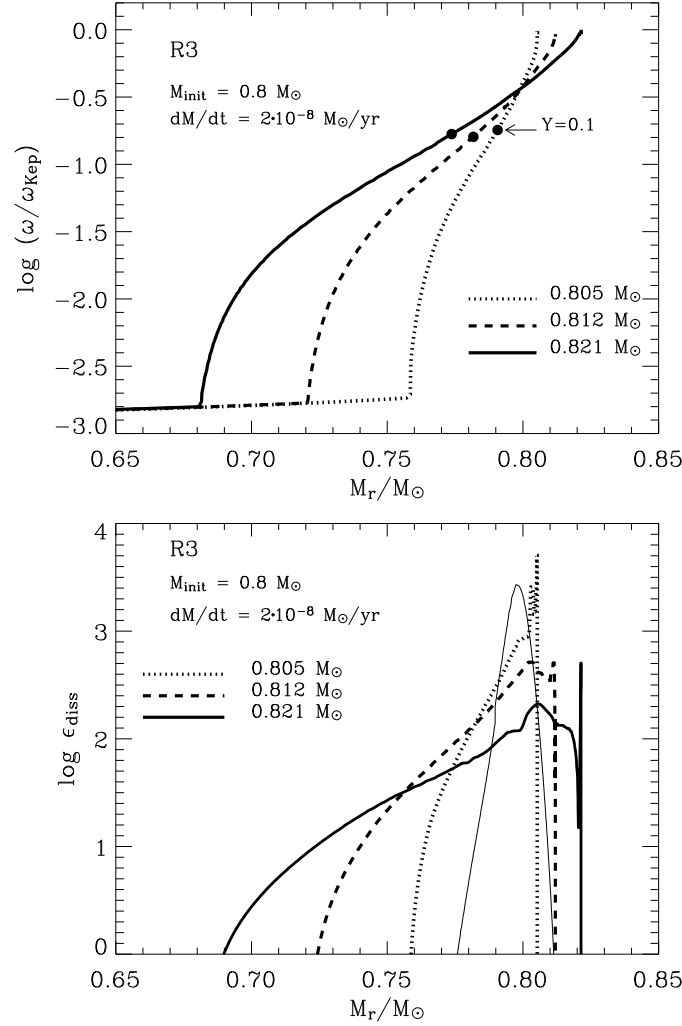
Figure 6.2: *Upper panel*: Angular velocity in units of the local Keplerian value as a function of the mass coordinate in model sequence R3 when $M_{WD} = 0.805$, 0.812 and 0.821 $M_\odot$. The filled circles indicate the boundary of the CO core and helium envelope, as defined in Fig. 6.1, where the helium mass fraction is 0.1. *Lower panel*: Rotational energy dissipation due to friction (Eq. 6.1) at the same evolutionary epochs as in the upper panel. The thin solid line denotes the energy generation rate due to nuclear reactions when $M_{WD} = 0.821$ $M_\odot$.

progressively with time, giving rise to rotational energy dissipation as shown in Fig. 6.2. In the upper panel of the figure, the angular velocity reveals a strong degree of differential

rotation. The consequent energy dissipation rate is given in the lower panel in the same figure. The total energy dissipation rate integrated over the spun-up layers in the given models amounts to 8.8 $L_\odot$, 6.2 $L_\odot$, and 3.6 $L_\odot$ for $M_{WD} = 0.805$ $M_\odot$, 0.812 $M_\odot$, and 0.821 $M_\odot$ respectively. Together with the accretion induced heating, this additional energy supply speeds up the temperature increase in the helium envelope, leading to the earlier helium ignition compared to the non-rotating case.

For comparison, the white dwarf evolution in sequence TB3, where the rotational energy dissipation is neglected while everything else is as in sequence R3, is shown in the third panel of Fig. 6.1. In this case, helium ignition occurs even later than in the corresponding non-rotating case (N3). This is due to the lifting effect of the centrifugal force, which reduces the accretion induced heating. The density at the bottom of the helium envelope when the helium burning is induced by the NCO reaction is about 1.36×10^6 g cm^{-3}, implying that a helium detonation might be triggered in this case.

As shown in Fig. 6.2, the surface layers of the white dwarf models in sequence R3, where $f = 1$ is used, rotate faster than 60 % critical, above which the effects of rotation are underestimated by our computational method. In the models with $M_{init} = 0.8$ $M_\odot$, i.e., in sequences R3 and R4, however, this fast rotating region is limited to only 1% of the white dwarf mass, which is not likely to affect the result significantly. On the other hand, about 7% in mass, which include a significant fraction of the helium envelope, exceed the limit at helium ignition in model sequences R1 and R2, for which $M_{init} = 0.6$ $M_\odot$ and $f = 1$ are adopted. Nevertheless, results from the corresponding sequences with $f = 0.6$ (TA1, TA2, TA3 and TA4), where the white dwarf models are forced to rotate below 60% critical throughout the white dwarf interior, lead us to the same conclusion as for $f = 1$: helium ignites at such a low density (even though it is somewhat higher than for $f = 1$) that a supernova event is unlikely to occur. For instance, in model sequence TA1, we have $\rho_{He} = 4.2 \times 10^5$ g cm^{-3} when the maximum temperature reaches 1.2×10^8 K. This is about 3.5 times lower than in the corresponding non-rotating case ($\rho_{He} = 1.48 \times 10^6$ g cm^{-3}) and about two times higher than for $f = 1$ ($\rho_{He} = 2.2 \times 10^5$ g cm^{-3}).

6.4   Discussion

6.4.1   Connection to recurrent helium novae

As discussed by Iben & Tutukov (1991) and Limongi & Tornambé (1991), a relatively low helium accretion rate of $\sim 10^{-8}$ $M_\odot$/yr onto a CO white dwarf can be realized, for example, in binary systems which consist of a $0.6 \cdots 1.0$ $M_\odot$ CO white dwarf and a less massive helium star. Mass transfer in such binary systems is driven by gravitational wave radiation, and the resulting mass transfer rate is found to be insensitive to the exact masses of white dwarf and helium star, at a few times 10^{-8} $M_\odot$/yr (Iben & Tutukov 1991; Limongi & Tornambé 1991). Many of such binary systems, if not all, could produce a supernova which will appear as Type Ia (Taam 1980; Nomoto 1982b; Iben & Tutukov 1991; Limongi & Tornambé 1991; Woosley & Weaver 1994; Livne & Arnett 1995), while the resulting

light curves and spectra may be abnormal (Höflich & Tutukov 1996; Nugent et al. 1997).
As mentioned in the introduction of this paper, binary population synthesis models show
that the production rate of such events may be comparable to the observed SN Ia rate (e.g.
Iben & Tutukov 1991; Regös et al. 2002), and therefore the apparent absence of such a
peculiar type of supernovae has been a puzzling matter.

The results of the present study offer a possible solution to this problem: helium ac-
creting CO white dwarfs with an accretion rate of $\sim 10^{-8}$ $M_{\odot}$/yr may not result in a
supernova at all, but may instead produce nova-like explosions. The accumulated helium
mass of $\Delta M_{\mathrm{He}} \simeq 0.02 \cdots 0.1$ $M_{\odot}$ in our rotating models indicates that in a low mass he-
lium star + CO white dwarf binary system, nova explosions will occur recurrently, with a
period of about 10^6 yr.

As pointed out by Iben & Tutukov (1991), various factors need to be considered for
predicting the further evolution of such a binary system after the first nova outburst. First,
any mass loss induced by the helium flash will affect the binary orbit. I.e., the nova induced
mass loss will widen the orbit and interrupt the mass transfer for some time (Iben & Tutukov
1991). However, the angular momentum loss due to gravitational wave radiation will lead
the helium star to fill its Roche lobe soon again (after $\sim 10^6$ yr) as discussed below.

Second, the first nova outburst may heat up the white dwarf significantly, and the white
dwarf may still be hot when the second mass transfer starts, compared to the case of the first
mass transfer. Model sequence TC, where an initially hot white dwarf with $\log L_{\mathrm{s}}/\mathrm{L}_{\odot} = $
2.508 is adopted, was computed in order to investigate the effect of a pre-heated white
dwarf. A value of $\dot{M} = 10^{-8}$ $M_{\odot}$/yr for this sequence, which is smaller than in other
model sequences, was chosen to consider the decrease of the mass transfer rate due to the
change of the orbit as the binary system loses mass via helium nova outbursts (cf. Fig 6.3).
A comparison of ΔM_{He} in sequence TC ($\Delta M_{\mathrm{He}} \simeq 0.002\,\mathrm{M}_{\odot}$) with the accumulated helium
masses in the sequences R3 and R4 ($\Delta M_{\mathrm{He}} \simeq 0.02\,\mathrm{M}_{\odot}$) implies that ΔM_{He} decreases by
more than a factor of 10 if the white dwarf is preheated. Therefore, the second and any
further helium flash may be much weaker than the first one.

In an attempt to make more detailed conjectures on the evolution and final fate of binary
systems of the considered kind, we made a simple experiment as follows. We constructed a
binary star model consisting of a zero-age helium main sequence star of 0.6 $M_{\odot}$ and a CO
white dwarf of 0.8 $M_{\odot}$ in an 1.08 h orbit ($A_{\mathrm{orbit,init}} = 0.6\,\mathrm{R}_{\odot}$, cf. Limongi & Tornambé
1991). Here, the white dwarf is approximated by a point mass. Since it appears likely that
the accreted helium will be ejected from the system by the violent helium shell flash when
about 0.02 $M_{\odot}$ of helium is accumulated as implied by the results of sequences R3 and R4,
we assume this for the evolution of our binary system. As discussed above, the subsequent
helium flashes may occur with a smaller ΔM_{He}. Therefore, for the subsequent evolution
the white dwarf is assumed to lose the accumulated matter at every time when $\Delta M_{\mathrm{He}} = $
0.002 $M_{\odot}$ is achieved. For comparison, a second binary evolution model with the same
initial condition is calculated, with the assumption of no mass loss due to helium flashes.
The evolution of the helium star and the change of the binary orbit due to the mass transfer,
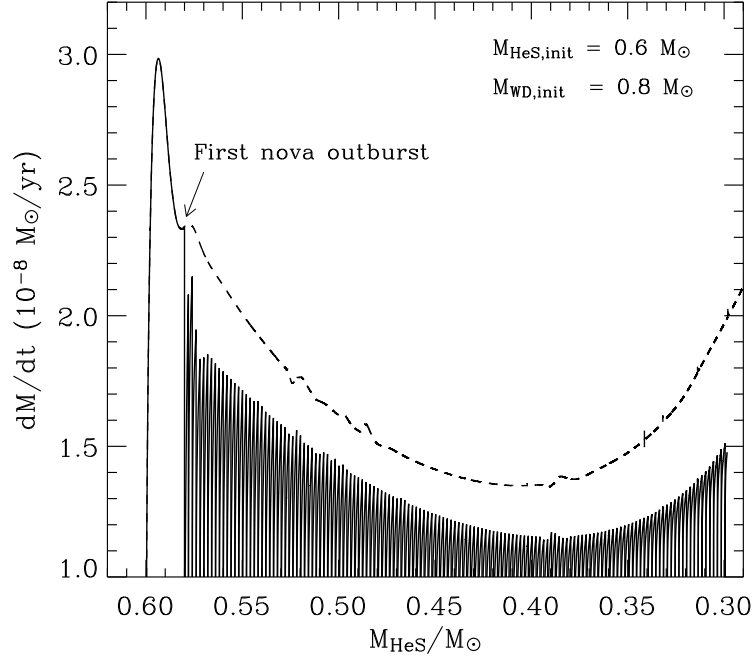stellar wind mass loss and gravitational wave radiation are followed by using a binary stellar

Figure 6.3: Mass transfer rate as a function of the helium star mass, for a binary system consisting initially of an 0.6 $M_\odot$ helium star and an 0.8 $M_\odot$ CO white dwarf (the latter here being approximated by a point mass). The initial orbital separation is 0.6 $R_\odot$. Mass transfer is initiated by gravitational wave radiation. The solid line illustrates the case where mass loss due to helium flashes is considered, while the dashed line was computed assuming that no mass loss occurs.

evolution code (see Langer et al. 2000 for more details about the code).

Fig. 6.3 shows the evolution of the mass transfer rate in the considered system, as a function of the helium star mass (M_{HeS}). The mass transfer from the helium star starts when the helium mass fraction in the helium star center equals 0.39. The orbital period at this moment is about 39 min. The mass transfer rate initially increases to 3×10^{-8} $M_\odot$/yr and has decreased to 2.3×10^{-8} $M_\odot$/yr by the time ΔM_{He} reaches 0.02 $M_\odot$. As the white dwarf is assumed to lose 0.02 $M_\odot$ at this point due to the helium nova flash, the system becomes detached for about 5.5×10^5 yr, after which the helium star again fills its Roche lobe. Further-on, the white dwarf loses mass whenever ΔM_{He} reaches 0.002 $M_\odot$, and thus the mass transfer is switched on and off repeatedly every $\sim 1.5 \times 10^5$ yr. We follow the evolution of the system until the helium star mass decreases to 0.30 $M_\odot$.

Fig. 6.4 shows the evolution of the helium star in the HR diagram. The helium star luminosity decreases continuously as it loses mass, and it will finally evolve into a white dwarf. At this stage, the binary system will resemble an AM CVn system.
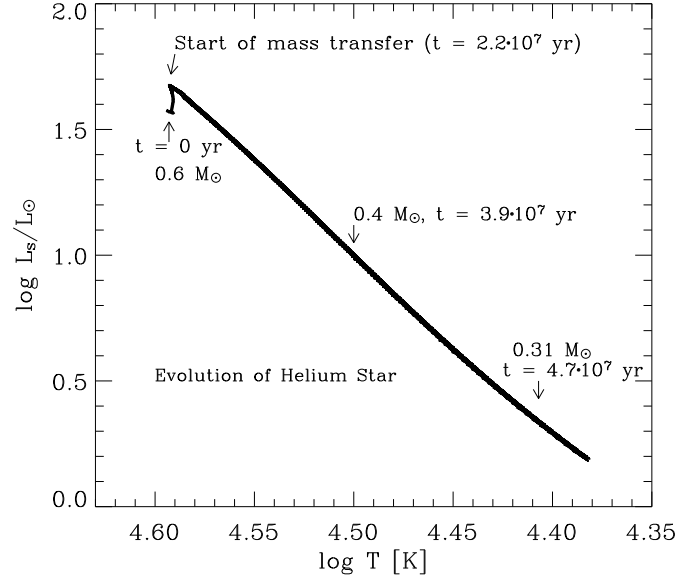
Figure 6.4: Evolution in the HR diagram of the helium star (initial mass 0.6 $M_\odot$) component of the binary system considered in in Fig. 6.3, for case with nova induced mass loss.

At the end of the calculation (i.e., $M_{\mathrm{HeS}} = 0.30\ M_\odot$), the central helium abundance has decreased to 0.16, and more than 0.1 $M_\odot$ of helium is still available in the envelope for further mass transfer. Since about 135 nova outbursts occurred until the end of the calculation, more than 180 recurrent nova outbursts in total are expected to occur throughout the evolution of the considered binary system. This implies that helium nova explosions in low mass helium star + CO white dwarf binary systems could be realized with a frequency of $\sim 0.1\ \mathrm{yr}^{-1}$ in our Galaxy, given that such binary systems are being produced at a frequency of $\sim 0.001\ \mathrm{yr}^{-1}$ (Iben & Tutukov 1991; Regös et al. 2002). The recently discovered outburst of V445 Puppis, which has been attributed to a helium nova (Ashok & Banerjee 2003; Kato & Hachisu 2003), may be a promising observational counterpart of such an event. The high observed carbon abundance in this system (Ashok & Banerjee 2003) might be explained by the rotationally induced chemical mixing in the accreting white dwarf, the effects of which are discussed in the next section.

6.4.2 Rotationally induced chemical mixing and neutron capture nucleosynthesis

As already suggested by Iben & Tutukov (1991), strong helium flashes in accreting CO white dwarfs may activate neutron capture nucleosynthesis, since neutrons can be provided
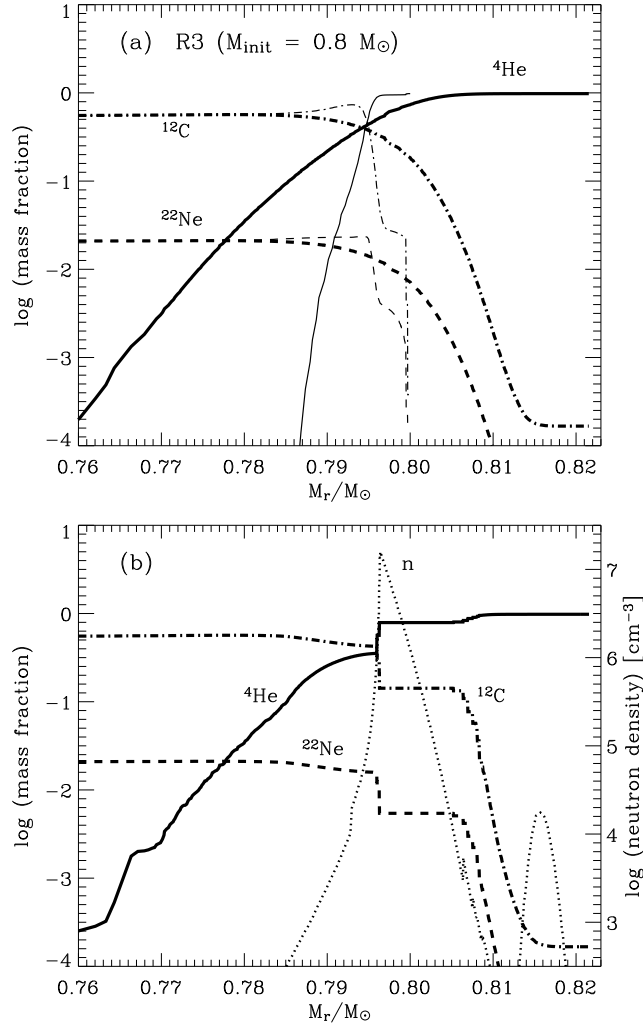
Figure 6.5: (a) Chemical profiles in the outer layers of the white dwarf models of sequence R3 when $M_{WD} = 0.8$ M$_\odot$ (initial model, thin lines), and $M_{WD} = 0.822$ M$_\odot$ (thick lines) which is immediate before the helium ignition. The solid and dotted-dashed lines give the mass fraction of ^{4}He and ^{12}C respectively, as a function of the mass coordinate. The dashed line denotes the mass fraction of ^{22}Ne. (b) Same as in (a) but after the ignition of helium. The dotted line denotes the neutron density, for which the scale is given at the right side.

via the ^{22}Ne$(\alpha, n)^{25}$Mg reaction. We note that favorable conditions for neutron capture nucleosynthesis might be achieved with rotation compared to the non-rotating case, due to

the rotationally induced chemical mixing (cf. Langer et al. 1999).

Fig. 6.5a gives the mass fraction of ^{4}He, ^{12}C and ^{22}Ne in the initial model (M_{WD} = 0.8 M$_\odot$) of sequence R3, as well as in the model with M_{WD} = 0.822 M$_\odot$, which is immediate before the helium ignition. It is found that ^{12}C and ^{22}Ne have been significantly dredged up into the helium envelope when helium ignites, due to rotationally induced mixing. For instance, comparing the two models shown in Fig. 6.5a reveals that the mass fraction of ^{12}C and ^{22}Ne at M_{r} = 0.8 M$_\odot$ has increased by about a factor of 10 when helium ignites.

The ignition of helium induces convection. Fig. 6.5b shows the chemical structure when T_{He} reaches 1.5×10^8 K. At this point, the convective layer has a mass of $\Delta M_{\text{conv}} \simeq$ 0.01 M$_\odot$, extending from M_{r} = 0.796 M$_\odot$ to M_{r} = 0.806 M$_\odot$. The abundance of the dredged up core material in the convective layer amounts to 0.15 for ^{12}C and 5.5×10^{-3} for ^{22}Ne, respectively. Neutrons are released by the ^{22}Ne$(\alpha, n)^{25}$Mg reaction, and a maximum neutron density of $\sim 10^7$ cm^{-3} is achieved at M_{r} = 0.76 M$_\odot$ in our last model. This neutron density may be somewhat overestimated in our calculation, since we did not include the reaction ^{14}N$(n, p)^{14}$C in our network (cf. Siess, Goriely & Langer 2003). However, we note that alpha particles are mixed significantly into the ^{22}Ne-rich region, and that large amount of neutrons will be released in the further evolution of the flash which is not covered any more by our model, as hydrodynamic effects in the exploding layers may become important. Therefore, we leave the exploration of the neutron capture nucleosynthesis effects in our models for the future.

6.5   Concluding remarks

We have shown that the effects of rotation in helium accreting white dwarfs may be incompatible with the scenario of double detonations in sub-Chandrasekhar mass CO white dwarfs as possible SNe Ia progenitors. In helium accreting white dwarfs, we find the thermal evolution to be affected by viscous heating due to differential rotation in the spun-up layers, such that helium ignition is induced at too low densities to develop a detonation. This may give a plausible solution to the long standing problem of the missing observational counterparts of sub-Chandrasekhar explosions, which are predicted to occur with a frequency comparable to the observed SN Ia rate.

We discussed that binary systems consisting of a CO white dwarf and a less massive helium star may be possible progenitors of recurrent helium novae (Iben & Tutukov 1991), which may be analogous to V445 Puppis (Ashok & Banerjee 2003; Kato & Hachisu 2003). After the first strong helium nova flash in such binary systems, rather mild nova outbursts are expected to occur recurrently with a period of $\sim 10^5$ yr. The realization frequency of such a helium nova may be as high as ~ 0.1 yr^{-1} in our Galaxy.

Rotation induces chemical mixing of ^{22}Ne and ^{4}He at the bottom of the helium envelope, which may provide interesting conditions for neutron capture nucleosynthesis to occur during the helium nova flashes.

Finally, we note that other important mechanisms for the angular momentum redistribution in white dwarfs may exist than those considered in the present study. In particular,

we neglected the possible role of magnetic fields, which may increase the efficiency of the angular momentum transport significantly (cf. Heger et al. 2003; Maeder & Meynet 2003). If the spin-up time scale is shorter than considered in the present study, the resulting shear strength will be weaker and the effect of rotational energy dissipation may not be as important as shown here. However, studies of magnetic effects in accreting white dwarfs have to be left for future investigations.

Chapter 7

Nederlandse Samenvatting

7.1 Witte dwergen

Sterren brengen het grootste deel van hun leven door op de zogenaamde *hoofdreeks*, de fase van hun leven waarin waterstof wordt gefuseerd. Eenmaal, wanneer alle waterstof in het centrum van een ster is opgebruikt, volgt in het centrum heliumfusie. Wanneer alle helium is opgebruikt, vormt zich in een ster met een massa lager dan ongeveer 8 zonsmassa ($\lesssim 8\,\mathrm{M_\odot}$), een compacte kern van koolstof en zuurstof (CO). Hierna treden er geen fusieprocessen meer op in de kern, alleen dunne schillen van waterstof en helium rondom de CO-kern ondergaan thermonucleaire reacties. De buitenste lagen van de ster, bestaande uit waterstof, worden meer en meer weggeblazen, tot uiteindelijk een naakte CO-kern overblijft. Zulke overblijfselen van sterevolutie worden *CO witte dwergen* genoemd.

In het binnenste van witte dwergen treedt geen fusie meer op en ze doven daarom langzaam uit als gevolg van het uitstralen van warmte vanuit hun binnenste. Een typische witte dwerg heeft een massa van $0.6\,\mathrm{M_\odot}$, maar een omvang die niet groter is dan de aarde. De materie binnenin een witte dwerg heeft zo'n grote dichtheid dat zelfs elektronen worden samengeperst in een klein volume. Zo'n toestand wordt een gedegenereerde toestand genoemd. Deze gedegenereerde elektronen zorgen voor de benodigde druk om tegenwicht te bieden aan de zwaartekracht, en daarom zijn zwaardere witte dwergen kleiner in afmetingen. Er bestaat echter een kritische massa voor witte dwergen, waarboven de druk binnenin een witte dwerg niet meer in staat is om tegenwicht te bieden aan de zwaartekracht. Deze kritische massa wordt de *Chandrasekhar-massa* genoemd, en is ongeveer $1.4\,\mathrm{M_\odot}$.

7.2 Massa invangende witte dwergen in dubbelstersystemen

Tal van witte dwergen maken deel uit van een dubbelstersysteem, waarin de begeleider van de witte dwerg een ster is met waterstof- of heliumfusie in het binnenste. Wanneer een ster uitzet en een kritisch volume in een dubbelstersysteem vult, waarbuiten de aantrekkingskracht van z'n begeleider domineert, wordt materie overgedragen op z'n begeleider.

Wanneer deze begeleider een witte dwerg is, en waterstof of helium van een andere ster

invangt, beginnen er een aantal interessante gebeurtenissen. De materie die is ingevangen wordt op de witte dwerg samengedrukt tot extreme dichtheden. Door deze samenpersing warmen de lagen met ingevangen materie sterk op, en komen waterstof en helium tot ontbranding. Thermonucleaire reacties bij zulke hoge dichtheden zijn gewoonlijk erg instabiel en heftig, en resulteren vaak in een snelle en drastische stijging van de helderheid. Dit wordt een nova-explosie genoemd.

De evolutie van massa invangende witte dwergen in een dubbelstersysteem is verschillend voor verschillende massaoverdrachtssnelheden. Wanneer de overdrachtssnelheid hoog genoeg is, kan waterstof en/of helium in een stabiel proces worden omgezet in koolstof en zuurstof, waarmee de massa van de witte dwerg dus groeit. Als de witte dwerg op deze manier groeit richting de Chandrasekhar massa, moet hij snel inkrimpen omdat anders de interne druk geen tegenwicht meer kan bieden tegen de zwaartekracht. Hierdoor wordt het centrum van de witte dwerg sterk samengedrukt en opgewarmd, waardoor explosieve verbranding van koolstof in gang wordt gezet. Grote delen van de witte dwerg nemen deel aan deze fusie van koolstof. Dit leidt uiteindelijk tot de explosie van de gehele witte dwerg en uiteindelijk tot een supernova explosie.

7.3   Type Ia supernova's en kosmologie

Wanneer het spectrum van een supernova geen waterstof- en heliumlijnen vertoont, maar wel sterke silicon-lijnen, wordt zo'n supernova gekarakteriseerd als Type Ia. Het is algemeen aanvaard dat zulke supernova's het gevolg zijn van thermonucleaire explosies van witte dwergen, volgens het hierboven uitlegde principe. Elk Type Ia supernova (SN Ia) produceert grote hoeveelheden ijzer. Feitelijk kunnen SN Ia's worden beschouwd als de grootste bron van ijzer in het heelal. SN Ia's worden ook gebruikt om afstanden te bepalen tot verweg gelegen sterrenstelsels. Dit is mogelijk dankzij de speciale eigenschap dat hoe helderder een SN Ia is, hoe langzamer de helderheid afneemt.

Recente systematische waarnemingen van SN Ia's met als doel het meten van extragalactische afstanden hebben geleid tot verrassende resultaten. Ze suggereren dat de uitdijing van het heelal momenteel versneld. Het is onmogelijk om dit feit te verklaren zonder de hulp in te roepen van mysterieuze *donkere energie* of *quintessence* in het heelal, hoewel we geen enkel idee hebben van de aard hiervan. Momenteel proberen astronomen, door waarnemingen te verrichten aan SN Ia's op extreme afstanden, aanwijzingen te vinden die de aard van donkere materie kunnen ontrafelen.

Er is echter nog een belangrijke vraag onopgelost. Hoe nauwkeurig zijn de schattingen van extra-galactische afstanden door gebruik te maken van SN Ia's? Het verband tussen de maximale helderheid en de afname van de helderheid van SN Ia's is alleen bevestigd voor waargenomen SN Ia's in nabije sterrenstelsels en de geldigheid voor verre sterrenstelsels is daarmee niet zeker omdat de omstandigheden kunnen verschillen van nabije stelsels. Het is algemeen bekend dat verschillen in de hoeveelheid zware elementen in sterren, dramatische verschillen kunnen veroorzaken in de evolutie van sterren. Om deze vraag te kunnen beantwoorden, moeten we tot in detail weten in welke soort dubbelstersystemen en op welke

manier, witte dwergen kunnen evolueren tot een SN Ia door het invangen van massa.

7.4   Dit onderzoek

Er is reeds veel studie gedaan naar de evolutie van massa invangende witte dwergen in dubbelstersystemen. Verrassend genoeg, veronachtzamen de meeste van deze onderzoeken het feit dat een witte dwerg sneller kan gaan roteren wanneer het massa invangt dat afkomstig is van een snel roterende schijf rond de ster (zie Fig. 1.3). In deze dissertatie wordt systematisch onderzocht hoe de evolutie van massa invangende witte dwergen kan veranderen als de effecten van rotatie op een juiste manier in aanmerking worden genomen. Meer specifiek; de evolutie van massa invangende witte dwergen is gesimuleerd inclusief de effecten van rotatie, door middel van een sterevolutiecode, die voor dit doel is aangepast. De belangrijkste resultaten volgen hieronder.

Hoewel de verbranding van ingevangen waterstof of helium in witte dwergen een stabiel proces is wanneer de snelheid waarmee de materie wordt ingevangen hoog genoeg is, zal een tè hoge invangssnelheid leiden tot het uitzetten van de witte dwerg waardoor het kritische volume wordt gevuld en er materie het systeem verlaat. Een 'fine-tuning' van de overdrachtssnelheid is daarom noodzakelijk om, door een gelijkmatige verbranding van ingevangen materie, een witte dwerg in massa te laten groeien. In werkelijkheid echter, zal de overdrachtssnelheid van de begeleider op de witte dwerg variëren in de tijd en daardoor niet altijd voldoen aan de noodzakelijke criteria voor gelijkmatige verbranding van ingevangen materie. Dat wil zeggen dat instabiele of zelfs heftige nucleaire verbrandingsprocessen, met als gevolg massa-verliezen vanaf de witte dwerg, een natuurlijke consequentie zijn van massa overdracht. Er wordt daarom getwijfeld of het mogelijk is om een witte dwerg te laten groeien totaan de Chandrasekhar limiet, door het invangen van waterstof of helium.

Dit onderzoek geeft een plausibele oplossing voor deze vraag. Onze simulaties laten zien dat nucleaire reacties in ingevangen materie op een witte dwerg minder heftig of zelfs stabiel worden, wanneer de effecten van het sneller roteren van de witte dwerg worden meegenomen. De belangrijkste reden voor het optreden van instabiele thermonucleaire reacties is dat in een witte dwerg de ingevangen materie sterk wordt samengedrukt tot dunne schillen als gevolg van de zwaartekracht. Wanneer echter een witte dwerg sneller gaat roteren, als gevolg van het invangen van massa, worden de schillen met die ingevangen materie opgetild als gevolg van de centrifugale kracht. Bovendien wordt de ingevangen materie gemengd met materie uit de kern van de witte dwerg als gevolg van turbulentie door rotatie. Dit heeft tot gevolg dat de schillen waarin nucleaire verbranding plaatsvindt, meer uitgebreid en een lagere dichtheid hebben, dat bijdraagt aan de stabilisatie van de thermonucleaire reacties. Dit resultaat is belangrijk omdat witte dwergen die sneller gaan roteren als gevolg van de het invangen van massa een grotere kans hebben om te groeien totaan de Chandrasekhar limiet.

Rotatie heeft ook andere interessante consequenties. Doordat de effectieve zwaartekracht wordt verminderd in snel roterende witte dwergen en daarmee de contractie als gevolg van de zwaartekracht, vindt er zelfs voorbij de Chandrasekhar limiet geen koolstof verbrand-

ing plaats in het centrum van een witte dwerg. Dit suggereed een grote spreiding in de
massa's van exploderende witte dwergen. Het is daarom hoogst noodzakelijk om te onder-
zoeken hoe de verschillende massa's van exploderende witte dwergen de uitkomsten van
supernova explosies beïnvloeden, om daarmee de waarde te bepalen van de methode om
extra-galactische afstanden te meten met behulp van SN Ia waarnemingen.

Een van de meest opwindende onderwerpen in de astrofysica aan het begin van de 21ste
eeuw is de detectie van zogenaamde zwaartekrachtsgolven, die worden voorspeld door de
Algemene Relativiteits Theorie van Einstein. In het bijzonder snel roterende compacte ob-
jecten zoals neutronensterren en zwarte gaten zijn veelbelovende bronnen zwaartekrachtsstral-
ing. Maar ook witte dwergen kunnen een bron van zwaartekrachtsstraling zijn, wanneer hun
rotatiesnelheid hoog genoeg is. Onze modellen laten zien dat witte dwergen in dubbelster-
systemen zo snel kunnen gaan roteren dat ze het punt bereiken waarop een instabiliteit zich
vormt, die aanleiding geeft tot het uitzenden van zwaartekrachtsstraling. De waarschijnli-
jkheid om ze te detecteren wordt significant geschat, hoewel gedetailleerdere onderzoeken
nodig zijn voor een precieze schatting.

Bovendien laten onze resultaten zien dat de mogelijkheid van een sterke explosie in een
dikke heliumschil met hoge dichtheid bovenop een CO witte dwerg moet worden uitges-
loten. Dit mechanisme is door veel mensen opgevoerd als een mogelijke verklaring voor
een soort supernova die moet worden geklassificeerd als Type Ia, maar in waarneembare
kenmerken verschilt van normale SN Ia's. CO witte dwergen met dikke heliumschillen
worden waarschijnlijk gevormd in een bepaald soort dubbelstersysteem bestaande uit een
CO witte dwerg en een heliumster met een lagere massa. Wanneer een witte dwerg in zo'n
dubbelstersysteem helium invangt, zal de ingevangen materie zich ophopen in lagen die
differentiëel roteren ten opzichte van lager gelegen lagen, waardoor er energie vrijkomt als
gevolg van wrijving. Dit heeft tot gevolg dat helium tot ontbranding komt op een tijdstip
dat veel eerder is dan in het geval waarin rotatie wordt verwaarloost. Het gevolg is dat de
dichtheid op de plek waar helium ontbrandt veel te laag is om een supernova te produceren.
Dit resultaat geeft een mooie verklaring voor een aloude puzzel in de astrofysica waarom
deze vorm van theoretisch voorspelde supernova's van een CO witte dwerg en een helium-
ster nooit zijn waargenomen ondanks de hoge frequentie die werd verwacht.

Appendix A

Solving the non-linear diffusion equation for the angular momentum transport

In our numerical code, the transport of angular momentum is approximated as a diffusive process, as in Heger et al. (2000), Heger & Langer (2000) and Endal & Sofia (1978), by solving the following diffusion equation:

$$
\left(\frac{\partial \omega}{\partial t}\right)_{M_{\mathrm{r}}} = \frac{1}{i}\left(\frac{\partial}{\partial M_{\mathrm{r}}}\right)_{t}\left[(4\pi r^2 \rho)^2 i\nu_{\mathrm{turb}}\left(\frac{\partial \omega}{\partial M_{\mathrm{r}}}\right)_{t}\right],
\tag{A.1}
$$

where ν_{turb} is the turbulent viscosity, i.e., the sum of all diffusion coefficients due to the considered rotationally induced hydrodynamic instabilities (see Heger et al. 2000). Here, i is the specific moment of inertia of a mass shell at M_r. In Heger et al. (2000) and Heger & Langer (2000), this equation is solved assuming ν_{turb} as constant over a time step Δt which is determined on the basis of secular time scales. In the case of the evolution of main sequence stars, the redistribution of angular momentum is dominated by Eddington Sweet circulations, which do not depends strongly on the degree of differential rotation. The linear approximation is thus justified, since the diffusion efficiency in main sequence stars does not change significantly over a time step Δt.

In accreting white dwarfs, however, the dynamical shear instability (DSI) can dominate the transport of angular momentum. The assumption of constant ν_{turb} over Δt does not hold any more, since the shear strength in differentially rotating layers may change on a dynamical time scale if they are dynamical shear unstable. Therefore, the above equation needs to be solved non-linearly in order to properly describe such a fast diffusive process. Here we explain our newly developed numerical method for this task.

A.1   Discretization

The equation A.1 can be rewritten in terms of the moment of inertia coordinate as

$$\left(\frac{\partial\omega}{\partial t}\right)_I = \left(\frac{\partial}{\partial I}\right)_t \left[\mathcal{D}\left(\frac{\partial\omega}{\partial I}\right)_t\right], \tag{A.2}$$

where

$$\partial I := i\partial M_\mathrm{r} \ ; \ I(M_\mathrm{r}) := \int_0^{M_\mathrm{r}} i(m)dm \tag{A.3}$$

and

$$\mathcal{D} := (4\pi^2\rho)^2 i^2 \nu_\mathrm{turb} \tag{A.4}$$

In our discretization of the physical quantities, the angular velocity ω is defined in the middle of a mass shell, while the integrated moment of inertia I and the turbulent viscosity ν_turb are defined at the inner edge of a mass shell as illustrated in Fig. A.1
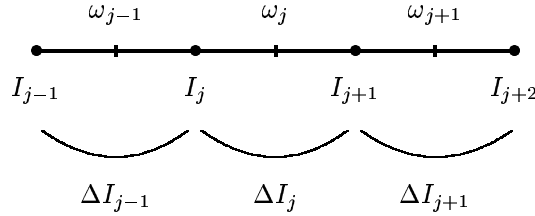
Figure A.1: Discretization of the physical quantities for solving the diffusion equation. The short vertical lines indicate the centers of mass shells, while the filled circles denote the boundaries of mass shells

Now, Eq. A.2 can be expressed in a discretized form using 3 neighboring grids points ($j-1$, j, and $j+1$):

$$\frac{\omega_j - \omega_j^*}{\Delta t} = \frac{1}{\Delta I_j}\left(\mathcal{D}_{j+1}\frac{\omega_{j+1} - \omega_j}{0.5(\Delta I_{j+1} + \Delta I_j)} - \mathcal{D}_j\frac{\omega_j - \omega_{j-1}}{0.5(\Delta I_j + \Delta I_{j-1})}\right), \tag{A.5}$$

where ω_j^* is the old value at t, while ω_{j-1}, ω_j and ω_{j+1} are new values at $t' = t + \Delta t$.

A.2 Solution

In our code, solutions for ω are obtained using the Newton-Raphson method (e.g. Press et al. 1992). I.e., by defining a function $f_j(\omega_{j-1}, \omega_j, \omega_{j+1})$ as

$$f_i(\omega_{j-1}, \omega_j, \omega_{j+1})$$
$$:= \omega_j - \omega_j^* + \frac{2\Delta t}{\Delta I_j}\left(\mathcal{D}_j \frac{\omega_j - \omega_{j-1}}{(\Delta I_j + \Delta I_{j-1})} - \mathcal{D}_{j+1}\frac{\omega_{j+1} - \omega_j}{(\Delta I_{j+1} + \Delta I_j)}\right), \quad \text{(A.6)}$$

a trial solution for ω is gradually improved until $f_i(\omega_{j-1}, \omega_j, \omega_{j+1}) \to 0$ is satisfied with a sufficient accuracy (see below).

The corrections $\delta\omega_j$ for a trial solution can be provided by means of the first order Taylor expansion:

$$f_j(\omega_{j-1} + \delta\omega_{j-1}, \omega_j + \delta\omega_j, \omega_{j+1} + \delta\omega_{j+1}) = 0$$
$$\approx f_i(\omega_{j-1}, \omega_j, \omega_{j+1}) + \frac{\partial f_j}{\partial \omega_{j-1}}\delta\omega_{j-1} + \frac{\partial f_j}{\partial \omega_j}\delta\omega_j + \frac{\partial f_j}{\partial \omega_{j+1}}\delta\omega_{j+1} . \quad \text{(A.7)}$$

This equation is rewritten in matrix form as

$$\mathcal{J} \cdot \begin{pmatrix} \delta\omega_1 \\ \delta\omega_2 \\ . \\ . \\ \delta\omega_j \\ . \\ . \\ \delta\omega_{N-1} \\ \delta\omega_N \end{pmatrix} = - \begin{pmatrix} f_1 \\ f_2 \\ . \\ . \\ f_j \\ . \\ . \\ f_{N-1} \\ f_N \end{pmatrix} \quad \text{(A.8)}$$

where $\mathcal{J}$ is the Jacobian matrix such that

$$\mathcal{J} = \begin{pmatrix} \frac{\partial f_1}{\partial \omega_1} & \frac{\partial f_1}{\partial \omega_2} & 0 & \cdots & \cdots & \cdots & \cdots & \cdots & 0 \\ \frac{\partial f_2}{\partial \omega_1} & \frac{\partial f_2}{\partial \omega_2} & \frac{\partial f_2}{\partial \omega_3} & 0 & \cdots & \cdots & \cdots & \cdots & 0 \\ & & & \cdots & & & & & \\ & & & \cdots & & & & & \\ 0 & \cdots & 0 & \frac{\partial f_j}{\partial \omega_{j-1}} & \frac{\partial f_j}{\partial \omega_j} & \frac{\partial f_j}{\partial \omega_{j+1}} & 0 & \cdots & 0 \\ & & & \cdots & & & & & \\ & & & \cdots & & & & & \\ 0 & \cdots & \cdots & \cdots & \cdots & 0 & \frac{\partial f_{N-1}}{\partial \omega_{N-2}} & \frac{\partial f_{N-1}}{\partial \omega_{N-1}} & \frac{\partial f_{N-1}}{\partial \omega_N} \\ 0 & \cdots & \cdots & \cdots & \cdots & \cdots & 0 & \frac{\partial f_N}{\partial \omega_{N-1}} & \frac{\partial f_N}{\partial \omega_N} \end{pmatrix} \quad \text{(A.9)}$$

The derivatives $\partial f_j / \partial \omega_m$, where $m = j - 1$, j, and $j + 1$, need to involve partial differentiation of $\mathcal{D}$ with respect to ω for the non-linear effect of diffusion to be considered.

Here we give an example for the calculation of $\partial\mathcal{D}/\partial\omega$ in a discretized form considering only the dynamical shear instability. In our code, the diffusion coefficient for the DSI is estimated as

$$D_{\mathrm{DSI}} = \frac{H_{\mathrm{P}}}{\tau_{\mathrm{dyn}}}\left(1 - \frac{R_{\mathrm{i}}}{R_{\mathrm{i,c}}}\right)^2 . \tag{A.10}$$

Here, H_{P} is the pressure scale hight, $R_{\mathrm{i,c}}$ the critical Richardson number, and τ_{dyn} the dynamical time scale ($:= \sqrt{r^3/(GM_r)}$). The Richardson number R_{i} is defined as $R_{\mathrm{i}} := N^2/\sigma^2$, where N^2 is the Brunt-Väisälä frequency and σ the shear factor ($\partial w/\partial\ln r$; see Eq. 4.3 – 4.6), which is numerically calculated as

$$\sigma_j = \frac{2r_j}{r_{j+1} - r_{j-1}}(\omega_j - \omega_{j-1}), \tag{A.11}$$

where r_j is defined at the inner edge of a mass shell like I_j. Therefore, we have

$$\frac{\partial\mathcal{D}_k}{\partial\omega_m} = 8(4\pi\rho_k)^2 i_k^2 \frac{H_{\mathrm{P},\,k}}{\tau_{\mathrm{dyn},\,k}} \frac{r_k}{r_{k+1} - r_{k-1}}\left(1 - \frac{N_k^2}{\sigma_k^2 R_{\mathrm{i,c}}}\right)\frac{N_k^2}{\sigma_k^3 R_{\mathrm{i,c}}}\delta_{k,m}, \tag{A.12}$$

where $k = (j,\ j+1)$ and $m = (j-1,\ j,\ j+1)$. $\delta_{k,m}$ is the Kronecker delta index.

Once the Jacobian matrix is constructed, $\delta\omega$ can be obtained by calculating the inverse matrix of $\mathcal{J}$. Then, ω is updated as

$$\omega_{j,\,\mathrm{new}} = \omega_{j,\,\mathrm{old}} + \lambda\delta\omega_j, \quad 0 < \lambda \leq 1. \tag{A.13}$$

It is well known that the Newton-Raphson method for solving non-linear systems of equations may fail to converge. A careful choice of λ is important, and the globally convergent method by Press at al. (1992, chapter 9) is found very useful for this purpose.

In our calculations, the above procedure is iterated until $\max_{1\leq j\leq N}(\delta\omega_j/\omega_j) < 10^{-10}$ is fulfilled. At every iteration, the diffusion coefficients for the angular momentum transport should be newly determined using the updated trial solution of ω.

A.3   Performance Test

For a test of the new scheme to solve Eq. A.1, we have constructed a rotating CO white dwarf model of 1.0 $\mathrm{M}_\odot$ such that the angular velocity profile has a discontinuity around $M_r = 0.65$, as shown by the line connecting open triangles in Fig. A.2. Then, we let the white dwarf evolve over one time step of $\Delta t = 10^5$ sec, with only the dynamical shear instability considered for the angular momentum transport. The consequent angular velocity profile is denoted by the line connecting filled circles in Fig. A.2. For a comparison, the same model is evolved with the old diffusion solver over the same duration of time (10^5 sec) but with a 10 times smaller time step ($\Delta t = 10^4$ sec). The result is given by the line connecting open squares in Fig. A.2. It is found that the angular velocity profile from the old scheme shows noisy steps, which is simply because the rapid change in angular
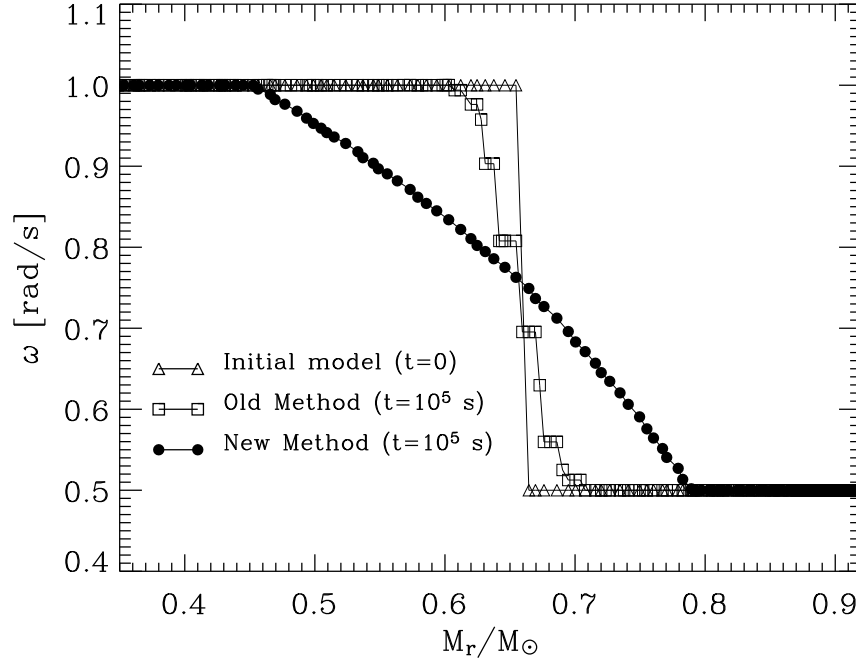
Figure A.2: Angular velocity profiles in a 1.0 M$_\odot$ white dwarf model. The line connecting open triangles denotes the initial model, where a discontinuity in ω is artificially introduced at $M_r = 0.65$ M$_\odot$. The line connecting filled circles gives the result of the evolution over one time step of 10^5 seconds, which is calculated with the new diffusion solver. The line connecting open squares shows the solution from the old diffusion solver, obtained by letting the initial model evolve over 10^5 sec with a fixed time step of 10^4 sec.

velocity induced by the dynamical shear instability could not be sufficiently resolved with the given time step. By contrast, we have a very clean solution with the new diffusion solver, which convincingly demonstrates its capability.

References

Anand, S.P.S., 1968, ApJ, 153, 135

Andersson, N., 1998, ApJ, 502, 708

Andersson, N., Kokkotas, K.D., 2001, Int. J. Mode. Phys. D, 10, 381

Andersson, N., Kokkotas, K.D., Stergioulas, N., 1999, ApJ, 516, 307

Ashok, N.M., Banerjee, D.P.K., 2003, A&A, 409, 1007

Bardeen, J.M., Friedman, J.L., Schutz, B.F., Sorkin R., 1977, ApJ, 217, L49

Baron, E., Lentz, E.J., Hauschildt, P.H., 2003, ApJ, 588, 29

Benz, W., Cameron, A.G.W., Press, W., Bowers, R.L., 1990, ApJ, 348, 647

Blinnikov, S.I., Dunina-Barkovskaya N.G., Nadyozhin D.K., 1996, ApJS, 106, 171

Branch, D., 1998, ARA&A, 36, 17

Branch, D., 2001, PASP, 113, 17

Branch, D., 2004, in: 3-D Signatures of Stellar Explosions, Cambridge, in press, [astro-ph/0310685]

Branch, D., Livio, M., Yugelson, L.R., Boffi, F.R., Baron, E., 1995, PASP, 107, 1019

Branch, D., Tammann, G.A., 1992, ARA&A, 20, 359

Braun, H., 1997, Ph.D. Thesis, LMU München

Brookshaw, L., Tavani, M., 1993, ApJ, 410, 719

Busso, M., Roberto, G., Lambert, D., Travaglio, C., Smith, V.V., 2001, ApJ, 557, 802

Cameron, A.G.W., Iben, I. Jr., 1986, ApJ, 305, 228

Canuto, V., 1970, ApJ, 159, 641

Cassisi, S., Iben, I.Jr., Tornamé, A., 1998, ApJ, 496, 376

Caughlan, G.R., Fowler, W.A., 1988, At. Data Nucl. Data Talbes, 40, 283

Caughlan, G.R., Fowler, W.A., Marris, M.J., Zimmerman, B.A., 1985, Atomic Dat. Nuc. Dat. Tables., 32, 197

Chaboyer, B., Zahn, J.-P., 1992, A&A, 253, 173

Chandrasekhar, S. 1970, Phys. Rev. L, 24, 611

Clark, D.H., Stephenson, F.R., 1997, The Historical Supernovae, Pergamon Press

Clayton, D.D. 1968, Principles of Stellar Evolution and Nucleosynthesis (New York: MacGraw-Hill)

Cutler, C., Thorne K., 2002, [gr-qc/0204090]

della Valle, M., Livio, M., 1994, ApJ, 423, L31

Dennis, T.R., 1971, ApJ, 167, 311

Domínguez, I., Höflich, P., Straniero, O., 2001, ApJ, 557, 279

Downes, R.A., Webbink, R.F., Shara, M.M., Ritter, H., Kolb, U., Duerbeck, H.K., 2001, PASP, 113, 764

Driebe, T., Blcker, T., Schnberner, D., Herwig, F., 1999, A&A, 350, 89

Durisen, R.H., 1973a, ApJ, 183, 205

Durisen, R.H., 1973b, ApJ, 183, 215

Durisen, R.H., 1975a, ApJ, 195, 488

Durisen, R.H., 1975b, ApJ, 199, 179

Durisen, R.H., 1977, ApJ, 213, 145

Durisen, R.H., Imamura, J.N., 1981, ApJ, 243, 612

Eggleton, P., 1983, ApJ, 268, 368

Endal, A.S., Sofia, S., 1976, ApJ, 210, 184

Ferreras, I., Silk, J., 2002, MNRAS, 336, 1181

Fisher, A., Branch, D., Hatano, K., Baron, E., 1999, MNRAS, 304, 67

Fliegner, J. 1993, Diplomarbeit, University of Göttingen

Fricke, K., 1968, ZfAP, 68, 317

Friedman, J.L., Morsink, S.M., 1998 ApJ, 502, 714

Friedman, J.L., Schutz, B., 1975, ApJ, 199, L157

Friedman, J.L., Schutz, B., 1978, ApJ, 222, 281

Fryer, C.L, Holz D.E., Hughes S., 2002, ApJ, 565, 430

Fujimoto, M.Y., 1982a, ApJ, 257, 752

Fujimoto, M.Y., 1982b, ApJ, 257, 767

Fujimoto, M.Y., 1988, A&A 198, 163

Fujimoto, M.Y., Hanawa T., Miyaji S., 1981, ApJ, 246, 267

Fujimoto, M.Y., Iben I., 1997, in Advances in Stellar Evolution, Cambridge University Press.

Fujimoto, M.Y., Sugimoto D., 1979, PASJ, 31, 1

Fujimoto, M.Y., Sugimoto D., 1982, ApJ, 257, 291

Gamezo, V.N., Khokhlov, A.M., Oran, E.S. et al., 2003, Science, 299, 77

Giannone, P., Weigert, A., 1967, Zs.f.Ap., 59, 242

Goldreich, P., Schubert, G., 1967, ApJ, 150, 571

Greiner, J., 2000, New Astron., 5, 137

Greiner, J., Hasinger, G., Kahabka, P., 1991, A&A, 246, L17

Greiner, J., Orio, M., Schwarz, R., 2000, A&A, 355, 1041

Hachisu, I., 1986, ApJS, 61, 479

Hachisu, I., Kato, M., 2001, ApJ, 558, 323

Hachisu, I., Kato, M., Kato, T., Matsumoto, K., 2000, ApJ, 528, L97

Hachisu, I., Kato, M., Nomoto, K., 1996, ApJ, 470, L97

Hachisu, I., Kato, M., Nomoto K., 1999, ApJ, 522, 487

Hamuy, M., Phillips, M.M., Maza, J., et al., 1995, AJ, 109,1

Hamuy, M., Phillips, M.M., Suntzeff, N.B., et al., 1996a, AJ, 112, 2398

Hamuy, M., Phillips, M.M., Suntzeff, N.B., et al., 1996b, AJ, 112, 2438

Hamuy, M., Phillips, M.M., Suntzeff, N.B., et al., 2003, Nature, 424, 651

Han, Z., Webbink, R.F., 1999, A&A, 349, L17

Hanato, K., Branch D., Qui Y.L., Baron E., Thielemann F.K., Fisher A., 2002, New Astron., 7, 441

Härm R., Schwarzshild M., 1972, ApJ 172, 403

Harris, M. J., Fowler, W. A., Caughlan, G. R., Zimmerman, B. A., 1983, ARA&A, 21, 165

Hashimoto, M.-A., Nomoto, K.I., Arai, K., Kaminisi, K., 1984, Phys. Rep. Kumamoto Univ., 6, 75

Hayashi, A., Eriguchi Y., Mashimoto M., 1998, ApJ 492, 286

Heber, U., Napiwotzki, R., Reid, I.N., 1997, A&A, 323, 819

Heger, A., Langer, N., 2000, ApJ, 544, 1016

Heger, A., Langer, N., Woosley, S.E., 2000, ApJ, 528, 368

Heger, A., Woosley, S., Langer, N., Spruit, H.C., 2003, in: Stellar Rotation, proc. IAU-Symp. 215, (San Francisco: ASP), A. Maeder, P. Eenens, eds., in press

Hillebrandt, W., Niemeyer, J.C., 2000, ARA&A, 38, 191

Hiscock, W., 1998, [gr-qc/9807036]

Höflich, P., Khokhlov, A., 1996, ApJ, 457, 500

Höflich, P., Khokhlov A., Wheeler J.C. et al., 1996, ApJ 472, L81

Höflich, P., Nomoto, K., Umeda, H., Wheeler, J.C., 2000, ApJ, 528, 590

Höflich, P., Stein, J., 2002, ApJ, 568, 779

Höflich, P., Wheeler, J.C., Thielemann, F.K., 1998, ApJ, 495, 617

Howell, D.A., 2001, ApJ, 554, 193

Howell, D.A., Höflich, P., Wang, L., Wheeler, J.C., 2001, ApJ, 556, 302

Hoyle, F., Fowler, W.A., 1960, ApJ, 132, 565

Huang, R.Q., Yu, K.N., 1998, Stellar Astrophysics, Springer-Verlag.

Hubbard, W.B., Lampe, M., 1969, ApJS, 18, 297

Hujeirat, A., 1995, A&A, 295, 268

Iben, I.Jr., 1982, ApJ 253, 248

Iben, I.Jr., 1982, ApJ, 259, 244

Iben, I.Jr., Livio, M., 1993, PASP, 105, 1373

Iben, I.Jr., Renzini, A., 1983, ARA&A, 27, 271

Iben, I.Jr., Tutukov, A.V., 1984, ApJS, 54, 335

Iben, I.Jr., Tutukov A.V., 1989, ApJ 342, 430

Iben, I.Jr., Tutukov, A.V., 1991, ApJ 370, 615

Iben, I.Jr., Tutukov, A.V., 1994, ApJ 431, 264

Iglesias, C.A., Rogers, F.J., 1996, ApJ, 464, 943

Imamura, J.N., Toman, J., Durisen, R.H., Pickett, B., Yang, S., 1995, ApJ, 444, 363

in't Zand, J.J.M., Kuulkers, E., Verbunt, F., Heise, J., Cornelisse, R., 2003, A&A, 411, L487

Itoh, N., Kohyama, Y., Takeuchi, H., 1987, ApJ, 317, 733

Iwamoto, K., Brachwitz, F., Nomoto, K. et al., 1999, ApJS, 125, 439

James, R.A., 1964, ApJ, 140, 552

Kahabka, P, van den Heuvel, E.P.J., 1997, ARA&A, 35, 69

Karino, S., Eriguchi, Y., 2002, ApJ, 578, 413

Karl, C.A., Napiwotzki, R., Nelemans, G., et al. 2003, A&A, 410, 663

Kasen, D., Nugent, P., Wang, L., et al., 2003, ApJ, 593, 788

Kato, M., Hachisu, I., 1999, ApJ, 513, L41

Kato, M., Hachisu I., 2003, ApJ, 598, L107

Kawai, Y., Saio, H., Nomoto, K., 1988, ApJ, 328, 207

Kawaler, S.D., 2003, In: Stellar Rotation, proc. IAU Symp. 215, A. Maeder, P. Eenes, eds., in press

Kenyon, S.J., Livio, M., Mikolajewska, J., Tout, C.A., 1993, ApJ, 407, L81

Khokhlov, A.M., 1991a, A&A, 245, 114

Khokhlov, A.M., 1991b, A&A, 246, 383

Khokhlov, A.M., Oran, E.S., Wheeler, J.C., 1997, ApJ, 478, 678

Kippenhahn, R., Möllenhoff, C., 1974, Ap. Space. Sci., 31, 117

Kippenhahn, R., Thomas, H.-C., 1970, in : Stellar Rotation, IAU Coll. 4, Ed. A. Slettebak

Kippenhahn, R., Thomas, H.-C., 1978, A&A, 63, 265

Kippenhahn, R., Weigert, A., 1990, Stellar Structure and Evolution, Springer-Verlag.

Kobayashi, C., Tsujimoto, T., Nomoto, K., 2000, ApJ, 539, 26

Koester, D., Dreizler, S., Weidemann, V., Allard, N.F., 1998, A&A, 338, 617

Koester, D., Napiwotzki, R., Christlieb, N., et al., 2001, A&A, 378, 556

Landau, L.D., Lifshitz, E.M., 1984, Fluid Mechanics, Course of theoretical physics, vol. 6, Pergamon Press

Langer, N., 1989, A&A 210, 93

Langer, N., 1998, A&A, 329,551

Langer, N., Deutschmann, A., Wellstein, S., Höflich P., 2000, A&A, 362, 1046

Langer, N., Heger, A., Wellstein, S., Herwig, F., 1999, A&A, 346, L37

Langer, N., Kiriakidis, M., El Eid, M.F., Fricke, K.J., Weiss, A., 1988, A&A, 192, 177

Langer, N., Yoon, S.-C., Petrovic, J., Heger, A., 2003, In: Stellar Rotation, proc. IAU Symp. 215, (San Francisco: ASP), A. Maeder, P. Eenens, eds., in press, [astro-ph/0302232]

Langer, N., Yoon, S.-C., Wellstein, S., Scheithauer, S., 2002, ASP Conference Proceedings, vol. 261, B.T. Gaensicke et al., eds., p. 252

Leibundgut, B., 2000, A&AR, 10, 179

Leibundgut, B, 2001, ARA&A, 39, 67

Limongi, M., Tornambé, A., 1991, ApJ, 371, 317

Lindblom, L, 1999, Phys. Rev. D, 60, 4007

Lindblom, L, Tohline J.E., Vallisneri M., 2002, Phys.Rev. D., 65, 4039

Lisewski, A.M., Hillebrandt, W., Woosley, S.E., 2000, ApJ, 538, 831

Livio, M., 2000, The accelerating universe : infinite expansion, the cosmological constant, and the beauty of the Cosmos, Wiley

Livio, M., 2001, In: Cosmic evolution, ed. E. Vangioni, R. Ferlet, M. Lemoine, New Jersey: World Sceintific

Livio, M., Pringle, J.E., 1998, ApJ, 505, 339

Livio, M., Truran, J., 1987, ApJ, 318, 316

Livne, E., 1990, ApJ, 354, L53

Livne, E., Arnett, D., 1995, ApJ, 452, 62

Li, W., Filippenko, A.V., Chornock, R., et al., 2003, PASP, 115, 453

Li, X.-D., van den Heuvel, E.P.J., 1997, A&A, 322, L9

Lugaro, M., Herwig, F., Lattanzio, J.C., Gallino, R., Straniero, O., 2003, ApJ, 586, 1305

Lynden-Bell, D., Ostriker, J.P., 1967, MNRAS, 136, 293

MacDonald, J.,1983, ApJ 273,289

Maeder, A., 1999, A&A 347, 185

Maeder, A., 2003, A&A 399, 263

Maeder, A., Meynet, G., 2000, ARA&A, 38, 143

Maeder, A, Meynet, G., 2003, A&A, 411, 543

Marrietta, E., Burrows A., Fryxell B. 2000, ApJS 218, 615

Matteucci, F., Recchi, S., 2001, ApJ, 558, 351

Maxted P.F.L., March, T.R., North R.C. 2000, MNRAS, 317, L41

Maza, J., van den Bergh, S., ApJ, 1976, 204, 519

McMillan, R.J., Ciardullo, R., 1996, ApJ, 473, 707

Meynet, G., Maeder, A., 1997, A&A, 321, 465

Mochkovitch, R., 1996, A&A 311, 152

Mochkovitch, R., Livio, M., 1989, A&A, 209, 111

Mochkovitch, R., Livio, M., 1990, A&A, 236, 378

Monaghan, J.J., 1966, MNRAS, 132, 305

Nandkumar, R., Pethick, C.J. 1984, MNRAS, 209, 511

Napiwotzki, R., Christlieb, N., Drechsel, H.-J., et al., 2003, The Messenger (ESO), 112, 25

Napiwotzki, R., Koester, D., Nelemens, G. et al., 2002, A&A, 386, 957

Narayan, R., Popham, R., 1989, ApJ, 346, L25

Neo, S., Miyaji, S., Nomoto, K., Sugimoto, D., 1977, PASJ, 29, 249

Niemeyer, J.C., 1999, ApJ, 523, L57

Niemeyer, J.C., Woosley, S.E., 1997, ApJ, 475, 740

Nomoto, K., 1982a, ApJ 253, 798

Nomoto, K., 1982b, ApJ 257, 780

Nomoto, K., Hashimoto, M., Tsujimoto, T., et al., 1997a, Nuc. Phys. A, 616, 79

Nomoto, K., Iben, I.Jr., 1985, ApJ, 297, 531

Nomoto, K., Iwamoto K., Kishimoto N., 1997b, Sci 276, 1378

Nomoto, K., Kondo, Y., 1991, ApJ, 367, 19

Nomoto, K., Thielemann, F.-K., Yokoi, K., 1984, ApJ, 286, 644

Nomoto, K., Uenishi, T., Kobayashi, C. et al., 2003, In : From Twilights to Highlights: The Physics of Supernovae, W. Hillebrandt & B. Leibundgut, eds, Springer, p. 115

Nugent, P., Baron, E., Branch, D., Fisher, A., Hauschildt, P.H., 1997, ApJ, 485, 812

Oppenheimer, B.R., Hambly, N.C., Digby, A.P., Hodgkin, S.T., Saumon, D., 2001, Science, 292, 698

Ostriker, J.P., 1966, ApJ, 71, 394

Ostriker, J.P., Bodenheimer, P., 1968, ApJ, 151, 1089

Ostriker, J.P., Bodenheimer, P., 1973, ApJ, 180, 171

Ostriker, J.P., Mark, J.W.-K., 1968, ApJ, 151, 1075

Ostriker, J.P., Tassoul, J.L., 1969, ApJ, 155, 987

Owocki, S.P., Gayley, K.G., 1997, In: Nota A., Lamers H.J.G.L.M. (eds.), Luminous Blue Variables:Massive stars in Transition. ASP Conf. Ser. Vol. 120

Paczyński, B., 1972, ApJ L11, 53

Paczyński, B., 1991, ApJ, 370, 597

Paczyński, B., Zytkow, A.N., 1978, ApJ, 222, 604

Perlmutter, S., Aldering, G., Goldhaber, G., et al., 1999a, ApJ, 517, 565

Perlmutter, S., Gabi, S., Godhaber, G. et al., 1997, ApJ 483, 565

Perlmutter, S., Schmidt, B.P., 2003, In: Supernovae & Gamma Ray Bursts, K. Weiler, Ed., Springer, Lecture Notes in Physics, in press, [astro-ph/0303428]

Perlmutter, S., Turner, M.S., White, M., 1999b, Phys.Rev.L, 83, 670

Phillips, M.M., 1993, ApJ, 413, L105

Piersanti, L., Cassisi, S., Iben, I.Jr., Tornambé, A., 1999, ApJ, 521, L59

Piersanti, L., Cassisi, S., Iben, I.Jr., Tornambé, A., 2000, ApJ, 535, 932

Piersanti, L., Cassisi, S., Tornambé, A., 2001, ApJ, 558, 916

Piersanti, L., Gagliardi, S., Iben, I.Jr., Tornambé, A., 2003, ApJ, 583, 885

Pinsonneault, M.H., Kawaler, S.D., Sofia, S., Demarque, P., 1989, ApJ, 338, 424

Pinto, P.A., Eastman, R.G., Rogers, T., 2001, ApJ, 551, 231

Podsiadlowski, Ph., Joss, P.C., Hsu, J.J.L., 1992, ApJ, 391, 246

Popham, R., Narayan, R., 1991, ApJ, 370, 604

Press, W.H., Teukolsky, S.A., Vetterling, W.T., Flannery, B.P., Numerical Recipes in Fortran, Second Edition, Cambridge Univ. Press

Prialnik, D., Shara, M.M., Shaviv, G., 1978, A&A, 278, L39

Rappaport, S.A., Di Stefano, R., Smith, M., 1994, ApJ 426, 692

Regös, E., Tout, C.A., Wickramasinghe, D., Hurley, J.R., Pols, O.R., 2002, New Astron., 8, 283

Reinecke, M., Hillebrandt, W., Niemeyer, J.C., 2002, A&A, 391, 1167

Renzini, A., 1999, In: Chemical Evolution from Zero to High Redshift, eds. J.R. Walsh, M.r. Rosa, Springer Verlag, p. 185

Riess, A.G., Filippenko, A.V., Challis, P. et al., 1998, ApJ, 116, 1009

Riess, A.G., Filippenko, A.V., Liu M.C. et al., 2000, ApJ, 536, 62

Riess, A.G., Press, W.H., Kirshner, R.P., 1996, ApJ, 473, 88

Ritter, H., 1985, A&A, 148, 207

Ritter, H., 1988, A&A, 202, 93

Roxburgh, I.W., 1965, Z. Astrophys., 62, 134

Sackmann, I.J., 1977, ApJ 212, 159

Saio, H., Nomoto, K., 1985, A&A, 150, L21

Saio, H., Nomoto, K., 1998, ApJ, 500, 388

Schmidtke, P.C., Cowley, A.P., McGrath, T.K., Hutchings, J.B., Crampto, D., 1996, AJ 111, 788

Schwarzshild, M., Härm, R., 1965, ApJ, 142, 855

Segretain, L., Chabrier, G., Mochkovitch, R., 1997, ApJ, 481, 355

Shapiro, S.L., Teukolsky, S.A., 1983, Balack Holes, White Dwarfs and Neutron Stars (New York:Wiley)

Siess, L., Goriely, S., Langer, L., 2003, A&A, in press

Sion, E.M., 1995, ApJ, 438, 876

Sion, E.M., 1999, PASP 111,532

Sion, E.M., Acierno, M.J., Tomczyk, K., 1979, ApJ, 230, 832

Sparks, W.M., Kutter, G.S., 1987, ApJ, 321, 394

Spitzer, L.J., 1962, Physics of fully Ionized Gases, Interscience Publ., New York

Spruit, H.C., 2002, A&A, 381, 923

Starrfield, 2003, in: Stellar Rotation, proc. IAU Symp. 215, A. Maeder, P. Eenens, eds.

Stein, J., Barkat, Z., Wheeler, J.C., 1999, ApJ, 523, 381

Stothers, R. & Chin, C.-W., 1972, ApJ, 177, 155

Taam, R.E., 1980, ApJ, 237, 142

Taam, R.E., Woosley, S.E., Lamb, D.Q., 1996, ApJ, 459, 271

Thoroughgood, T.D., Dhillon, V.S., Littlefair, S.P., Marsh, T.R., Smith, D.A.,2001, MN-RAS, 327, 1323

Tout, C.A., Regös, E., Wickramasinghe, D., Hurley, J., Pols, O.R., 2001, In: Evolution of Binary and Multiple Star Systems, ASP Conf. Ser., Vol 229

Townsley, D. M., Bildsten, L., 2002, In:Physics of Cataclysmic Variables and Related Objects, ASP Conf. Proc. Ser. vol. 261, Ed. B.T. Gaensicke et al., p. 31

Trümper, J., Hasinger, G., Aschenbach, B. et al., 1991, Nature, 349, 597

Uenishi, T., Nomoto, K., Hachisu, I., 2003, ApJ, 595, 1094

Umeda, H., Nomoto, K., Kobayashi, C., Hachisu, I., Kato, M., 1999, ApJ, 522, L43

Unno, W., 1970, PASJ, 22, 299

van den Heuvel, E.P.J., Bhattacharya, D., Nomoto, K., Rappaport, S.A., 1992, A&A, 262, 97

Walleborn, J., Baus, M., 1978, Phys. Rev. A., 18, 1737

Wang, L., 2004, in: 3-D Signatures of Stellar Explosions, Cambridge, in press, [astro-ph/0311299]

Wang, L., Baade, L., Höflich, P. et al., 2003, ApJ, 591, 1110

Wang, L., Höflich, P., Wheeler, J.C., 1997, ApJ, 483, L29

Weaver, T.A., Woosley, S.E., 1993, Phys. Rep., 227, 65

Webbink, R.F., 1984, ApJ, 277, 355

Weigert, A., 1966, Z. Astrophys., 64, 395

Weller, J., Albrecht, A., 2002, Phys.Rev.D, 65, 3512

Wellstein, S., Langer, N., 1999, A&A, 350, 148

Wellstein, S., Langer, N., Braun, H., 2001, A&A, 369, 939

Wheeler, C.J., 1996, In: Evolutionary Processes in Binary Stars, Dordrecht, Kluwer

Whelan, J., Iben, I.Jr., 1973, ApJ, 186, 1007

Woosley, S.E., Weaver, T.A., 1986, ARA&A, 24, 205

Woosley, S.E., Weaver, T.A., 1994, ApJ, 423, 371

Woosley, S.E., Wunsch, S., Kuhlen, M., 2003, [astro-ph/0307565]

Yoon, S.-C., Langer, N., 2002, In: Physics of Cataclysmic Variables and Related Objects, ASP Conf. Proc. Ser. vol. 261, Ed. B.T. Gaensicke et al., p. 79

Yoon, S.-C., Langer, N., 2003, A&A, 412, L53, [Chapter 3]

Yoon, S.-C., Langer, N., 2004a, A&A, accepted, [Chapter 4]

Yoon, S.-C., Langer, N., 2004b, A&A, accepted, [Chapter 6]

Yoon, S.-C., Langer, N., Scheithauer, S., 2004, A&A, submitted, [Chapter 5]

Yoon, S.-C., Langer, N., van der Sluys, M., 2004, A&A, submitted, [Chapter 2]

Yungelson, L., Livio, M., Tutukov, A., Kenyon, S.J., 1995, ApJ, 447, 656

Zahn, J.-P., 1974, in Stellar Instability and Evolution, ed. P. Ledoux, A. Noels, A.W. Rogers, IAU Symp. 59, Reidel, Dortrecht, p. 185

Zahn, J.-P., 1975, Mem. Soc. Roy. Liège 8, 31

Zahn, J.-P., 1992, A&A 265, 115

List of some abbreviations:

A&A :	Astronomy and Astrophysics
A&AR :	Astronomy and Astrophysics Review
AJ :	Astronomical Journal
ApJ :	Astrophysical Journal
ApJS :	Astrophysical Journal Supplement
ARA&A :	Annual Review of Astonomy and Astrophysics
MNRAS :	Monthly Notices of the Royal Astronomical Society
Nuc. Phys. A :	Nuclear Physics A
PASJ :	Publications of the Astronomical Society of Japan
PASP :	Publications of the Astronomical Society of of the Pacific
Phys. Rev. L :	Physical Review Letters
Phys. Rev. A :	Physical Reviews A
Phys. Rev. D :	Physical Reviews D
ZfAp :	Zeitschrift für Astrophysik

Curriculum Vitae

Date and place of birth:	15 November 1970, Seoul, Korea
Bachelor of Science:	Astronomy, Seoul National University, Korea (1989 – 1993)
Master of Science:	Astronomy, Seoul National University, Korea (1993 – 1995)
Diplôme d'Etudes Approfondies:	Applied Mathmatics, l'Université de Versailles-Saint-Quentin, France (1998 – 1999)
Diplôme d'Etudes Approfondies:	Astrophysics, l'Institut d'Astrophysique de Paris, France (1999 – 2000)
Doctorate:	Astrophysics, Sterrenkundig Insituut, Univsersiteit Utrecht, The Netherlands (2000 – 2004)

Acknowledgments

It is a great pleasure for me to express my sincere gratitude to Prof. Norbert Langer, who supervised this work with discretion. During the last three years, I have been nourished with his broad knowledge of stellar evolution and nucleosynthesis, inspired by his brilliant insights, and guided by his scientific rigorousness. At the same time, he endowed me with maximal freedom for developing my ideas. I am also indebted to him for the helps with various non-scientific matters, to which he has never been indifferent. Above all, I enjoyed a lot working with him.

I am grateful to the thesis committee: prof. John Heise, prof. Ed van den Heuvel, prof. Thomas Peitzmann, Dr. Philipp Podsiadlowski and prof. Frank Verbunt, for their careful reading of the manuscript. I would like to thank to Dr. Philipp Podsiadlowski who had great interest in my work, for the invitation to Oxford and many fruitful discussions. He also let me involved in the European Research and Training Network "The Physics of Type Ia Supernovae", which stimulated this research work. Many thanks to Dr. Alexander Heger for the helps with the stellar evolution code as well as for the discussion about rotationally induced hydrodynamic instabilities and magnetic fields in stars. I thank Dr. Peter Höflich for the intuitive discussion on the explosion physics of rotating white dwarf models. I am deeply grateful to Prof. Seung-Soo Hong at Seoul National University, who initiated me into the fantastic world of theoretical astrophysics, for his continuous encouragement and warm affection toward his old disciple.

I would like to thank to all colleagues in Sterrenkundig Instituut in Utrecht. Many thanks to Dr. Onno Pols for numerous discussions on both scientific and non-scientific matters and his friendly helps with various problems. I thank Axel Bončić for his nice explanation about the r-mode instability, which served to significantly expand the discussion on the final fate of rapidly rotating massive white dwarfs in chapter 4. I thank to Joeri van Leeuwen, Jelena Petrovic, Pui-Kei Fung, Jerôme Petri, Marc van der Sluys, Jorrit Wiersma and Jeroen Bergmans, especially for many useful tips and advice with regard to dutch life. I thank to Ed van der Zalm and Sake Hogeveen for their support with computer related matters. Special thanks to Arend Jan Poelarends for his painstaking dutch translation of the thesis summary and his support for my calculating some models in his computer. I am grateful to Marion Wijburg not only for her administrative service but also for having introduced me to Voces Intimae, thanks to which I could enjoy pleasant moments of singing together with its members on Tuesdays.

Memo

....